NASA CONTRACTOR REPORT 166461

Forward Velocity Effects on Fan Noise and the Influence of Inlet Aeroacoustic Design as Measured in the NASA-Ames 40 x 80 Foot Wind Tunnel

R.G. Holm
L.E. Langenbrunner
E.O. McCann

CONTRACT NAS2- 8675
July 1981

NASA

NASA CONTRACTOR REPORT 166461

Forward Velocity Effects on Fan Noise and the Influence of Inlet Aeroacoustic Design as Measured in the NASA-Ames 40 x 80 Foot Wind Tunnel

R.G. Holm
L.E. Langenbrunner
E.O. McCan
General Electric Company
Aircraft Engine Group
Cincinnati, Ohio 45215

prepared for
Ames Research Center
Under Contract NAS2-8675

National Aeronautics and
Space Administration

Ames Research Center
Moffett Field, California 94035

FOREWORD

This report was prepared by the Technical Programs and Program Technology Department, Aircraft Engine Group, General Electric Company, Evendale, Ohio, under the sponsorship of the National Aeronautics and Space Administration, Ames Research Center, Moffett Field, California, under Contract NAS2-8675. This report covers the work done under Modifications 7 and 8 during the period 8 November 1979 to 31 January 1981. Prior work was reported under NASA CR-152328. Mr. Allen Karchmer was the Technical Project Monitor for NASA and Mr. Ray Holm was the Program Technical Manager for the General Electric Company. Acknowledgment is made to the fine technical support provided by the Ames personnel associated with the program. Particular recognition is due to the engine operators, C. Huie and W. Douglas; the computer support of M. Campbell and J. Jope; instrumentation support of M. Alberry; mechanical support of C. Shiller; and technical engineering support of C. Horne. The technical support of the NASA-Langley personnel is providing the Blade-Mounted Transducer System was excellent; J. Preisser, R. Golub, V. Knight, R. Ingram, and D. McClure are acknowledged for their fine efforts. Also, the General Electric personnel who assisted in data reduction and reporting are gratefully acknowledged. The contributions of J. Gilbert, N. Allen, R. Coffin, and the assistance of the General Electric Installed Performance Group, including W. Ruehr, D. Paul, and D. Dietrich were extremely valuable to the conduct of the program.

TABLE OF CONTENTS

TABLE OF CONTENTS (Concluded)

LIST OF ILLUSTRATIONS

LIST OF ILLUSTRATIONS (Continued)

LIST OF ILLUSTRATIONS (Continued)

LIST OF ILLUSTRATIONS (Continued)

LIST OF ILLUSTRATIONS (Continued)

LIST OF ILLUSTRATIONS (Concluded)

LIST OF TABLES

1.0 SUMMARY

The NASA-Ames Research Center 40 x 80 Foot Wind Tunnel was utilized as a principal test facility to evaluate the influence of inlet aeroacoustic design and other forward velocity-related effects on the inlet-radiated fan noise of a small turbofan engine. Three inlet geometries were specifically evaluated, with concentration on the influence of the circumferential static pressure distortion aerodynamically induced as a result of the inlet design. In addition, test environmental considerations were evaluated by performing outdoor static tests using a turbulence control device and comparing these acoustic measurements to those obtained in the wind tunnel. The effect of the fan operating line on acoustic characteristics and the effectiveness of a bulk absorber treatment design were also investigated.

The influence of the test environment on the fan-radiated tones was very significant. Typical reductions of 10 to 15 dB in the first, second, and third harmonics of the blade passage frequency (BPF) were measured upon utilization of a turbulence control structure (TCS) for outdoor static testing or testing in the wind tunnel at a forward velocity of 41 m/sec (135 ft/s). The comparison of outdoor static with TCS and wind tunnel broadband acoustic data indicated differences on the order of 1 to 3 dB at frequencies above 1 kHz. The cause of these differences may be related to dynamic effects, changes in the turbulence spectrum interacting with the fan to produce noise, or transmission effects through the TCS. The tonal directivities between wind tunnel and outdoor TCS testing were generally in fair agreement in level, but shifts in the angular energy distribution were apparent. The cause of these shifts may in part be due to forward velocity-related coordinate transformations. However, lip shape and inlet flow-field effects may also be important contributing factors, and redirection of the sound field by introduction of the TCS should not be discounted. In general, the tonal directivities were more lobular in the wind tunnel testing and had broader humps in outdoor static (TCS) testing.

The treatment design evaluated was very effective in suppressing the BPF tone at typical sideline angles. Narrowband suppressions of up to 20 dB were achieved in the tip speed range corresponding to a high flap approach. This suppression translated into a rather modest 3- to 5-dB effect when scaled and extrapolated to perceived noise level (PNL) values for an engine four times the size of the JT15D used for the test program at an overhead distance of 61 m (200 ft).

The fan operating line noise impact was evaluated during the test program and broadband differences of 3 dB were shown over a wide engine speed range by lowering the design operating line from a peak pressure ratio of 1.5 to a peak pressure ratio of 1.30 at the engine's maximum operating speed of 16,000 rpm.

The evaluation of the influence of circumferential static pressure distortion on inlet radiated noise was partially masked by the treatment effectiveness previously denoted. Using an aerodynamically contoured inlet (i.e., curved inlet) to reduce the circumferential static pressure distortion produced using a canted inlet, the noise source mechanism was interpreted to be diminished by up to 12 dB as implied from blade-mounted transducer (BMT) results.

However, the far-field noise differences between the canted diffusing treated inlet and curved diffusing treated inlet configurations indicated differences of only 1 PNdB when scaled to an engine four times the size of that used in the test program. A straight diffusing treated inlet configuration that reduced the static pressure distortion (SPD) to 0.2% indicated slight improvements on the order of 1 PNdB over the curved inlet (SPD = 0.8%) and 2 PNdB over the canted inlet (SPD = 2.3%) for simulated high-flap-approach conditions. The differences measured previously (Reference 1) using nondiffusing untreated inlets were as great as 7 PNdB between nondiffusing canted and straight geometries at this engine speed, hence, the treatment effectiveness is largely responsible for the 5 PNdB incremental difference.

2.0 INTRODUCTION

The inlet radiated noise of a turbofan engine has been the subject of extensive research. The principal research objectives have been to characterize or suppress such noise with particular regard to its tonal characteristics. The major portion of this research has been conducted by using ground-based static testing without simulation of aircraft forward speed or aircraft installation-related aeroacoustic effects. Hence, wind tunnel testing is a necessary and viable alternative to the conduct of expensive flight test programs. The necessity of conducting flight-simulation research test programs in this area is provided by the discrepancies incurred when comparing static test noise data with that measured during turbofan flyovers. However, in flight, the resolution of the details of the inlet-radiated tonal noise component flight effects are masked by other aircraft or engine noise sources. Therefore, the impact of flight effects on the inlet radiated noise characteristics and their interdependence on inlet design features should be accomplished in the simulated flight environment provided by a wind tunnel.

Previous test experience (Reference 1) demonstrated that the NASA-Ames Research Center (ARC) 40 by 80 Foot Wind Tunnel (40 x 80) offered an excellent facility for performing controlled aeroacoustic tests. ARC provided a 21-inch fan diameter, 3.3 bypass ratio turbofan engine to perform this inlet-radiated noise research program.

The inlet designs selected for aeroacoustic evaluation were based on the data obtained under the previous test experience (Reference 1). The results of the earlier program demonstrated that the downward canting of a turbofan engine inlet produces a significant noise radiation impact over an engine speed range that coincides with a high-flap landing approach condition. Prior results were measured on inlets of a cylindrical hard-wall geometry. In this current test program, inlets of a diffusing nature were tested. The inlets tested were designed to be representative of those currently installed on commercial turbofan engines and in fleet service at this time.

Three specific designs were chosen for evaluation: a straight diffusing inlet, a canted diffusing inlet, and a curved diffusing inlet. These inlets were aerodynamically contoured to achieve various levels of static pressure distortion at the fan face. This parameter was anticipated to be the noise impact mechanism which caused the increased noise levels at the simulated high approach test condition as discussed in Reference 2.

The inlet aeroacoustic testing included the effects of inlet diffusion, inlet acoustic treatment, fan operating line, and a comparative assessment to static outdoor test measurements made with an inlet lip shape designed to match the inlet's internal aerodynamics of the wind tunnel installation. The outdoor testing was accomplished using a turbulence control device to achieve a turbulence structure more representative of that incurred during the wind tunnel evaluation.

Section 3.0 contains a summary of the tests and data reduction procedures along with a description of the test facilities, turbofan engine, inlets, instrumentation, and test setup.

Section 4.0 consists of a description of the data analysis techniques and a discussion of the results.

Section 5.0 completes the report by summarizing the results in terms of conclusions and recommendations.

3.0 TEST DESCRIPTION

3.1 TEST FACILITIES

3.1.1 NASA-ARC 40 by 80 Foot Wind Tunnel

The simulated-flight tests were conducted in the Large-Scale Aerodynamics Branch 40 by 80 Foot Wind Tunnel (40 x 80) at the Ames Research Center (ARC). A plan-view sketch of the 40 by 80 is shown in Figure 1. This facility has the capability, with an engine installed in the test section, to simulate flight speeds up to 91 m/s (300 ft/s). However, due to the fact that the wind tunnel is a closed-circuit facility, operation of an engine with the wind off circulates airflow around the circuit creating a minimum forward velocity range of 4 m/s (13.5 ft/s) to 8 m/s (26.3 ft/s), depending on the fan airflow. The wind-off operation provided quasi-static conditions of a low speed flow across the test section.

The use of the 40 by 80 for previous acoustic testing was significantly enhanced by lining the floor and part of the walls of the test section with a 7.62-cm (3-inch) layer of polyurethane foam. The foam mat virtually removed reverberant reflections from the noise data at all frequencies above 500 Hz. To ensure consistency in the noise measurements, the same foam was placed on the ground between the microphone and the engine during outdoor static tests.

3.1.2 NASA-ARC Outdoor Test Stand

Outdoor static tests were performed on the NASA-ARC large-scale aerodynamics test stand. These tests were conducted during early morning hours to take advantage of calm wind conditions and to avoid background noise contamination from an active runway adjacent to the test site. A plan-view sketch of the test stand is shown in Figure 2. The operations, which include the engine operator's console and data acquisition systems, are housed underground to provide a reflection-free test-bed for acoustic measurements.

3.2 TEST VEHICLE

3.2.1 JT15D Turbofan Engine

The test vehicle supplied by ARC was a modified JT15D turbofan engine; a cross section is shown in Figure 3. The physical and aerodynamic parameters for the modified JT15D engine are listed in Table 1. The JT15D is a moderate bypass ratio engine with a single-stage, supersonic tip speed fan. With regard to forward radiated fan noise, the JT15D has many of the design features incorporated into the approximately four-times-larger modern turbofan engines in commercial service. Features such as the absence of inlet guide vanes

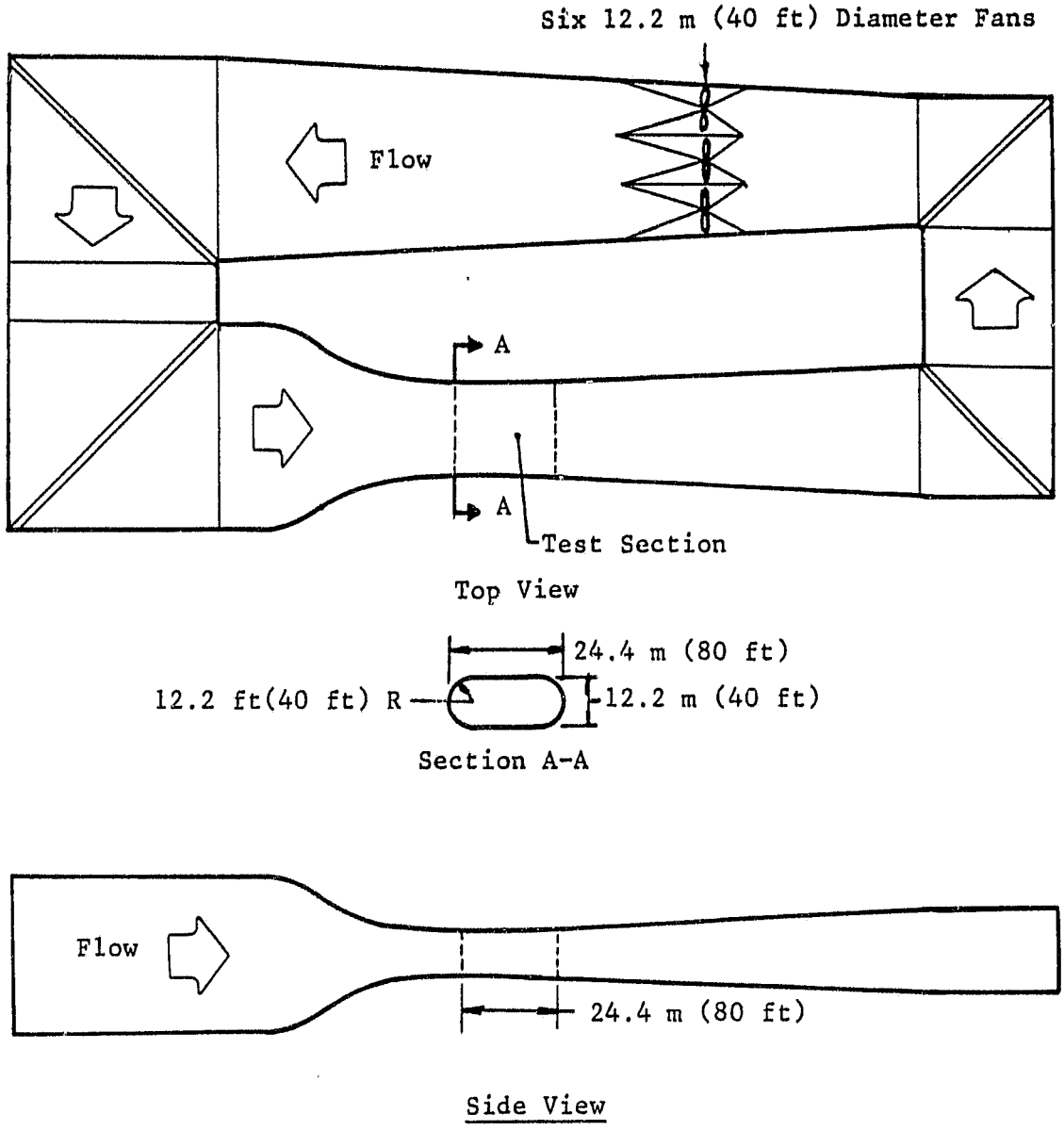

Figure 1. NASA-ARC 40 by 80 Wind Tunnel.

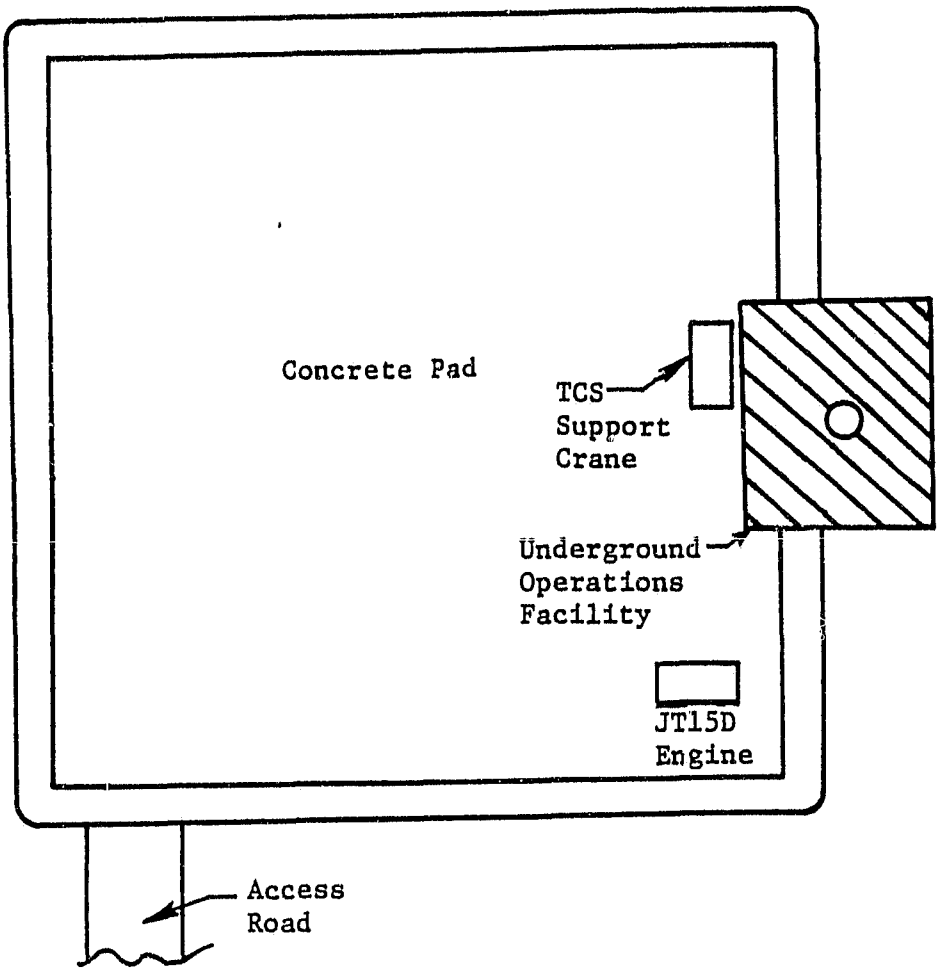

Figure 2. NASA-ARC Test Stand.

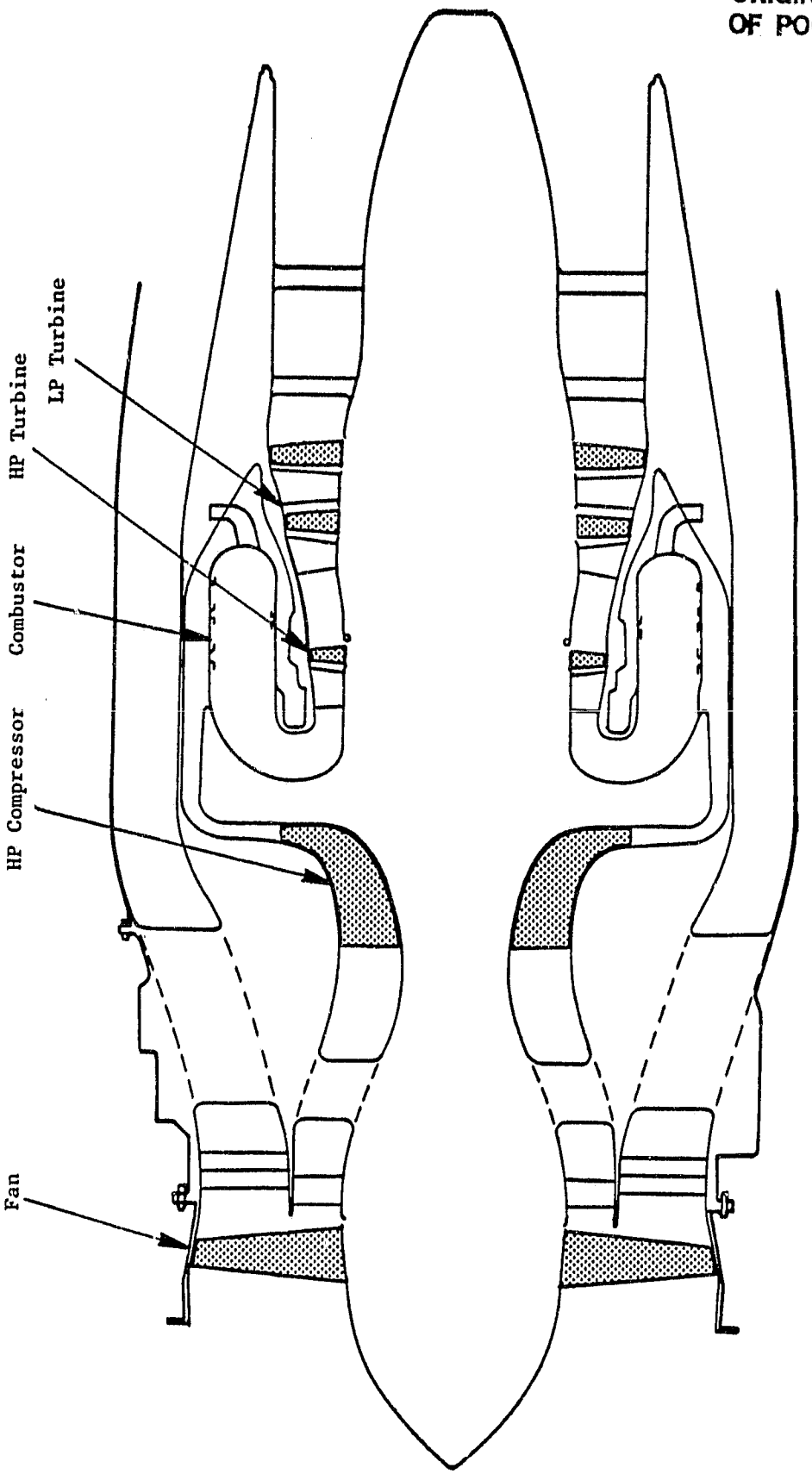

Figure 3. Modified JT15D Turbofan Engine.

Table 1. Modified JT15D Parameters.

Fan Pressure Ratio	1.5
Bypass Ratio	3.3
Hub/Tip Ratio	0.405
Rotor Diameter, cm (in.)	53 (21)
Maximum Fan, rpm	16,000
Rotor Blades	28
Bypass Stator Vanes	66
Core Stator Vanes	71
Bypass Vane/Blade Ratio	2.36
Core Vane/Blade Ratio	2.54
Bypass Rotor/Stator Spacing	1.65
Core Rotor/Stator Spacing	0.85

(IGV's), large spacing between the fan blades and outlet guide vanes (OGV's), and at least twice as many OGV's as fan blades are common design features between the JT15D and the CF6, JT9D, and RB211 turbofan engines. The engine utilized for this series of tests was modified by ARC as a result of the research of Hodder (Reference 3). The inlet temperature sensor was made flush with the wall in order to eliminate the tone noise from the interaction of its wake with the fan blades. Also, the number of core stator vanes was increased and spaced further downstream from the fan to diminish the impact of the fan blade wakes impinging on the vanes. The increase in core vane number produced a cutoff of tonal noise generated from this interaction.

3.2.2 Nacelle, Nozzle, and Mounting Assembly

The JT15D engine used during the advanced inlet testing was housed in a special quiet nacelle designed by ARC engineers. The nacelle was completely lined with sound-absorbent material to minimize the radiation of engine casing noise to the forward quadrant. Also designed by ARC engineers was a new coannular nozzle system for the JT15D. The new fan nozzle included a larger exit area to provide more flow to accommodate the operating line studies and had both walls lined with acoustic treatment to suppress the aft radiated fan noise. The JT15D, with its nacelle and nozzle system, is shown in cross sec-

tion in Figure 4, and the complete assembly is shown on the mount in Figure 5.

The mount is a leaned strut that supports the engine assembly 4.6 m (15 ft) over the wind tunnel floor as shown by the photo in Figure 6. The strut carries all the plumbing and instrumentation lines to the engine assembly and is fastened to a turntable. The axis of rotation is through the fan face which allows angle of attack to be accomplished by rotating the engine assembly about this vertical axis without changing the distances from the fan face to the noise measurement field. The engine assembly and its mount were installed on a nonrotating frame at the outdoor test stand to duplicate the wind tunnel setup during outdoor static testing.

3.3 INLET CONFIGURATIONS

The new inlet hardware tested in this program was fabricated under the supervision of the General Electric Co. The aerodynamic and mechanical designs were provided by General Electric, as was the acoustic treatment design. The inlets were selected to be representative of conventional commercial engines, apart from advanced aerodynamic concepts and advanced acoustic treatment designs. The aerodynamic design points for all inlets are listed in Table 2. The throat Mach number listed for each inlet is the one-dimensional calculation based on airflow and physical area. The acoustic design goals for the program were to achieve maximum perceived noise level (PNL) suppression when scaled to larger turbofan engines typical of those on modern commercial aircraft. There was also a goal to design as much of the hardware as possible to be common between the inlets, with configuration changes capable of being made simply and efficiently.

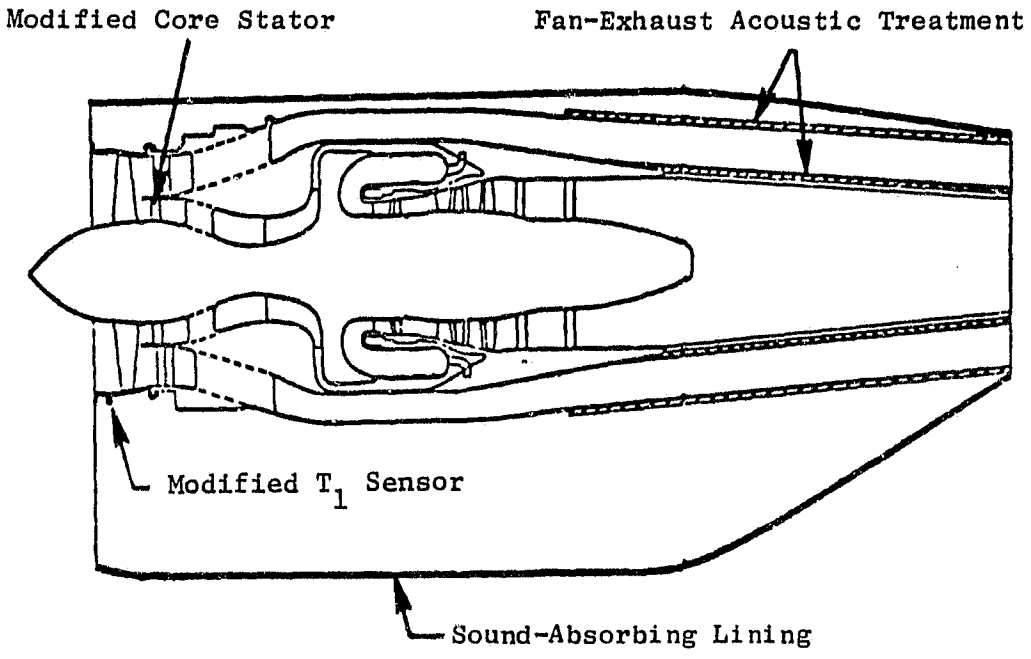

Figure 4. Modified NASA Test Engine Installed in the Quiet Nacelle.

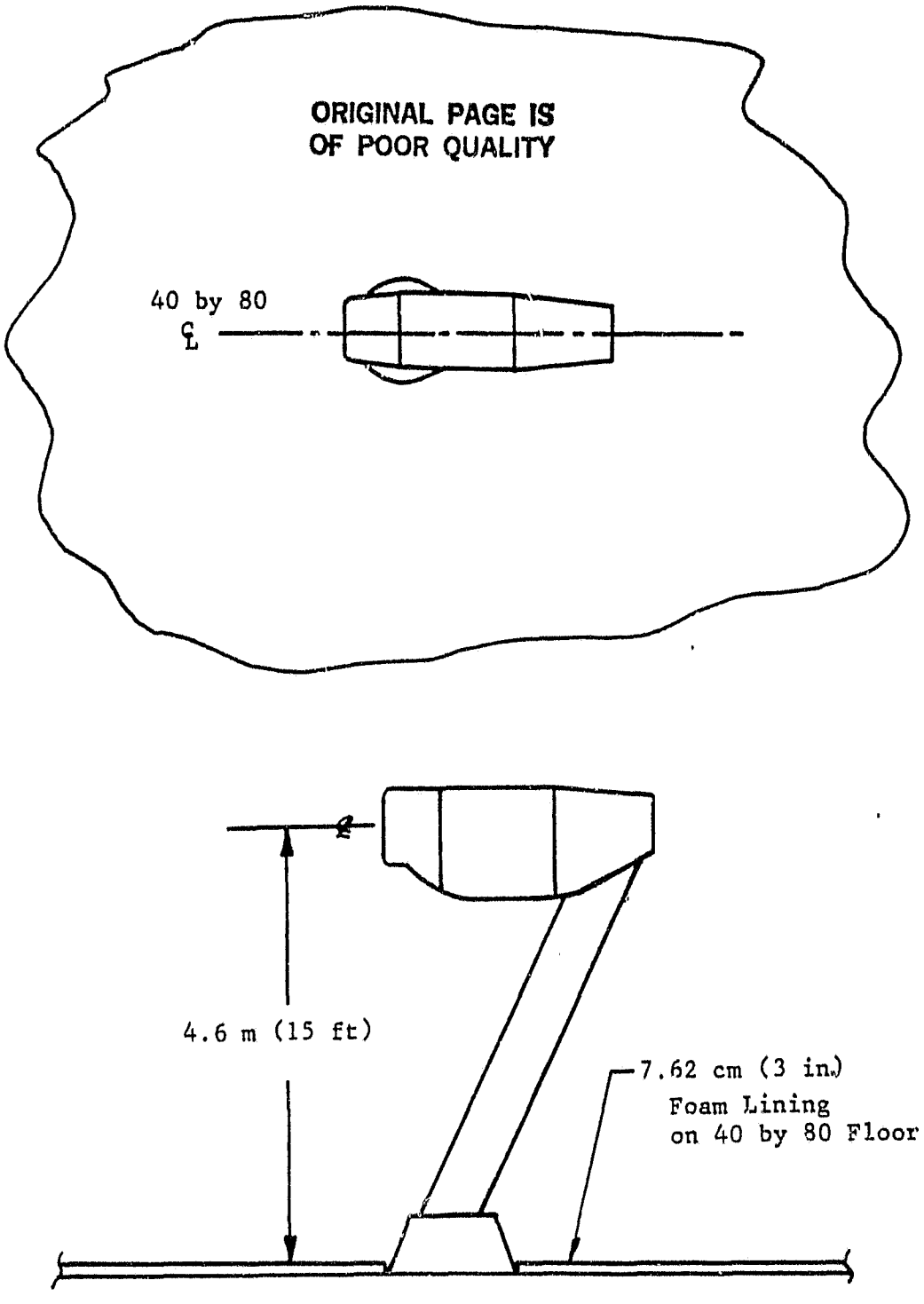

Figure 5. JT15D/Quiet Nacelle and Mount Assembly Schematic.

Figure 6. Photo of Engine Support Assembly.

Table 2. Inlet Design Parameters.

	Baseline	Diffusing
V_o, m/s (ft/s)	82 (270)	82 (270)
α, degrees	15	15
$\dot{w}$, kg/s (lb/s)	34 (75)	32.9 (73)
M_{th}	0.40	0.59
V_T, m/s (ft/s)	405 (1330)	405 (1400)
N_c, rpm	14,520	16,000
L/D	1.01	0.70
L/D Treated	---	0.38

3.3.1 Baseline Cylindrical Inlet

The baseline inlet is cylindrical in shape with a length-to-diameter ratio of 1.01. The inlet attaches to the JT15D fan casing with four drag links which compress a rubber seal around the circumference to ensure no leaks in the flowpath at the interface.

The baseline inlet was tested in the previous series of tests reported in Reference 1 and was retested in a similar wind tunnel configuration in order to provide a common data link between the two test programs.

3.3.2 Straight Diffusing Inlet

The straight diffusing inlet has a diffusion rate consistent with designs found in commercial service. The fan area to throat area ratio is 1.26 with a length-to-diameter ratio of 0.70. A schematic comparison of the baseline inlet and the straight diffusing inlet is shown in Figure 7(a).

The straight diffusing inlet is equipped with a flight lip for wind tunnel testing and a reverse cone aeroacoustic lip for outdoor static testing. A schematic of the two configurations is presented in Figure 8. The reverse cone outdoor configuration is designed to mate to the turbulence control screen (TCS) device which is utilized in the outdoor testing. A schematic of the TCS installed on the reverse cone is displayed in Figure 9.

The straight diffusing inlet is acoustically treated as shown in Figure 10(a). The treatment is a bulk absorber Kevlar material having a thickness of 0.09 inches which is compressed to 0.05 inches on installation. The Kevlar is covered with an aluminum 28% porosity faceplate of 0.025 inch thickness and pocketed in 1.75 inch cavities as indicated in Figure 10(b).

The attachment of the straight diffusing inlet to the fan casing is similar to the baseline inlet configuration. Any imperfections in the mating of the inlet hardware to the fan casing were smoothed over by using an RTV compound to ensure the flow field was as aerodynamically clean as possible when entering the fan.

3.3.3 Canted Diffusing Inlet

The canted diffusing inlet is designed to simulate the 5° canting of typical commercial aircraft engine inlets. This inlet's diffusing section is common hardware to the straight diffusing inlet, with the canting accomplished by inserting a canted ring between the diffusing section and the fan casing. The canted ring replaces a straight cylindrical ring used in straight diffusing inlet cases so that the average overall length of the two inlets is identical. The canting ring aerodynamically realigns the flowpath between the 5° canting diffuser and the axial fan assembly. The upper surface of the

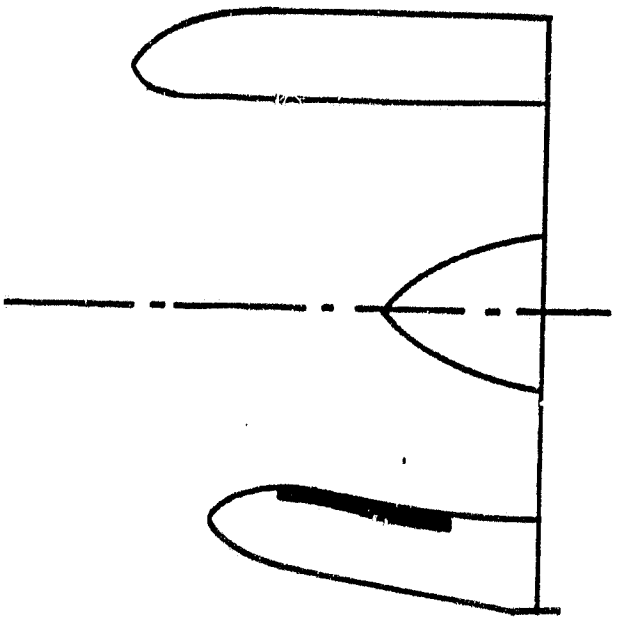

(a) Baseline Cylindrical (Upper) and Straight Diffusing (Lower) Inlets

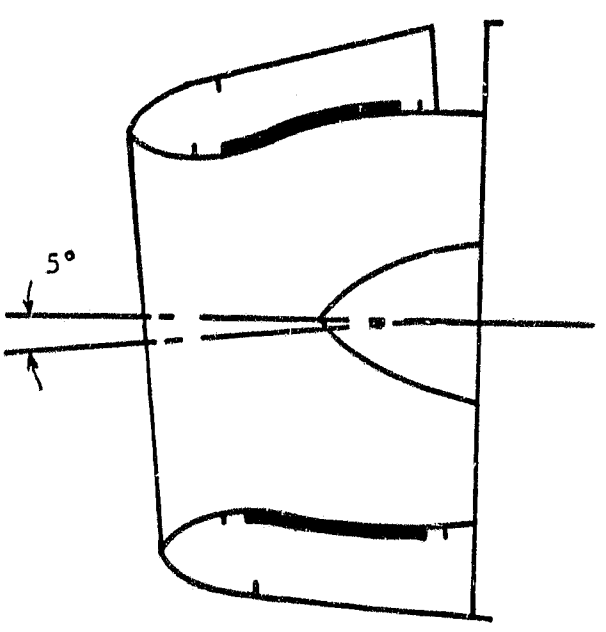

(b) Canted Inlet

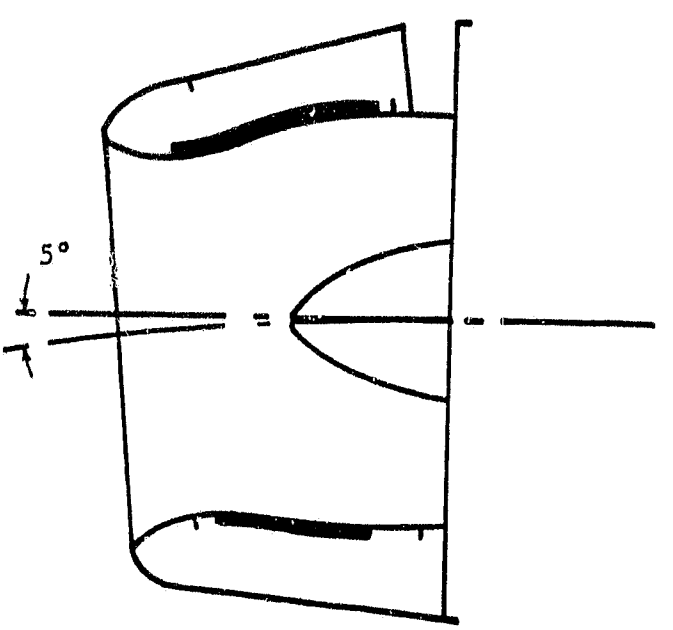

(c) Curved Inlet

Figure 7. Schematic of Wind Tunnel Inlets Tested.

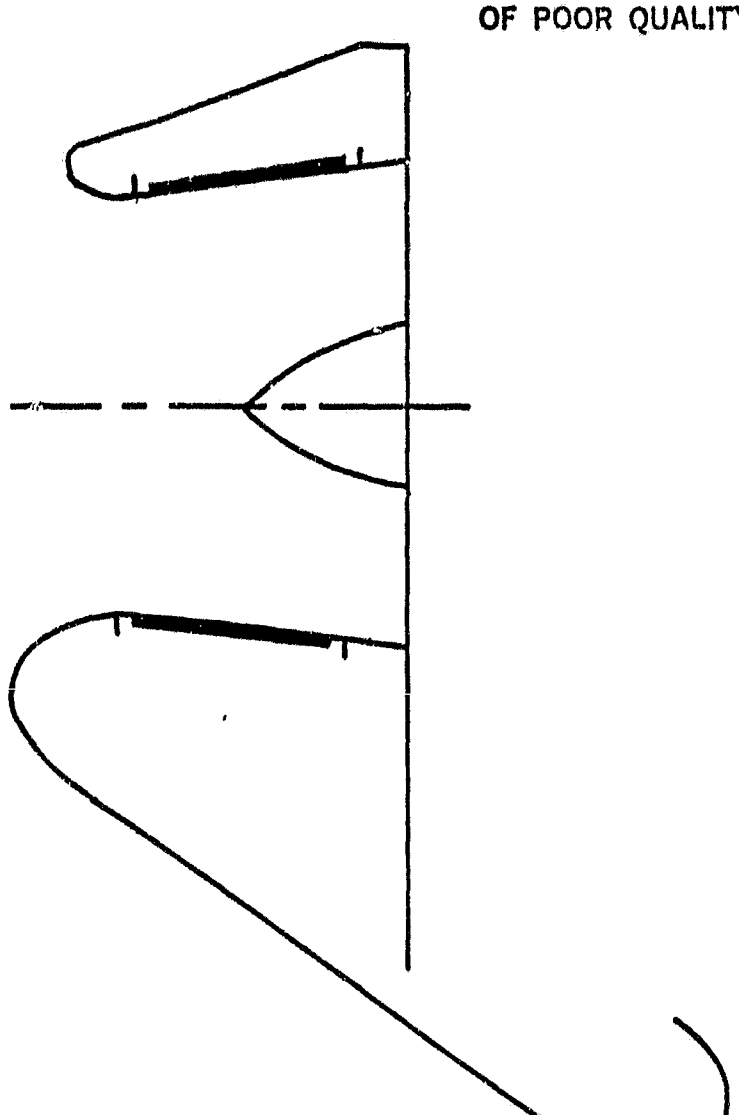

Figure 8. Schematic of Wind Tunnel (Upper) and Outdoor Test (Lower) Configurations.

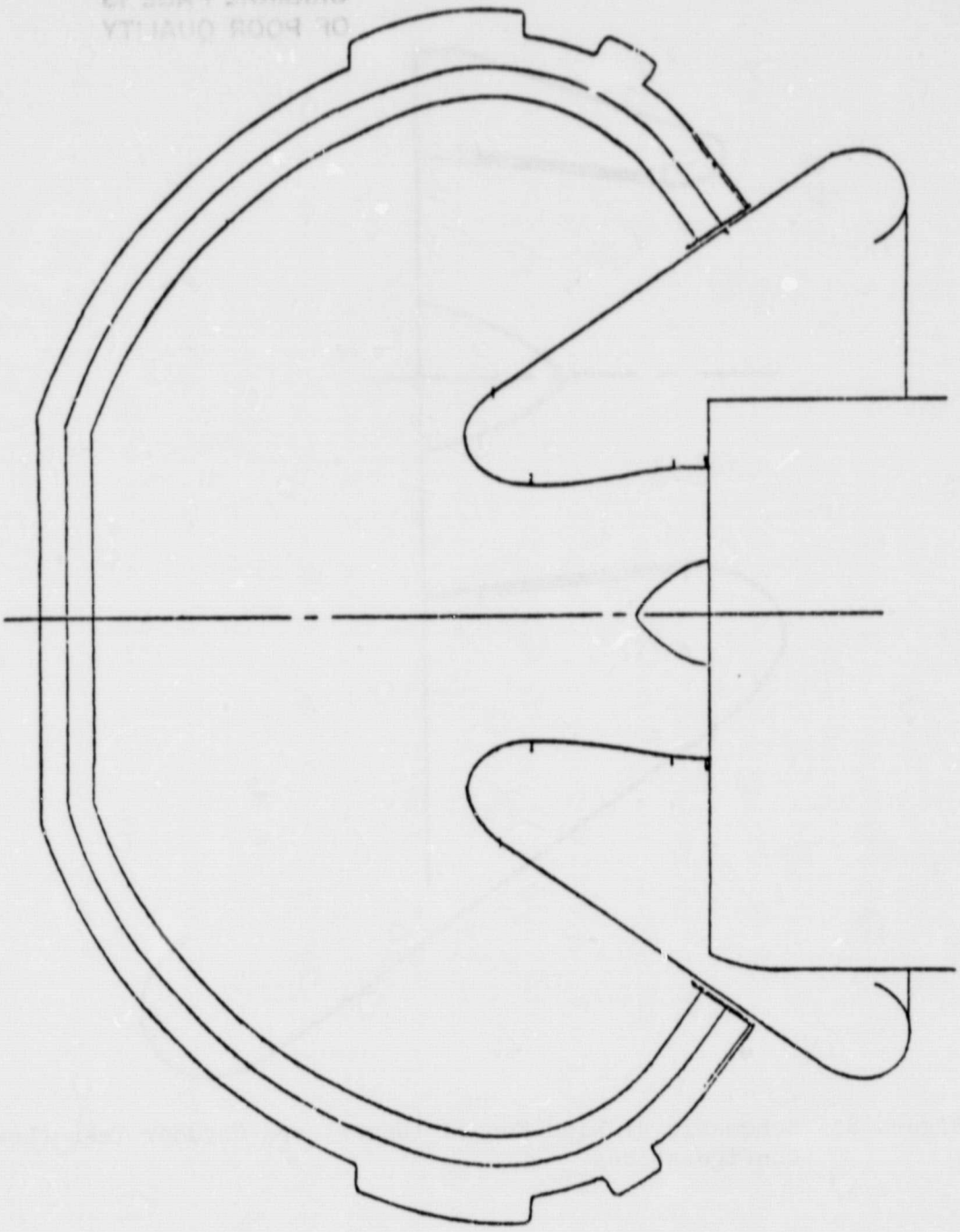

Figure 9. Schematic of TCS Installed on JT15D Engine.

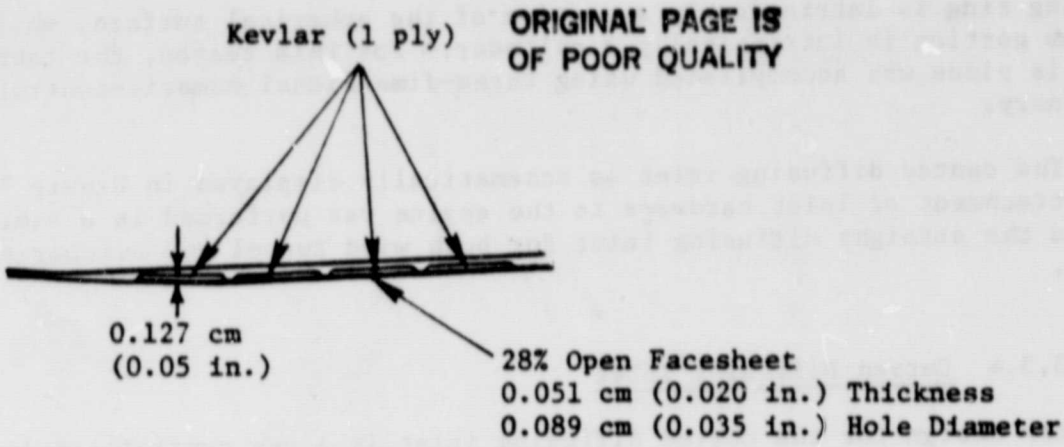

(a) Axial Treatment Deployment

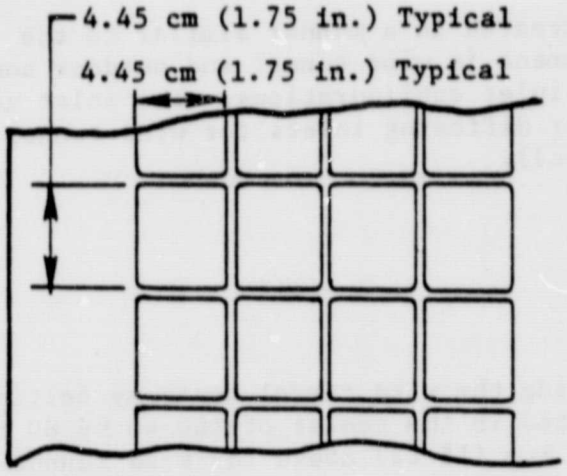

(b) Projection of Treatment Deployment

Figure 10. Inlet Treatment Details.

canting ring is intrinsically a portion of the spherical surface, while the bottom portion is intrinsically a cylinder. For this reason, the fabrication of this piece was accomplished using three-dimensional numeric-controlled machinery.

The canted diffusing inlet is schematically displayed in Figure 7(b). The attachment of inlet hardware to the engine was performed in a similar manner to the straight diffusing inlet for both wind tunnel and outdoor static tests.

3.3.4 Curved Diffusing Inlet

The design for the curved diffusing inlet is a new concept resulting from prior NASA-ARC testing. This inlet's throat is effectively oriented at 5° to the fan axial centerline. The entire diffusing section is utilized to turn the aerodyanmic flowpath back to parallel with the engine fan face centerline. The additional turning length allows flow alignment to be done more effectively, reducing circumferential static pressure distortion. The design was accomplished via a computer code of the GE Installed Performance Group entitled the "Stream Tube Curvature (STC) Program."

The curved diffusing inlet was treated in a manner similar to the straight diffusing inlet. Its attachment in wind tunnel and outdoor configurations was similar to the other inlet configurations. The inlet utilized the same flight lip as the other diffusing inlets for wind tunnel testing (schematically shown in Figure 7(c)).

3.4 TEST SETUP

3.4.1 Wind Tunnel Tests

The test vehicle was mounted during the wind tunnel tests by bolting the support strut to a turntable located in the center of the 40 by 80 test section. The engine centerline was 4.6 m (15 ft) above the wind tunnel floor with the turntable capable of yawing the test vehicle up to 40° for angle-of-attack operation. The floor and part of the walls were covered with foam to minimize reflection interference in the noise data. Noise measurements were made using a traversing microphone that covered angles from -5° to 138° on a 3.7-m (12-ft) arc. In addition, fixed microphones on a 4.5-m (14.5-ft) arc relative to the fan plane were located 30°, 50°, 60°, 70°, 90°, and 110° relative to the tunnel centerline. A schematic of the test setup is shown in Figure 11 with a photograph overview in Figure 12. Two other photographs showing the test setup are presented in Figures 13 and 14.

3.4.2 Outdoor Static Tests

The test vehicle was mounted during the outdoor static tests by bolting the support strut to a support frame located in the southwest corner of the

JT15D Far-Field Microphones

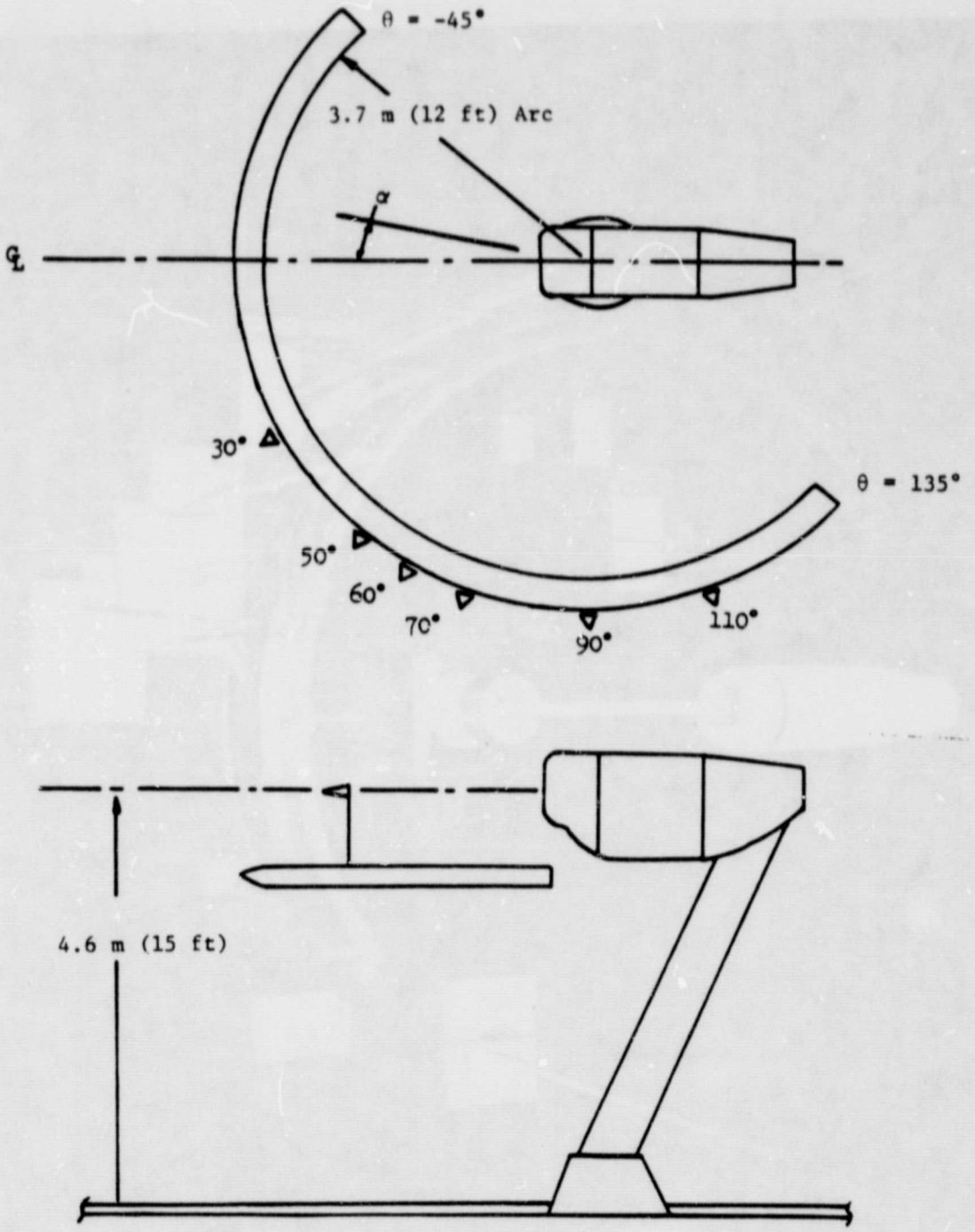

Figure 11. Test Setup for Wind Tunnel and Outdoor Static Tests.

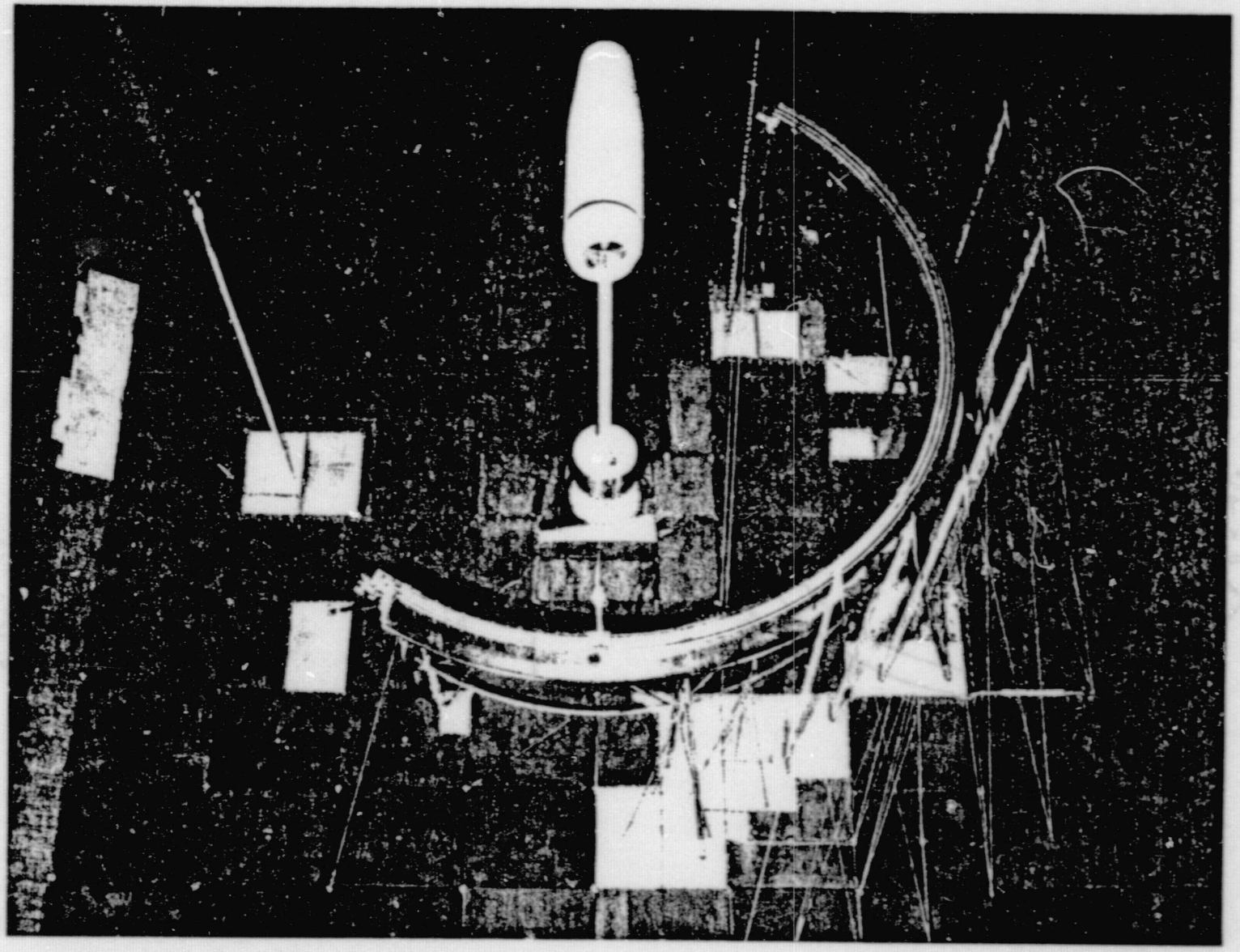

Figure 12. Photo of Wind Tunnel Test Configuration.

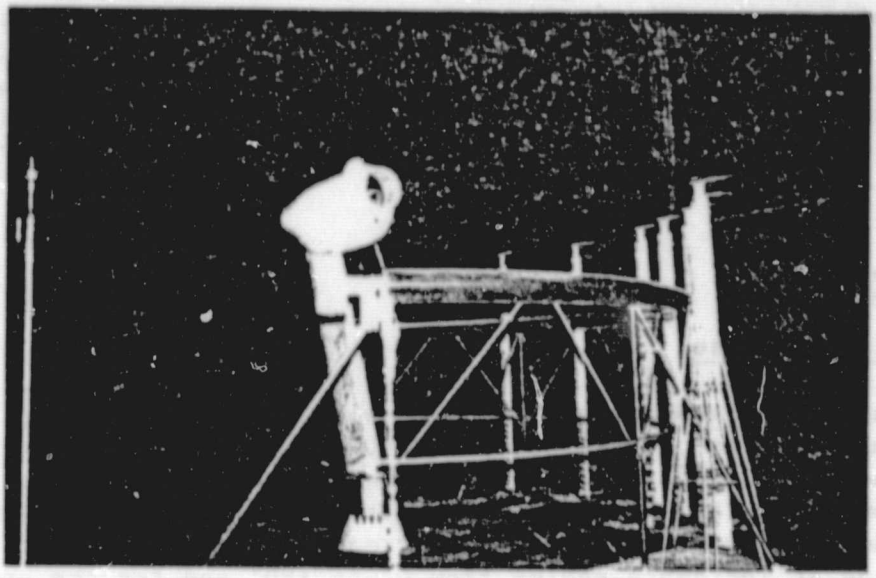

Figure 13. Frontal View of Microphone Deployment.

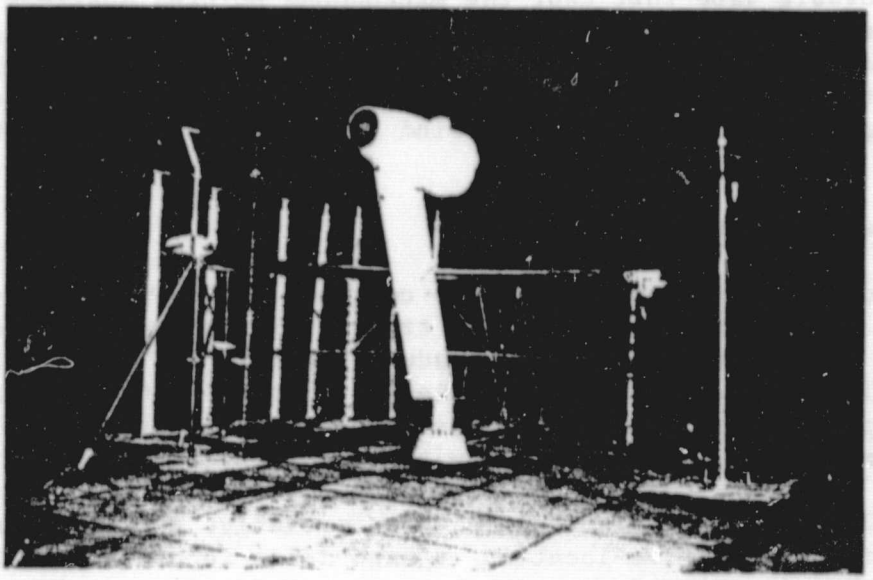

Figure 14. Aft View of Microphone Deployment

test area (see Figure 2). The engine centerline was 4.6 m (15 ft) above the ground and pointed in a northerly direction. The noise measurements were made at the same arc and fixed locations as those used in the wind tunnel tests. To minimize ground reflection interference in the noise measurements, large pieces of the wind tunnel foam were used to cover the ground under the engine and microphones. Two photographs of the test setup are presented in Figures 15 and 16.

3.5 INSTRUMENTATION

3.5.1 External Noise

All external noise measurements were made with B&K microphones. During all tests the microphones used were 0.64 cm (0.25 in.) B&K 4135's with B&K UA0385 nose cones attached. By using the same microphone/nose cone configuration for both outdoor static and wind tunnel tests, direct comparisons of the data can be made. However, B&K provides correction curves for noise arriving at the microphone at incidence angles from 0° to 180° and for the presence of nose cones. These curves were used to correct all the 1/3-octave-band data so that absolute sound pressure levels could be determined.

During the outdoor static and wind tunnel tests the fixed microphones were oriented pointing forward parallel to the engine centerline or wind tunnel centerline. The circular traversing microphone used during the tests was attached to a movable vane that kept the microphone pointed upstream during forward speed testing in the wind tunnel. However, during quasi-static wind tunnel and outdoor static testing, the vane was locked so that the microphone pointed toward the engine at all angles. Photos of the microphone setup are presented in Figures 11, 17, and 18 for wind tunnel, outdoor, and TCS tests.

3.5.2 Internal Noise

Internal noise measurements were made on the diffuser walls of each inlet with Kulite (XTMS-1-190-25D) pressure transducers during all outdoor static and wind tunnel testing. The transducers have a 0.32-cm (0.125-in.) pressure sensitive diaphragm mounted in the end of a 10/32 threaded bolt. Each inlet was provided with threaded holes through its diffuser walls which enabled the transducers to be installed with the diaphragms flush with the inner surface. The locations of the transducers for each of the inlets are given in Table 3. Since the transducers were removable, the same sensors were used at the same relative location in each inlet to minimize data errors, except for replacement due to instrumentation fatality during the test program.

3.5.3 Aerodynamic Performance

Static pressure distributions along the surfaces of each inlet at various circumferential positions were an essential part of the data acquired for each

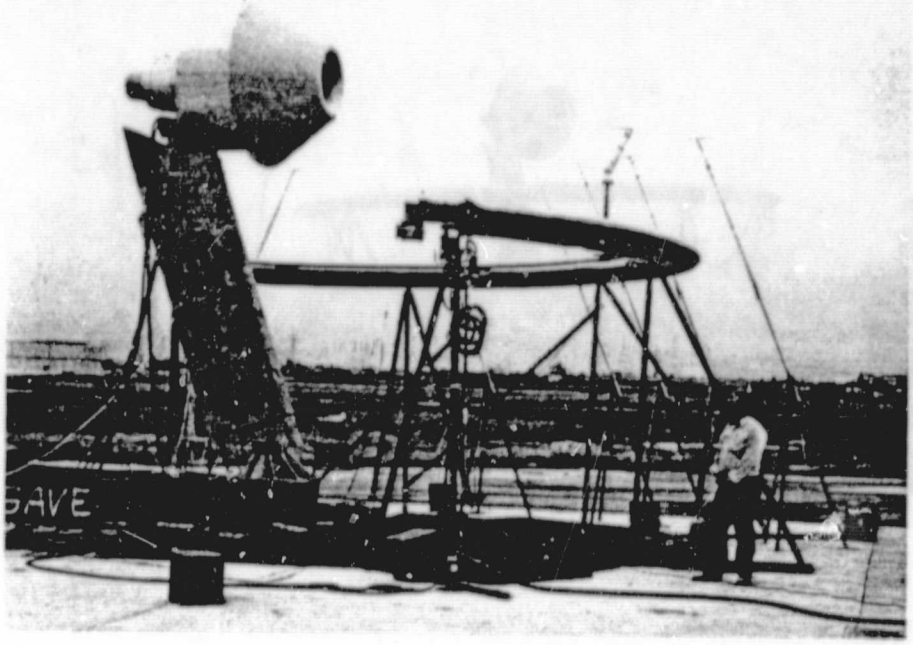

Figure 15. Photo of Outdoor Support Assembly.

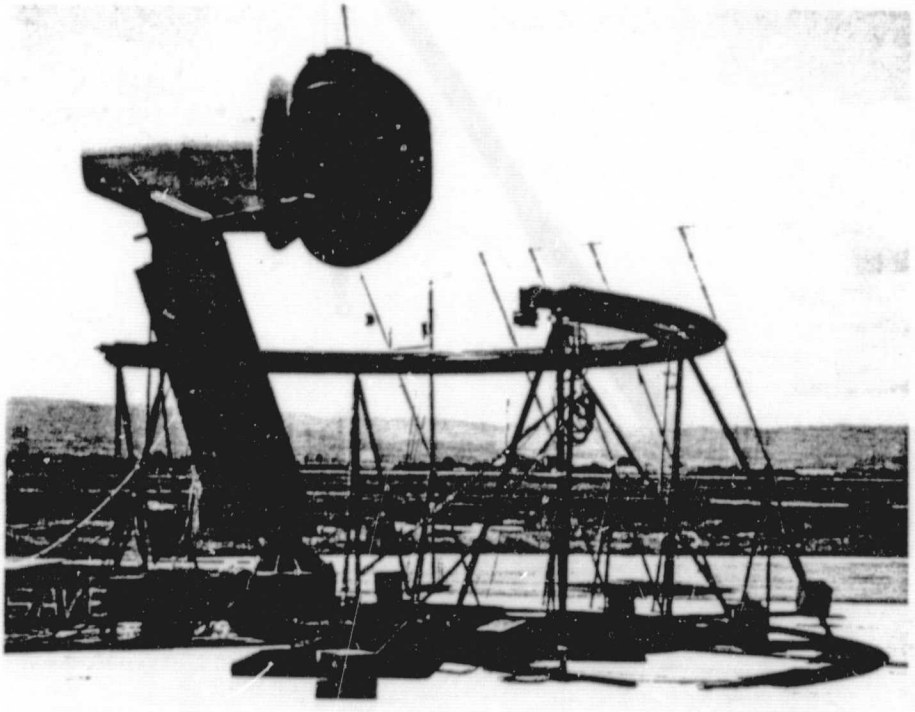

Figure 16. Photo of TCS Installation.

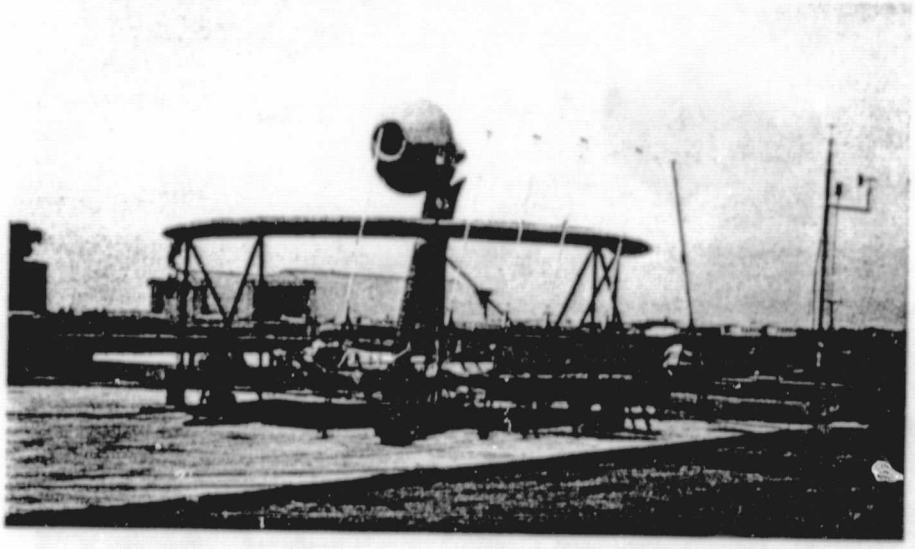

Figure 17. Photo of Outdoor Microphone Deployment.

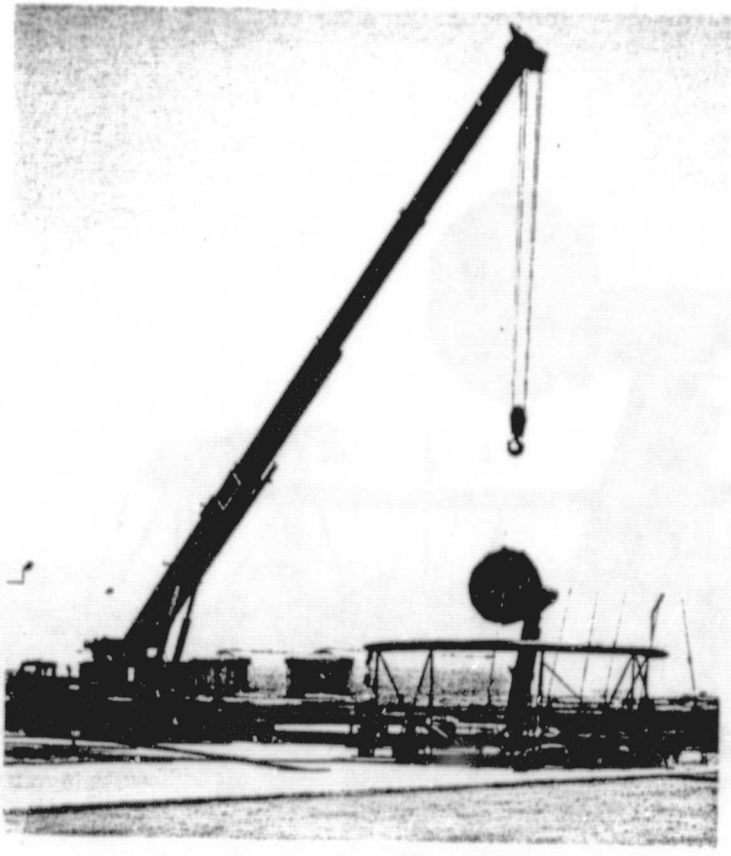

Figure 18. Photo of TCS and Instrumented Sound Field.

Table 3. Kulite Locations (Fan Casing Reference X = 0).

Transducer No.	Straight Diffusing Inlet (Canted Diffusing Inlet)		Curved Diffusing Inlet	
	Degrees	Inches	*Degrees	Inches
1	0	-2.800	0	-2.800
2	90	-2.800	90	-2.990
3	180	-2.800	180	-2.800
4	270	-2.800	270	-2.620
5	0	-10.750	0	-10.750
6	90	-10.750	90	-11.507
7	180	-10.750	180	-10.750
8	270	-10.750	270	-9.988

*90° = Upper Surface

test condition. In addition, eight static pressure taps mounted circumferentially 2.65 inches ahead of the fan face were closely monitored in-line during the testing. The static pressure tap locations for each of the inlets are tabulated in Table 4.

The JT15D fan pressure ratio was also of central concern during fan noise testing. The fan operating line was monitored during the wind tunnel testing utilizing a set of three NASA-supplied 6-headed total pressure rakes installed in the bypass duct.

3.5.4 Blade/Vane-Mounted Transducers

A special blade/vane-mounted instrumentation package on loan from the NASA-Lewis Research Center and operated by NASA-Langley Research Center personnel was provided for the test series. The locations and installation details of these transducers are shown in Figures 19 and 20. A more detailed discussion of this instrumentation can be found in References 4 and 5.

In general, the transducer system was a set of 14 Kulites - 8 blade-mounted and 6 vane-mounted. The blade-mounted transducers (BMT) were activated by a light switch, and information was telemetered to a receiving antenna mounted axially in the wall of the inlet. A schematic of the system installation details is also provided in Figure 19.

Table 4. Inlet Static Pressure Tap Locations (Fan Casing Reference X = 0).

Tap No.	Straight/Canted/Curved Inlets θ	X
1	0	-0.72
2	45	-0.72
3	90	-0.72
4	135	-0.72
5	180	-0.72
6	225	-0.72
7	270	-0.72
8	315	-0.72

	Straight (Canted) Diffuser θ	X	Curved Diffuser θ	X
9	0	-2.65	0	-2.65
10	45	-2.65	90	-2.839
11	90	-2.65	180	-2.65
12	135	-2.65	270	-2.469
13	180	-2.65	270	-3.720
14	225	-2.65	270	-4.928
15	270	-2.65	270	-6.135
16	315	-2.65	0	-6.6
17	270	-4.0	90	-7.055
18	270	-5.3	180	-6.6
19	270	-6.6	---	---
20	90	-6.6	---	---
21	270	-7.6	270	-7.071
22	270	-8.6	270	-8.00
23	270	-9.6	270	-8.931
24	0	-9.6	0	-9.6
25	90	-9.6	90	-10.269
26	180	-9.6	180	-9.6
27	270	-10.3	270	-9.583
28	270	-10.9	270	-10.138
29	0	-10.9	0	-10.9
30	90	-10.9	90	-11.657
31	180	-10.9	180	-10.9
32	270	-11.45	270	-10.649

	Flight Lip θ	X		Aeroacoustic Lip θ	X
33	270	-12.0		270	-12.0
34	90	-12.0		90	-12.0
35	270	-12.4		270	-12.4
36	270	-12.8		270	-12.8
37	0	-12.8		0	-12.8
38	90	-12.8		90	-12.8
39	180	-12.8		180	-12.8
40	270	-13.2		270	-13.2
41	270	-14.1		270	-13.9
42	270	-14.7		270	-14.8
43	270	-14.1		270	-16.2
44	270	-13.2	External	270	-16.79
45	270	-12.4		270	-16.1
46	270	-11.5		270	-14.1

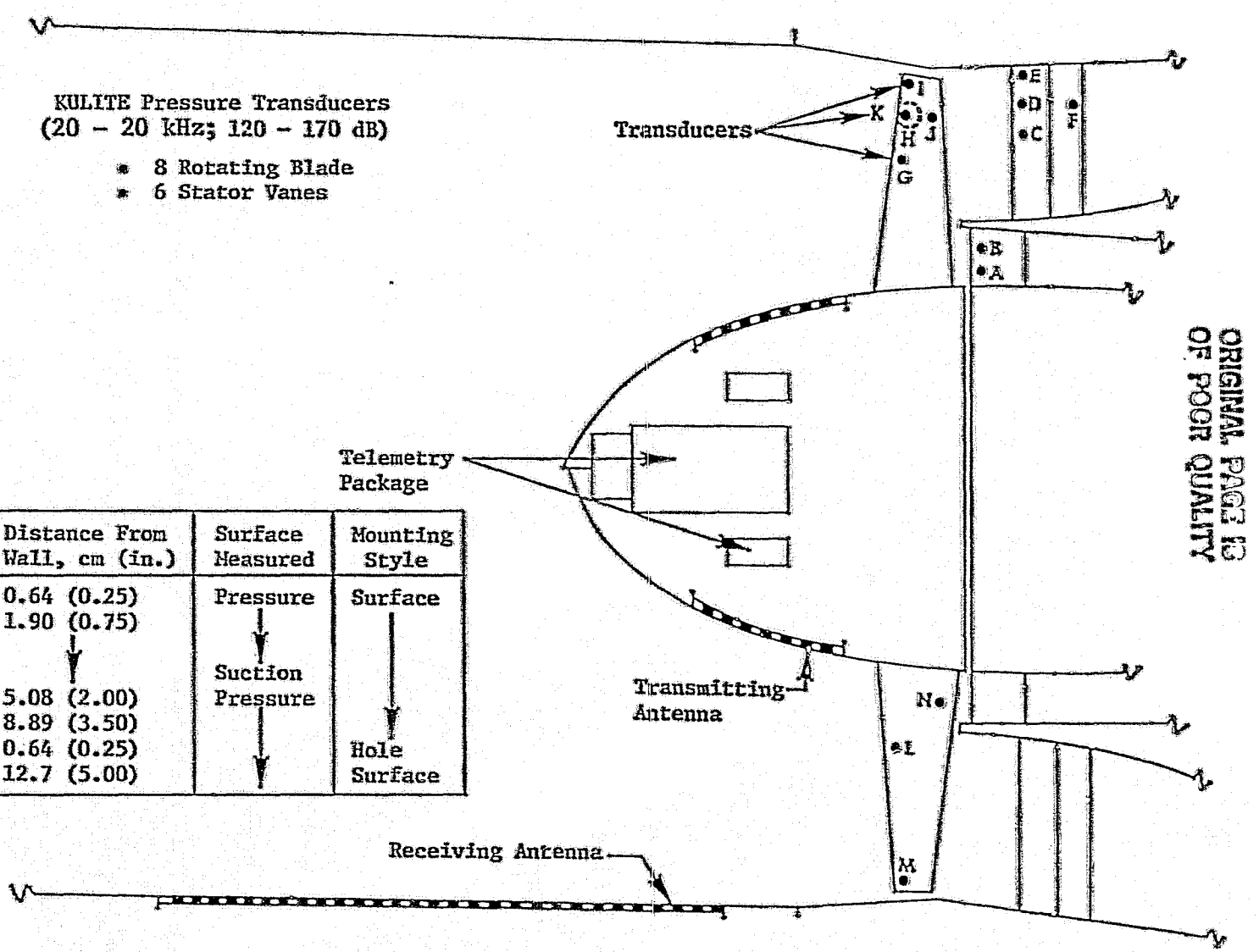

Transducer	Distance From Wall, cm (in.)	Surface Measured	Mounting Style
I	0.64 (0.25)	Pressure	Surface
J	1.90 (0.75)		
H			
K		Suction	
G	5.08 (2.00)	Pressure	
L	8.89 (3.50)		
M	0.64 (0.25)		Hole
N	12.7 (5.00)		Surface

Figure 19. Schematic of Internal Dynamic Instrumentation.

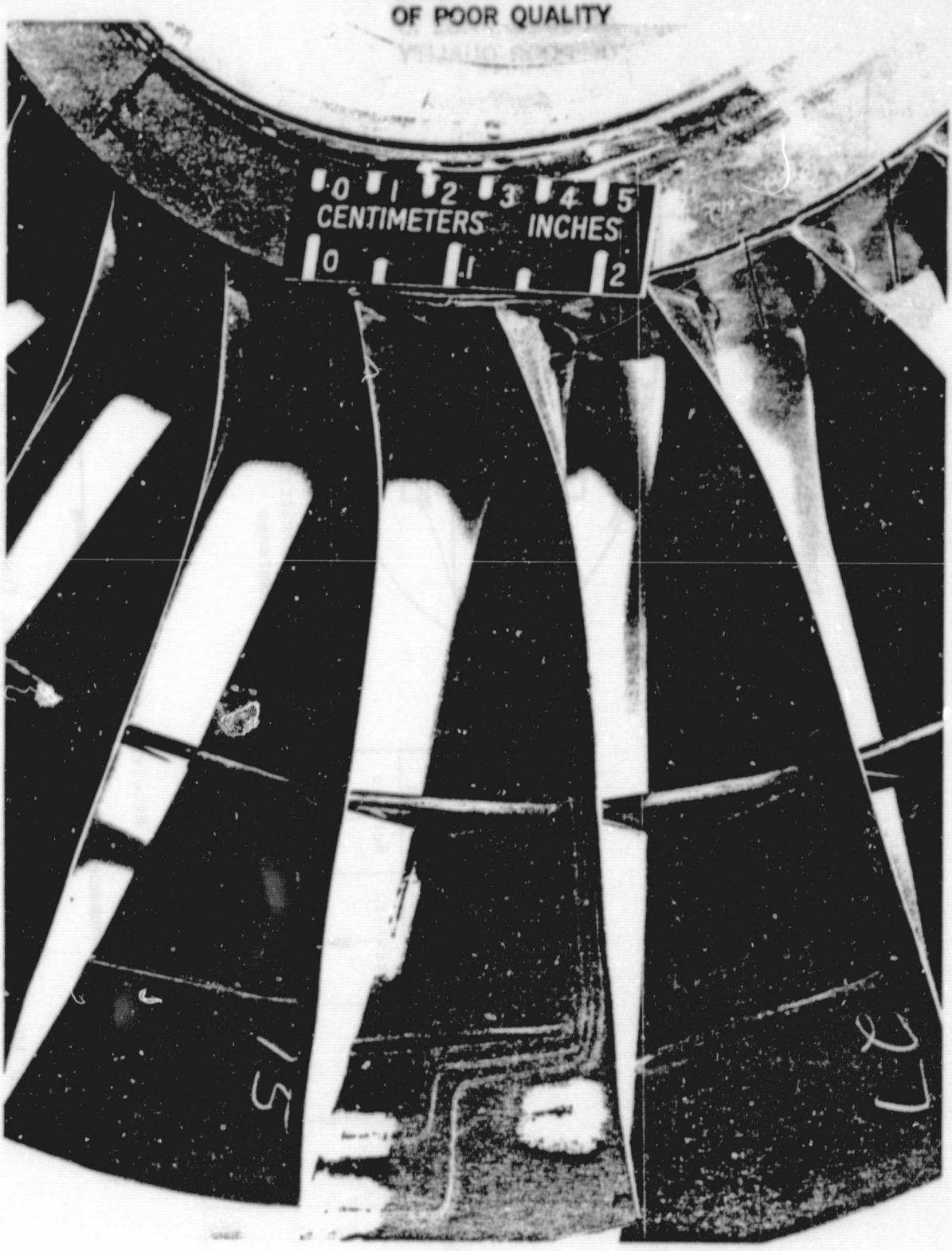

Figure 20. Photo of BMT Installation.

3.5.5 Hot Film Probe

During the outdoor static test program, a single hot film probe, TSI Model 1054A, was inserted at a station approximately 2.54 cm (1.0 in.) upstream of the fan rotor. Tests were conducted with this probe to measure axial turbulence parameters with and without the turbulence control device installed to determine its impact on the flow impinging onto the fan. Three radial immersions were tested coincident with the BMT radial locations of 0.25, 0.75, and 2.0 inches. Subsonic, transonic, and supersonic fan tip speeds were investigated with this hot film instrumentation.

3.6 TEST SUMMARY

3.6.1 Wind Tunnel Tests

The wind tunnel tests were conducted in the 40 x 80 during the period of 18 March 1980 to 22 March 1980. A summary of the 85-data-point test program is contained in Table 5. The primary objectives of the program were to obtain a complete characterization of the inlets tested, both aerodynamically and acoustically. The tests were conducted over the entire operating range of the JT15D engine; however, an emphasis was placed on the high subsonic fan tip speed region of 11,300 to 12,320 rpm.

Table 5. Run Log - Wind Tunnel Test.

Run	Inlet	Lip	Treatment	α	V_o* (knots)	Test Points	Operating Line
1	Curved	Flight	Yes	0°	0, 40	Check-Out	Upper
2	Curved	Flight	Yes	0°	0, 80	12	Upper
3	Curved	Flight	Yes	0°, 5°	0, 80	13	Lower
4	Straight	Flight	No	0°	0, 80	12	Lower
5	Straight	Flight	Yes	0°, 5°	0, 80	14	Lower
6	Canted	Flight	Yes	0°	0, 80	4	Lower
7	Canted	Flight	Yes	0°, 5°	0, 80	10	Lower
8	Baseline	Flight	No	0°	0, 80	9	Upper
9	Baseline	Flight	No	0°	0, 80	9	Lower

*V_o = 0 implies minimum tunnel velocity.

For each noise data point, the fan corrected speed was set based on aeroacoustic considerations and allowed to stabilize. All amplifier gain settings were optimized for internal and external noise measurements and then at least 30 seconds of internal dynamic data was tape recorded with the traversing microphone in the 138° position. An aerodynamic data sample was computer printed during this recording time. The traverse microphone sweep was then initiated and the recorders ran continuously for the approximate 4 minutes required to complete the traverse.

3.6.2 OUTDOOR STATIC TESTS

The outdoor static tests were conducted at the test stand during the period 23 April 1980 to 1 May 1980. Complete summaries of the tests are contained in Table 6 which includes the details of the 65-data-point test program. The objectives of the outdoor static tests were, first, to compare the engine's aeroacoustic performance with the production exhaust configuration to that produced by modifying the quiet nacelle engine to the production fan operating line. The other objectives were to operationally check out the turbulence control structure's aeroacoustic performance and obtain noise data for comparisons with the wind tunnel noise data.

Table 6. Run Log - Outdoor Static Test.

Run	Inlet	Lip†	Treatment	Test Points	Operating Line
1	Straight	Reverse Cone*	No	10	Design
2	Straight	RC/TCS	No	10	Design
3	Straight	RC/TCS	No	10	Upper
4	Straight	RC/TCS	No	10	Lower
5	Canted	RC/TCS	Yes	10	Upper
6	Curved	RC/TCS	No	5	Upper
7	Curved	RC/TCS	Yes	10	Upper
8	Curved	RC/TCS	Yes	12	Upper
9	Curved	RC/TCS	Yes	12	Upper

*Denoted as RC in other runs.

†TCS implies Turbulence Control Structure.

For each noise data point the fan corrected speed was set based on throat Mach number, if applicable, and allowed to stabilize. All amplifier gain settings were optimized for the internal/external noise measurements and then at least 30 seconds of data were tape recorded. During traverse operation of each outdoor static test, the recorders ran continuously for the 3 to 4 minutes required to complete the traverse. To minimize errors in data reduction the traverse microphone amplifier gain settings, which were preestablished based on peak overall noise levels, were not changed during data acquisition.

3.7 DATA REDUCTION

The reduction and processing of test data were shared by NASA and General Electric. Steady-state aerodynamic performance data for the inlets and the test facilities was calculated on-line by the NASA computers. Data editing and correcting were performed by GE and NASA engineers, and the final computed results were supplied by NASA posttest to GE. The external/internal noise measurements were monitored on-line during the tests by GE personnel to ensure signal validity. Posttest noise data reduction and processing were accomplished at the GE facilities.

3.7.1 Aerodynamic Performance Data

As part of the pretest effort, GE engineers conducted a compressible flow analysis of the inlets. This analysis determined the relationships between the airflow rate, the surface pressure distribution, and the throat Mach number for each inlet at outdoor static and wind tunnel test conditions. The results of this analysis were incorporated into the on-line aerodynamic performance computer program used for all wind tunnel testing. This program computed throat Mach number for all zero angle-of-attack test points using selected wall static pressures from each inlet. The computer program also computed the average total pressure distortion and the area-weighted average total pressure for all test points. These computer programs were a valuable asset to the wind tunnel testing because preliminary results were available on-line for each test point and final checked results were available at the completion of the tests.

3.7.2 Traverse Microphone Data

The 3.7 m (12 ft) arc microphone data from the wind tunnel and outdoor static tests were reduced to 1/3-octave-band spectra from 400 Hz to 16,000 Hz by special techniques developed to process moving microphone data. While the traverse is moving, narrowband spectra are being continuously computed with an angular spacing that depends on the number of spectral averages. The number used was 0.2 seconds which provides the smallest angular resolution between spectra on the 3.7 m (12 ft) arc, yet keeps the statistical errors below ±1 dB in the sound pressure levels. For each data point, the narrowband spectra are computed every 1.5° around the arc and then converted to 1/3-octave-band spectra that are corrected to standard day conditions.

To verify the traverse microphone data reduction technique, the data acquired with the traverse was compared to fixed microphone data at selected angles at the same test conditions. Typical comparisons of the spectra computed from fixed microphone data reduction to spectra computed from traverse microphone data reduction are shown in Figure 21. The baseline inlet was used because it changes more with frequency and angle than data from the other inlets and, therefore, presents a tougher test case for comparison of the methods. These comparisons, obtained from Reference 1, indicate that the traverse microphone data reduction method provides spectrum levels within ±2 dB of those computed by conventional fixed microphone techniques. In addition, traverse microphone data have an advantage over fixed microphone data in that no errors exist due to calibrating and recovering data from several microphones.

3.7.3 Fixed Microphone/Internal Noise Data

Selected fixed microphone and internal noise data from the outdoor static and the wind tunnel tests were reduced to 25 Hz narrowband spectra from 0 to 20,000 Hz using digital fast Fourier transform techniques. A 4.0-second average time was used which results in a 90% confidence that errors are less than ±0.5 dB in the sound pressure level.

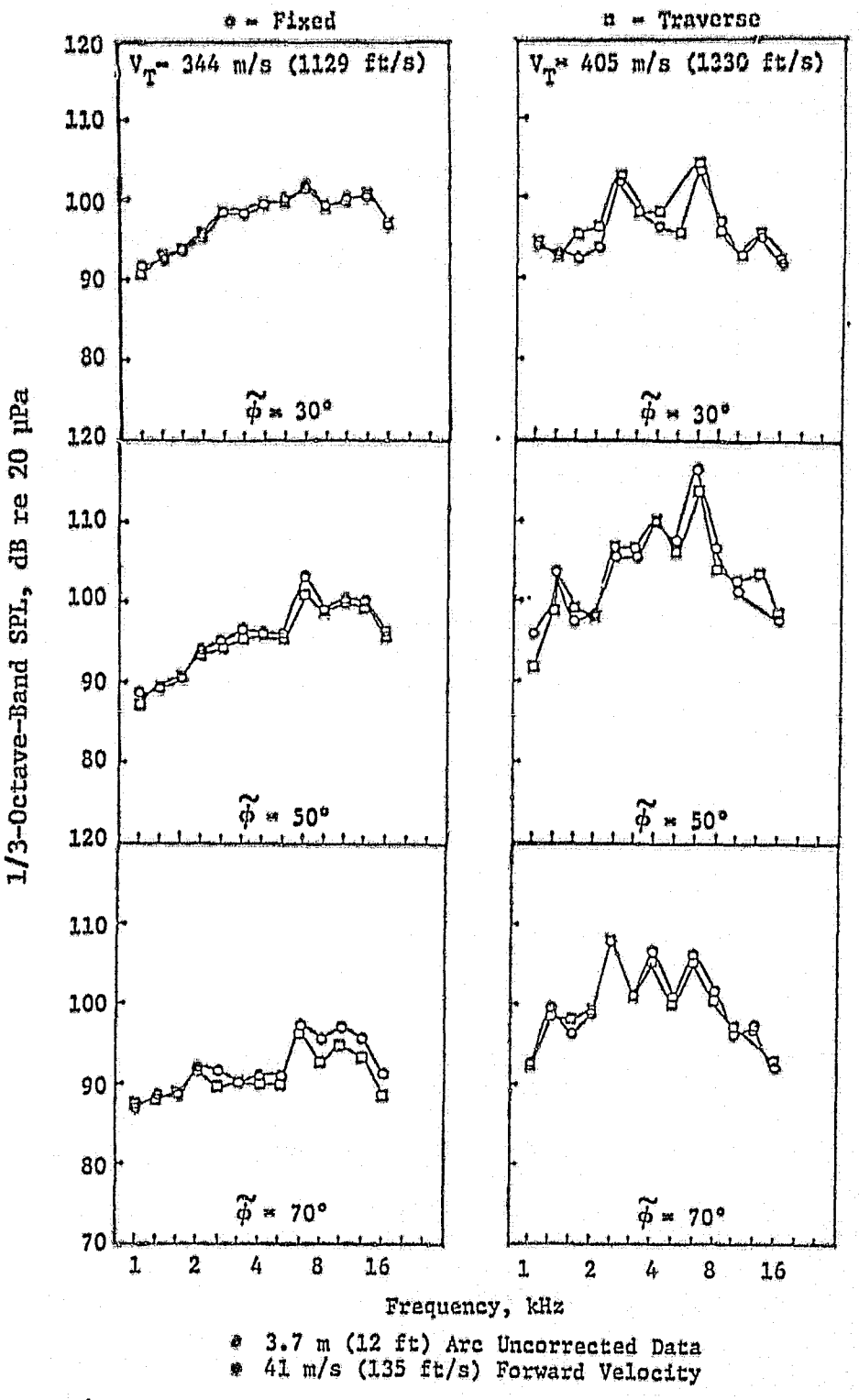

Figure 21. Verification of Traverse-Microphone Data Reduction.

4.0 DATA ANALYSIS

4.1 ANALYSIS TECHNIQUES

The techniques used to analyze acoustic data from the outdoor static and wind tunnel tests use 25-Hz narrowband and 1/3-octave-band formats. The 1/3-octave-band format is used to detect system noise differences, whereas the 25 Hz narrowband format can distinguish componential noise differences in greater detail. In addition, the directivity of fan blade passage frequency (BPF) is analyzed via a narrowband tracking filter in order to reveal additional details of this important element of the inlet radiated fan noise.

The reduction of the wind tunnel test data involves several steps. The initial step is to transform the coordinate system to account for the forward wind velocity effects. The next steps are to correct the narrowband stored spectra obtained at 1.5° increments on the 12 foot arc for wind tunnel background and system response effects. These stored spectra are then averaged at 10° incremental locations (i.e., the stored spectra between 47° and 53° are used to determine the 50° averaged spectrum). The 10° increment spectra are corrected for atmospheric attenuation, reconstituted to 1/3-octave bands, scaled to a large turbofan engine size, and extrapolated to a 61-m (200-ft) overhead condition. The 1/3-octave-band spectra are next weighted and summed to obtain overall sound pressure level (OASPL) and perceived noise level (PNL) at the arc angles from 10° to 130° in 10° increments. Tabulated 1/3-octave-band information was transmitted to NASA ARC. Atmospheric corrections were made on the basis of Reference 6.

4.1.1 Wind Tunnel/Static Transformation

The relationship between acoustic pressure and angle in the far field for static and wind tunnel situations can be expressed (as in Reference 7) by Equations 1 and 2 with reference to Figure 22.

The transformations of Equations 1 and 2 allow for the wind tunnel data to be adjusted for comparison to outdoor static results. It should be noted, however, that a simulated flyover calculation would utilize the static angle ϕ as opposed to the wind tunnel angle $\tilde{\phi}$, and would adjust the static results for forward velocity. The forward velocity adjustments would include two features - a doppler shift and a "dynamic effect." It is concluded that the wind tunnel data has no doppler shift; however, it possesses the dynamic-effect correction as a result of the wavelength contraction imposed due to the variation in the speed of sound identical to the variation in wavelength induced by frequency changes for the flight case. Thus, wind tunnel testing provides a basis for assessments of the dynamic effect corrections made for simulated flyover calculations. This effect is not accounted for in Equation 2. Another effect not accounted for in the transformations of Equations 1 and 2 is sound propagation effects through the velocity gradients near the engine inlet.

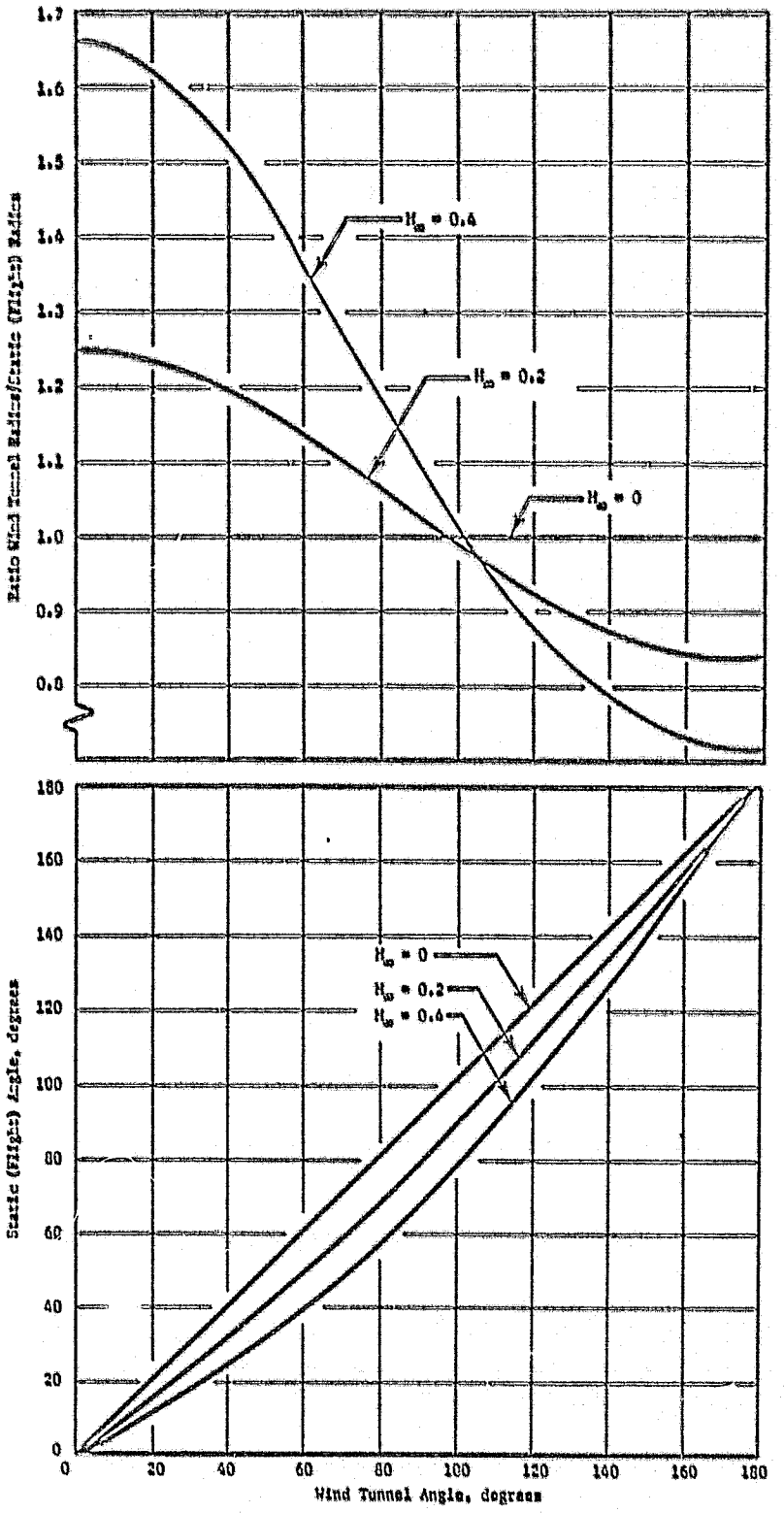

Figure 22. Relationship Between Wind Tunnel and Static (Flight) Coordinates.

$$\tilde{\phi} = \cos^{-1} \frac{\cos \phi - M_\infty}{(1 + M_\infty^2 - 2M_\infty \cos \phi)^{1/2}} \quad (1)$$

$$\frac{\tilde{p}^2}{p^2} = (1 + M_\infty^2 - 2M_\infty \cos \phi)^{3/2} / (1 - M_\infty \cos \phi) \quad (2)$$

The values $\tilde{P}$ and $\tilde{\phi}$ are the actual wind tunnel parameters and M_∞ is the (uniform) tunnel Mach number.

4.1.2 Wind Tunnel Background Noise

A plot of the typical wind tunnel background noise spectrum at two locations for the wind tunnel in operation at an 80-knot wind condition is presented in Figure 23. The levels indicate that only below 400 Hz does the wind tunnel background noise interfere with the JT15D noise measurements. Since this program was principally concerned with the higher frequency inlet radiated noise, this low frequency masking presented minimal limitations to the conduct of the testing.

Since the wind tunnel background was fairly constant with angle, an angularly averaged narrowband background spectra was logarithmically subtracted from the narrowband noise measurements.

4.1.3 Large-Scale Turbofan Noise

The projection of the JT15D results obtained under this test program to a large-scale turbofan engine was a desirable objective. A scaling factor of four was selected to simulate a 2.1-m (7.0-ft) fan diameter representative of the size currently found in commercial operation. The scaling procedure to accomplish this objective is outlined in the following:

- Correct the 12 ft data for atmsopheric absorption to a 0.3-m (1.0-ft) reference.
- Correct the 12 ft arc data for spherical divergence to a 0.3-m (1.0-ft) reference.
- Increase 1/3-octave-band sound pressure levels (SPL) by a factor of 12 dB, equivalent to an airflow increase of 16 which is proportional to the scale diameter squared.
- Frequency-adjust the 1/3-octave-band SPL's by a scaling ratio that will ensure a constant Strouhal number.
- Extrapolate the scaled source data to a distance of 61 m (200 ft).

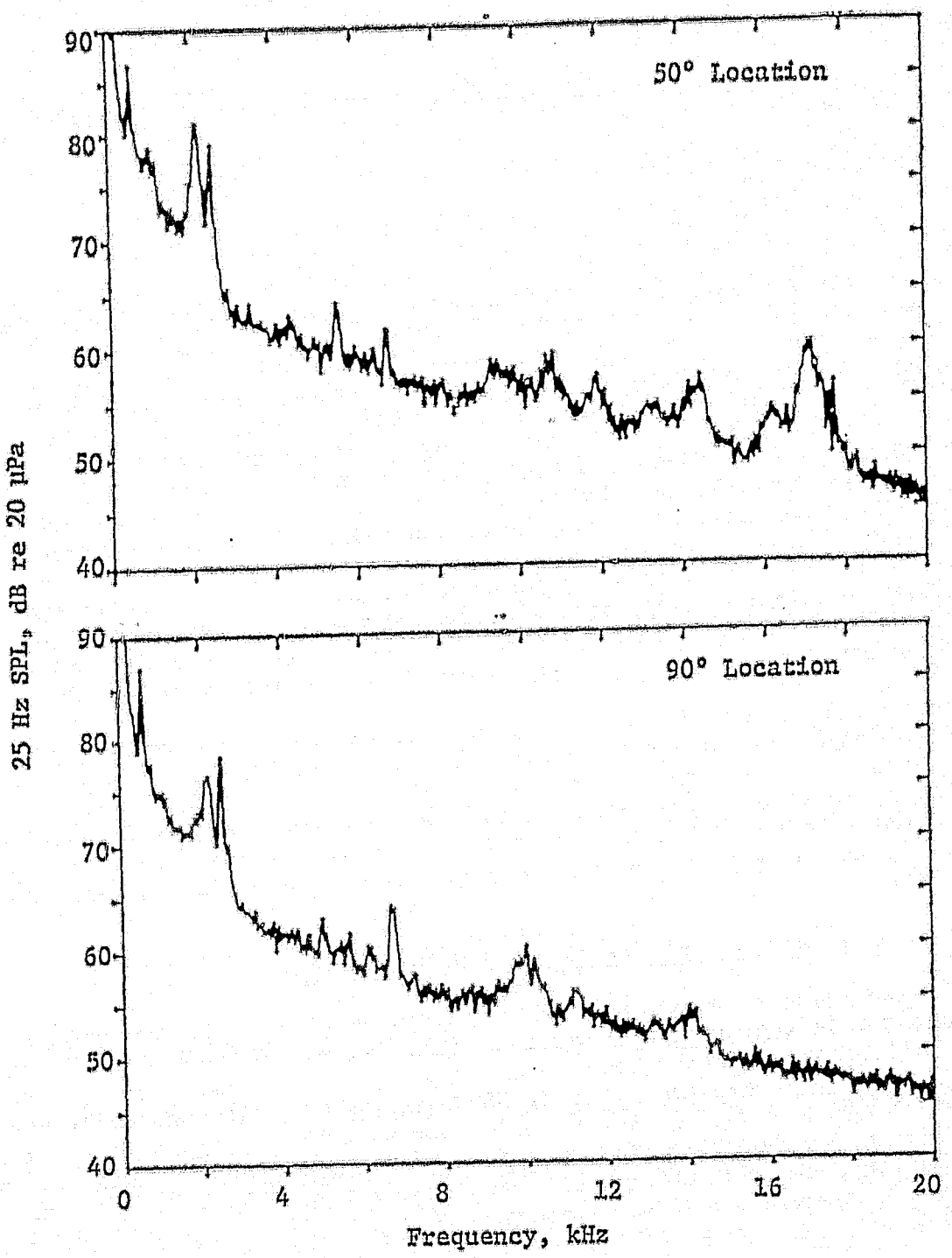

Figure 23. Typical 80 Knot Wind Tunnel Background Noise Spectra.

- Adjust the scaled 1/3-octave-band array for standard day atmospheric attenuation and spherical divergence sideline corrections at 10° increments.

- The scaled and extrapolated spectra are appropriately weighted to obtain power levels and at each 10° increment are summed to obtain OASPL and PNL.

4.1.4 Normalized Narrowband Differencing

The spectral difference in noise level between two configurations can best be determined by direct differencing of the 25 Hz narrowband spectrum measured at identical far-field locations. This procedure can produce some peculiar results if the tonal components do not align. To alleviate this problem the sampling rate, which is used to convert the analog noise signal recorded on magnetic tape to a digital number stream for conversion into the frequency domain, needs to be normalized. For example, if the BPF occurs at a frequency of 5600 Hz in one configuration and a frequency of 5625 Hz in a second configuration, then by sampling the data from the second configuration at a reduced sampling rate, the tonal component may be repositioned into the same spectral band. As a result of this normalization process, the two narrowband spectral components may be differenced directly. Performing this normalization does not impact the broadband energy distribution significantly, since the two configuration speed points being differenced were run at the same corrected speed to effectively normalize any aerodynamic differences.

The utilization of this narrowband differencing process required data of high statistical accuracy. Consequently, when this technique was utilized each narrowband spectrum was the result of 100 averages of a 2048-point data sample. This allowed the analysis to produce a 90% confidence level that the narrowband spectra were within ±0.5 dB of the true level. A frequency-smoothing and segment-averaging technique as discussed in Reference 8 was utilized.

4.1.5 Blade-Mounted Transducer (BMT) Analysis

The pressure measured on a BMT is composed of periodic and random signal variations. To segregate the periodic contribution to this signal, a technique called Signal Enhancement is utilized. The pressure signal is analog to digitally converted at a rate of 360 times per revolution, triggered from an optical blade sensor (refer to Reference 4). The enhanced waveform is then computed by averaging the records of 500 revolutions in order to obtain the mean pressure at each degree. The Fourier transform of this signal shows which harmonics of the circumferential periodic distortion are most dominant.

4.2 FAN/INLET AERODYNAMIC PERFORMANCE

The fan/inlet aerodynamic performance was an important element in the aeroacoustic measurement program. Prior to a detailed discussion of inlet acoustic performance, a summary of inlet aerodynamic performance is given.

4.2.1 Fan Operating Characteristics

The fan operating line characteristic was an important consideration in this acoustic measurement program. Utilizing the data measured by the NASA-supplied bypass duct pressure rakes and the results of the NASA/ARC-generated computer program, the two operating lines on which the fan performed were mapped as shown in Figure 24.

The success with which the NASA/ARC JT15D fan exhaust nozzle area was modified to match the JT15D fan design operating line is indicated in Figure 25. Production-nozzle data were obtained outdoors in the test configuration shown in Figure 15. The minimal impact of the TCS on operating line characteristics is illustrated in Figure 25.

4.2.2 Inlet Throat Mach Number Determination

The inlet throat Mach number was computed on-line during the wind tunnel tests by means of the computer programs provided by NASA/ARC. This capability assured that proper inlet performance was achieved at comparable corrected speed points for each configuration. Eight static pressure taps at four axial and four circumferential locations were monitored during the testing. These inputs were utilized in the computations of throat Mach number with analytically derived equations to permit this on-line, steady-state, data-reduction capability. This information was obtained prior to and after each acoustic test point along with computations of corrected fan speed, inlet airflow, and fan pressure ratio. Table 7 is a summary of the test parameters.

Table 7. Inlet Test Parameters.

N_c	V_T		M_{th}	M_{th}	M_{th}	$\dot{\omega}$		
rpm	m/s	(ft/s)	Straight	Canted	Curved	kg/s	(lb/s)	PR
10,500	293	(962)	0.360	0.360	0.357	24.7	(54.3)	1.128
10,800	302	(990)	0.370	0.371	0.370	25.3	(55.6)	1.137
11,300	315	(1035)	0.392	0.392	0.392	26.7	(58.3)	1.147
11,500	321	(1054)	0.400	0.400	0.400	27.0	(59.3)	1.154
11,800	329	(1081)	0.413	0.414	0.412	27.7	(60.9)	1.164
12,000	335	(1100)	0.420	0.421	0.421	28.1	(61.8)	1.173
12,300	344	(1127)	0.436	0.435	0.436	28.9	(63.5)	1.182
12,500	349	(1145)	0.444	0.443	---	29.3	(64.5)	1.187
12,800	358	(1173)	0.459	0.459	0.459	30.0	(66.1)	1.194
13,500	377	(1237)	0.492	0.493	0.494	31.7	(69.8)	1.216
14,500	405	(1329)	0.543	0.545	0.545	34.0	(74.7)	1.252
15,000	419	(1375)	---	---	0.578	35.3	(77.6)	1.268

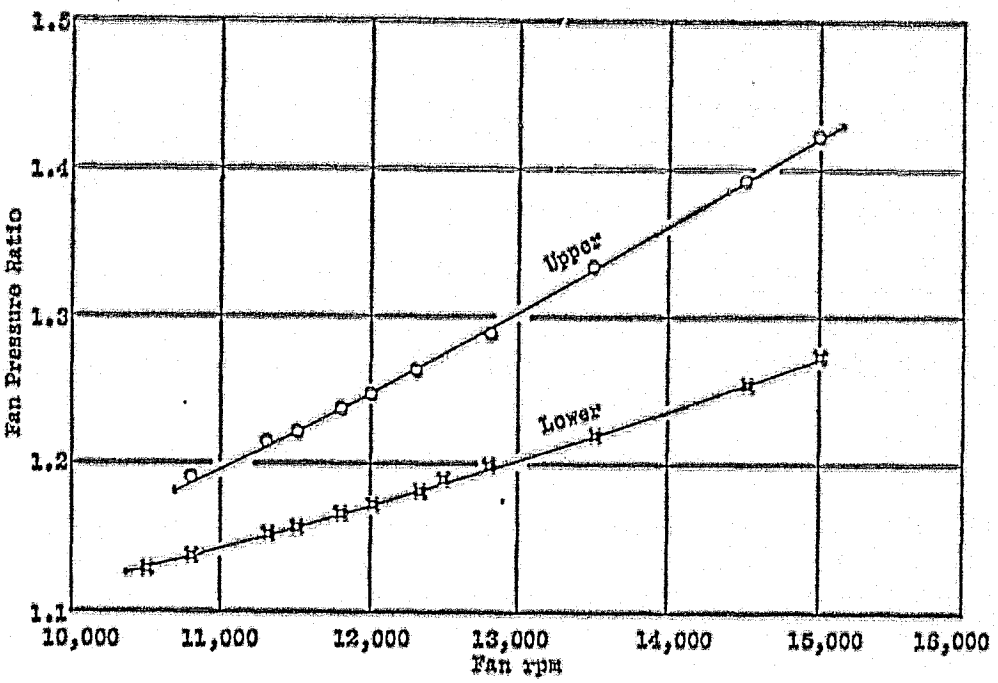

Figure 24. Plot of Two Fan Operating Lines

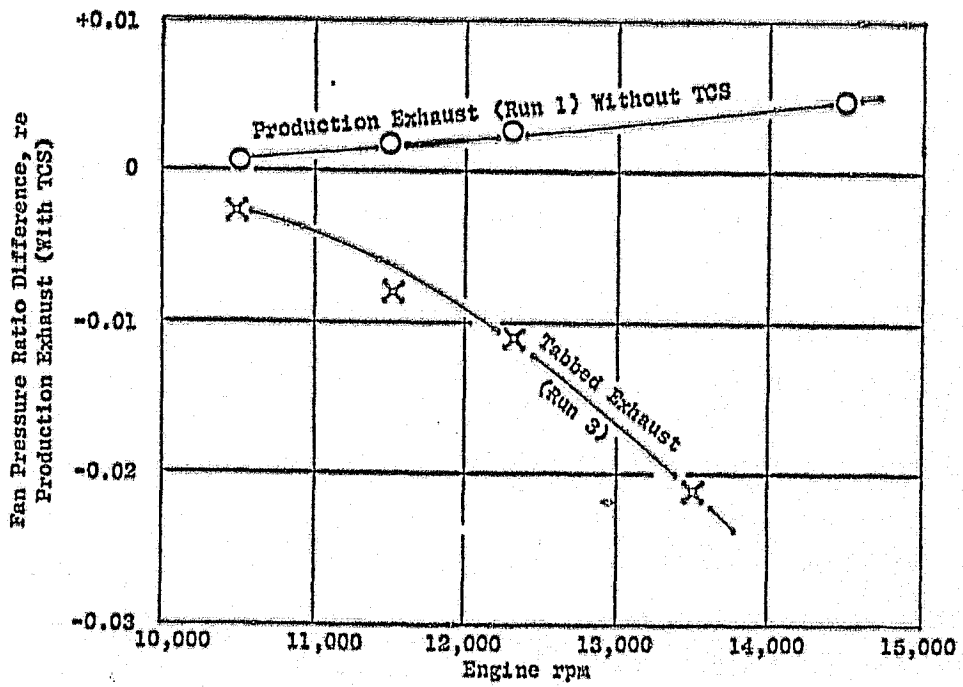

Figure 25. Pressure Ratio Differences for Production and Tabbed Exhaust Nozzles.

4.2.3 Inlet Wall Static Pressure Distribution

The inlet walls were well instrumented with static pressure taps as described in Section 3.5.4. These taps served to monitor the proper aerodynamic operation on the internal lip and in the diffusing section. Plots of the curved and canted inlet Mach number distributions for various corrected airflow conditions are presented in Figures 26 and 27. A comparison of the curved and canted inlet wall Mach number distributions versus axisymmetric projections of the Stream Tube Curvature (STC) program are is presented in Figure 28.

4.2.4 Inlet Wall Circumferential Static Pressure Distortion

The circumferential static pressure distortion (SPD) was monitored at eight equally spaced static pressure taps 6.73 cm (2.65 in.) upstream of the fan face. The static to total pressure ratio from these taps is presented in Figures 29 and 30 for the canted and curved diffusing inlet cases. A significant difference is indicated in these results; the curved inlet displayed a large reduction in circumferential distortion as anticipated. A specific comparison of the canted and curved inlets is shown in Figure 31 for a corrected engine speed of approximately 12,000 rpm; this corresponds to a fan tip speed of 336 m/s (1100 ft/s).

The results of this distortion may also be expressed in terms of a distortion parameter as shown in Figure 32. The cross-hatched areas represent the data obtained from the wind tunnel test program, while the symbols represent posttest derivations of the anticipated results using a GE three-dimensional flow computation computer code. General agreement in distortion trend with inlet configuration is shown.

4.3 TEST ENVIRONMENT INFLUENCE ON INLET ACOUSTIC CHARACTERISTICS

The environment in which an engine is tested influences the noise generation process and may affect other aspects of noise propagation and radiation processes. These influences cause differences in the measured noise and are central to the issue of what test environment can be utilized to successfully simulate flight conditions. The outdoor testing in this program utilized a turbulence control structure (TCS) which was installed to alleviate the problem of long, coherent, turbulent eddies interacting with the fan. This interaction process is attributed to the production of noise that contaminates the far-field noise measurements and renders them nonrepresentative of flight acoustic characteristics. A more detailed understanding of this interaction process was sought as a part of this program.

The simulation of a flight environment is provided by the NASA-ARC 40 x 80 wind tunnel testing. In this environment the turbulence interaction is alleviated by the tunnel's forward velocity which is believed to accurately simulate flight aerodynamics, thereby reproducing an environment conducive to obtaining flight-quality acoustic measurements. Thus, the 40 x 80 testing was performed such that selected results of these tests could be compared to those

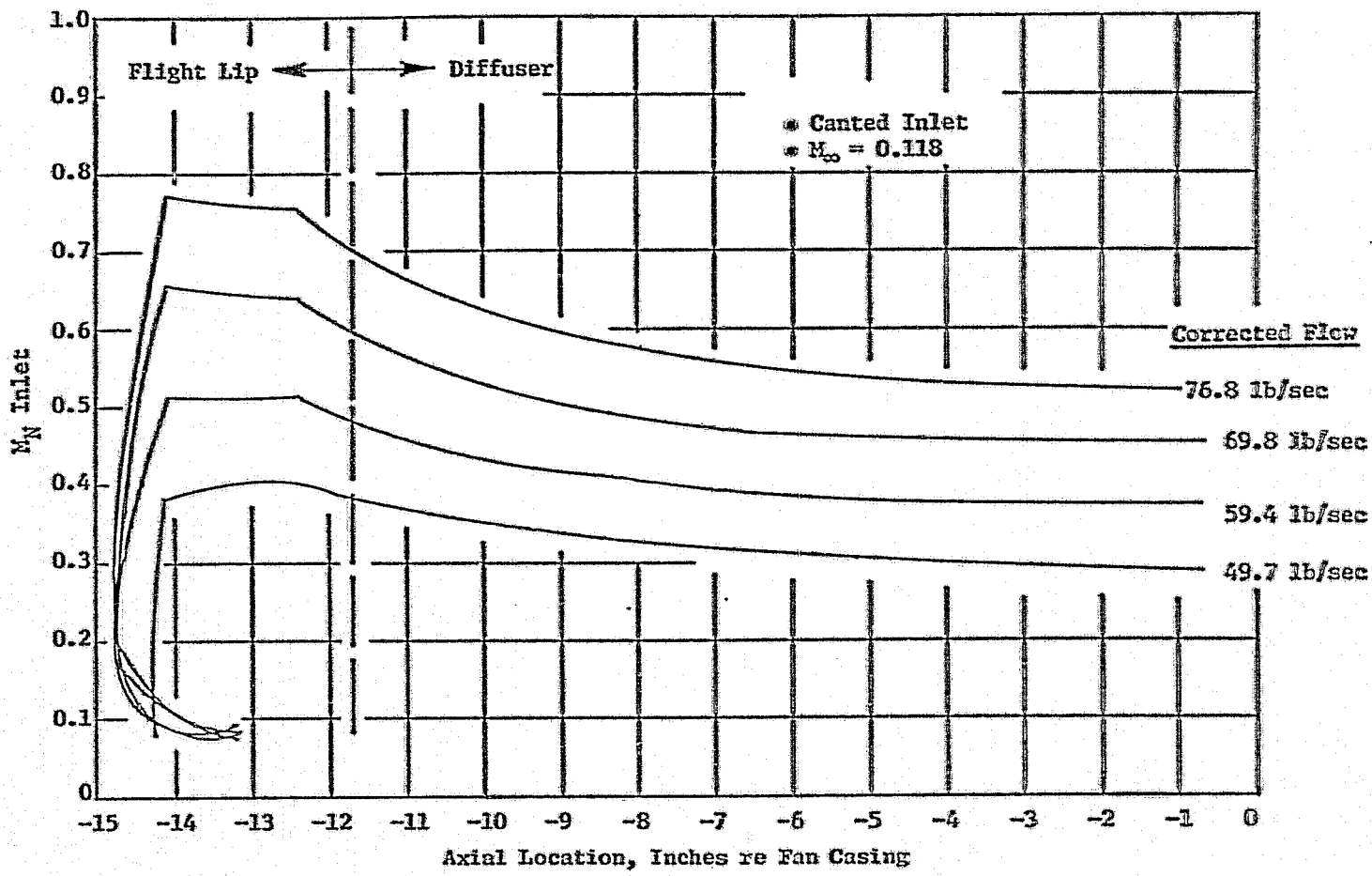

Figure 26. Comparison of Inlet Wall Mach Number Distributions.

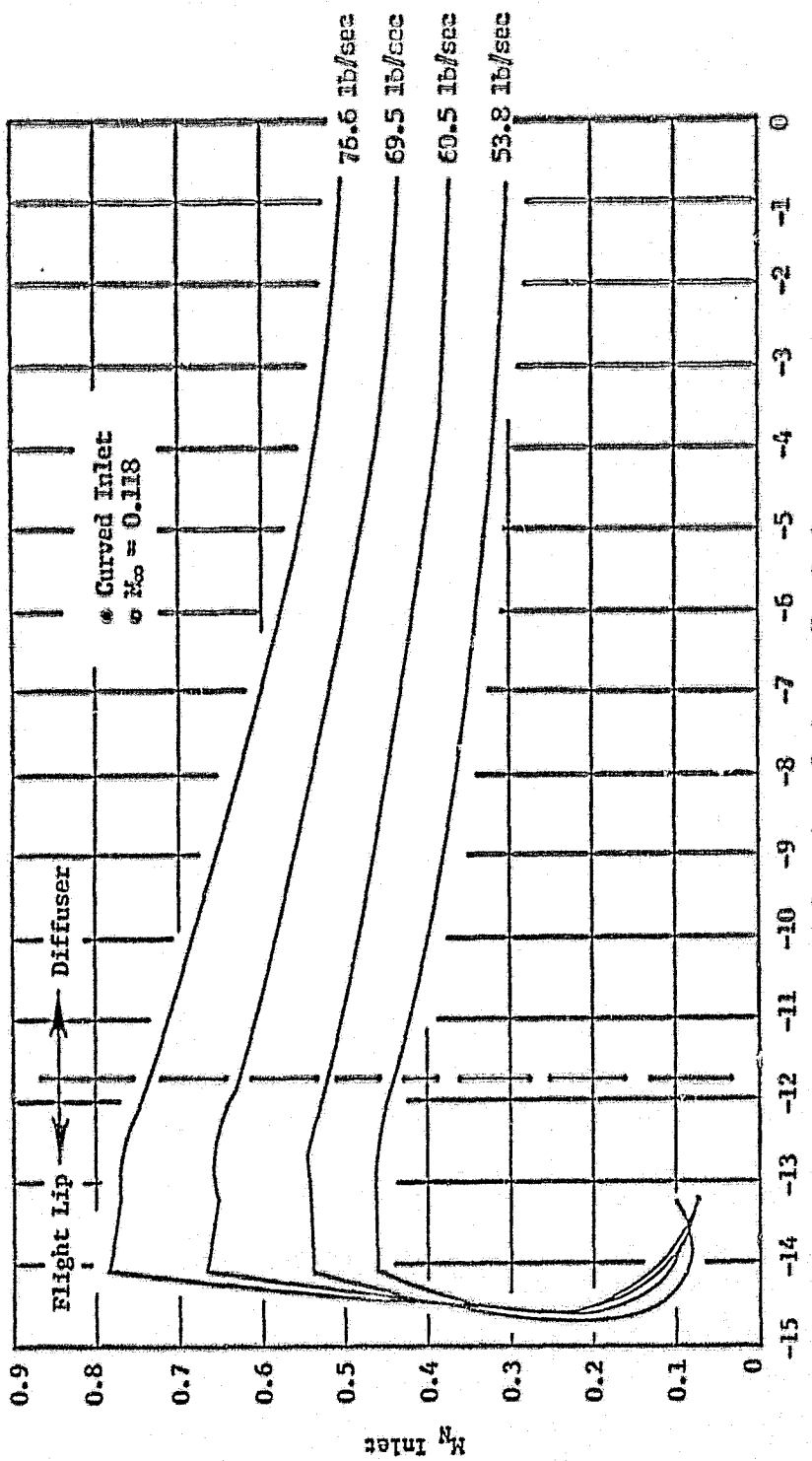

Figure 27. Curved Inlet Wall Mach Number Distributions.

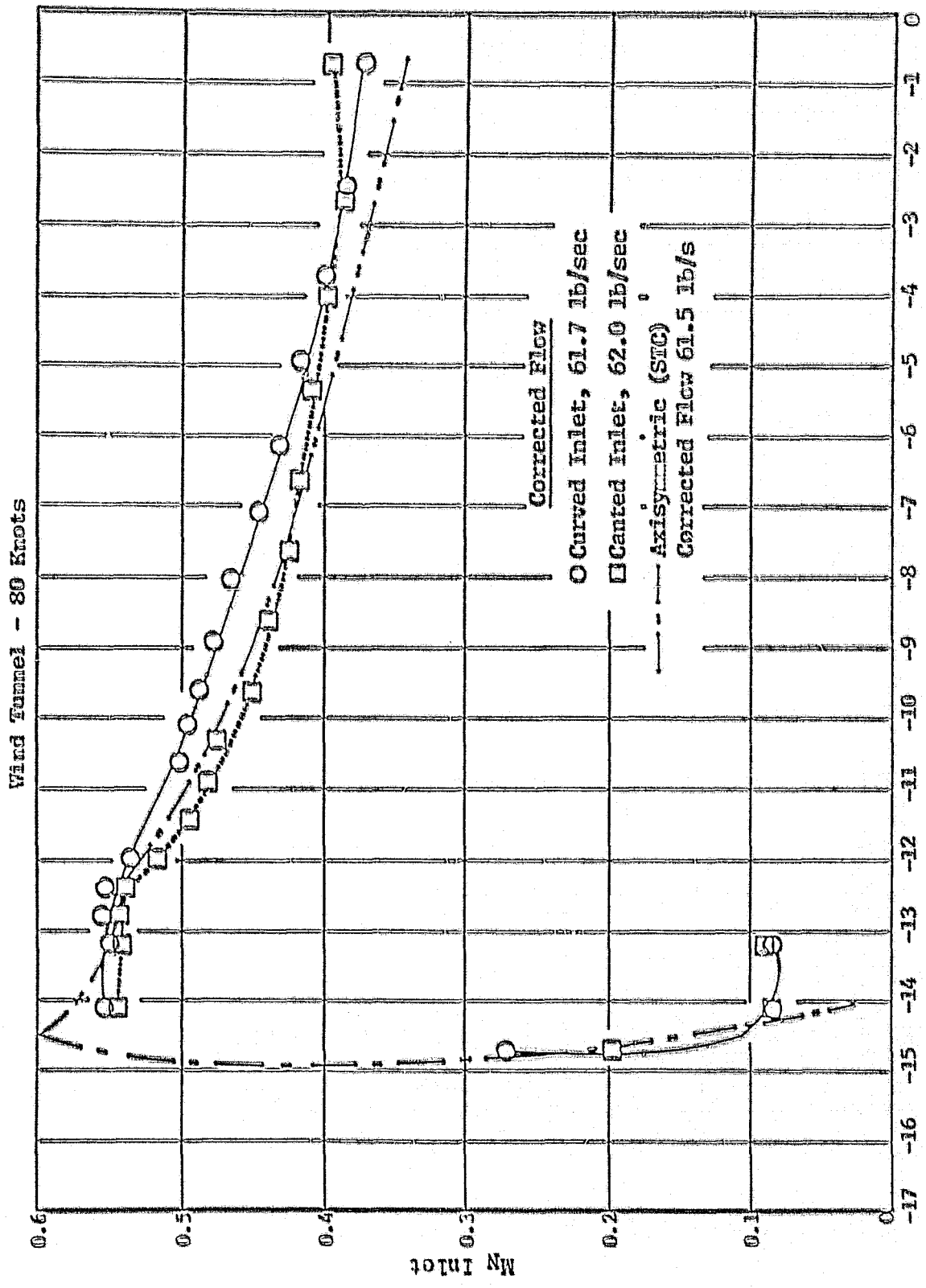

Figure 28. Comparison of Curved and Canted Inlet Wall Mach Number Distributions.

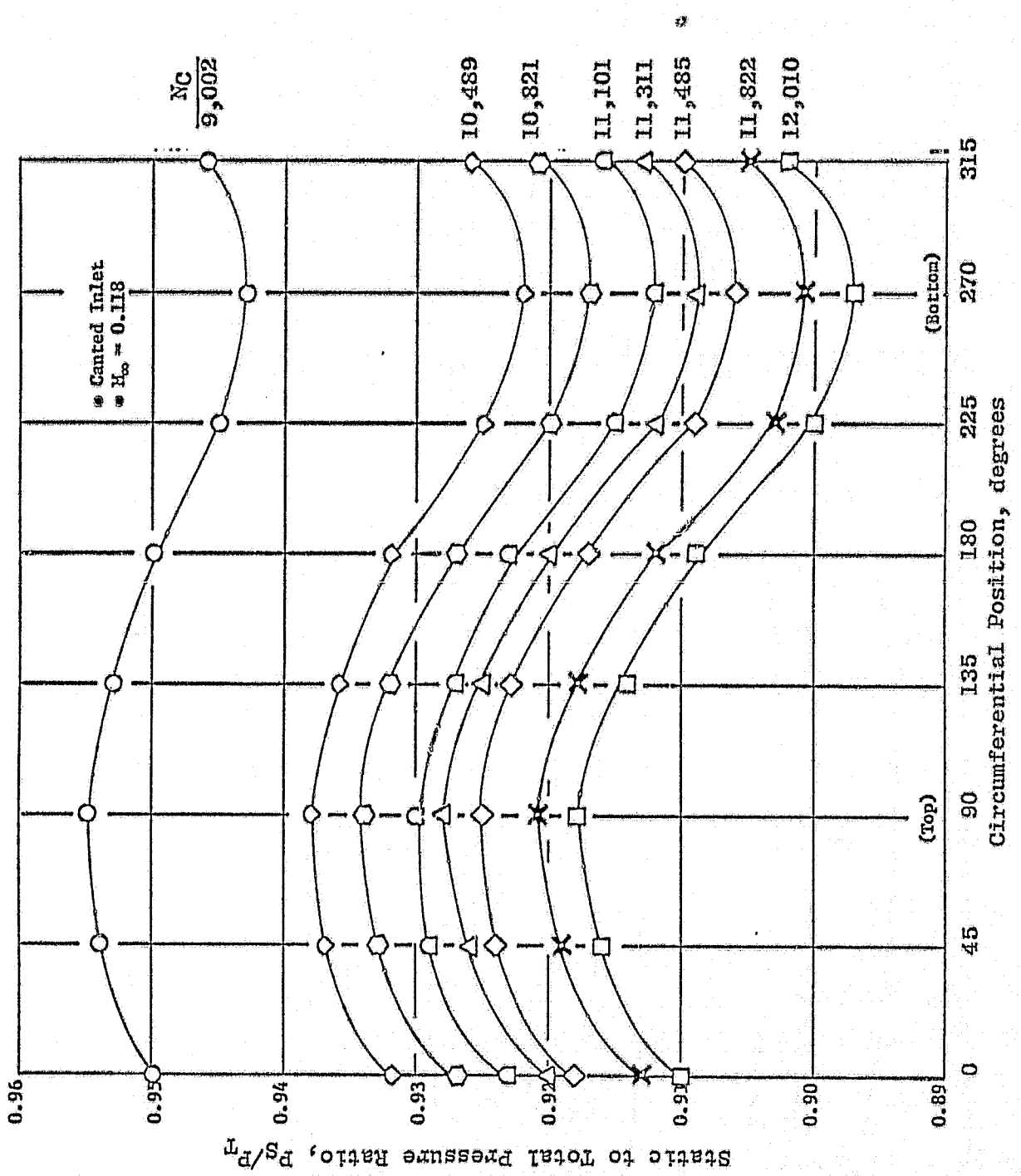

Figure 29. Canted Diffusing Inlet Circumferential Pressure Coefficient Summary.

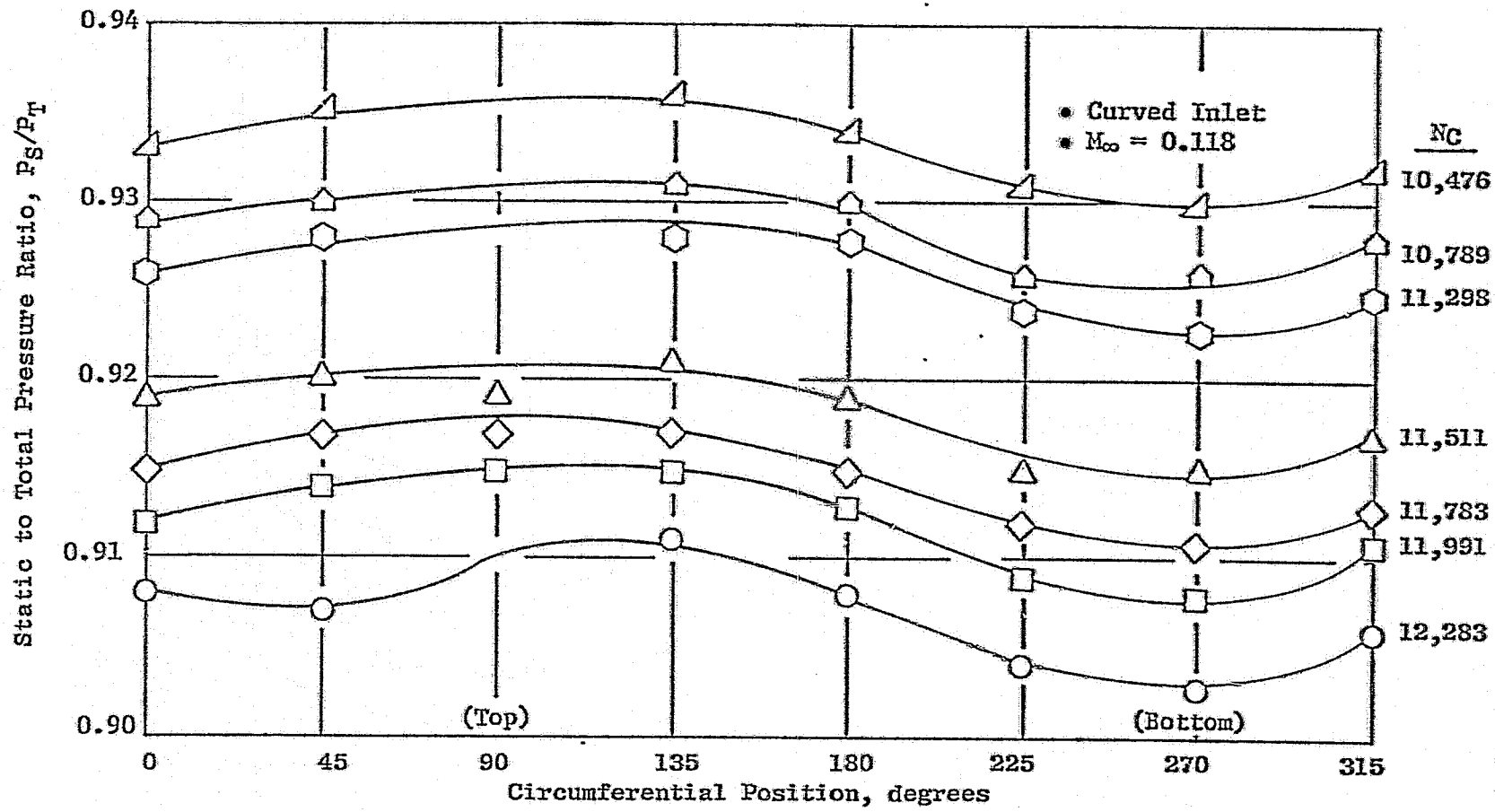

Figure 30. Curved Diffusing Inlet Circumferential Pressure Coefficient Summary.

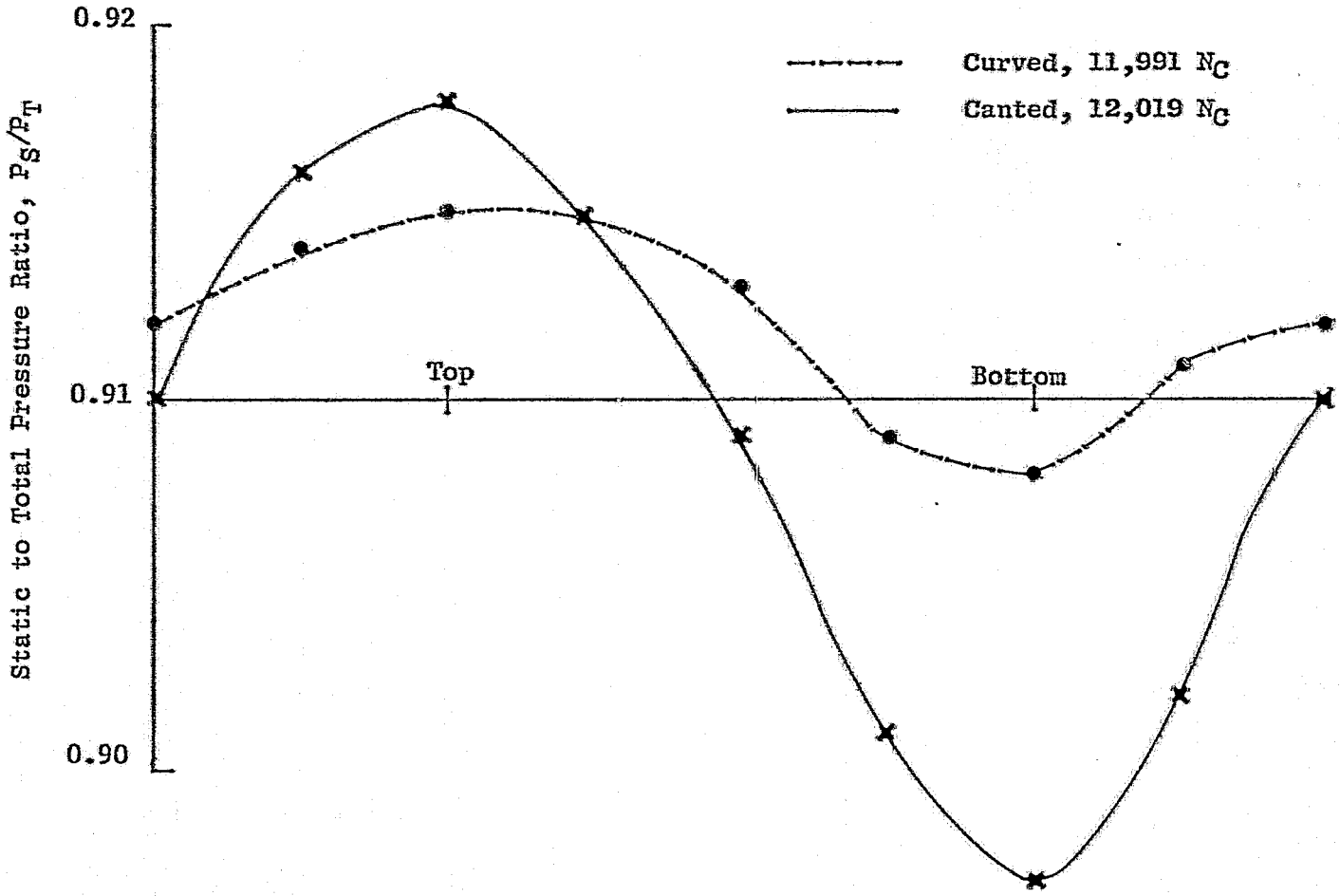

Figure 31. Comparison of Canted and Curved Inlet Circumferential Static Pressure Coefficient.

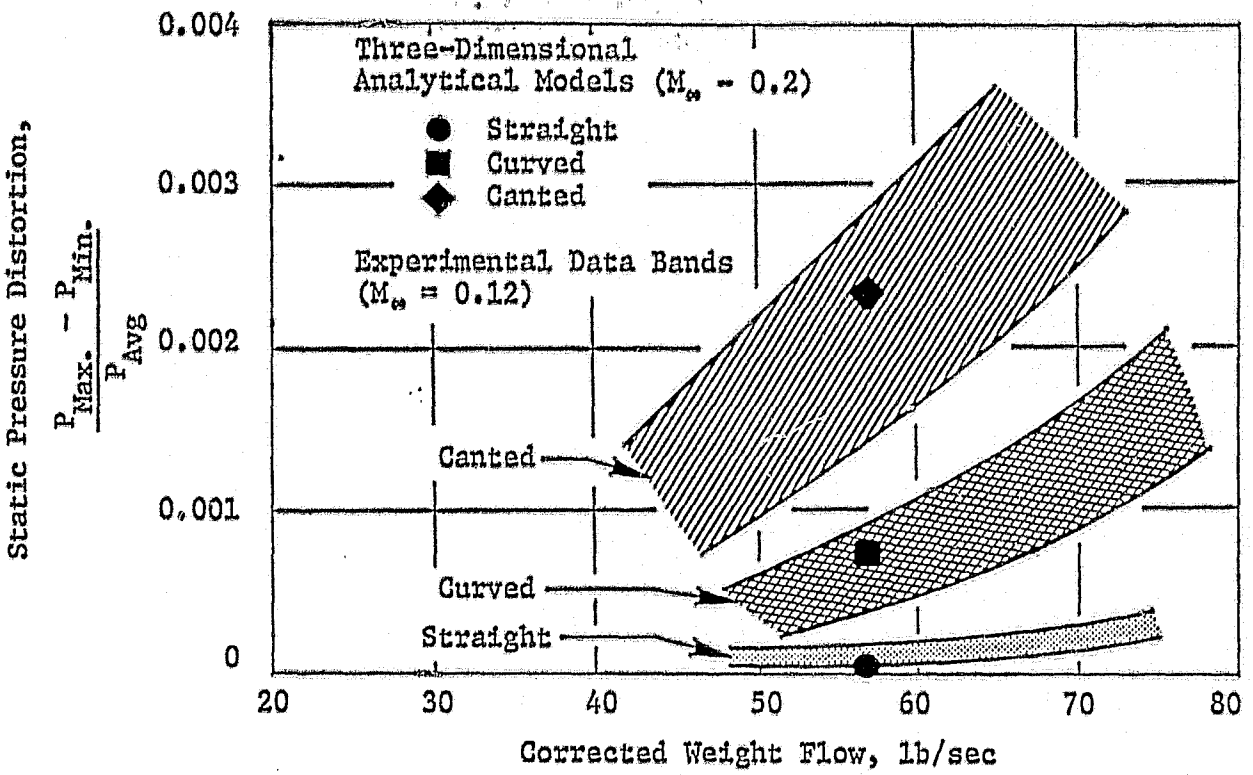

Figure 32. Static Pressure Distortion Based on the Ames Inlet Studies.

obtained statically outdoors using the TCS. This comparison forms the basis of an assessment of how well outdoor static testing with a TCS can reproduce the flight simulation of the ARC 40 x 80 wind tunnel.

4.3.1 Effects of Turbulence Control Structure on Inlet Radiated Noise

During the outdoor phase of the test program, a TCS was utilized. This device shown in Figure 16 was installed to break up elongated eddies due to random atmospheric turbulence which is stretched as it accelerates through the inlet during static testing. These eddies are believed to produce strong fan blade loading distortions which generate tonal noise.

An area of concern was the attachment of the TCS to the inlet, since the boundary layer turbulence is hypothesized to be a sensitive noise source mechanism due to its interaction with the fan blade tips. For this reason, a reverse cone was designed to aerodynamically simulate the inflow characteristics achieved in the wind tunnel with the flight lip configuration. Thus, the TCS was mated to the inlet using the reverse cone assembly shown in Figure 15. This attachment ensured the boundary layer flow would be minimally disturbed by the introduction of the TCS.

A measure of the success of the TCS in accomplishing the goals outlined is provided by comparing back-to-back runs of the same engine configuration

displayed in terms of PNL and OASPL for subsonic, transonic, and supersonic fan tip speeds in Figures 33 and 34. The scaled BPF 1/3-octave results are also presented in Figure 35.

Substantial differences are observed in the subsonic and transonic cases, with the supersonic case producing less difference in the PNL and OASPL results. The 1/3-octave results indicate the principal cause for the noise differences as the BPF tonal component. Its influence has been diminished by the installation of the TCS at the subsonic and transonic speed points.

Comparative 25 Hz bandwidth spectra are presented for three speed points at the 30°, 50°, and 70° angles in Figures 36, 37, and 38. These narrowband plots also indicate that the observed spectral differences principally occur in the tonal components, reaffirming the results of Reference 9. Using the normalized narrowband differencing procedure described in Section 4.1.4, the level differences for selected angles are noted in Figure 39. Only slight nontonal differences are observed at frequencies below 5 kHz. But when the wavelength becomes comparable to the honeycomb size of the TCS at higher frequencies, greater differences are observed. The initial suggestion is that the TCS may create a transmission loss device to these frequency components. An alternate explanation is that the turbulence spectrum is altered by the introduction of the TCS, thereby affecting the broadband noise generation process as well as the tone noise generation process.

The resolution of these differences can only be answered by detailed studies involving hot film probes in the inlet and calibrated sound-source TCS testing. However, some preliminary findings based on the use of a single-element hot film are displayed in Figure 40. This figure presents the turbulence spectrum results from a series of independent measurements performed with and without the TCS using the hot-film probe system described in Section 3.5.4. It is noted from this figure that the higher frequency broadband turbulence components are greater with TCS installed, in addition to the dramatic reduction in the tone influencing low-frequency turbulence components similar to the results of Reference 10. This finding gives credence to the suggestion that the TCS may impose a transmission loss which is further reinforced by the work reported in Reference 11. It should be noted that the hot film results are only of the axial turbulence component; the transverse turbulence components also need to be evaluated, such as in the analytical studies of Reference 12, to obtain a complete characterization of the noise generation process. Figure 41 details the large tonal differences of up to 20 dB observed in Figure 39. The results indicate the angular distribution of energy for TCS and non-TCS cases. Observing that the peak lobular locations are unaltered when using the TCS, the conclusion is reached that no significant redirection of sound energy is caused by its installation.

4.3.2 Comparison of Outdoor Static and Wind Tunnel Test Results

A direct comparison of outdoor static with TCS and wind tunnel (80 knots) tests of an equivalent engine configuration is presented using narrowband spectra at various angles. Figures 42, 43, and 44 present these comparisons

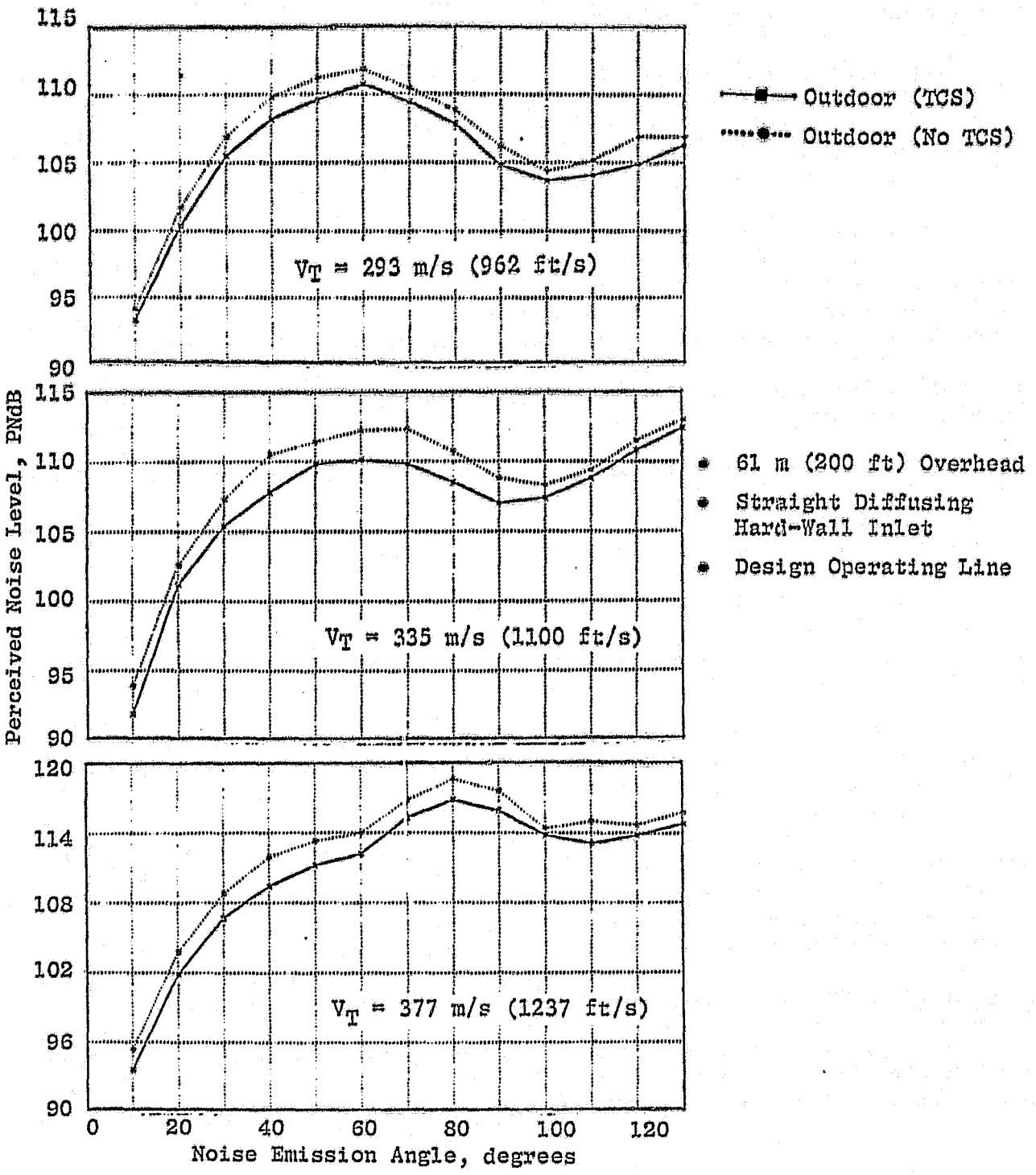

Figure 33. Scaled Perceived Noise Level Directivities for Subsonic, Transonic, and Supersonic Fan Tip Speeds.

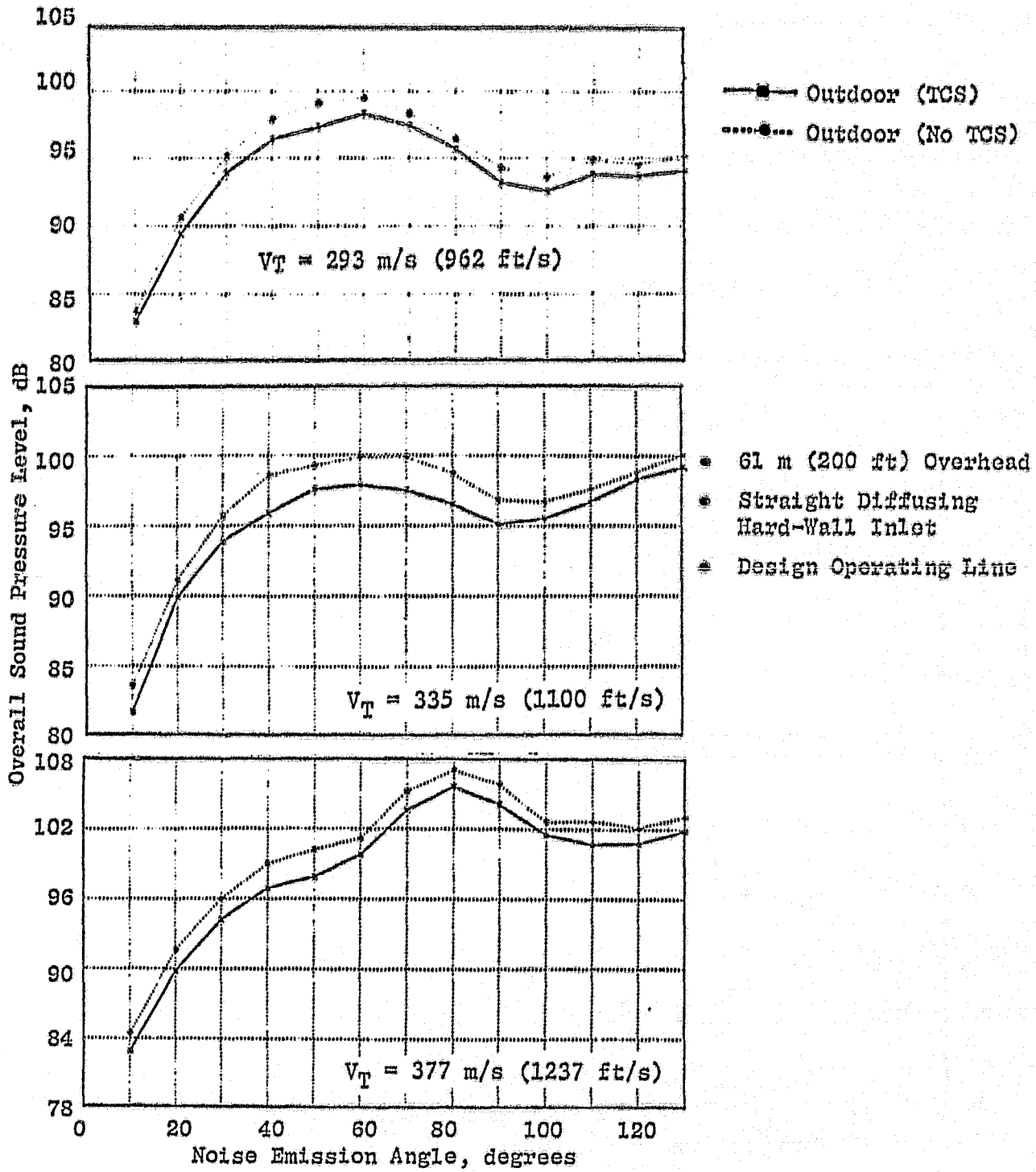

Figure 34. Scaled OASPL Directivities for Subsonic, Transonic, and Supersonic Fan Tip Speeds.

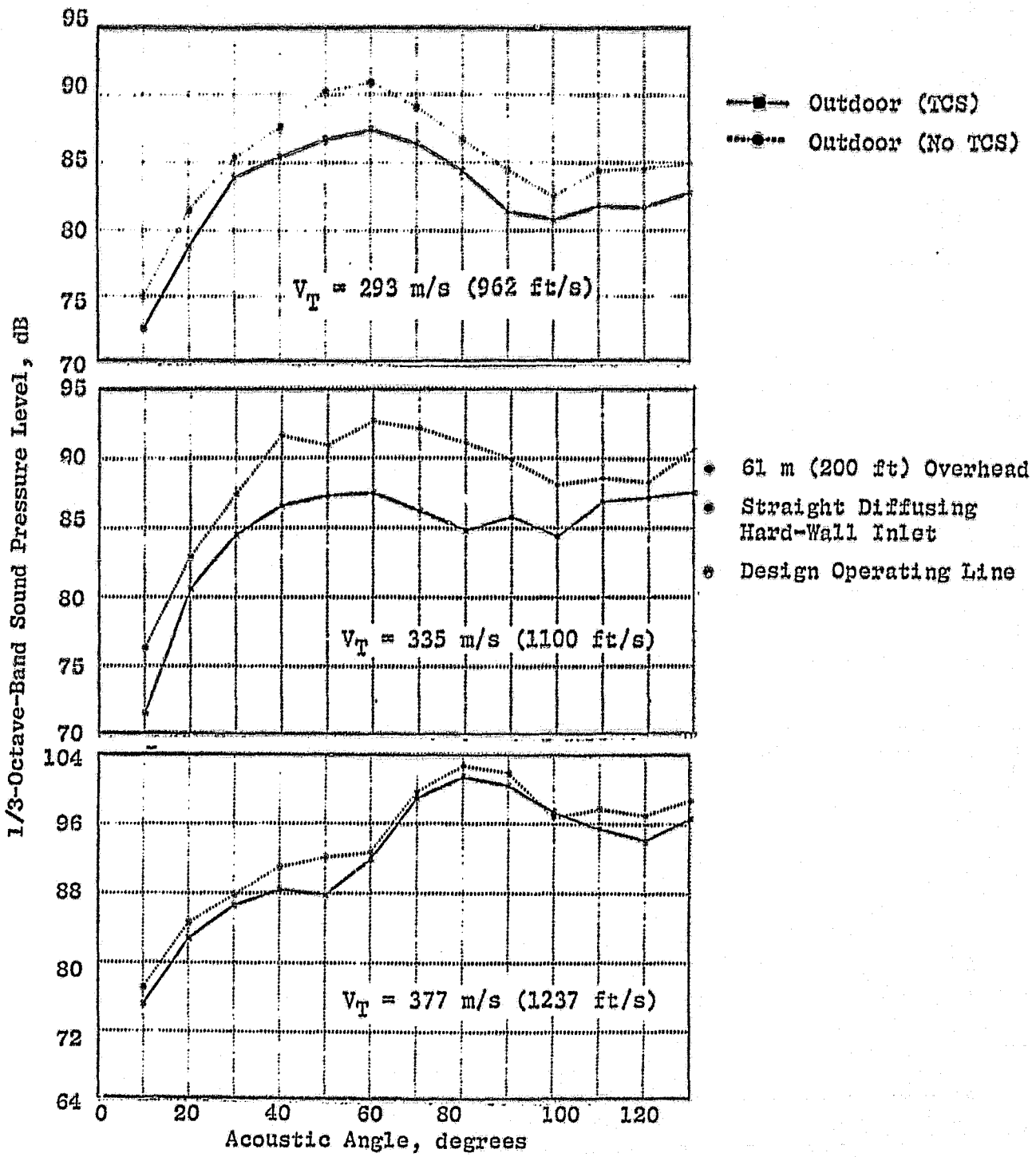

Figure 35. Scaled BPF 1/3-Octave-Band SPL for Subsonic, Transonic, and Supersonic Fan Tip Speeds.

- 30° Noise Emission Angle
- 14.5 Foot Microphone
- Straight Diffusing Hard-Wall Inlet
- V_T = 302 m/s (990 ft/s)
- Design Operating Line

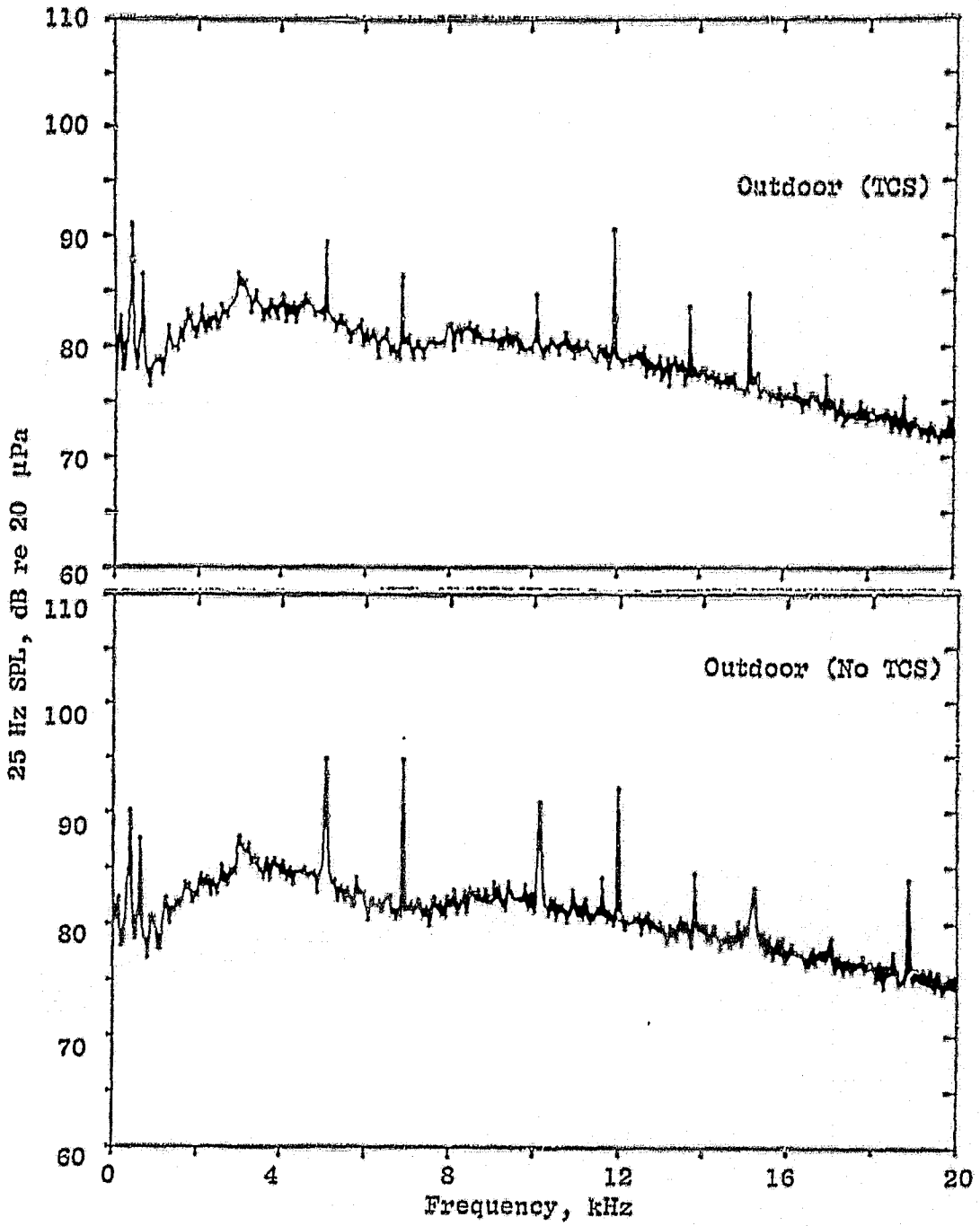

Figure 36. Comparison of No TCS/TCS Narrowband Spectra at Subsonic Tip Speed.

- 50° Noise Emission Angle
- 14.5 Foot Microphone
- Straight Diffusing Hard-Wall Inlet
- V_T = 302 m/s (990 ft/s)
- Design Operating Line

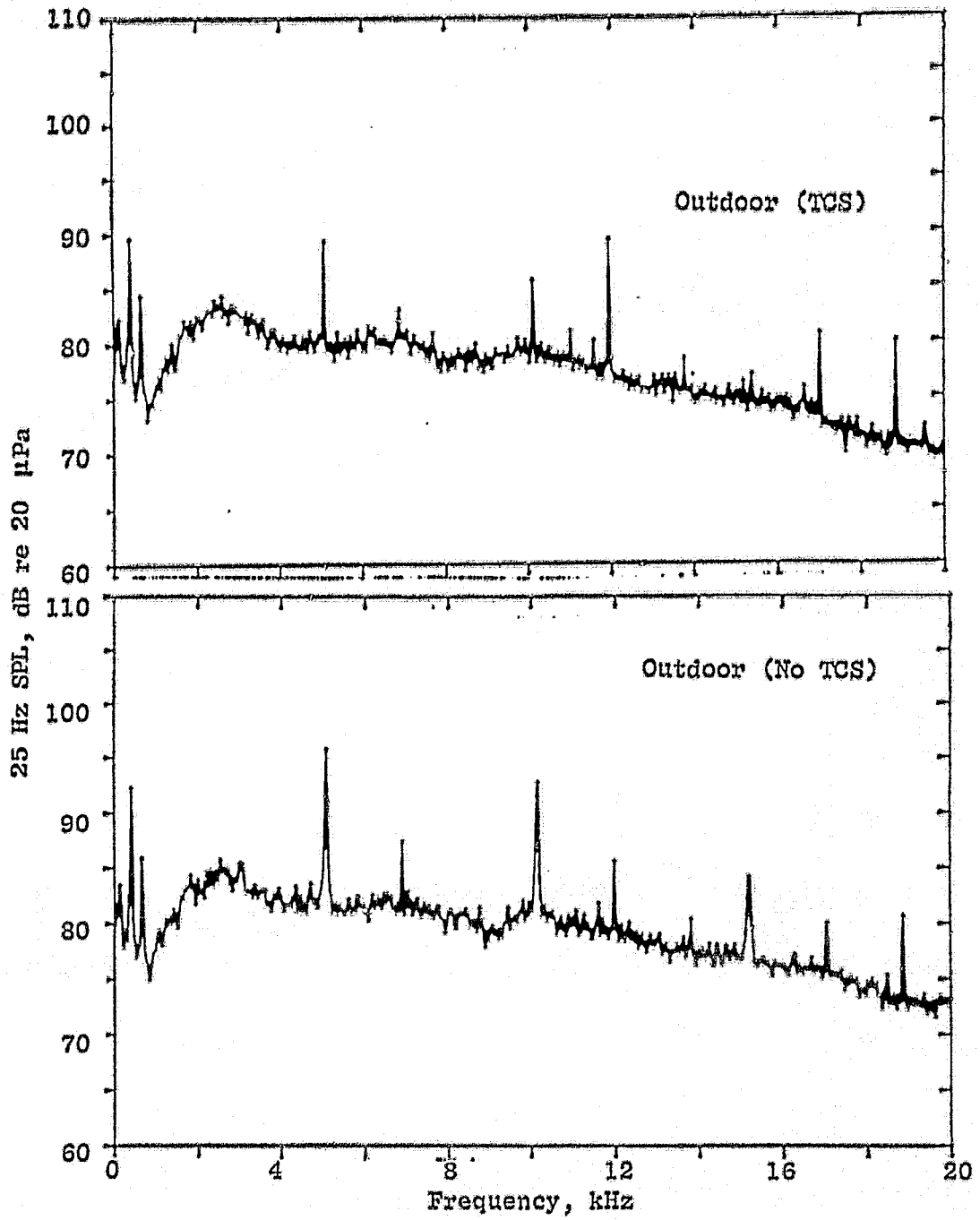

Figure 36. Comparison of No TCS/TCS Narrowband Spectra at Subsonic Tip Speed (Continued).

- 70° Noise Emission Angle
- 14.5 Foot Microphone
- Straight Diffusing Hard-Wall Inlet
- V_T = 302 m/s (990 ft/s)
- Design Operating Line

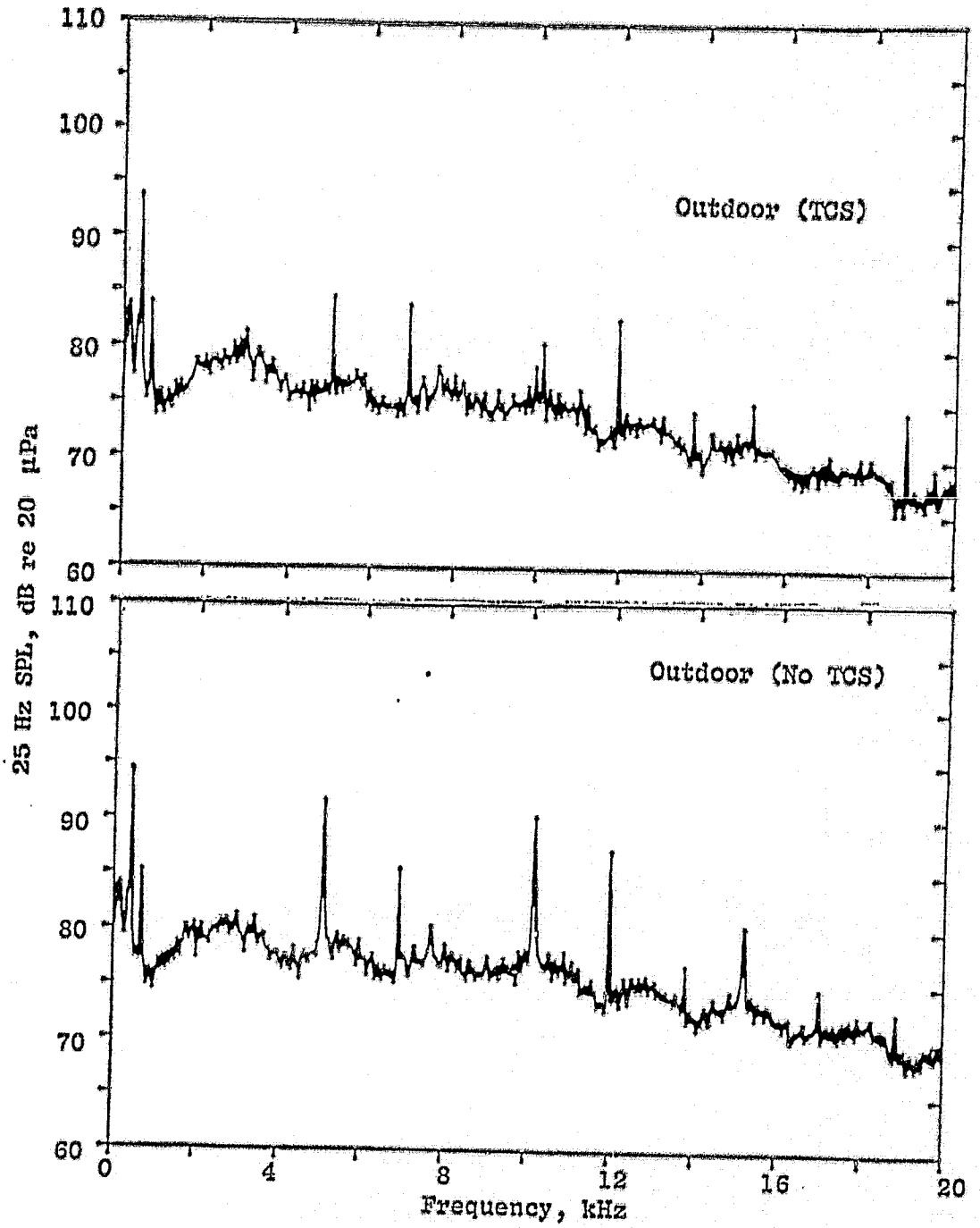

Figure 36. Comparison of No TCS/TCS Narrowband Spectra at Subsonic Tip Speed (Concluded).

- 30° Noise Emission Angle
- 14.5 Foot Microphone
- Straight Diffusing Hard-Wall Inlet
- V_T = 335 m/s (1100 ft/s)
- Design Operating Line

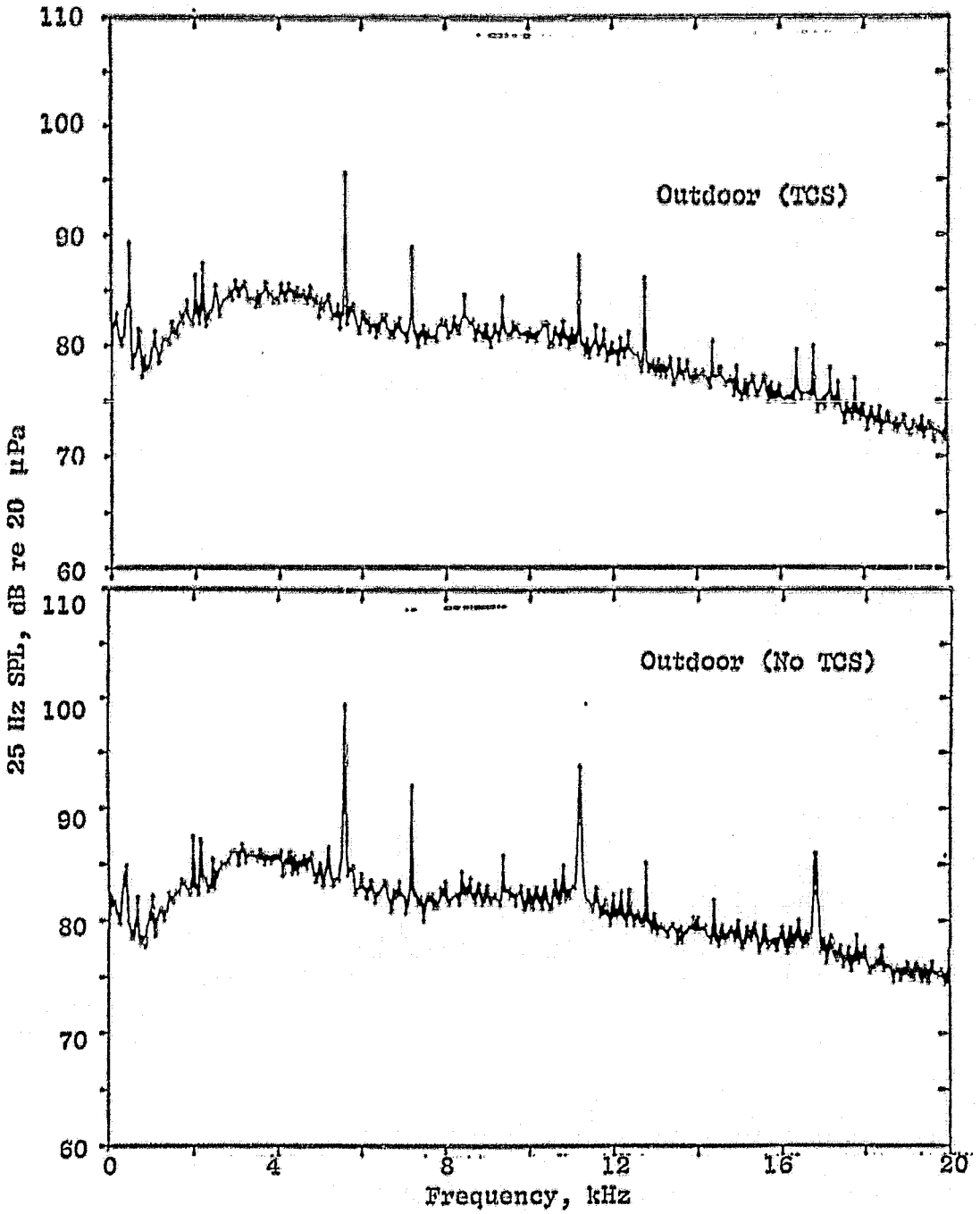

Figure 37. Comparison of No TCS/TCS Narrowband Spectra at Transonic Tip Speed.

- 50° Noise Emission Angle
- 14.5 Foot Microphone
- Straight Diffusing Hard-Wall Inlet
- V_T = 335 m/s (1100 ft/s)
- Design Operating Line

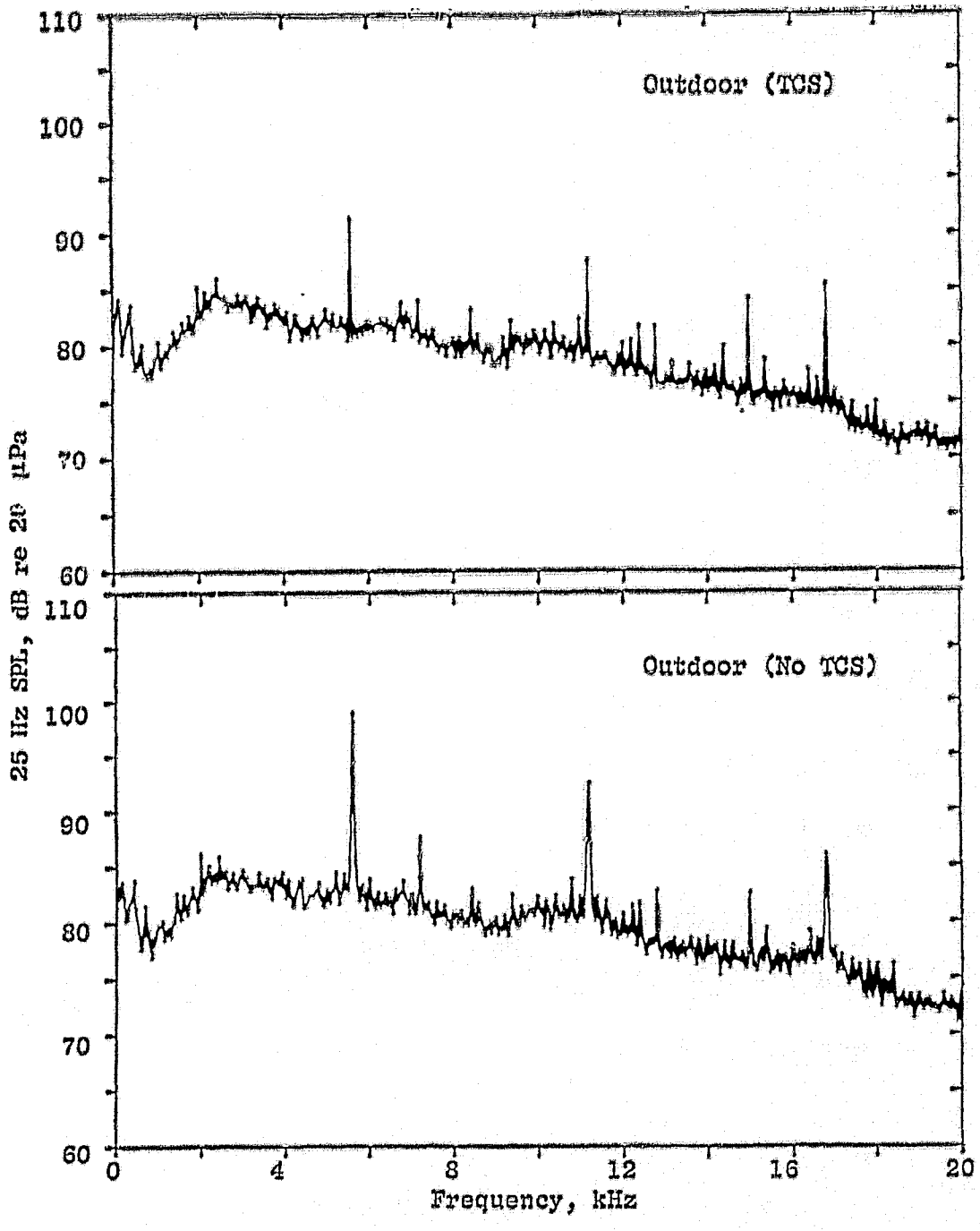

Figure 37. Comparison of No TCS/TCS Narrowband Spectra at Transonic Tip Speed (Continued).

- 70° Noise Emission Angle
- 14.5 Foot Microphone
- Straight Diffusing Hard-Wall Inlet
- V_T = 335 m/s (1100 ft/s)
- Design Operating Line

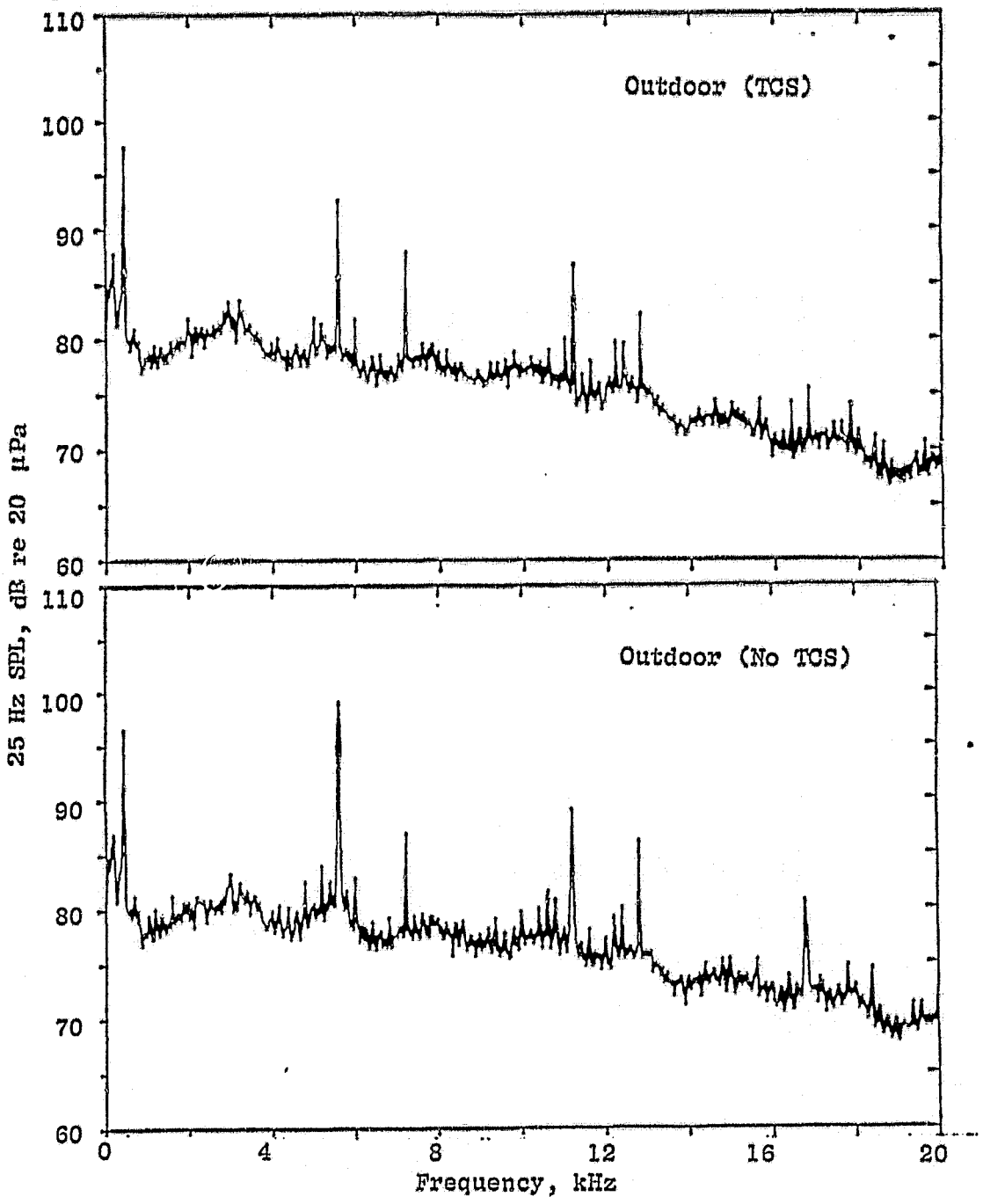

Figure 37. Comparison of No TCS/TCS Narrowband Spectra at Transonic Transonic Tip Speed (Concluded).

- 30° Noise Emission Angle
- 14.5 Foot Microphone
- Straight Diffusing Hard-Wall Inlet
- V_T = 377 m/s (1237 ft/s)
- Design Operating Line

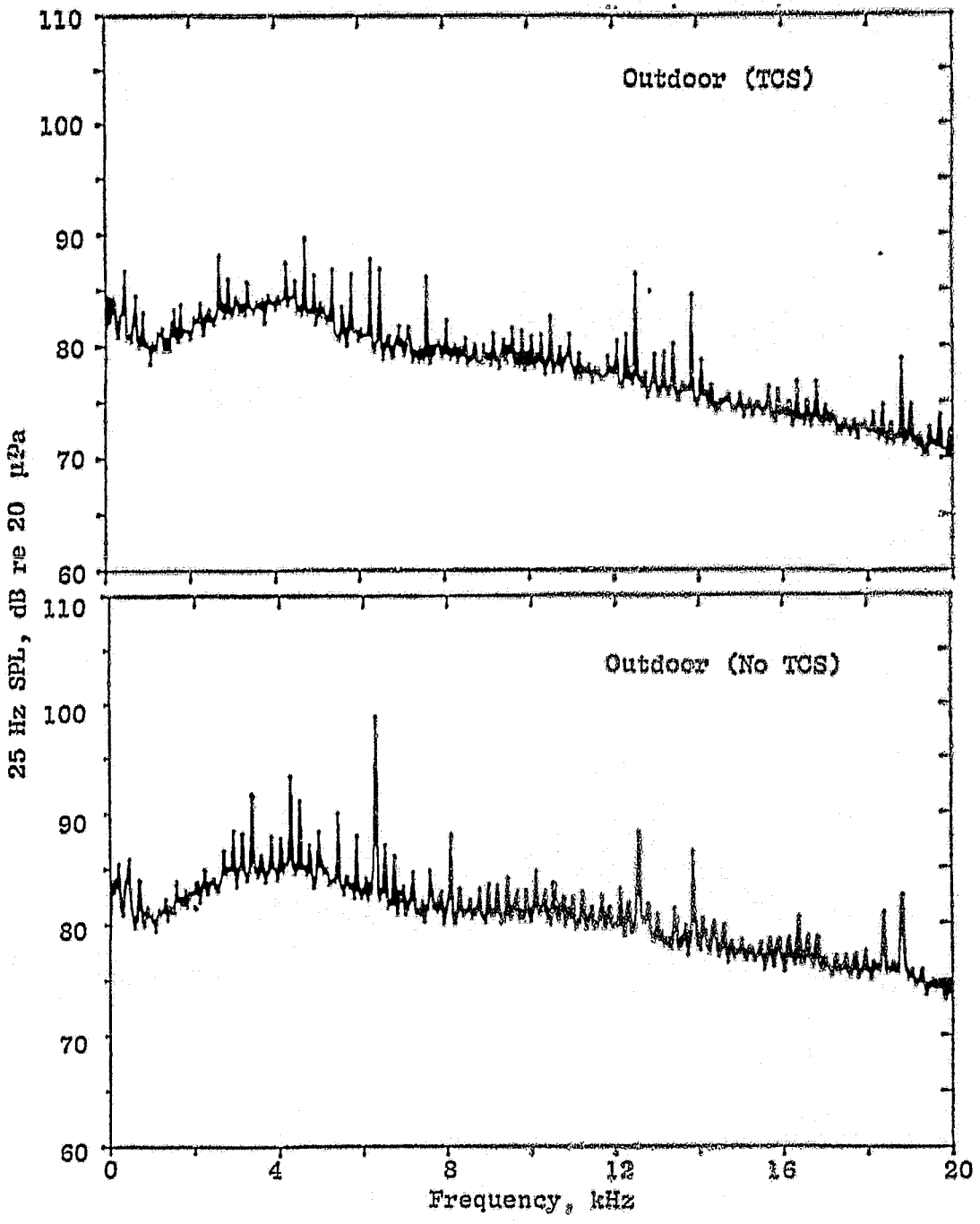

Figure 38. Comparison of No TCS/TCS Narrowband Spectra at Supersonic Tip Speed.

- 50° Noise Emission Angle
- 14.5 Foot Microphone
- Straight Diffusing Hard-Wall Inlet
- V_T = 377 m/s (1237 ft/s)
- Design Operating Line

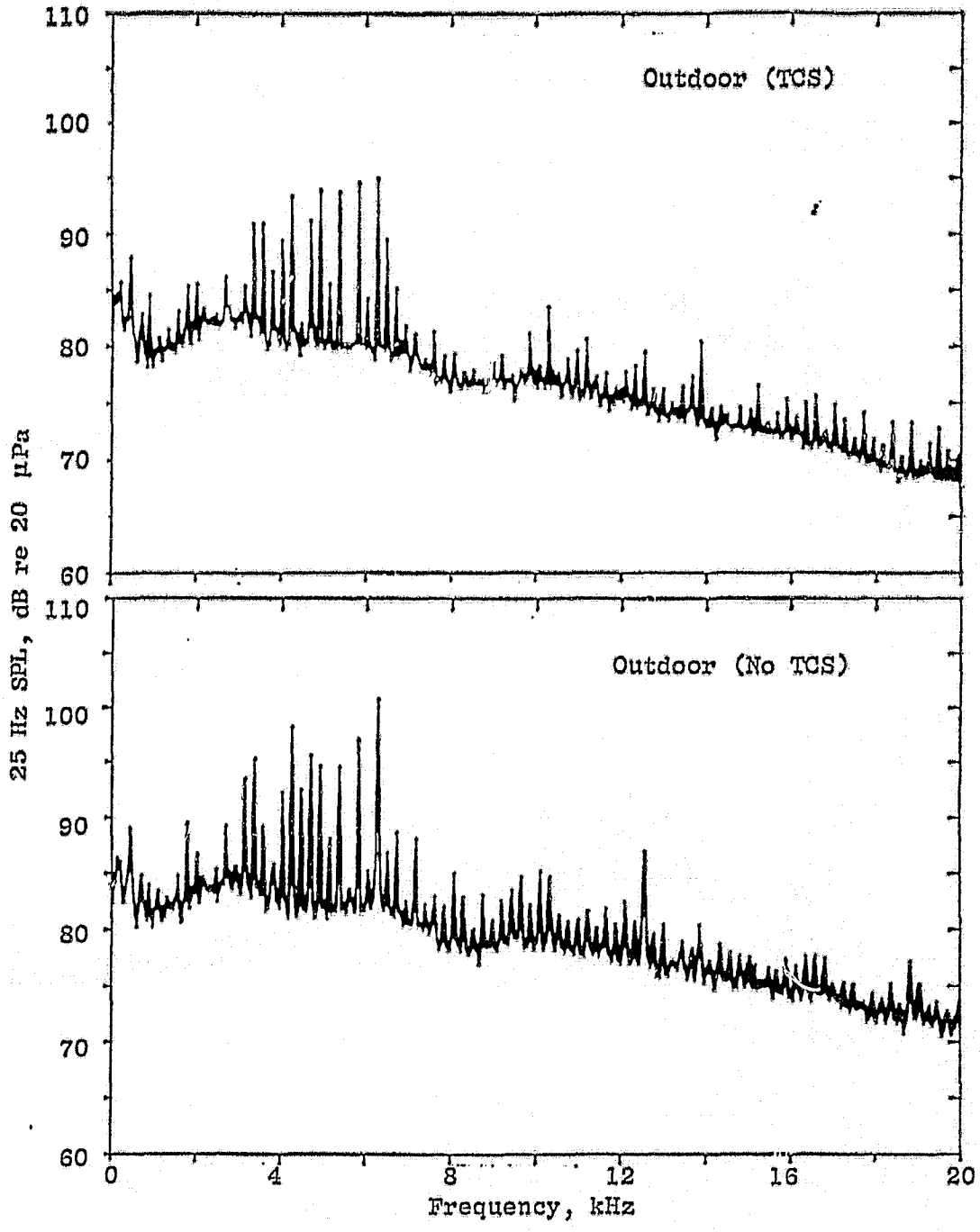

Figure 38. Comparison of No TCS/TCS Narrowband Spectra at Supersonic Tip Speed (Continued).

- 70° Noise Emission Angle
- 14.5 Foot Microphone
- Straight Diffusing Hard-Wall Inlet
- V_T = 377 m/s (1237 ft/s)
- Design Operating Line

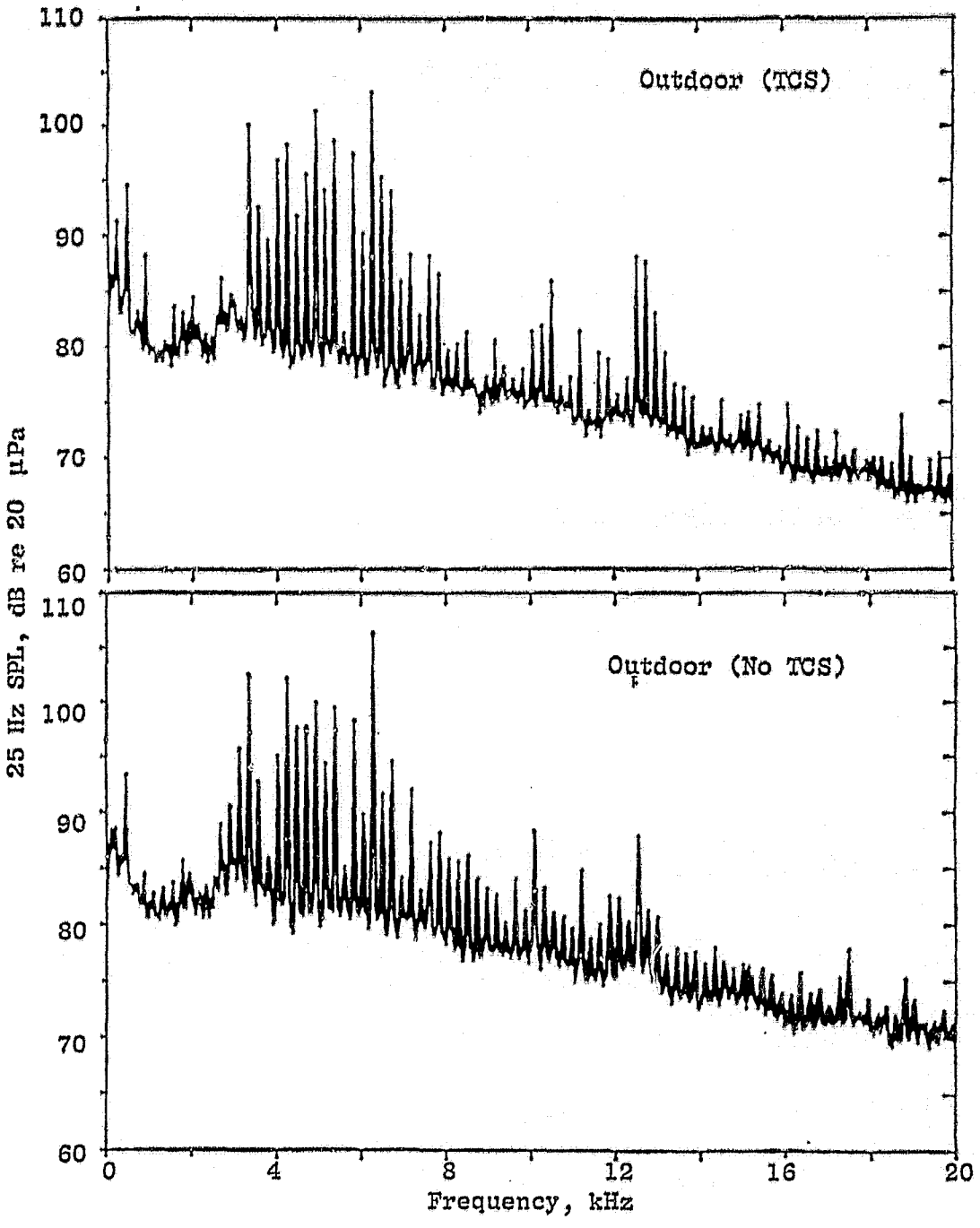

Figure 38. Comparison of No TCS/TCS Narrowband Spectra at Supersonic Tip Speed (Concluded).

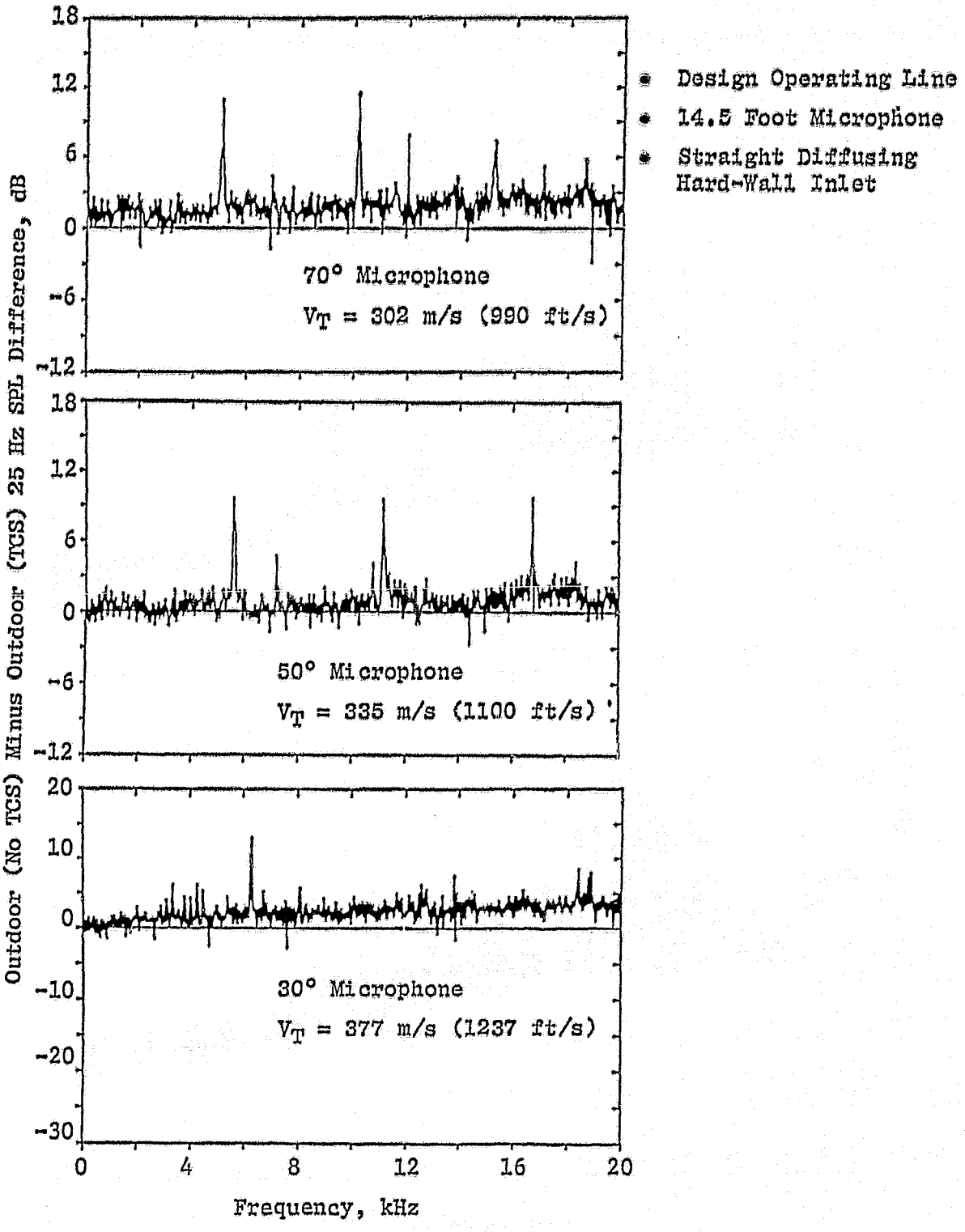

Figure 39. Comparison of Spectral Differences Between Outdoor TCS and No TCS Configurations.

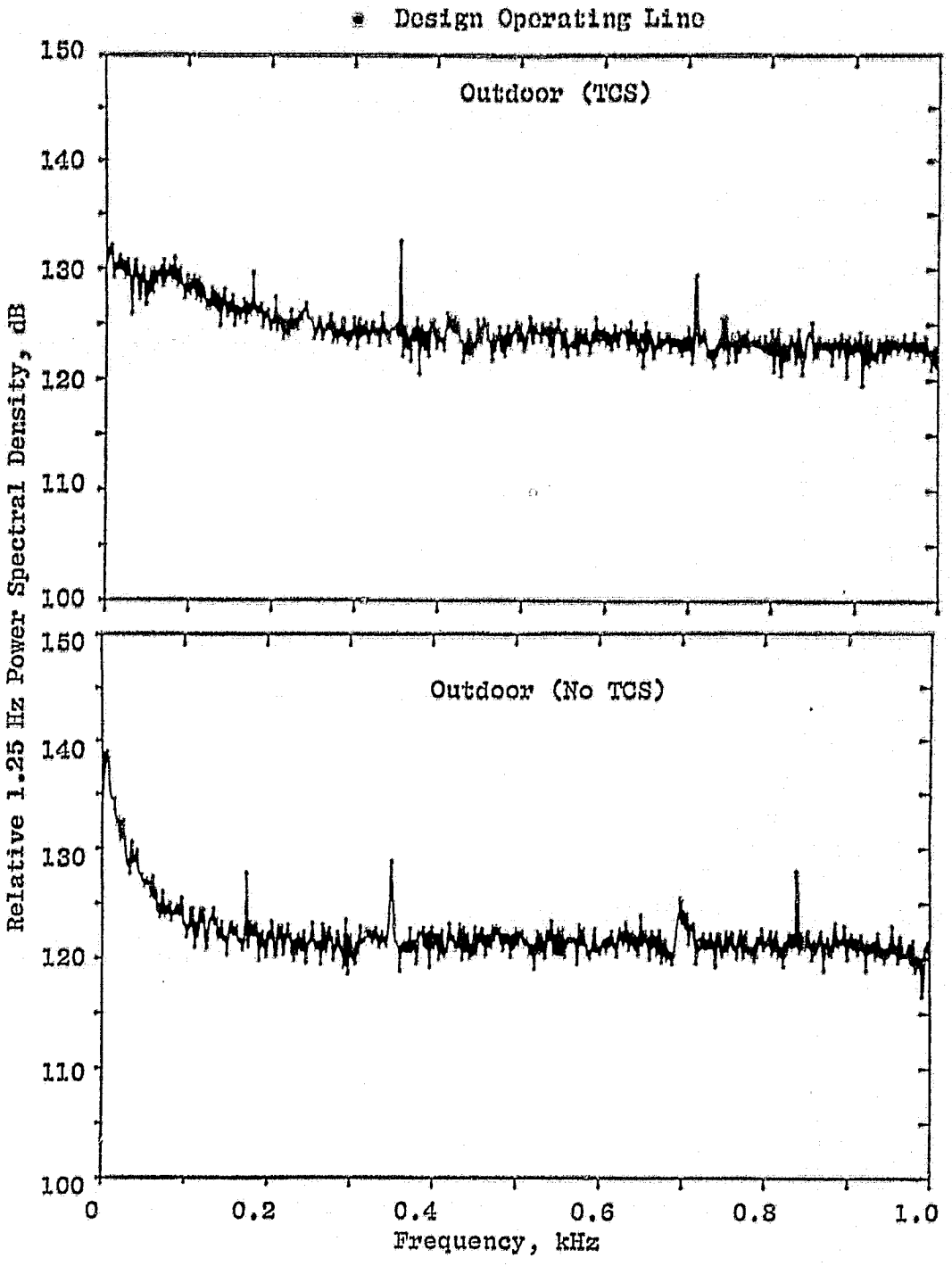

a. Subsonic Tip Speed, 223 m/s (962 ft/s)

Figure 40. Comparative Turbulence Spectra for TCS and No TCS Tests.

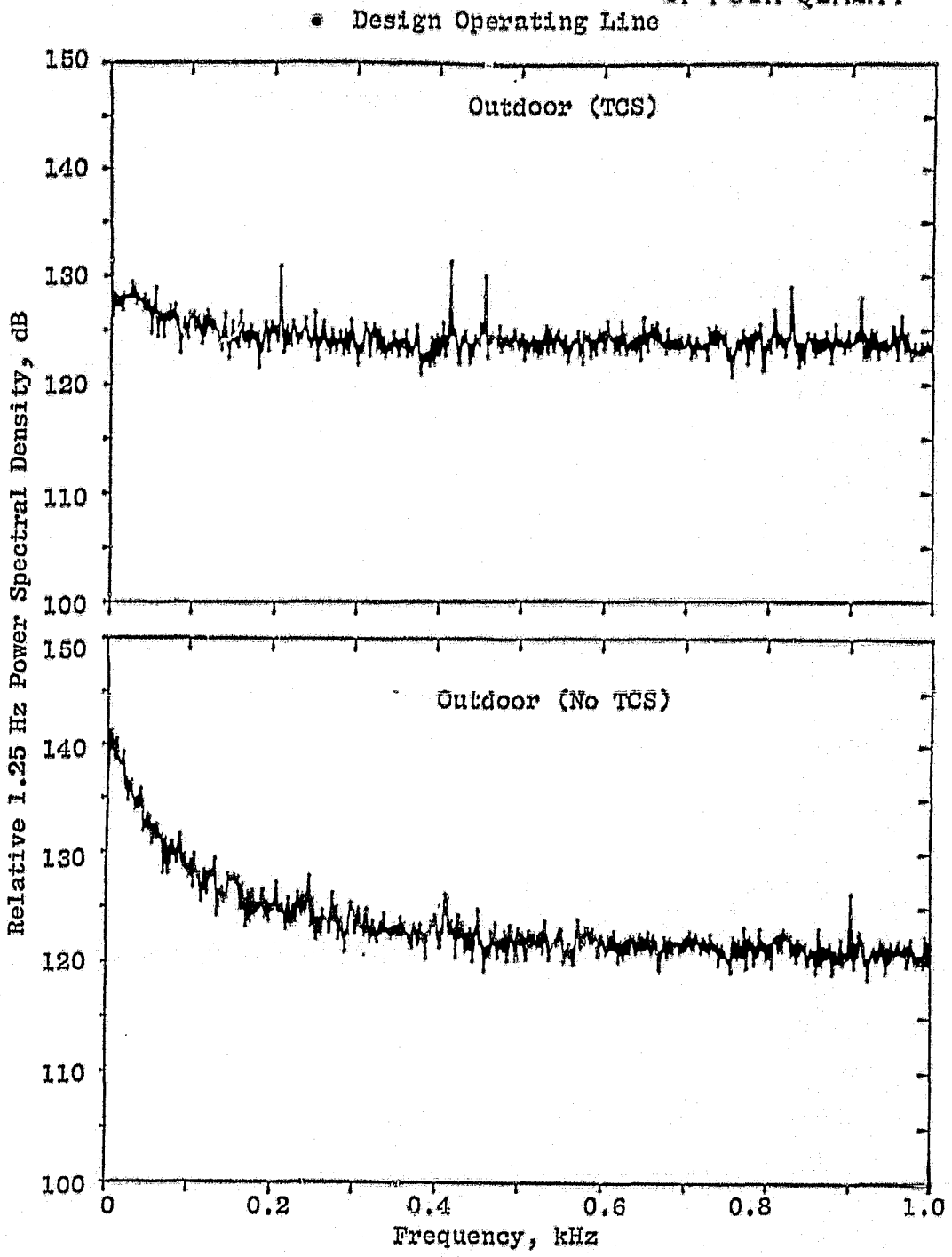

b. Transonic Tip Speed, 344 m/s (1127 ft/s)

Figure 40. Comparative Turbulence Spectra for TCS and No TCS Tests (Continued).

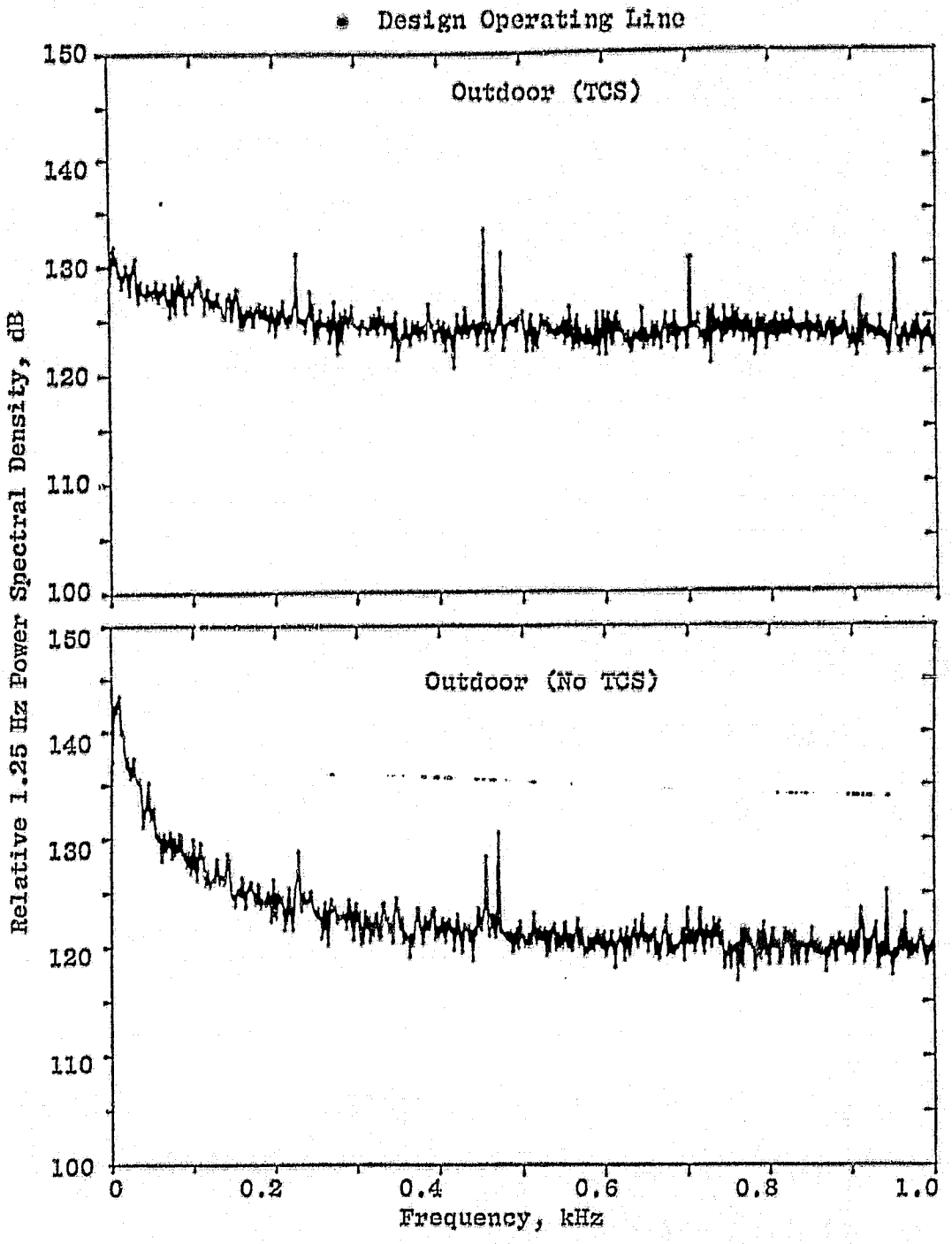

c. Supersonic Tip Speed, 377 m/s (1237 ft/s)

Figure 40. Comparative Turbulence Spectra for TCS and No TCS Tests (Concluded).

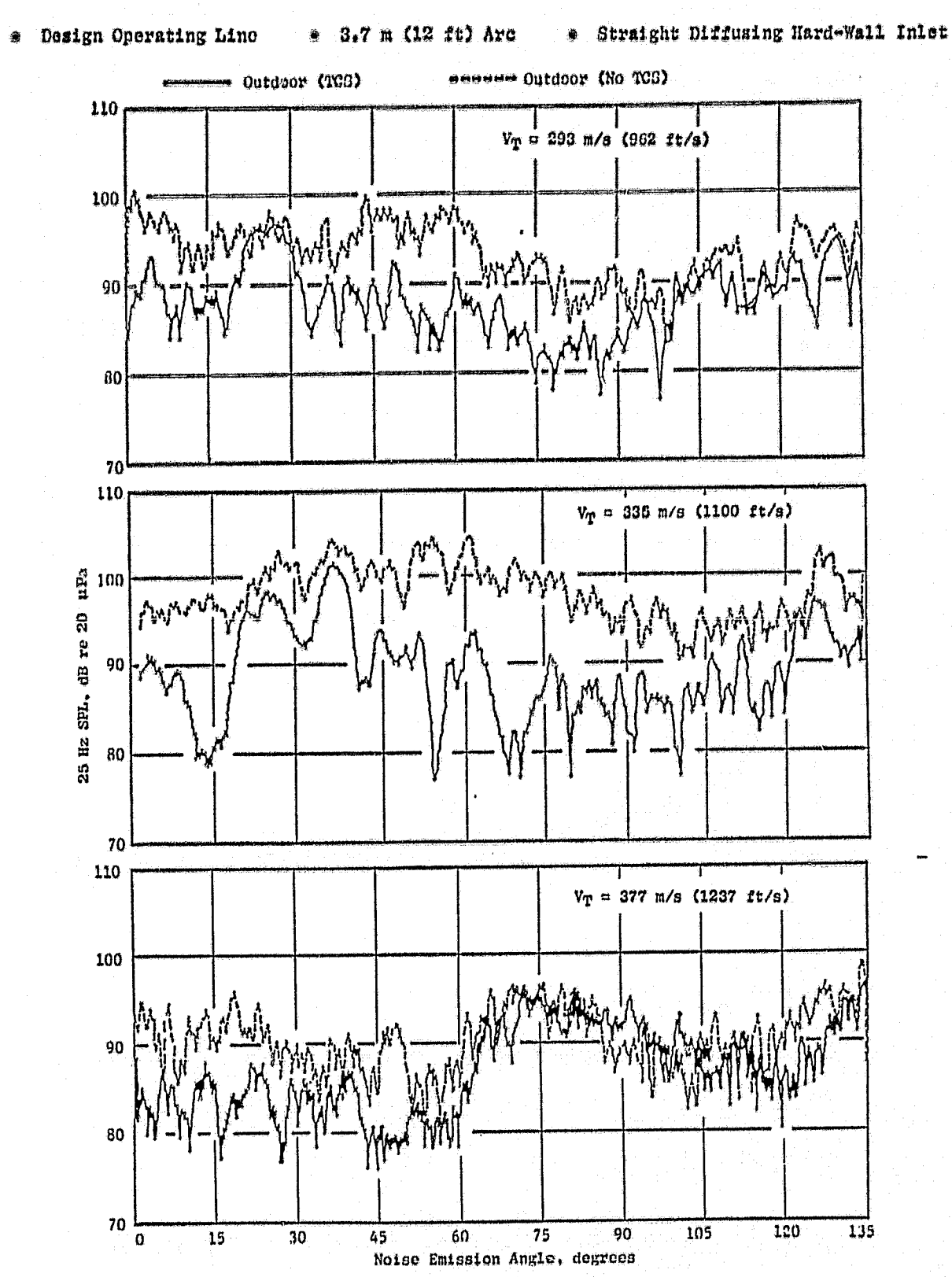

Figure 41. Comparison of TCS and No TCS BPF Directivities.

- 30° Noise Emission Angle
- 14.5 Foot Microphone
- Straight Diffusing Hard-Wall Inlet
- V_T = 302 m/s (990 ft/s)
- Lower Operating Line

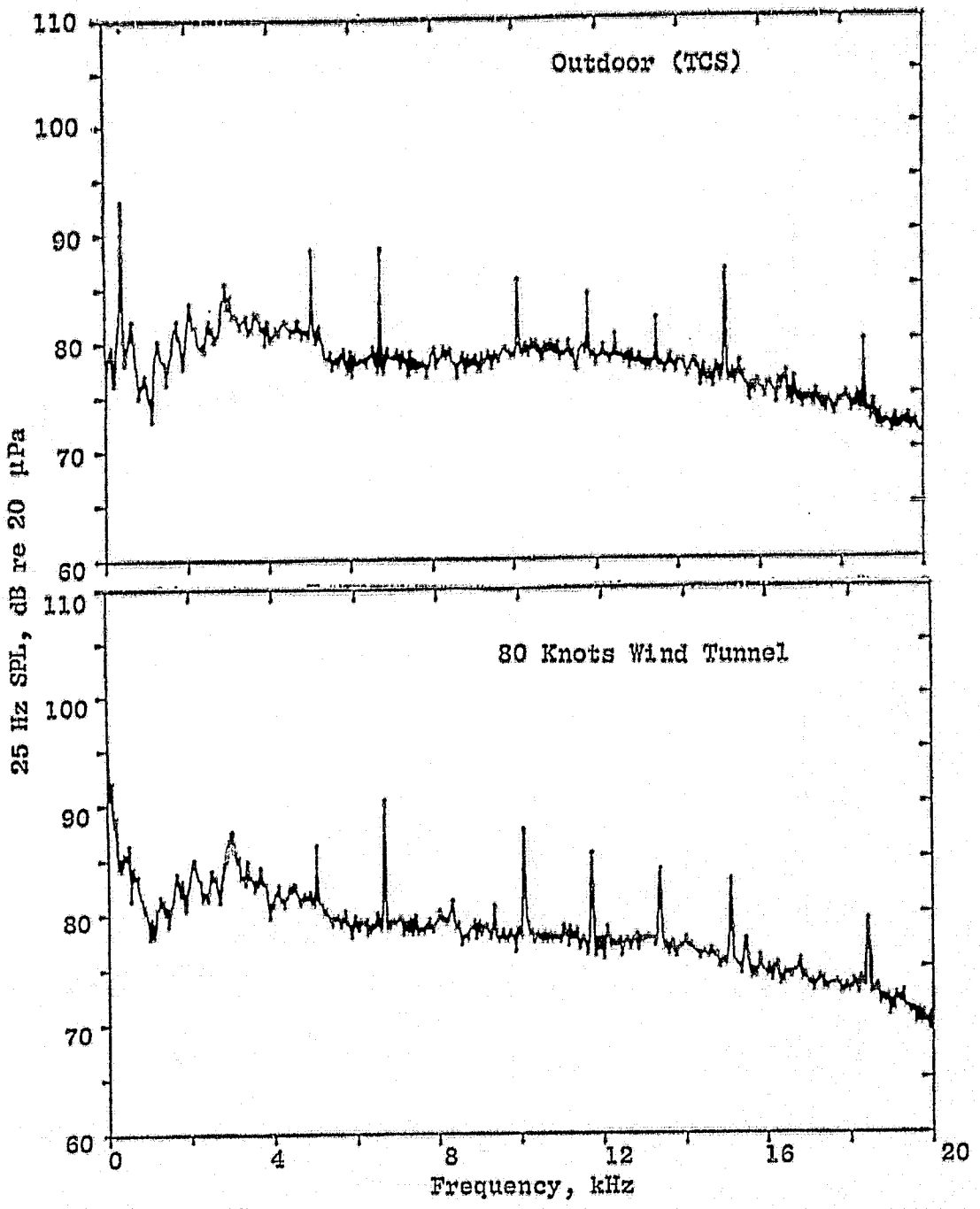

Figure 42. Comparison of Wind Tunnel and Outdoor with TCS Narrowband Spectra at Subsonic Tip Speed.

- 50° Noise Emission Angle
- 14.5 Foot Microphone
- Straight Diffusing Hard-Wall Inlet
- V_T = 302 m/s (990 ft/s)
- Lower Operating Line

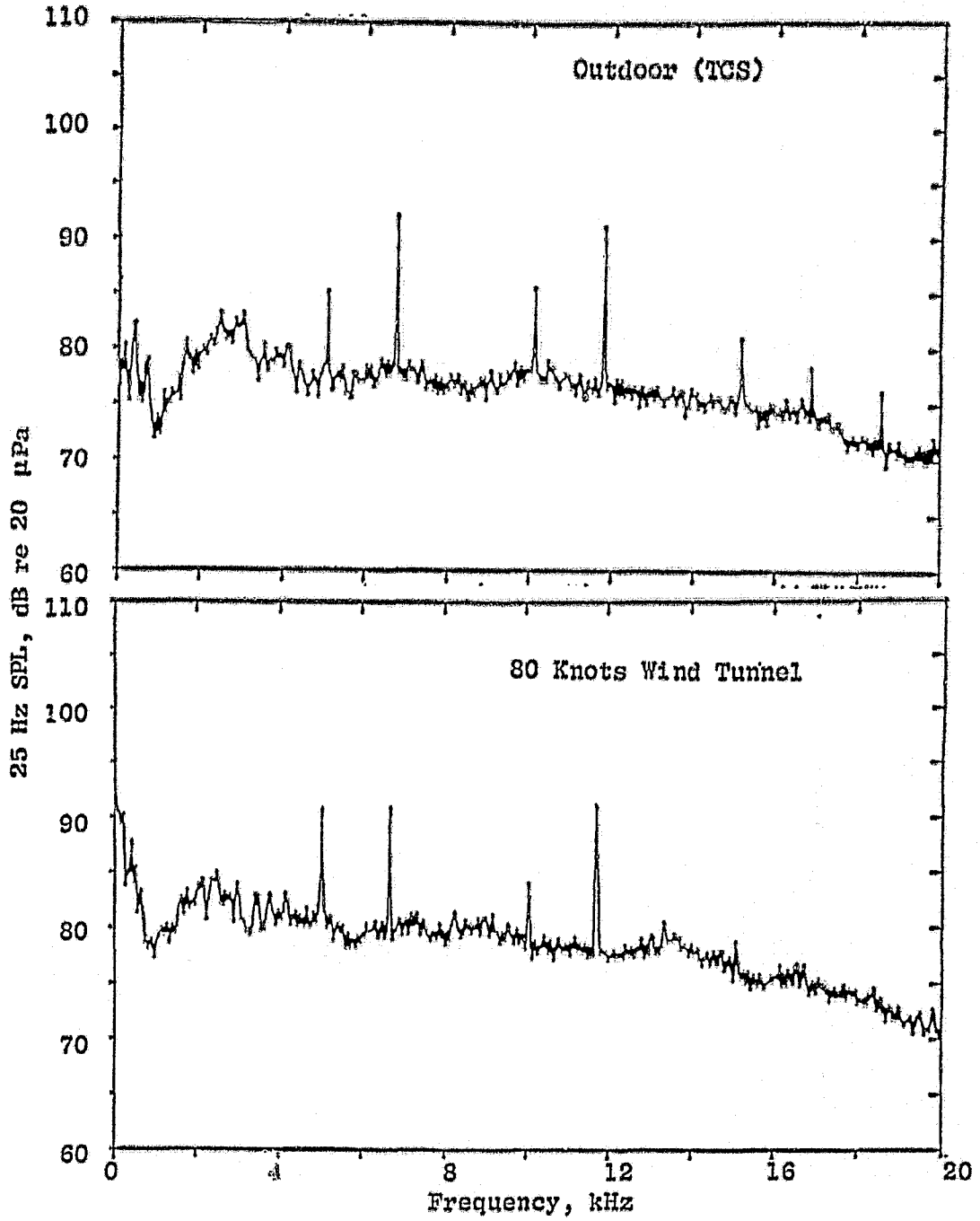

Figure 42. Comparison of Wind Tunnel and Outdoor with TCS Narrow-Band Spectra at Subsonic Tip Speed (Continued).

- 70° Noise Emission Angle
- 14.5 Foot Microphone
- Straight Diffusing Hard-Wall Inlet
- V_T = 302 m/s (990 ft/s)
- Lower Operating Line

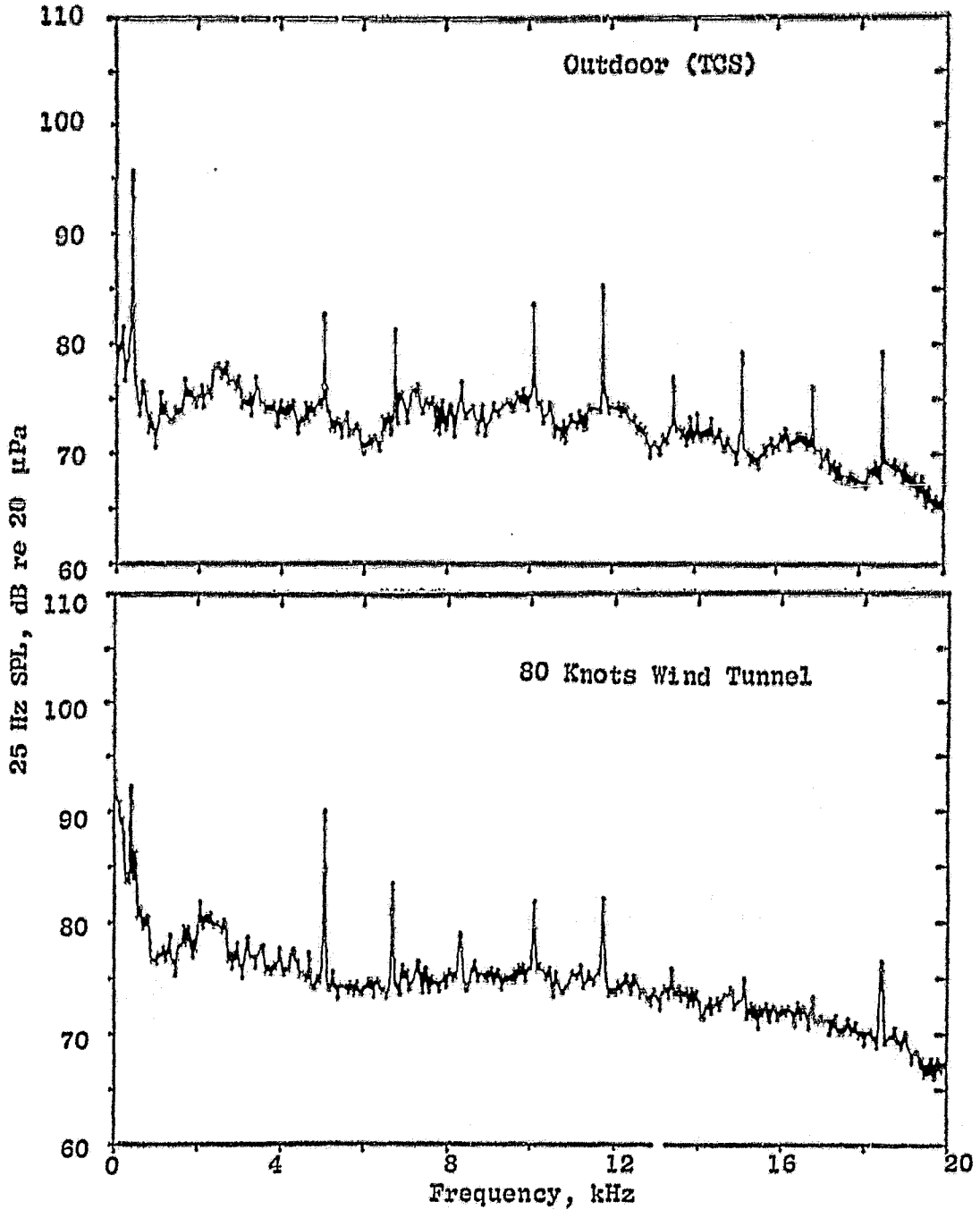

Figure 42. Comparison of Wind Tunnel and Outdoor with TCS Narrow-Band Spectra at Subsonic Tip Speed (Concluded).

- 30° Noise Emission Angle
- 14.5 Foot Microphone
- Straight Diffusing Hard-Wall Inlet
- V_T = 335 m/s (1100 ft/s)
- Lower Operating Line

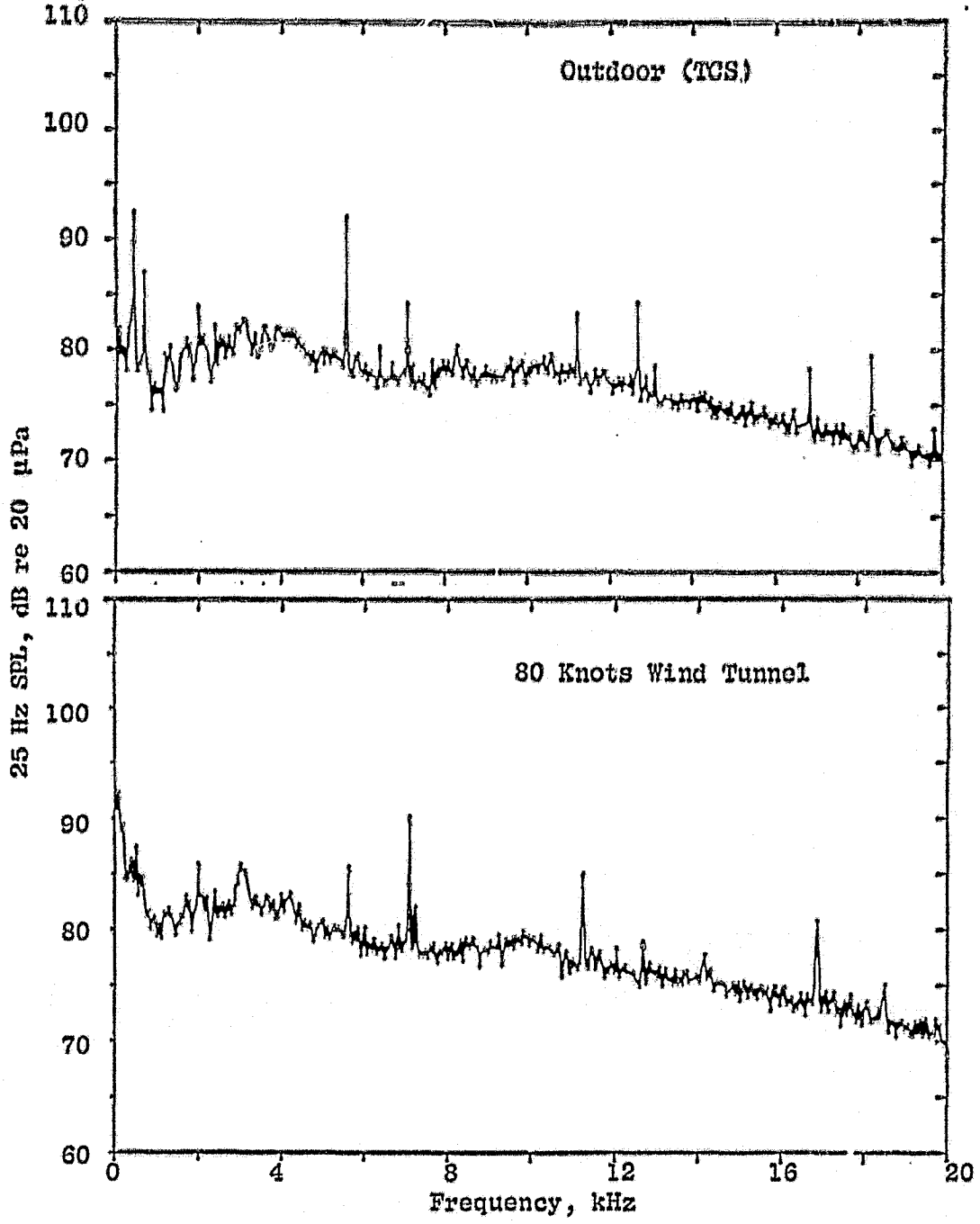

Figure 43. Comparison of Wind Tunnel and Outdoor with TCS Narrow-Band Spectra at Transonic Tip Speed.

- 50° Noise Emission Angle
- 14.5 Foot Microphone
- Straight Diffusing Hard-Wall Inlet
- V_T = 335 m/s (1100 ft/s)
- Lower Operating Line

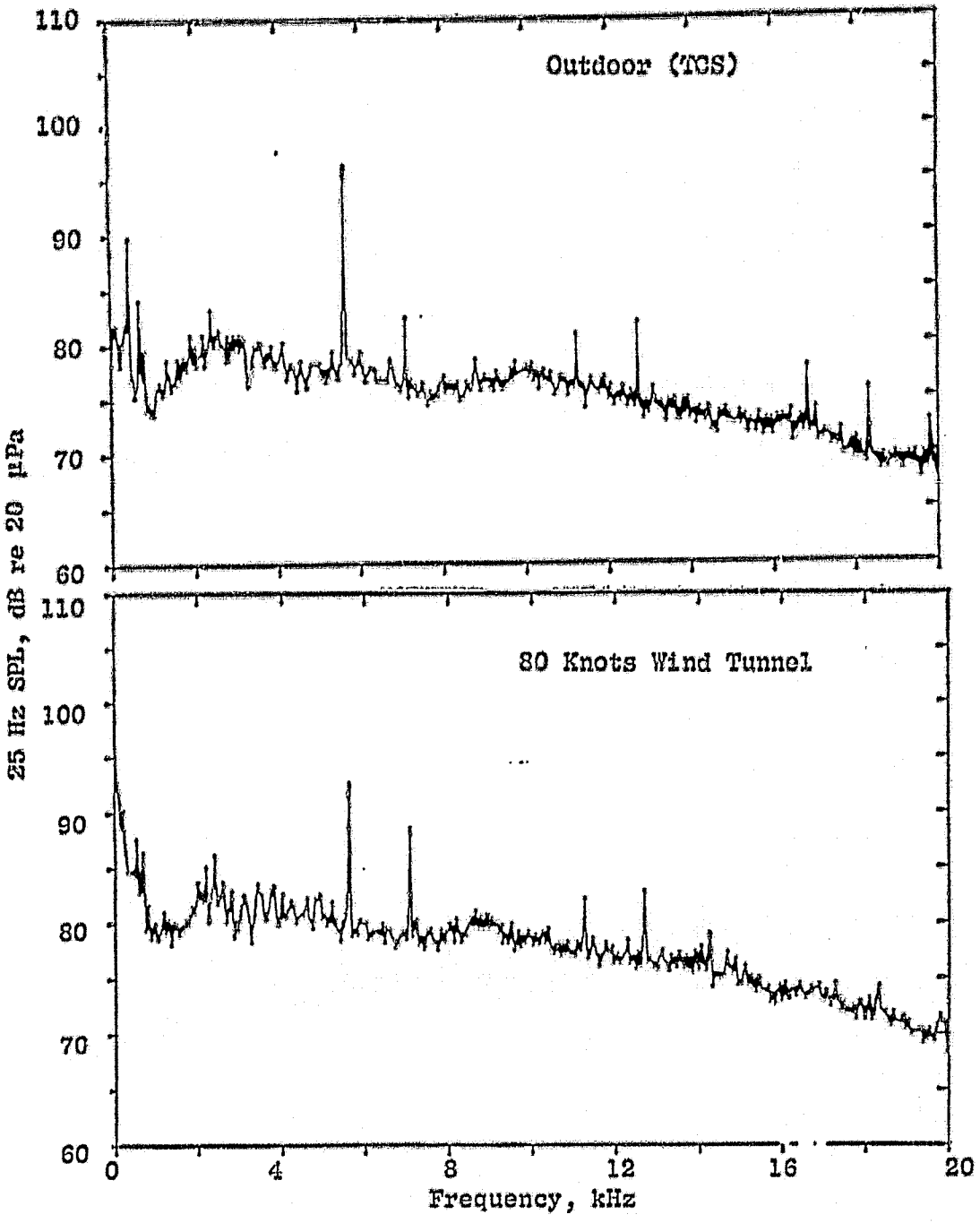

Figure 43. Comparison of Wind Tunnel and Outdoor with TCS Narrow-Band Spectra at Transonic Tip Speed (Continued).

- 70° Noise Emission Angle
- 14.5 Foot Microphone
- Straight Diffusing Hard-Wall Inlet
- V_T = 335 m/s (1100 ft/s)
- Lower Operating Line

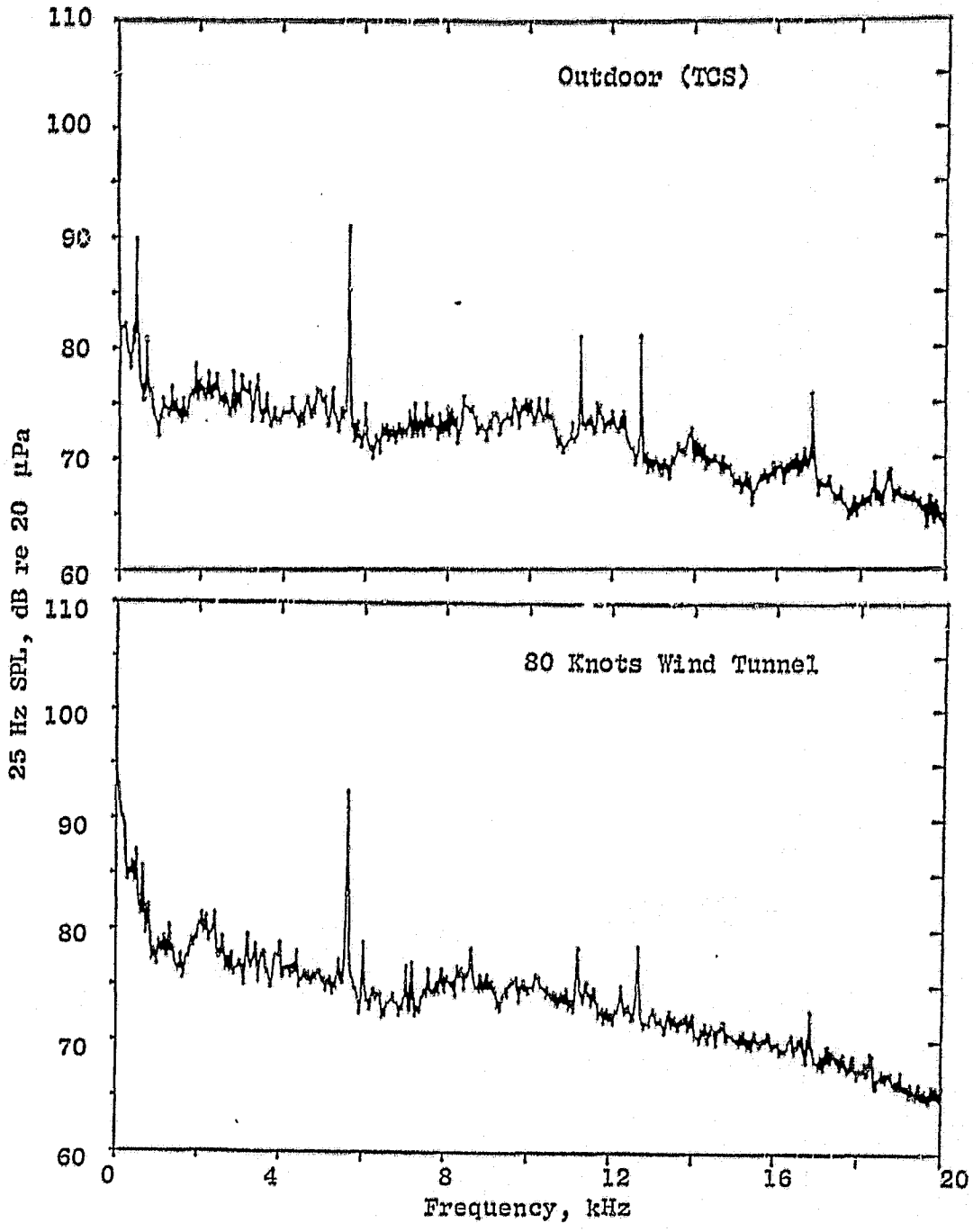

Figure 43. Comparison of Wind Tunnel and Outdoor with TCS Narrow-Band Spectra at Transonic Tip Speed (Concluded).

- 30° Noise Emission Angle
- 14.5 Foot Microphone
- Straight Diffusing Hard-Wall Inlet
- V_T = 377 m/s (1237 ft/s)
- Lower Operating Line

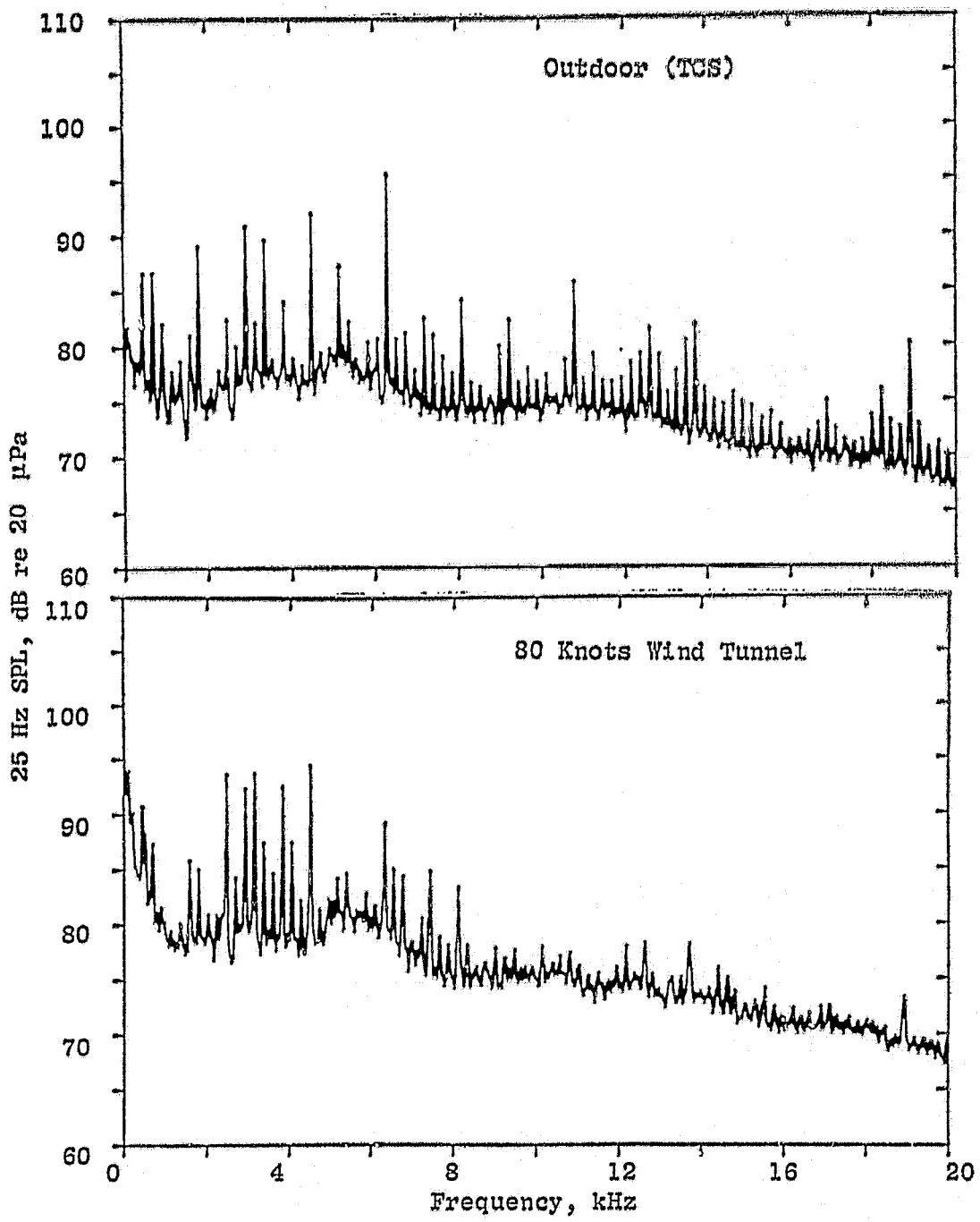

Figure 44. Comparison of Wind Tunnel and Outdoor with TCS Narrow-Band Spectra at Supersonic Tip Speed.

- 50° Noise Emission Angle
- 14.5 Foot Microphone
- Straight Diffusing Hard-Wall Inlet
- V_T = 377 m/s (1237 ft/s)
- Lower Operating Line

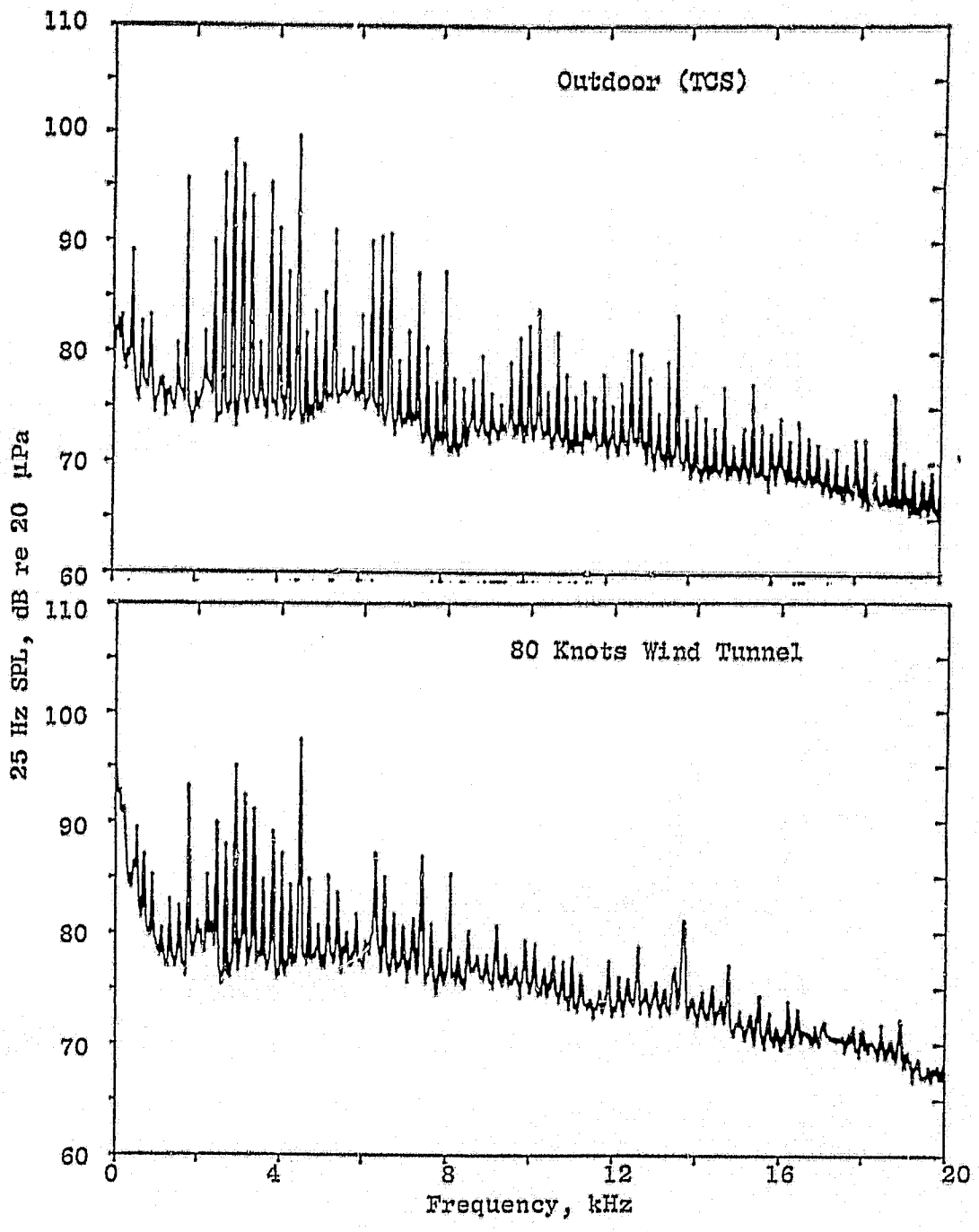

Figure 44. Comparison of Wind Tunnel and Outdoor with TCS Narrow-Band Spectra at Supersonic Tip Speed (Continued).

- 70° Noise Emission Angle
- 14.5 Foot Microphone
- Straight Diffusing Hard-Wall Inlet
- V_T = 377 m/s (1237 ft/s)
- Lower Operating Line

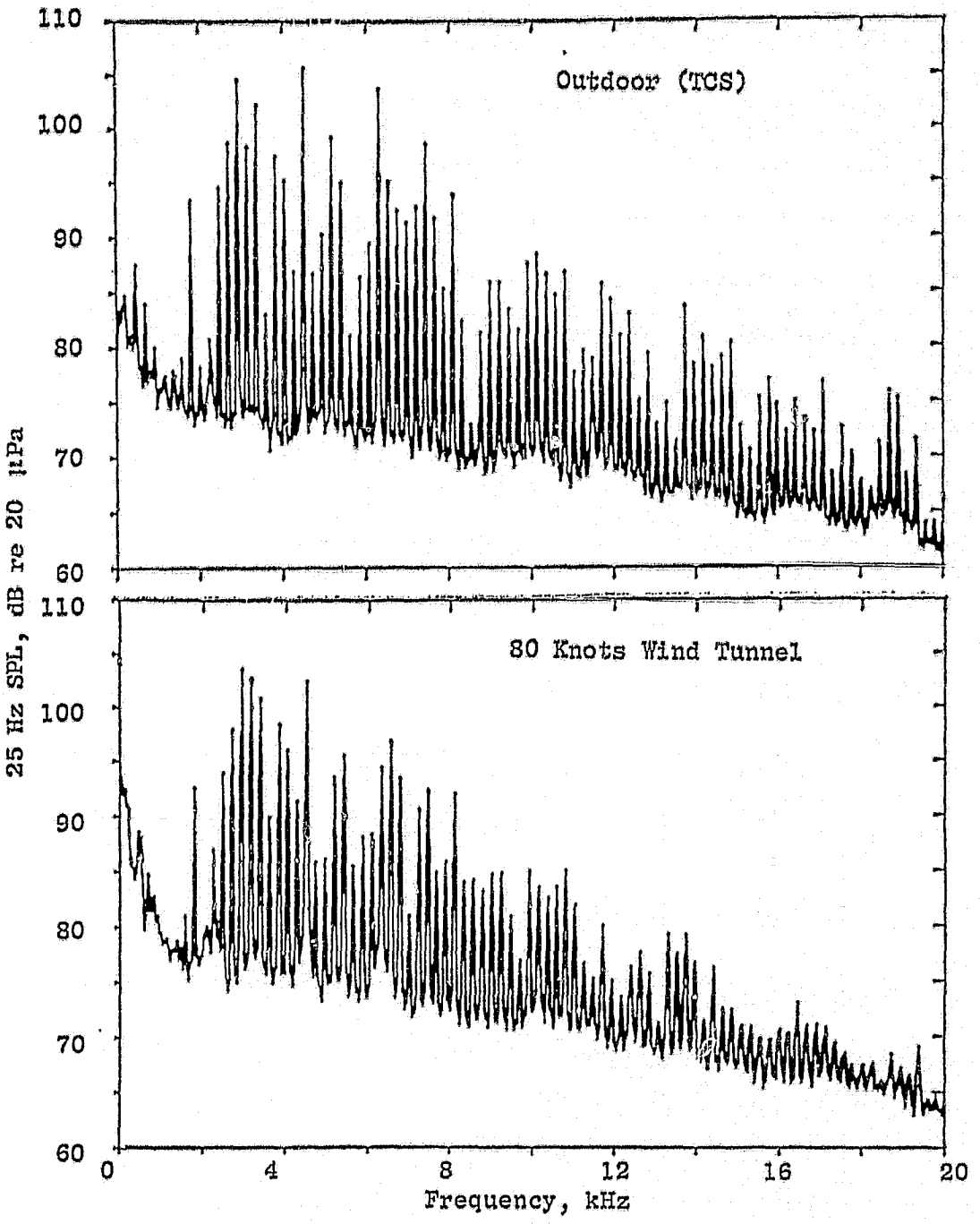

Figure 44. Comparison of Wind Tunnel and Outdoor with TCS Narrow-Band Spectra at Supersonic Tip Speed (Concluded).

for the hard-wall straight diffusing inlet condition, and in Figures 45 through 47, similar results are presented for the curved diffusing treated inlet. These two test configurations were common to both the wind tunnel and outdoor test programs. Utilizing the normalized narrowband differencing technique, Figure 48 shows that the wind tunnel spectral results are considerably higher in the first 500 Hz of the spectrum due to wind tunnel background, then slightly higher in broadband level at angles other than 30°. On the basis of the wind tunnel-to-static coordinate transformation formulas (refer to Section 4.1), the anticipated result is that the wind tunnel data should be on the order of 1 dB lower than the static results. However, as was noted previously, a dynamic effect correction was not included. The conventionally applied dynamic-effect correction is given by Equation 3.

$$\text{Dynamic Effect Increment} = -40 \text{ Log } [1 - M_\infty \cos \phi] \qquad (3)$$

By applying Equation 3 in conjunction with Equations 1 and 2, the increments presented in Table 8 are anticipated, independent of frequency. The results in Figure 48 indicate the wind tunnel results are typically 1 to 3 dB higher at the 50° and 70° angles. Unfortunately, a direct comparison of a wind tunnel run to a non-TCS run is not possible, yet these results tend to reinforce the conclusion that a small but non-negligible transmission loss may be attributed to the utilization of the TCS. The implication is that more testing needs be done to (1) determine if the TCS does induce a transmission loss which is angularly dependent or (2) if the dynamic-effect corrections need modifications in order to appropriately account for the differences. Only flight testing can resolve the adequacy of the dynamic correction formulas.

Table 8. Projected Noise Differences - Wind Tunnel Minus Static.

Angle, degrees	Coordinate Δ, dB	Dynamic Δ, dB	Total Δ, dB
10	-1.1	+2.1	+1.0
20	-1.0	+2.0	+1.0
30	-0.9	+1.9	+1.0
40	-0.8	+1.6	+0.8
50	-0.7	+1.4	+0.7
60	-0.5	+1.0	+0.5
70	-0.3	+0.7	+0.4
80	-0.2	+0.4	+0.2
90	-0.0	+0	0

- 30° Noise Emission Angle
- 14.5 Foot Microphone
- Curved Diffusing Treated Inlet
- V_T = 302 m/s (990 ft/s)
- Upper Operating Line

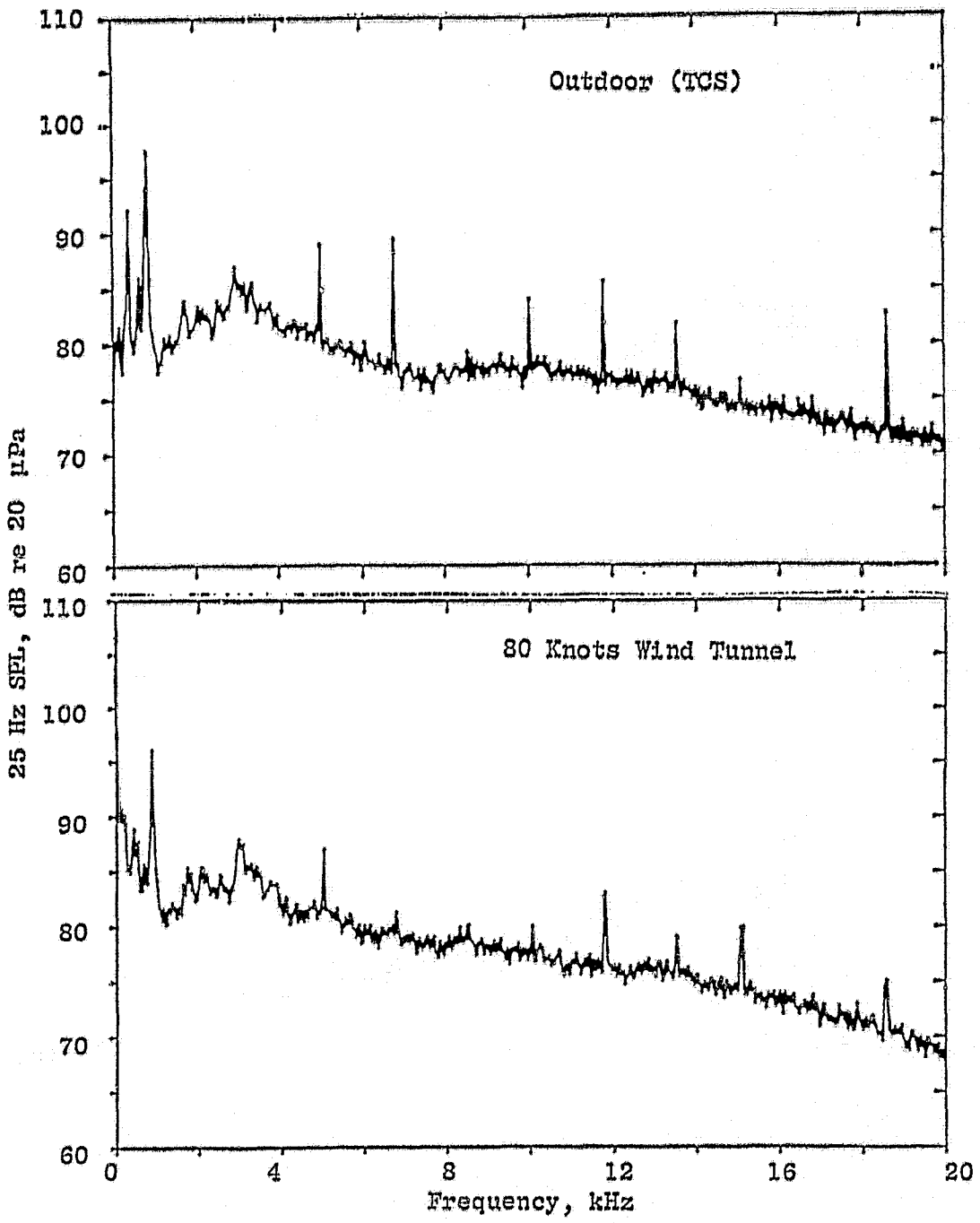

Figure 45. Comparison of Wind Tunnel and Outdoor with TCS Narrow-Band Spectra at Subsonic Tip Speed.

- 50° Noise Emission Angle
- 14.5 Foot Microphone
- Curved Diffusing Treated Inlet
- V_T = 302 m/s (990 ft/s)
- Upper Operating Line

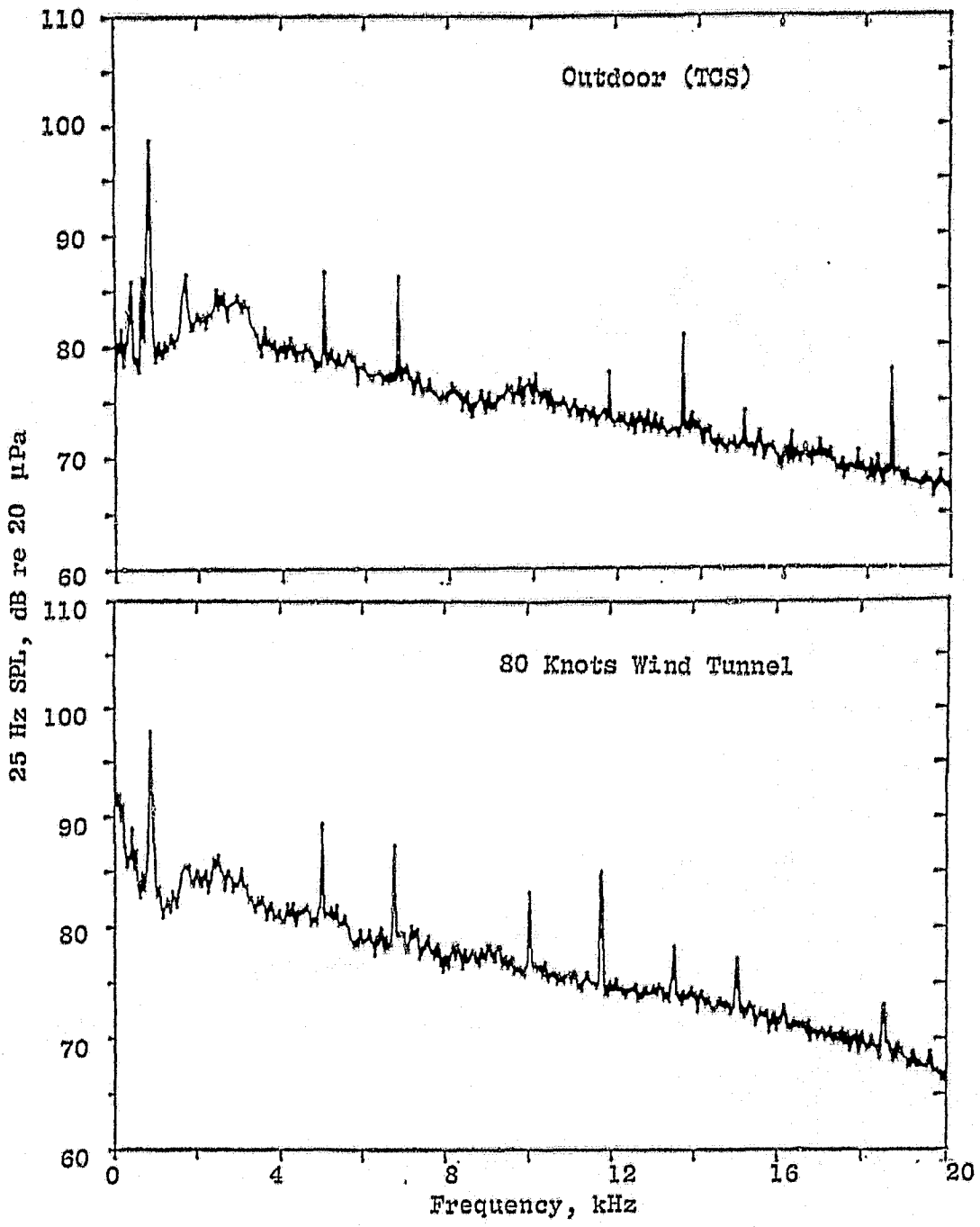

Figure 45. Comparison of Wind Tunnel and Outdoor with TCS Narrow-Band Spectra at Subsonic Tip Speed (Continued).

- 60° Noise Emission Angle
- 14.5 Foot Microphone
- Curved Diffusing Treated Inlet
- V_T = 302 m/s (ft/s)
- Upper Operating Line

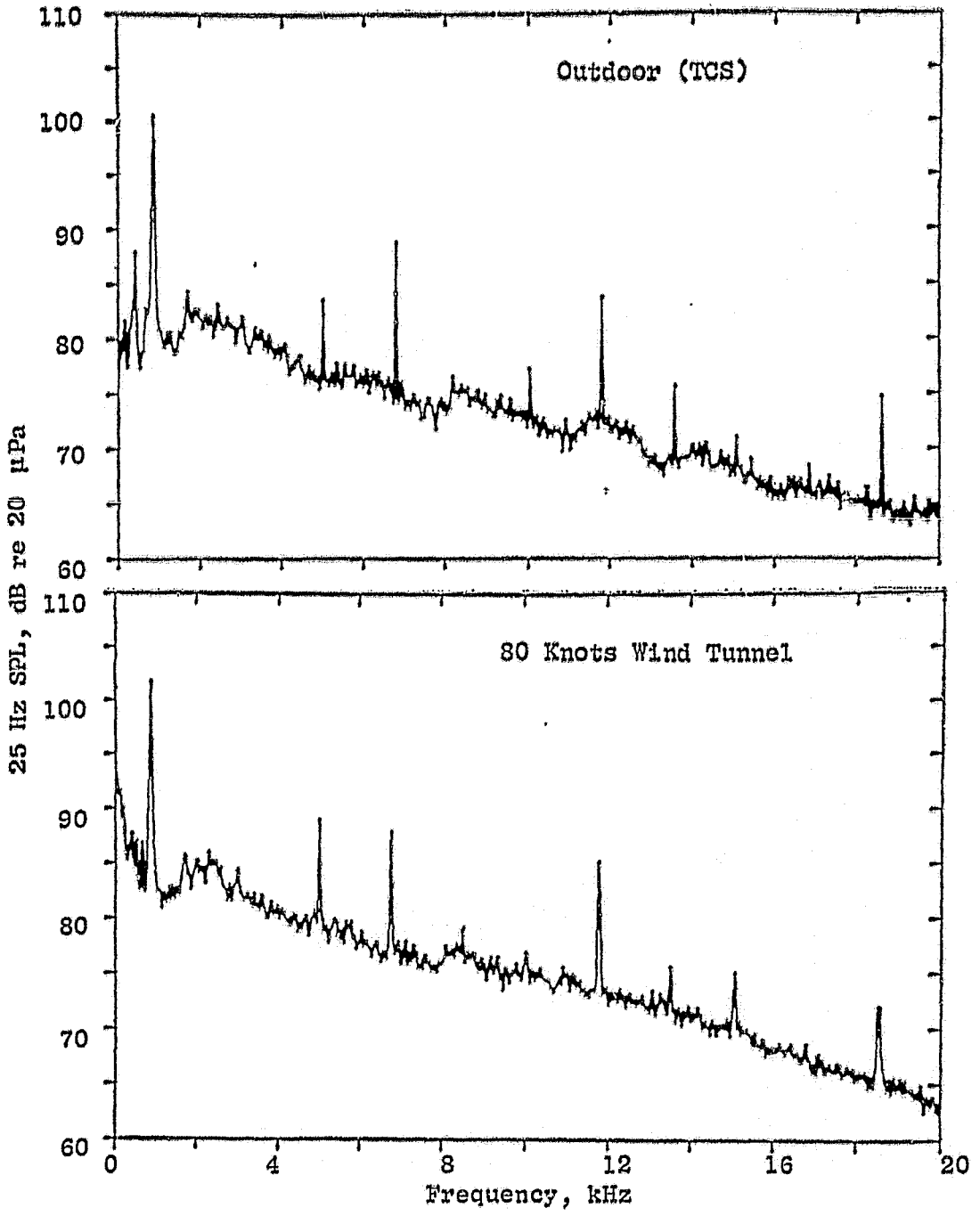

Figure 45. Comparison of Wind Tunnel and Outdoor with TCS Narrow-Band Spectra at Subsonic Tip Speed (Concluded).

- 30° Noise Emission Angle
- 14.5 Foot Microphone
- Curved Diffusing Treated Inlet
- V_T = 335 m/s (1100 ft/s)
- Upper Operating Line

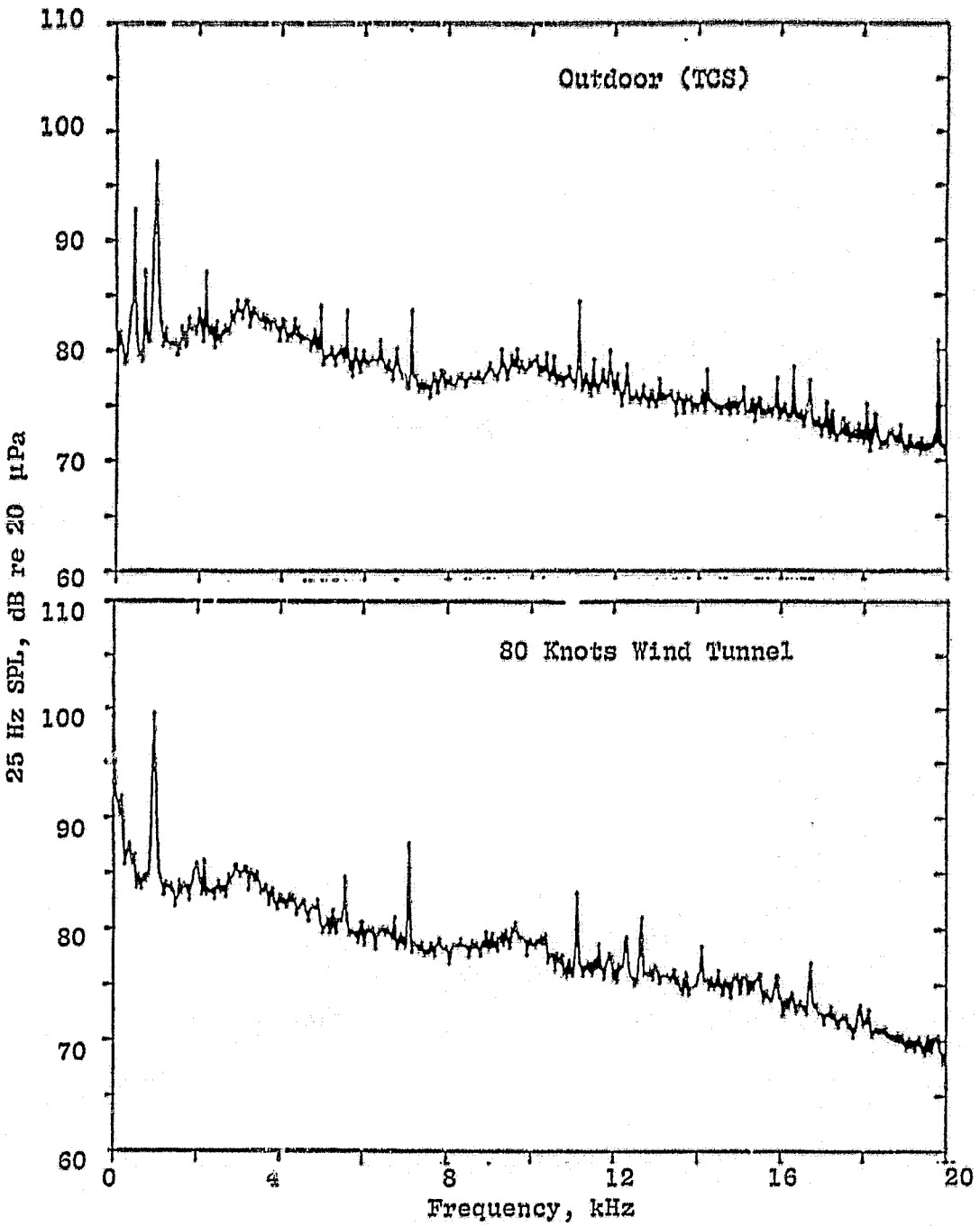

Figure 46. Comparison of Wind Tunnel and Outdoor with TCS Narrow-Band Spectra at Transonic Tip Speed.

- 50° Noise Emission Angle
- 14.5 Foot Microphone
- Curved Diffusing Treated Inlet
- V_T = 335 m/s (1100 ft/s)
- Upper Operating Line

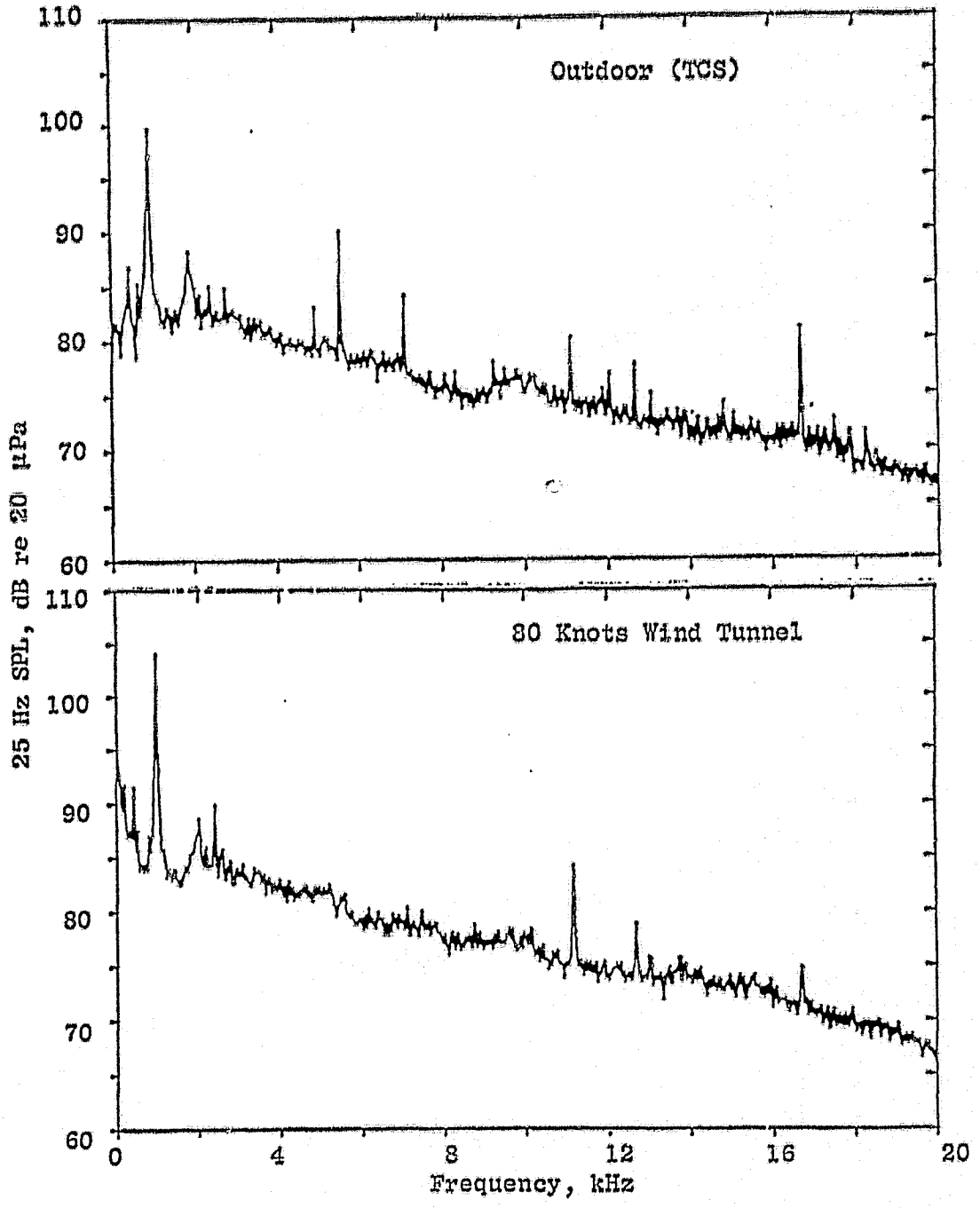

Figure 46. Comparison of Wind Tunnel and Outdoor with TCS Narrow-Band Spectra at Transonic Tip Speed (Continued).

- 60° Noise Emission Angle
- 14.5 Foot Microphone
- Curved Diffusing Treated Inlet
- V_T = 335 m/s (1100 ft/s)
- Upper Operating Line

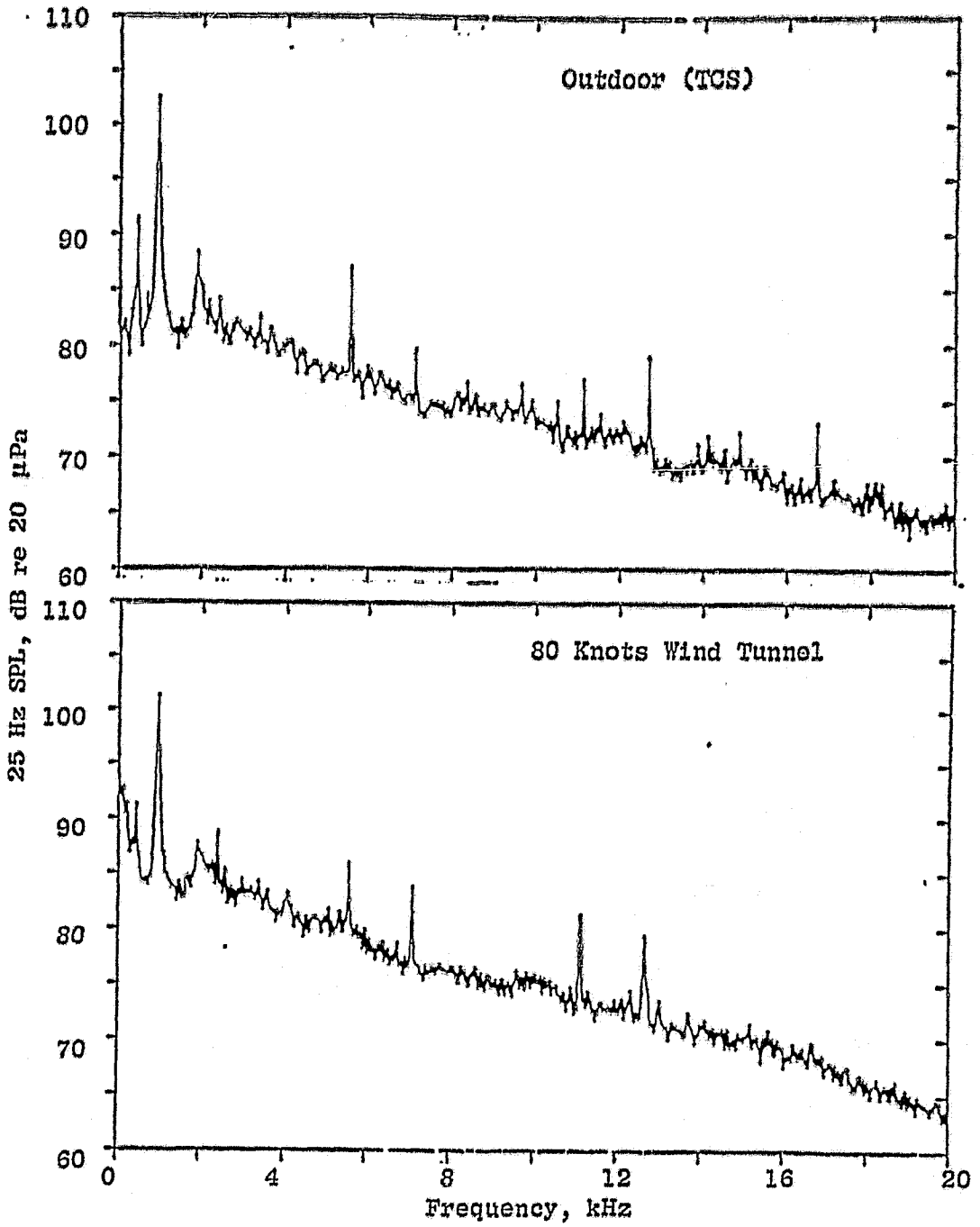

Figure 46. Comparison of Wind Tunnel and Outdoor with TCS Narrow-Band Spectra at Transonic Tip Speed (Concluded).

- 30° Noise Emission Angle
- 14.5 Foot Microphone
- Curved Diffusing Treated Inlet
- V_T = 377 m/s (1237 ft/s)
- Upper Operating Line

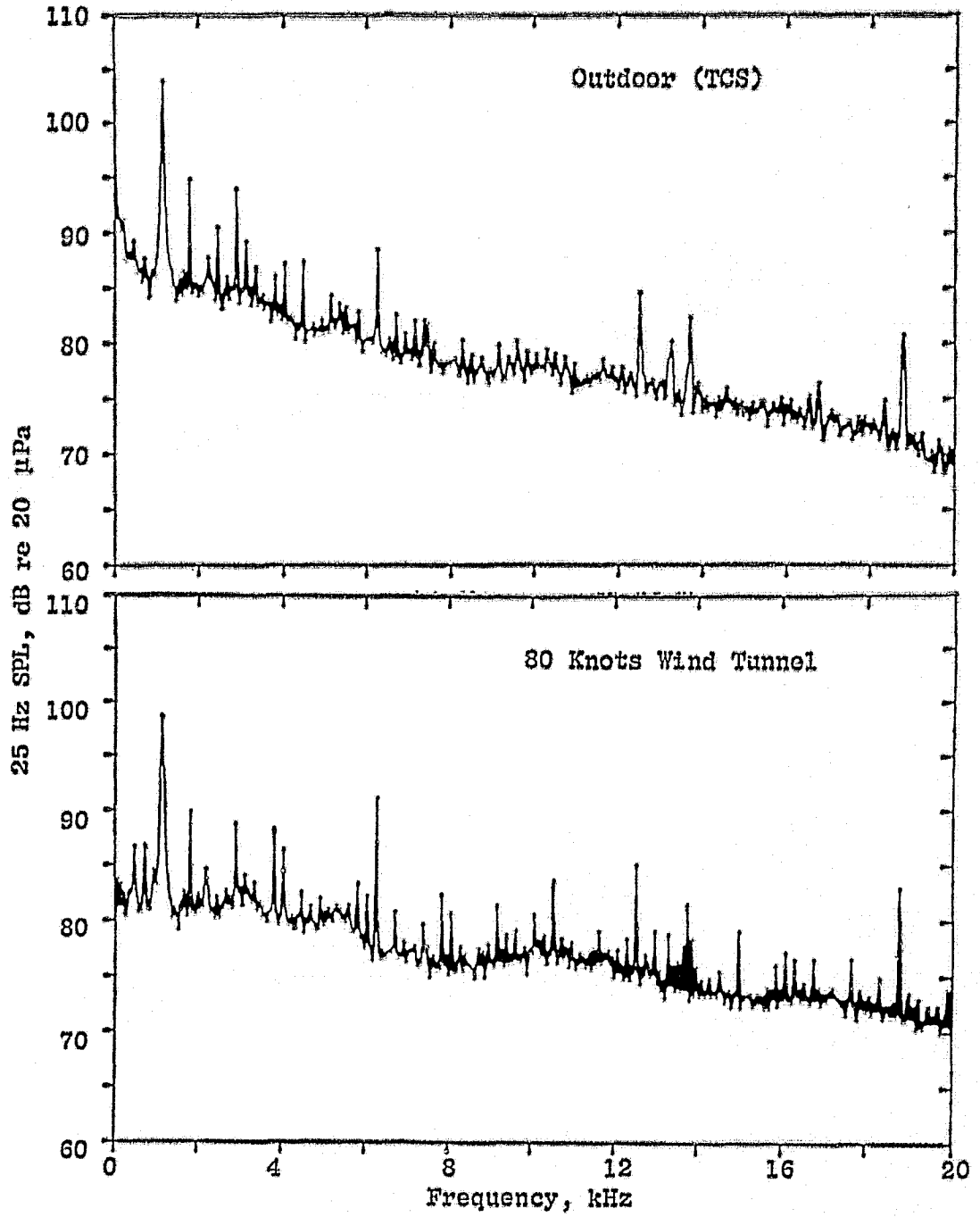

Figure 47. Comparison of Wind Tunnel and Outdoor with TCS Narrow-Band Spectra at Supersonic Tip Speed.

- 50° Noise Emission Angle
- 14.5 Foot Microphone
- Curved Diffusing Treated Inlet
- V_T = 377 m/s (1237 ft/s)
- Upper Operating Line

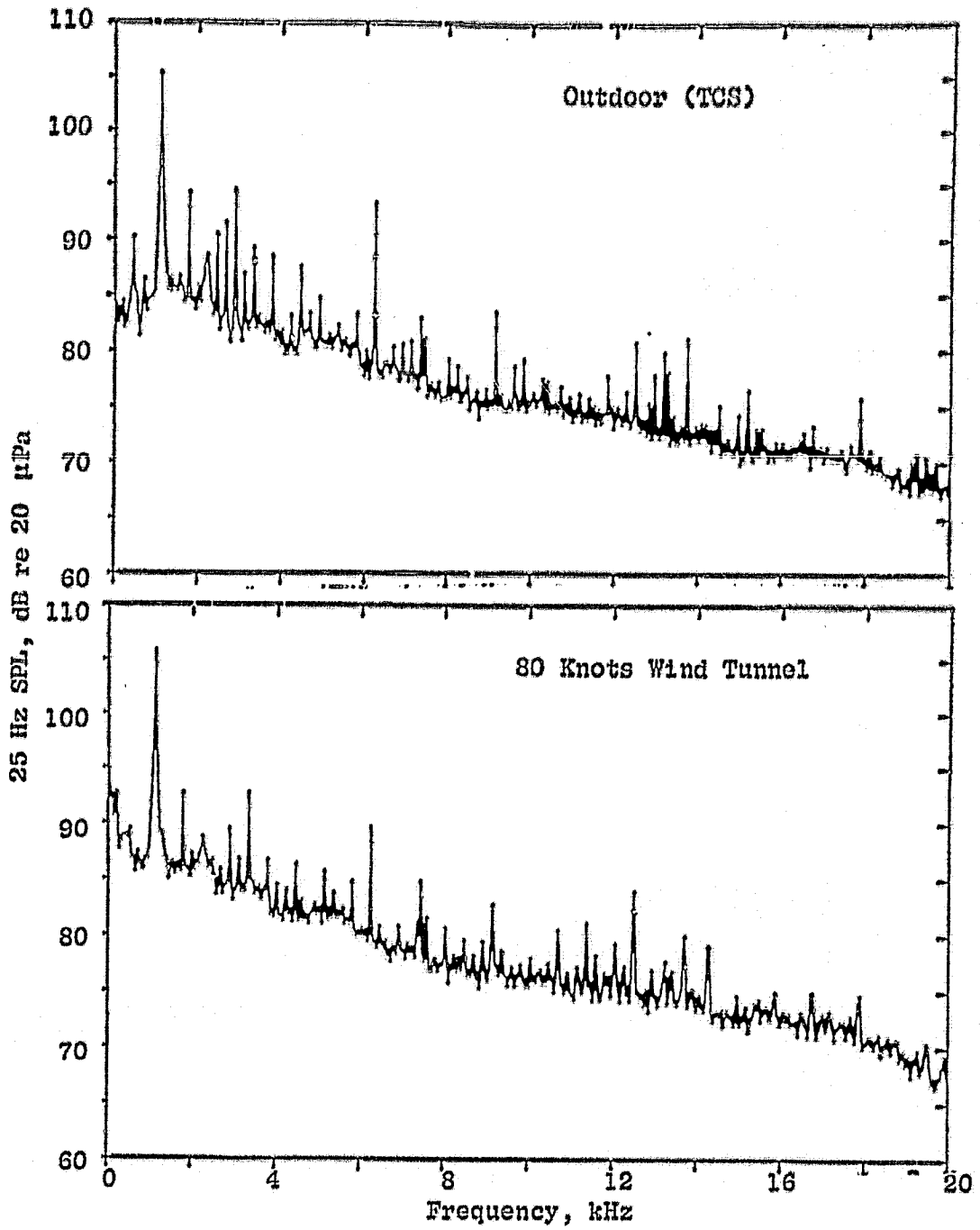

Figure 47. Comparison of Wind Tunnel and Outdoor with TCS Narrow-Band Spectra at Supersonic Tip Speed (Continued).

- 60° Noise Emission Angle
- 14.5 Foot Microphone
- Curved Diffusing Treated Inlet
- V_T = 377 m/s (1237 ft/s)
- Upper Operating Line

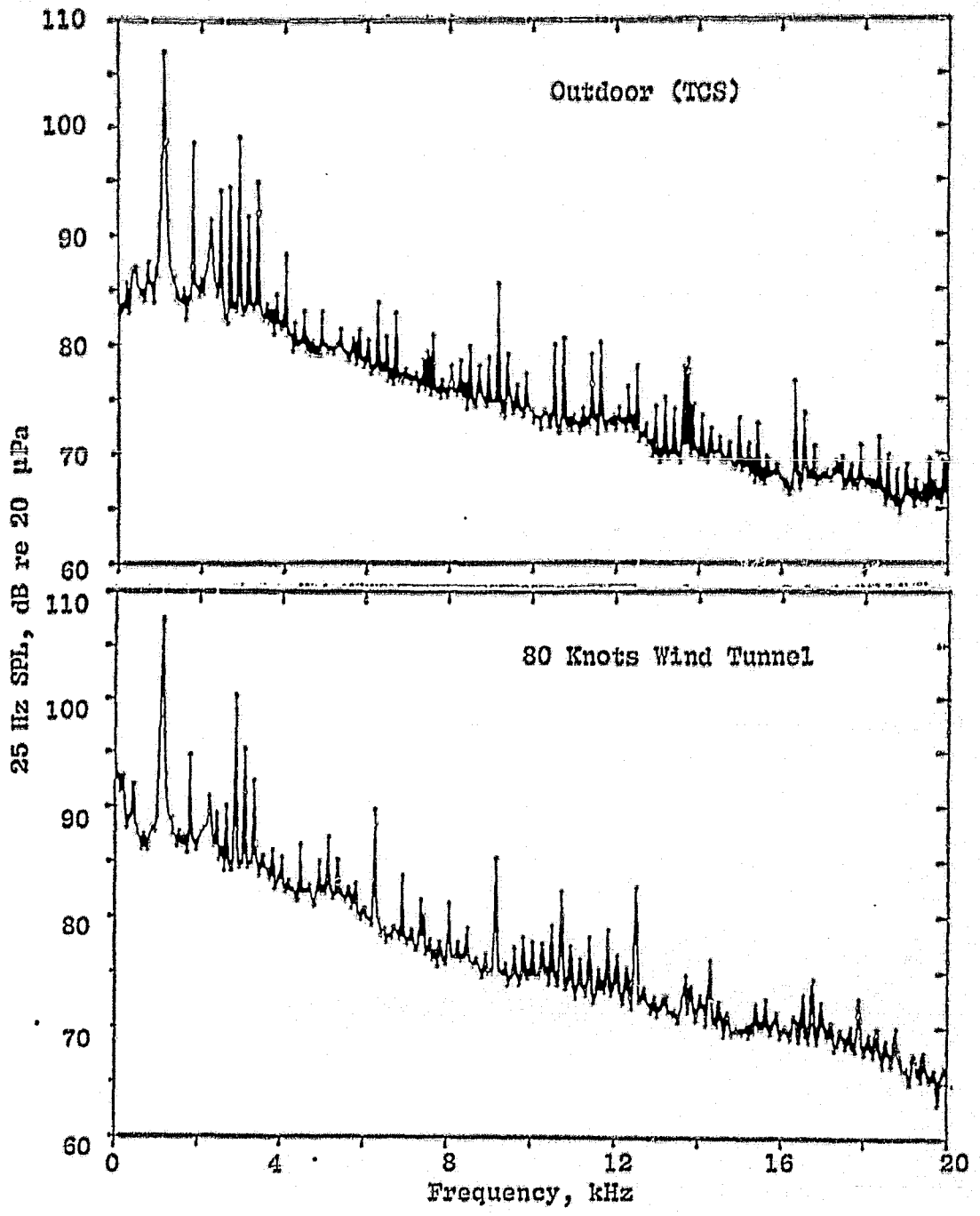

Figure 47. Comparison of Wind Tunnel and Outdoor with TCS Narrow-Band Spectra at Supersonic Tip Speed (Concluded).

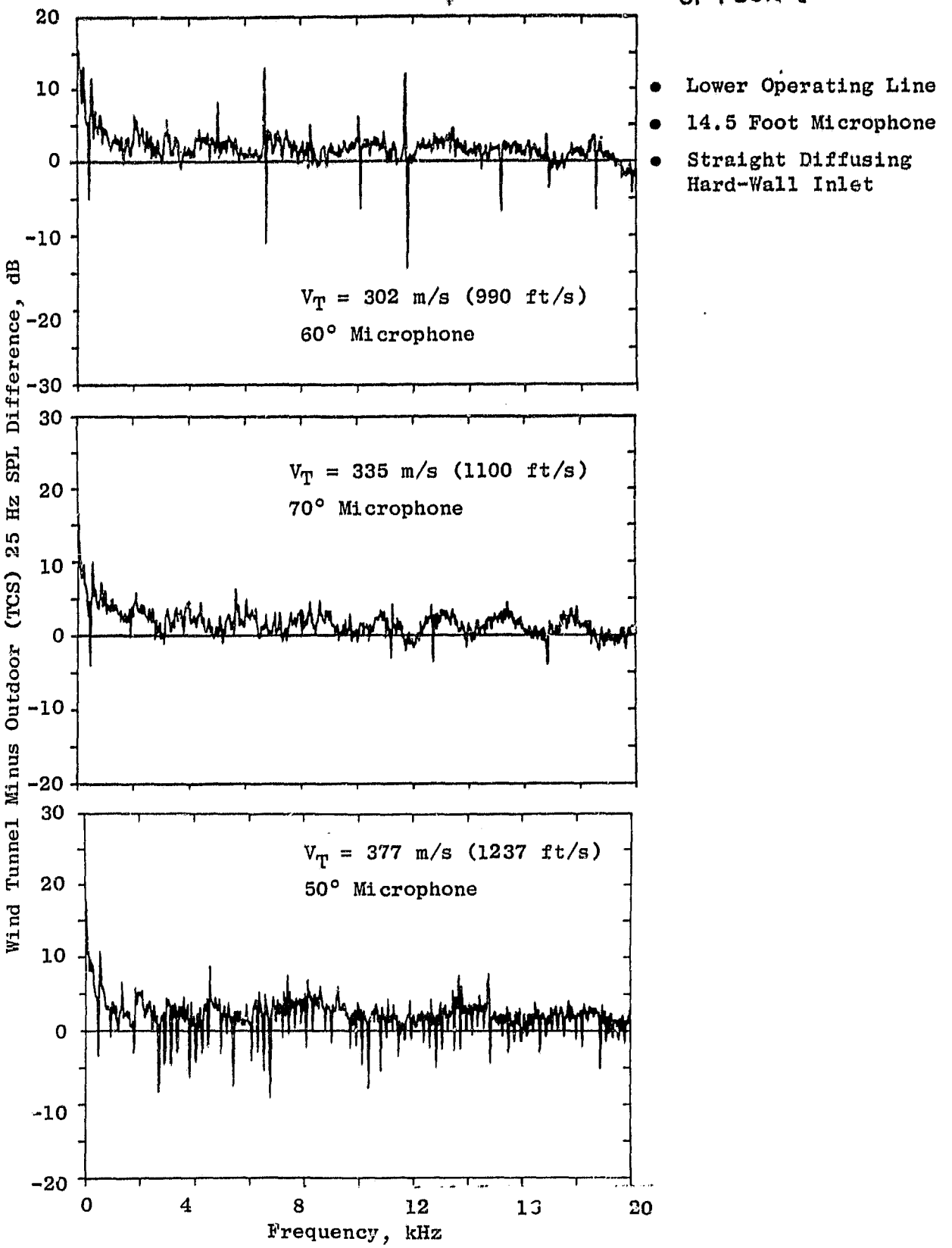

Figure 48. Comparative Narrowband Spectral Differences for Wind Tunnel and Outdoor/TCS Configuration.

C-2

The comparisons presented in Figure 48 are inappropriate to evaluate tonal differences. Therefore, BPF directivities are compared in Figures 49 and 50. The results indicate a general agreement in the sound pressure level, unlike the 10-15 dB discrepancies previously encountered without the TCS in Reference 1. However, the angular distribution of energy is not in good agreement, particularly in the 60° to 70° range which is extremely important in terms of sideline noise. These differences indicate that inlet flow effects may influence the directivity patterns more than previously anticipated, and this feature, in conjunction with inlet geometry, needs to be evaluated for projections of static noise data to flight.

4.4 FAN OPERATING LINE INFLUENCE ON INLET ACOUSTIC CHARACTERISTICS

The operating line on which the engine operates produces an effect on the fan broadband noise. This effect is well described by Reference 13 where a correlation to angle of incidence on the fan blade is documented. In this test program, emphasis was placed on detecting tonal differences such that much of the test program was run on the lower operating line (refer to Figure 24) to reduce the relative broadband levels and better reveal the tonal characteristics. This is particularly true for the treated inlet cases where the effectiveness of the treatment made analysis of the fan tonal contributions on the elevated or design operating line more difficult.

The broadband effect was demonstrated to follow the trends of Reference 14, while the tonal contributions were also impacted by this alteration of the fan operating line. The effect on the tonal contributions may be viewed in terms of the propagation of various duct modes. The determination of modal cut-off frequencies needs to be considered in terms of the axial Mach number influence. A plot of the cut-on duct mode map is displayed in Figure 51. The aerodynamic measurements described in Section 4.2 were utilized as input in the computation of this modal coupling map. To the left of the lines graphed, pressure patterns generated at the fan face are exponentially attenuated and do not propagate as was shown in Reference 7. But to the right, the duct would allow these pressure patterns to be transmitted forward without exponential attenuation in the absence of acoustic treatment on the duct walls. Hence, even in a hard-walled duct, significant differences in the propagating modes may be created by the operating line influence as shown in Figure 51. Note that the lower operating line that generates less broadband noise produces more propagational duct modes at a given corrected engine speed condition. Thus, if fan interaction is producing patterns with these characteristics, the potential for higher modally generated fan tone noise exists. This effect was investigated as part of the test program.

4.4.1 Straight Hard-wall Diffusing Inlet

A test of the effect that the fan operating line has on the system noise parameters for a straight diffusing hard-wall inlet was performed at the NASA-ARC outdoor test site. The tests were performed back-to-back with the TCS installed in order to control the turbulence-related tonal components as dis-

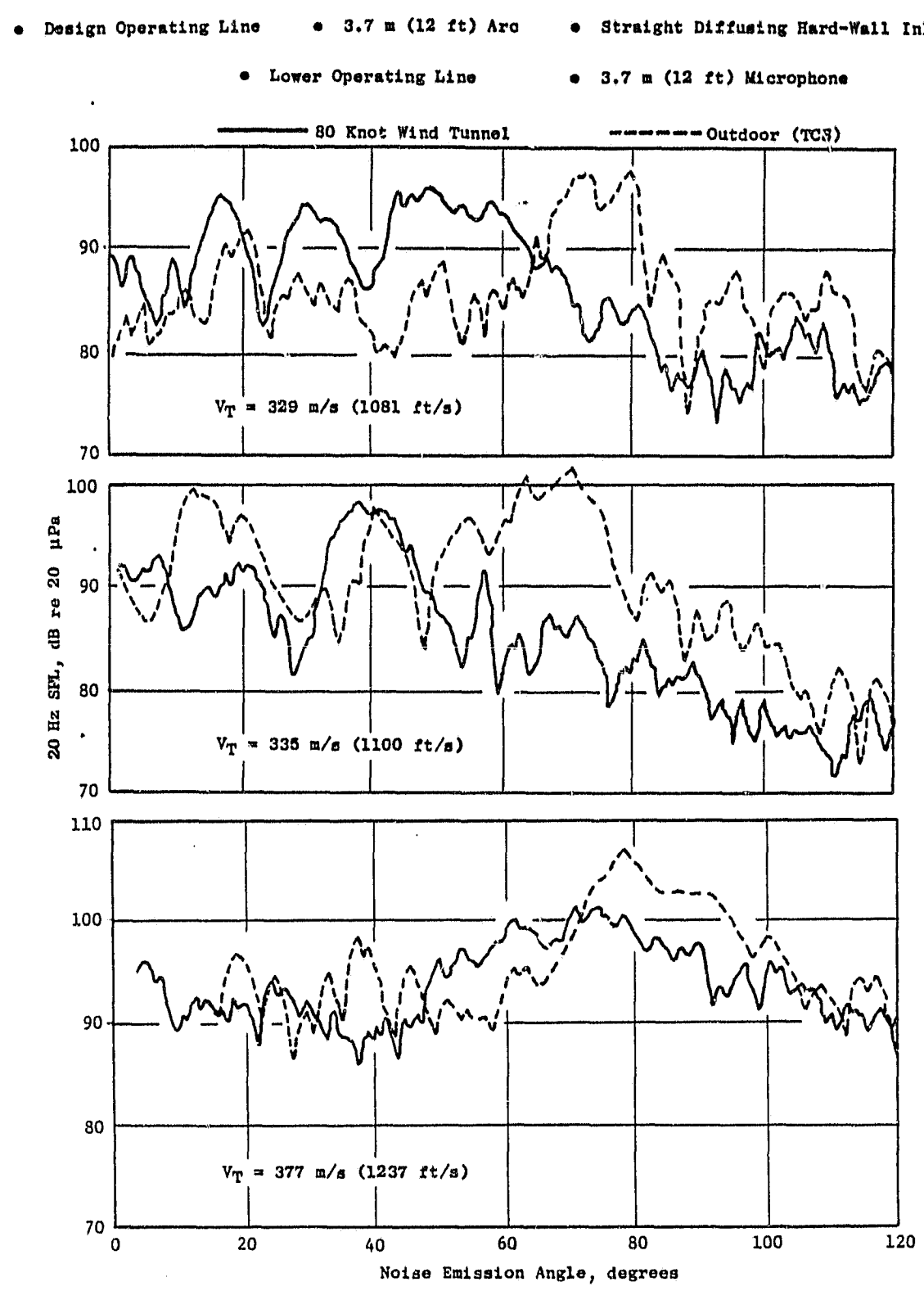

Figure 49. Comparison of Wind Tunnel and Outdoor TCS BPF Directivity at Subsonic, Transonic, and Supersonic Tip Speeds, Straight Hard-Wall Diffusing Inlet.

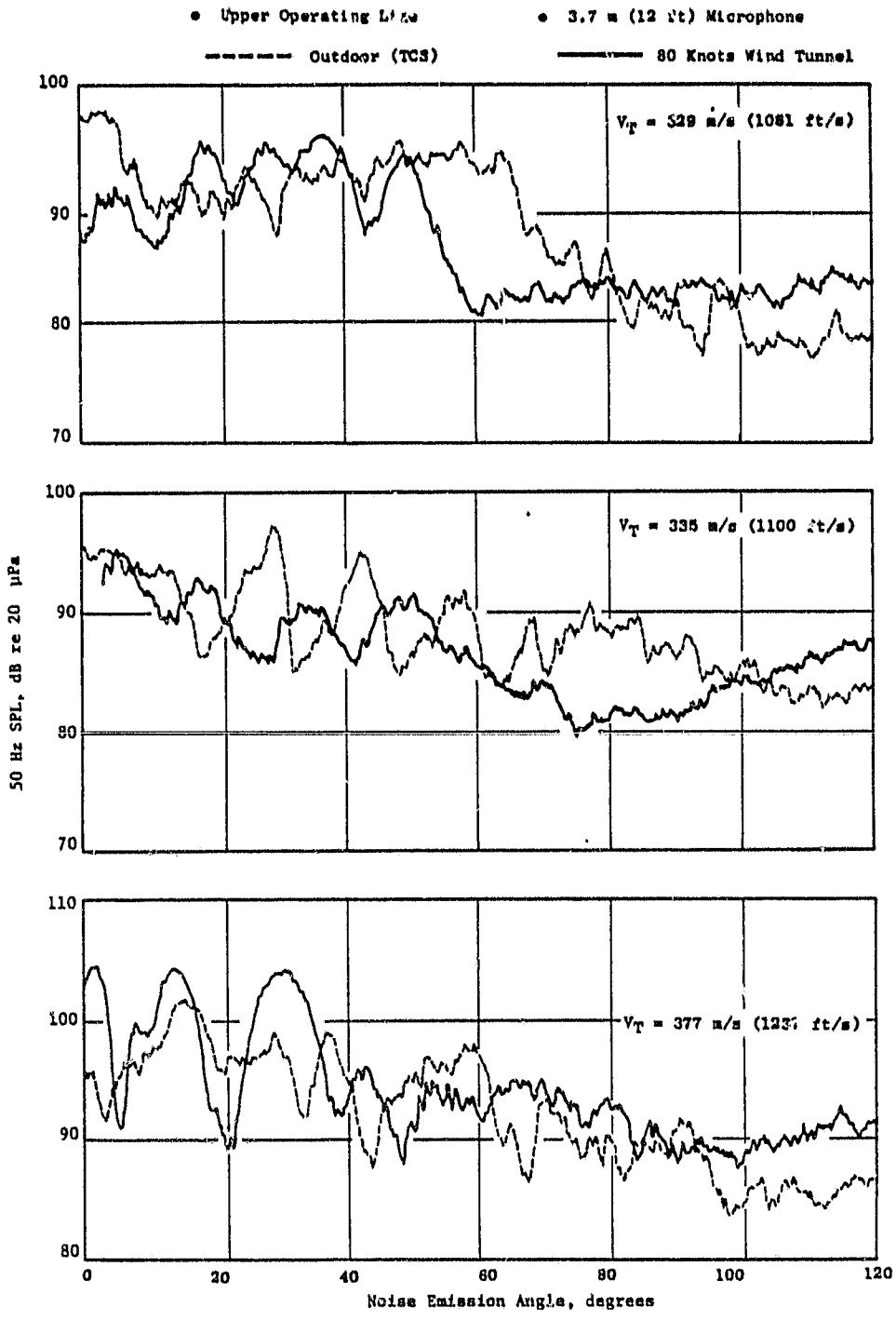

Figure 50. Comparison of Wind Tunnel and Outdoor TCS BPF Directivity at Subsonic, Transonic, and Supersonic Tip Speeds, Curved Treated Diffusing Inlet.

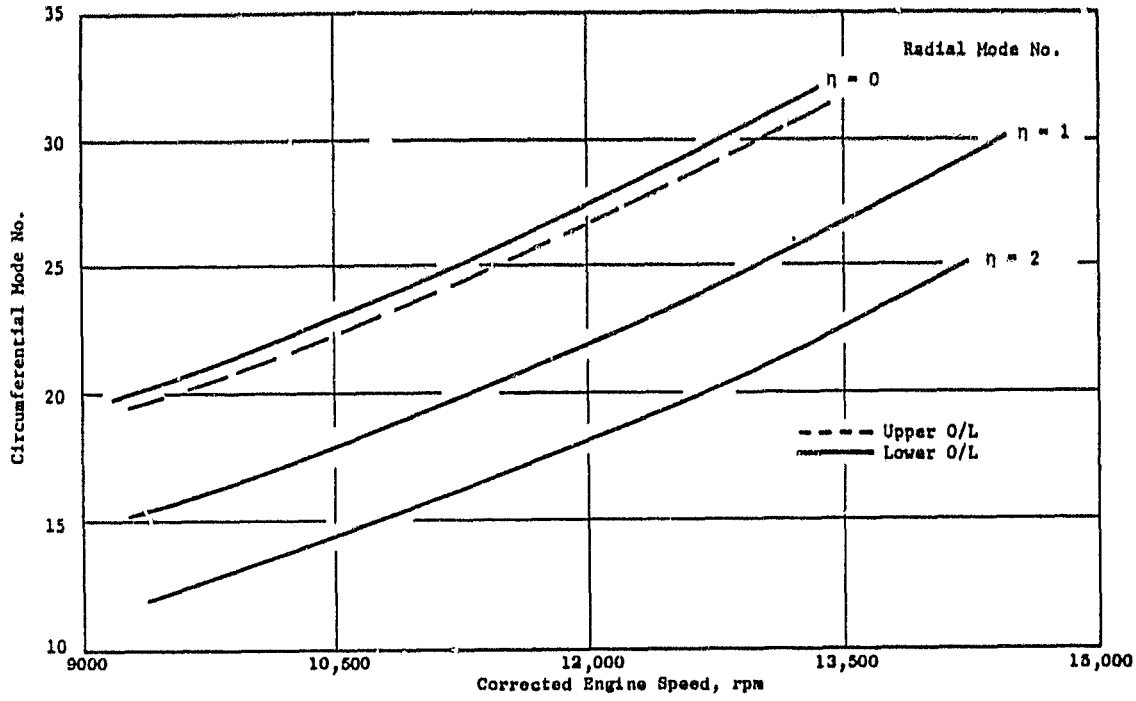

Figure 51. Duct Modal Coupling Map.

cussed previously. The scaled PNL and OASPL results are presented for subsonic, transonic, and supersonic fan tip speed points in Figures 52 and 53. The forward quadrant noise levels are noted to be lowered fairly uniformly independent of speed for the lowered operating line.

The upper operating line was generated by inserting a wedge-shaped section at the inner diameter of the bypass duct acoustic treatment; consequently, the aft quadrant results are biased by this effect. Analytical estimates of an improvement in the operating line change indicate the broadband noise level change should be on the order of 2.7 dB independent of angle. The forward quadrant results are of this order of magnitude.

Comparative 25 Hz bandwidth narrowband results are presented in Figures 54, 55, and 56. These figures show the dominant nature of the tonal components when the fan operating line is lowered and the broadband noise level is reduced. The results demonstrate the practicality of carrying out the major portion of the test program on the lowered operating line to detect the detailed nature of various inlet changes on the tonal components.

4.4.2 Curved Treated Diffusing Inlet

Results similar to those determined for the straight hard-wall diffusing inlet were measured for operating line changes associated with the curved

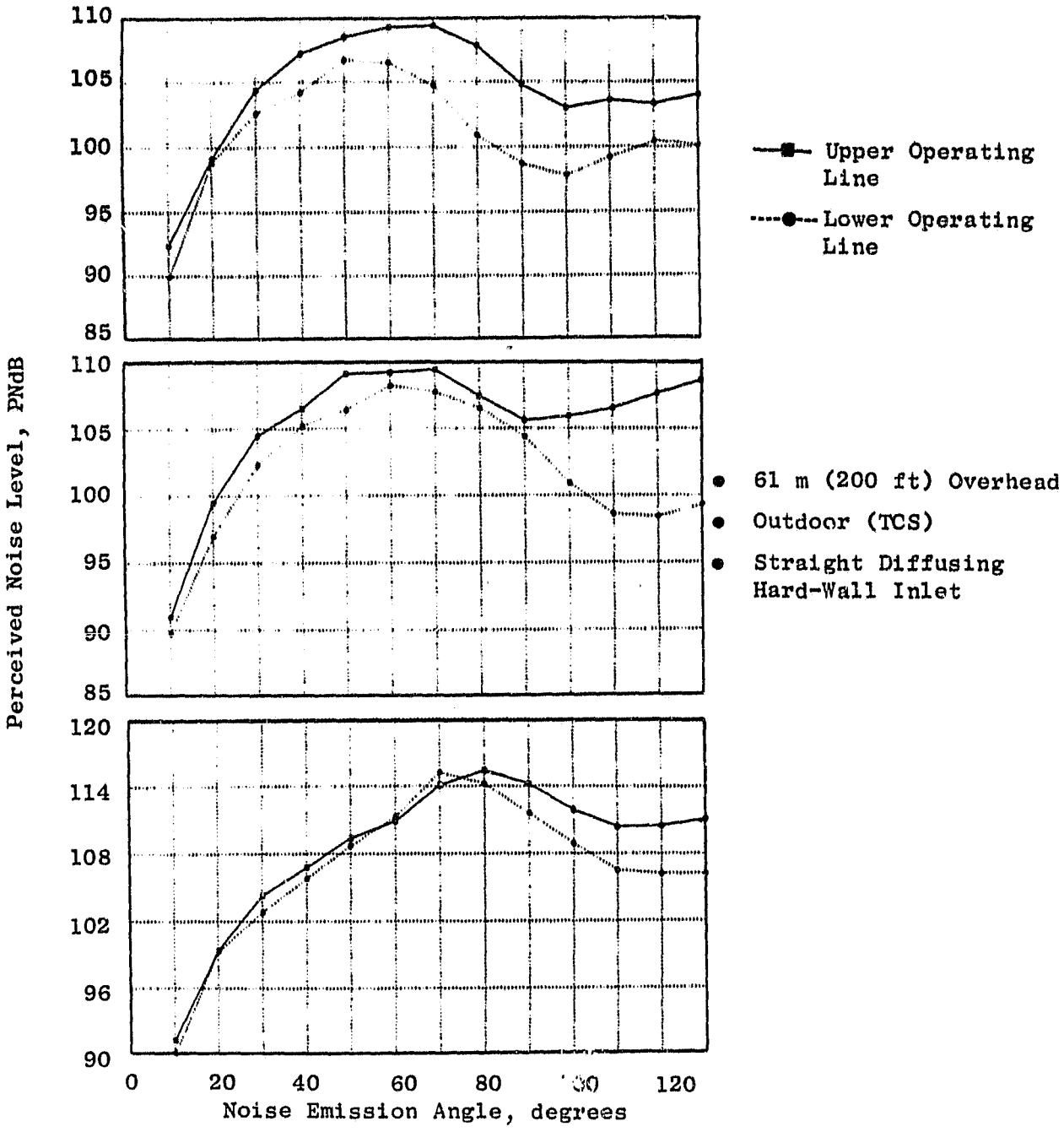

Figure 52. Scaled Perceived Noise Level Directivities for Two Fan Operating Lines.

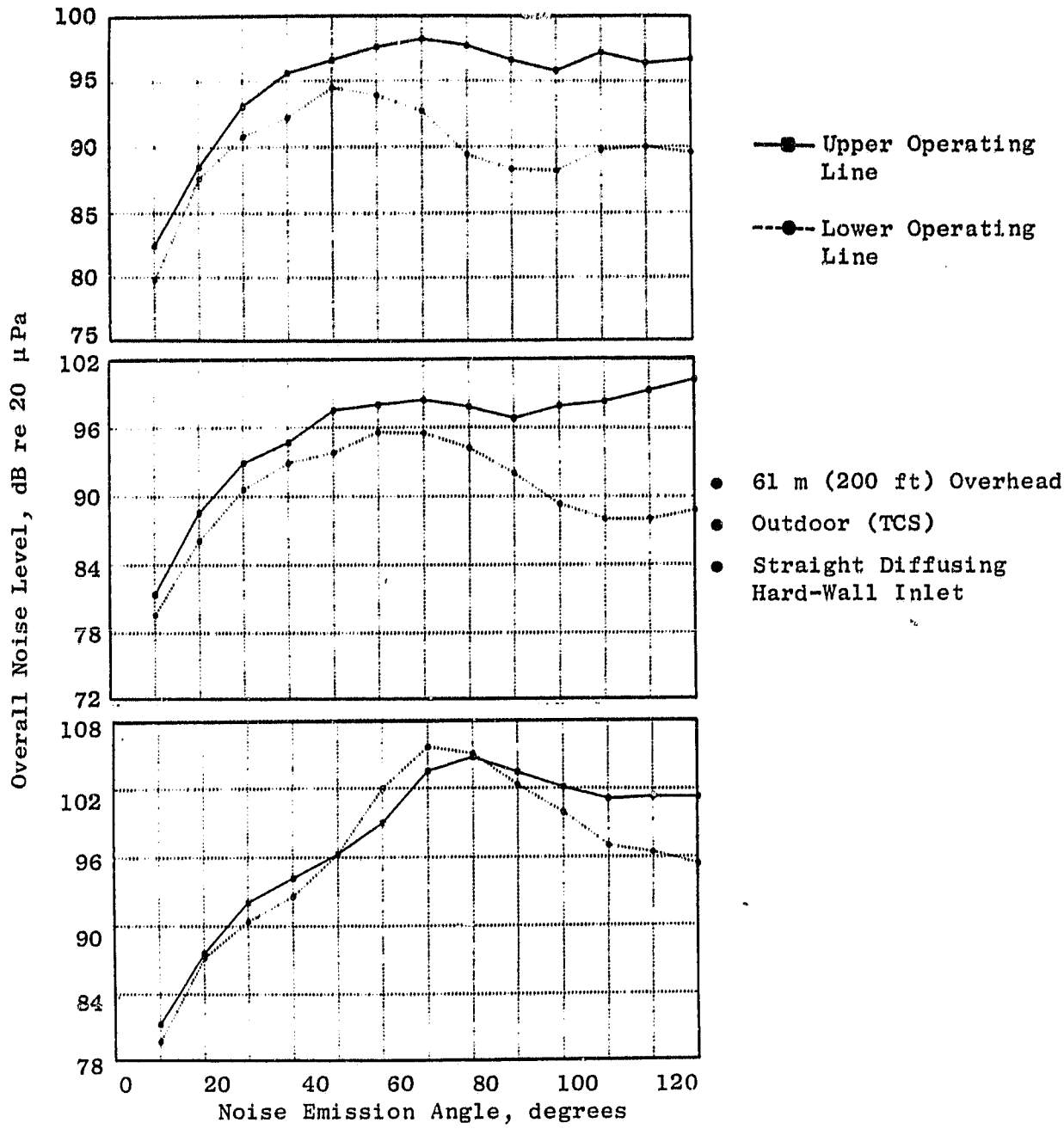

Figure 53. Scaled Overall Noise Level Directivities for Two Fan Operating Lines.

- 30° Noise Emission Angle
- 14.5 Foot Microphone
- Outdoor (TCS)
- Straight Diffusing Hard-Wall Inlet
- V_T = 302 m/s (990 ft/s)

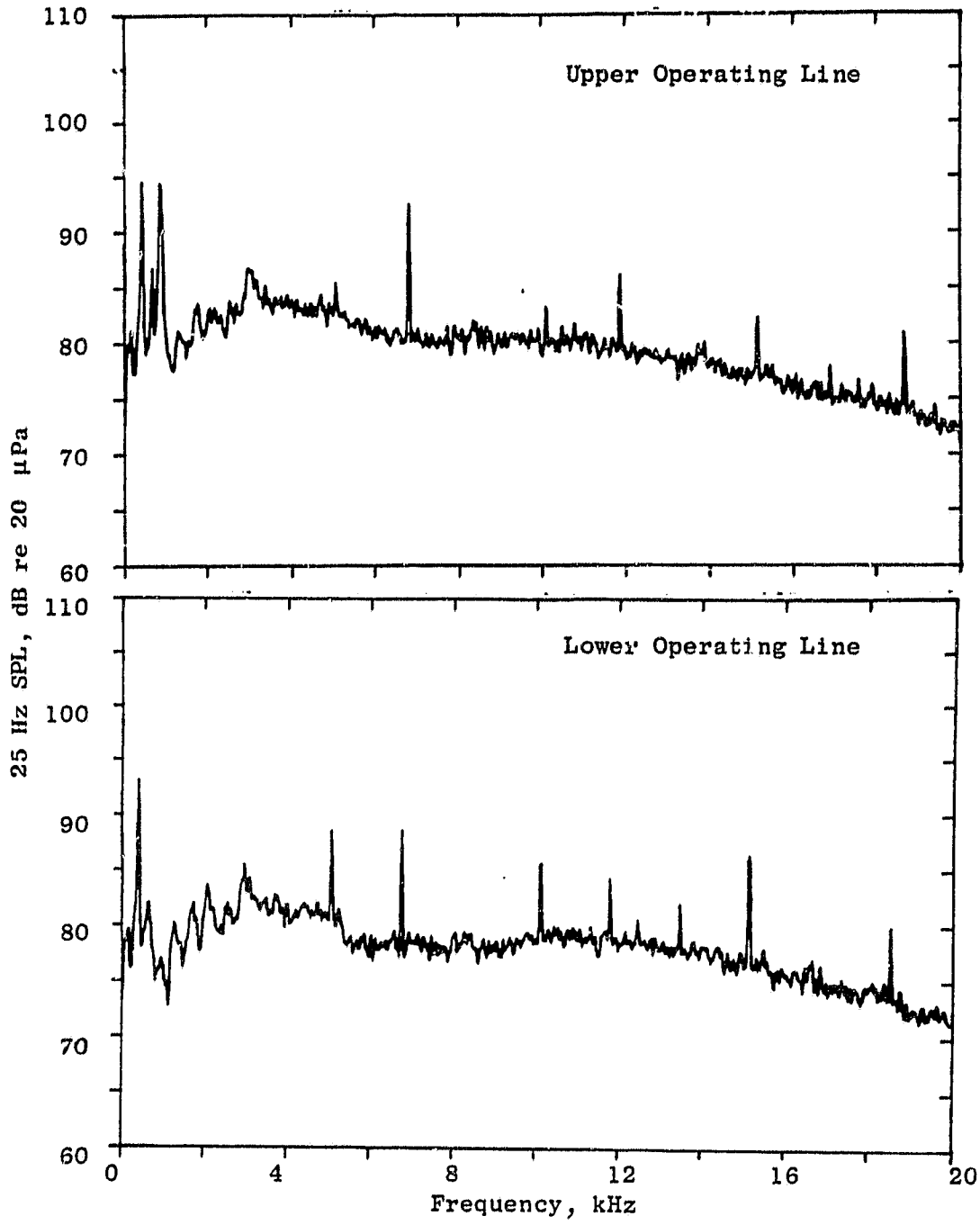

Figure 54. Comparison of Narrowband Spectra for Two Fan Operating Lines at Subsonic Tip Speed.

- 50° Noise Emission Angle
- 14.5 Foot Microphone
- Outdoor (TCS)
- Straight Diffusing Hard-Wall Inlet
- V_T = 302 m/s (990 ft/s)

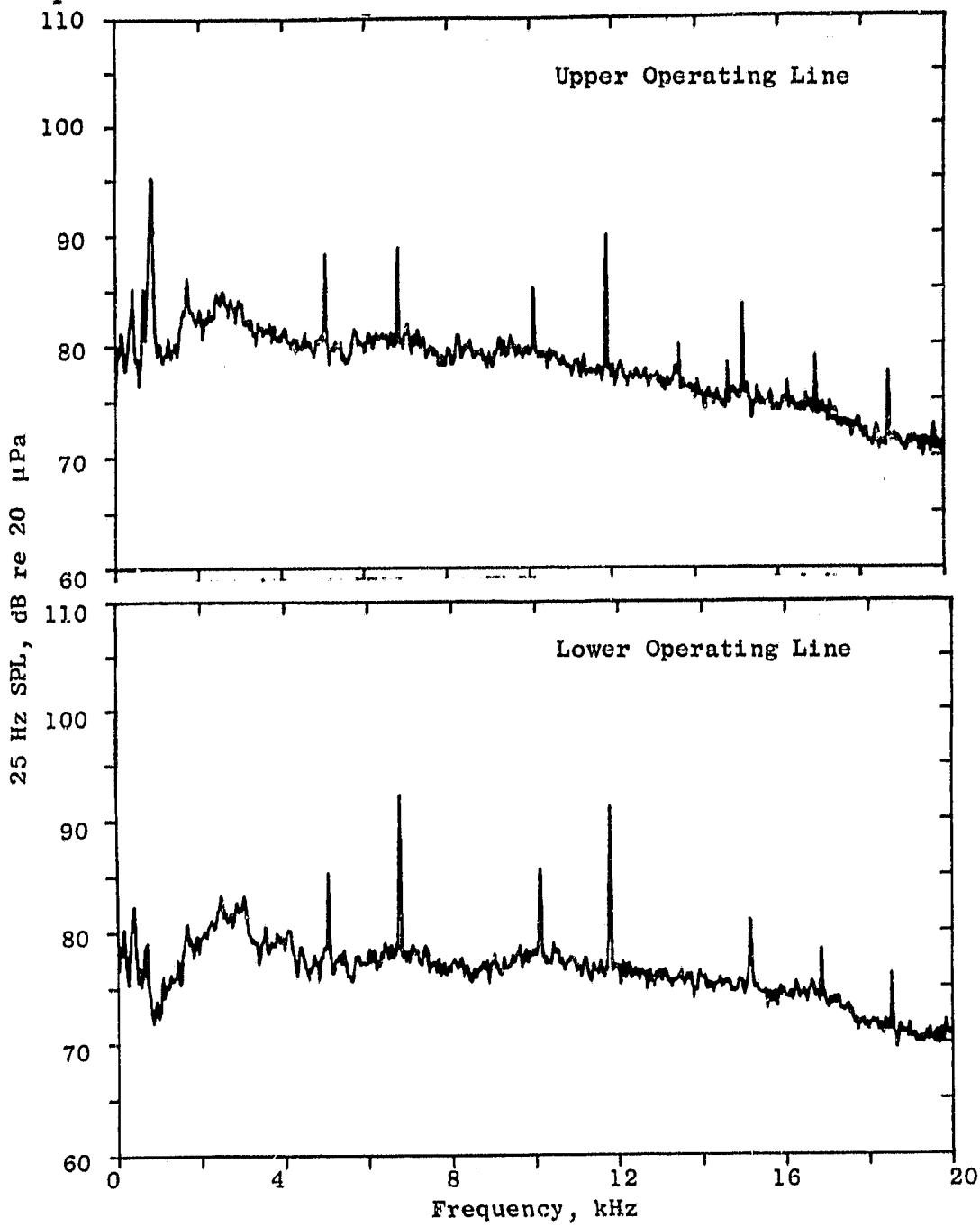

Figure 54. Comparison of Narrowband Spectra for Two Fan Operating Lines at Subsonic Tip Speed (Continued).

- 70° Noise Emission Angle
- 14.5 Foot Microphone
- Straight Diffusing Hard-Wall Inlet
- V_T = 302 m/s (990 ft/s)

Outdoor (TCS)

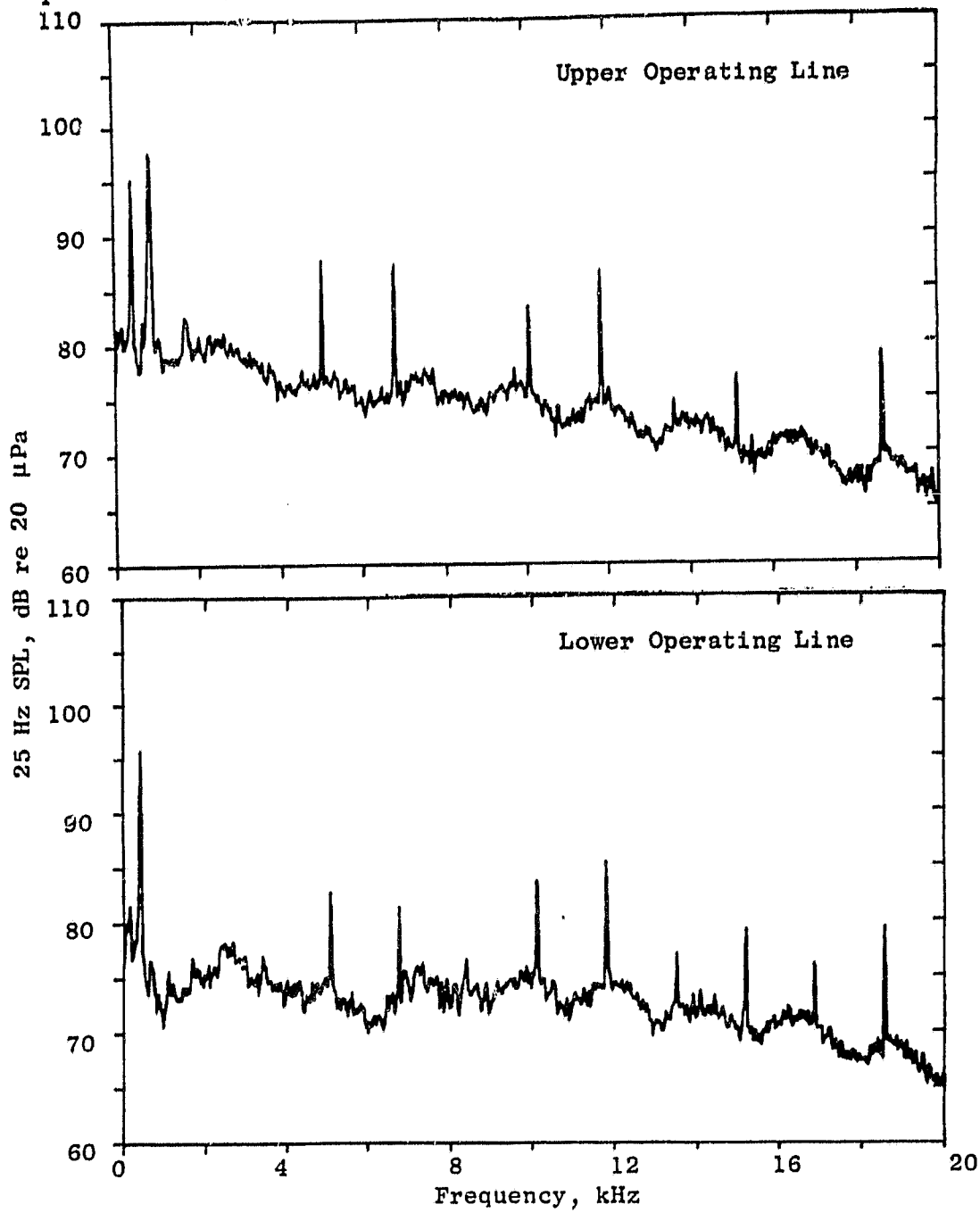

Figure 54. Comparison of Narrowband Spectra for Two Fan Operating Lines at Subsonic Tip Speed (Concluded).

- 30° Noise Emission Angle
- 14.5 Foot Microphone
- Straight Diffusing Hard-Wall Inlet
- V_T = 335 m/s (1100 ft/s)
- Outdoor (TCS)

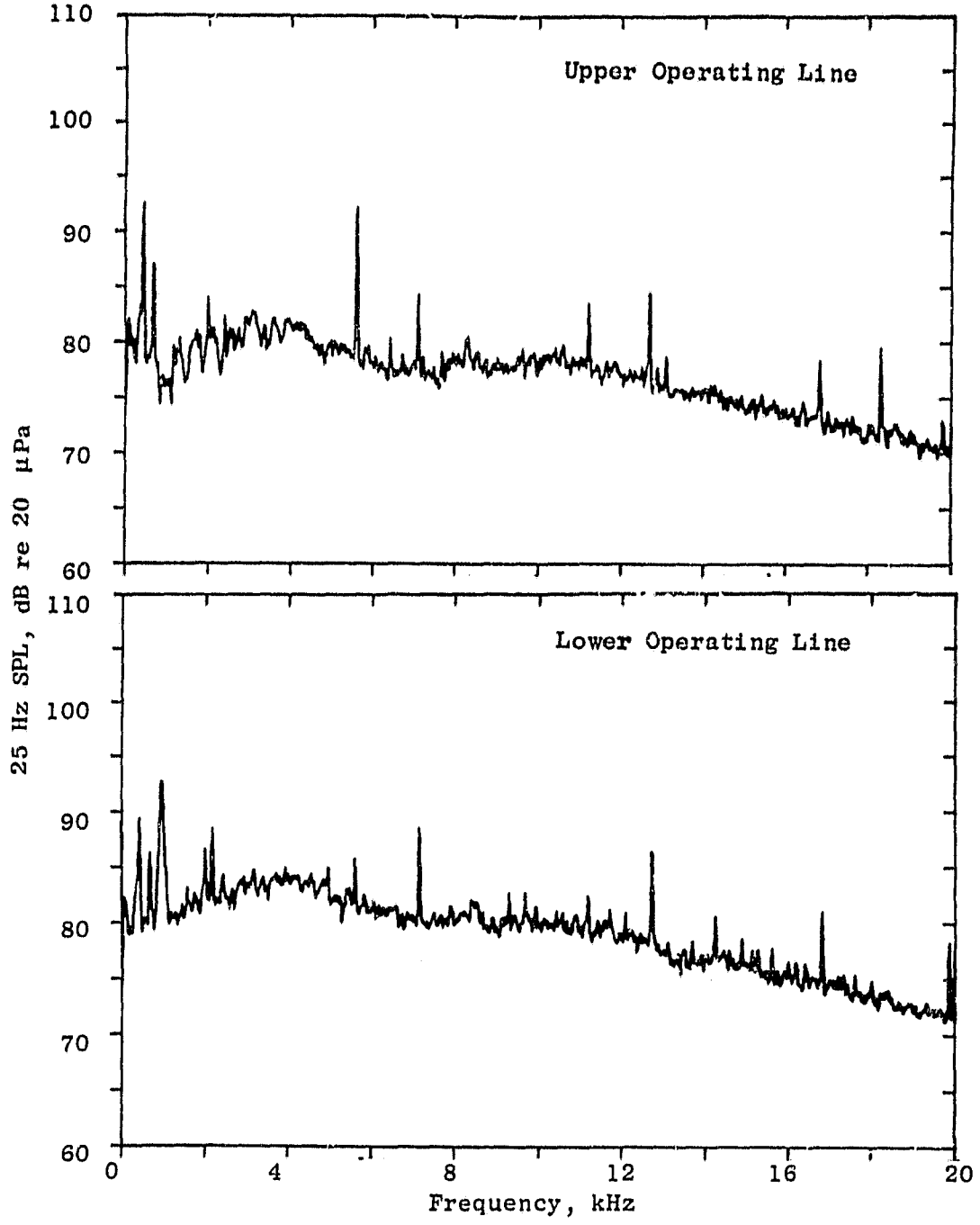

Figure 55. Comparison of Narrowband Spectra for Two Fan Operating Lines at Transonic Tip Speed.

- 50° Noise Emission Angle
- 14.5 Foot Microphone
- Straight Diffusing Hard-Wall Inlet
- V_T = 335 m/s (1100 ft/s)
- Outdoor (TCS)

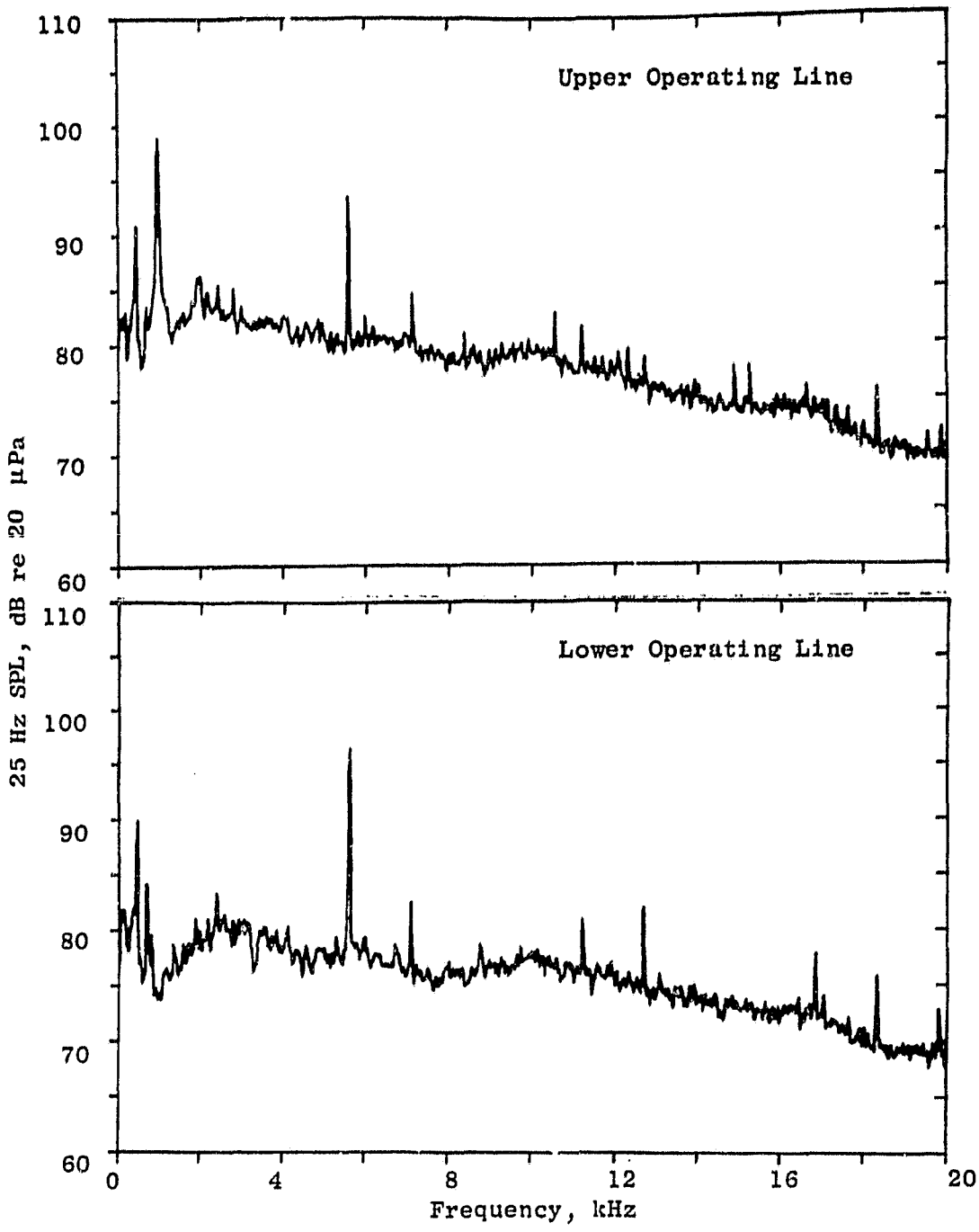

Figure 55. Comparison of Narrowband Spectra for Two Fan Operating Lines at Transonic Tip Speed (Continued).

- 60° Noise Emission Angle
- 14.5 Foot Microphone
- Straight Diffusing Hard-Wall Inlet
- V_T = 335 m/s (1100 ft/s)
- Outdoor (TCS)

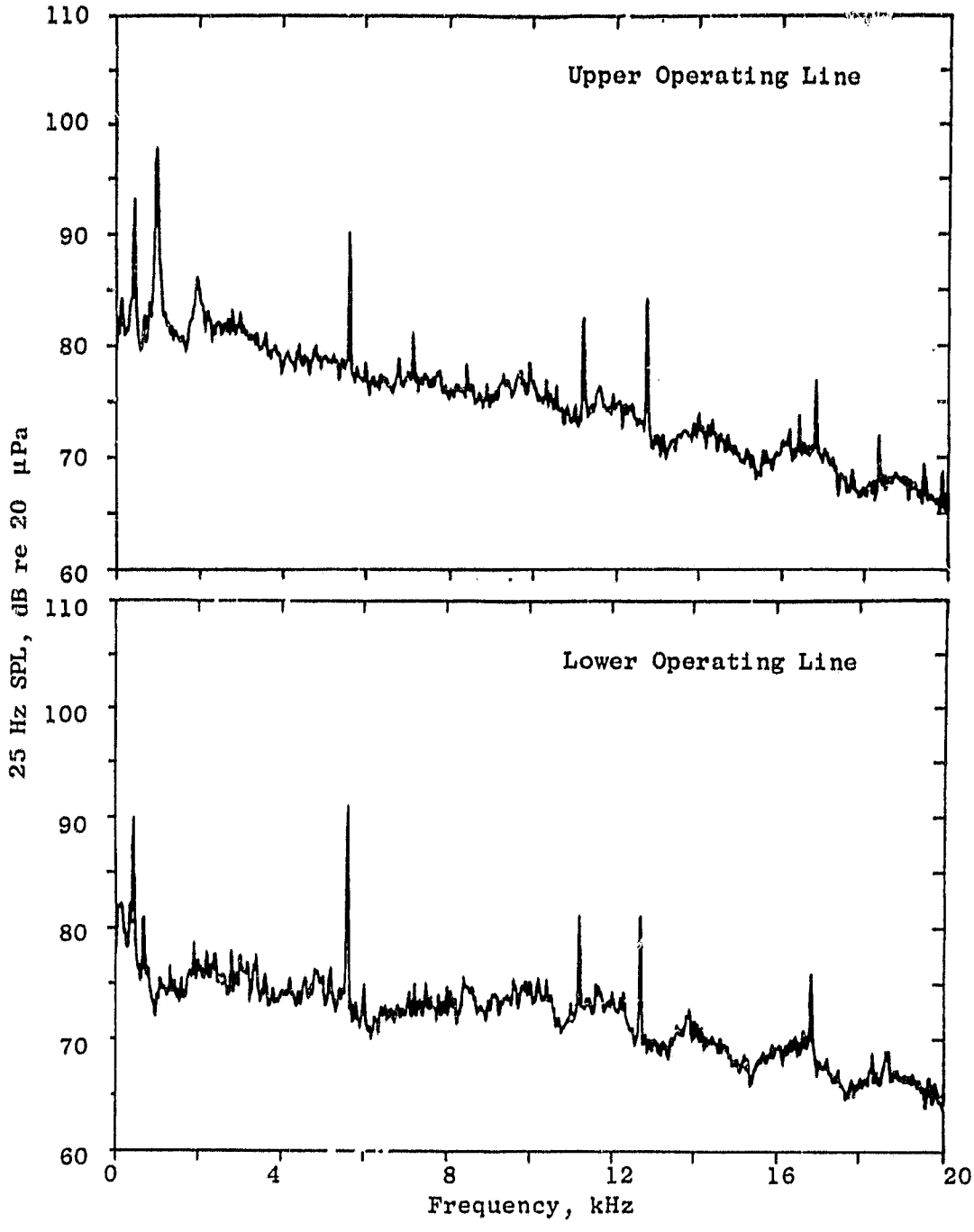

Figure 55. Comparison of Narrowband Spectra for Two Fan Operating Lines at Transonic Tip Speed (Concluded).

- 30° Noise Emission Angle
- 14.5 Foot Microphone
- Straight Diffusing Hard-Wall Inlet
- 377 m/s (1237 ft/s)
- Outdoor (TCS)

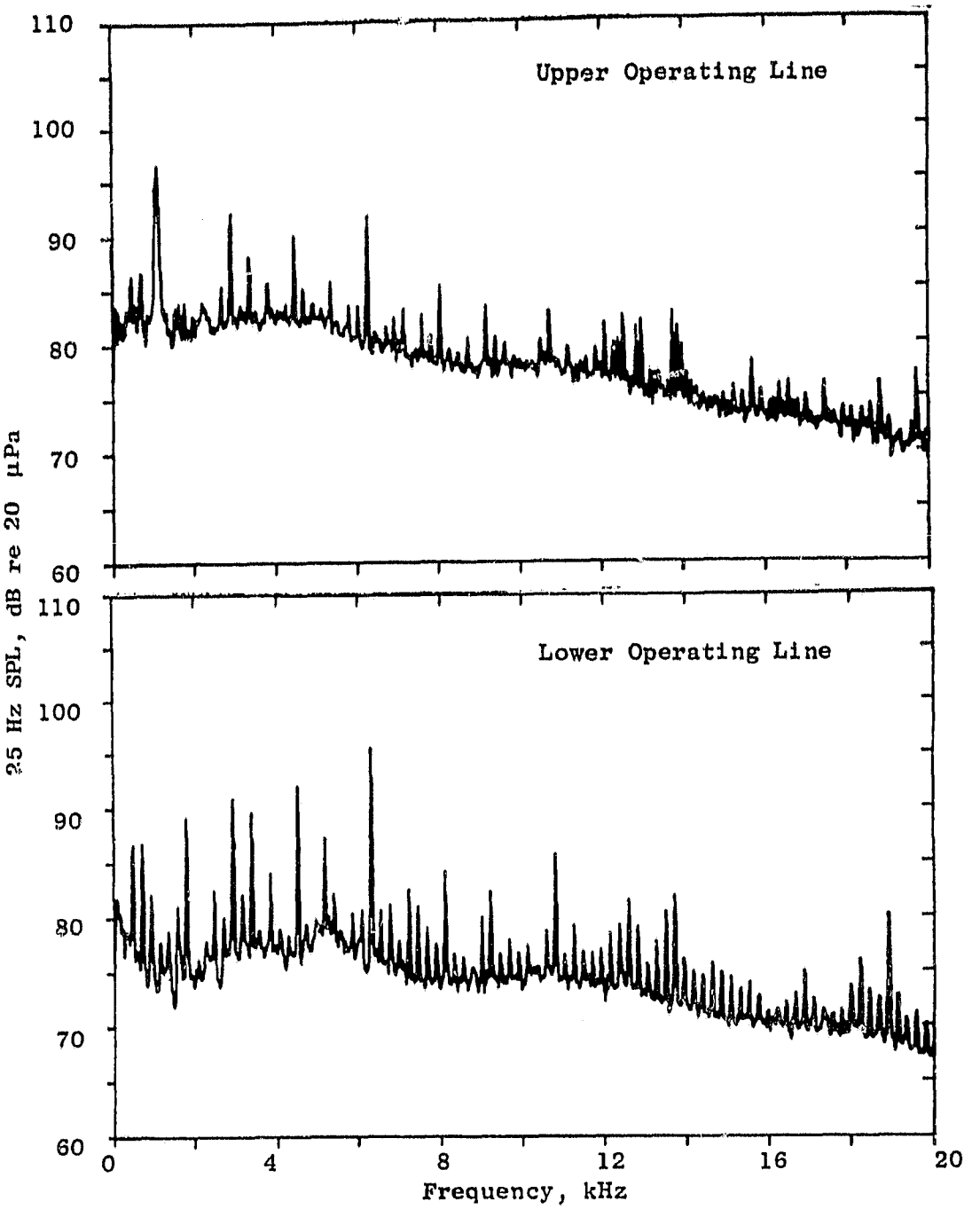

Figure 56. Comparison of Narrowband Spectra for Two Fan Operating Lines at Supersonic Tip Speed.

- 50° Noise Emission Angle
- 14.5 Foot Microphone
- Straight Diffusing Hard-Wall Inlet
- V_T = 377 m/s (1237 ft/s)
- Outdoor (TCS)

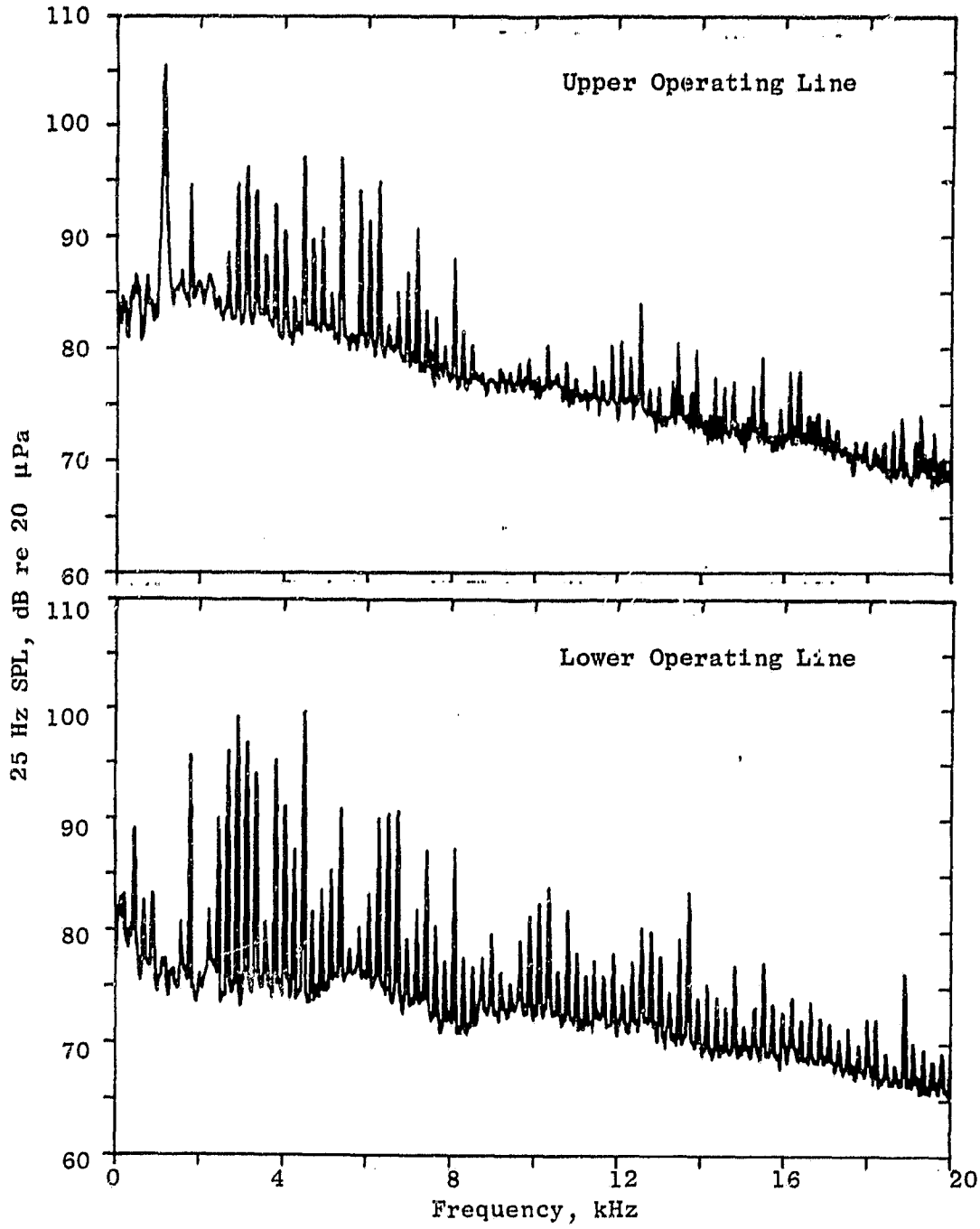

Figure 56. Comparison of Narrowband Spectra for Two Fan Operating Lines at Supersonic Tip Speed (Continued).

- 70° Noise Emission Angle
- 14.5 Foot Microphone
- Straight Diffusing Hard-Wall Inlet
- V_T = 377 m/s (1237 ft/s)
- Outdoor (TCS)

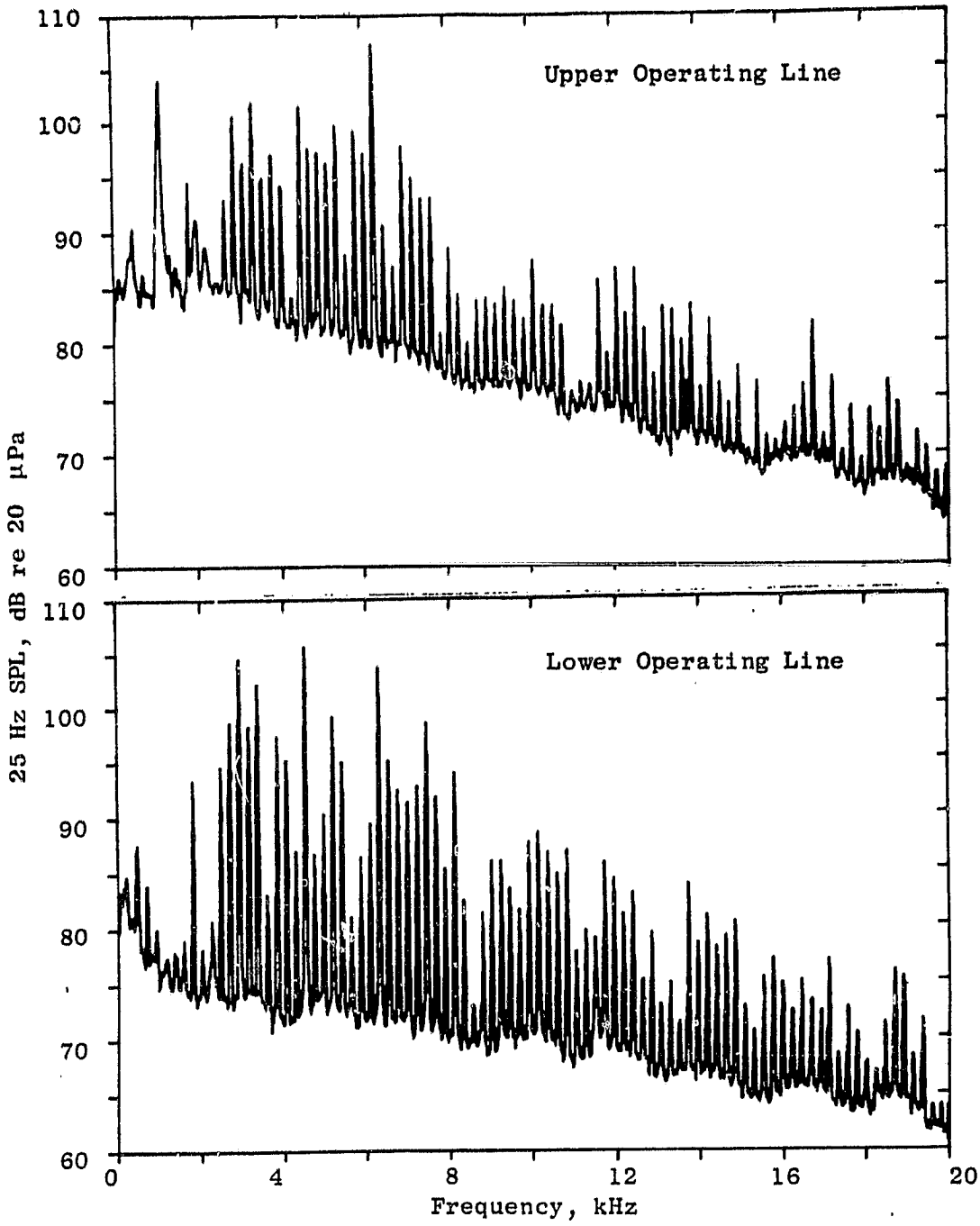

Figure 56. Comparison of Narrowband Spectra for Two Fan Operating Lines at Supersonic Tip Speed (Concluded).

treated diffusing inlet case in the wind tunnel. The scaled PNL and OASPL results are shown in Figures 57 and 58 with actual narrowband spectral information presented in Figures 59, 60, and 61. The normalized spectral differences are presented in Figure 62 where forward quadrant differences are about 3 dB independent of engine speed.

The tonal differences are shown in Figure 63 using a BPF directivity format. These plots indicate that at lower subsonic speeds the lower operating line produces less tonal noise; however, at the transonic speed the lower operating line yields a higher tonal contribution consistent with the duct modes in the engine speed region being cut on for the lowered operating line but cut off for the design operating line.

4.5 SUPPRESSION EFFECTS ON INLET RADIATED FAN NOISE

The major suppression effect investigated during the conduct of this test program was the inlet acoustic suppression attributable to acoustic treatment in the diffusing section of the inlet. The treatment utilized, and described in Section 3.0, was selected to be effective in suppressing the fan BPF tonal component. The other inlet suppression effect studied to a lesser degree was the acceleration suppression achieved by the diffusing nature of the inlet.

4.5.1 Inlet Treatment

The effectiveness of the inlet treatment on system noise parameters is displayed in Figures 64 and 65. The treatment was designed to be most effective in attenuating the sideline propagation of fan tone noise. This is best demonstrated at the supersonic speed where differences of 5 PNdB are noted in the 60° to 90° angular range. At subsonic and transonic speed points, differences of 3 PNdB are typical in this sideline angular range.

Although the system noise suppressions displayed are rather modest, the impact on the fan tone noise was substantially greater. Narrowband spectra are shown in Figures 66, 67, and 68 where the impact on the tone is illustrated. Utilizing the normalized narrowband differencng technique, described in Section 4.1.4, typical narrowband spectral differences at selected angles are seen in Figure 69. The effectiveness of the acoustic treatment is apparent from the results displayed in this manner.

The BPF directivities for the untreated and treated cases are displayed in Figure 70. The sideline attenuation effectiveness is dramatically demonstrated by these plots, as up to 20 dB tonal suppression is observed in the 60° to 90° angular range.

4.5.2 Inlet Acceleration Suppression

The suppression attainable due to inlet flow acceleration effects are examined in Figures 71, 72, and 73. These figures present the scaled PNL,

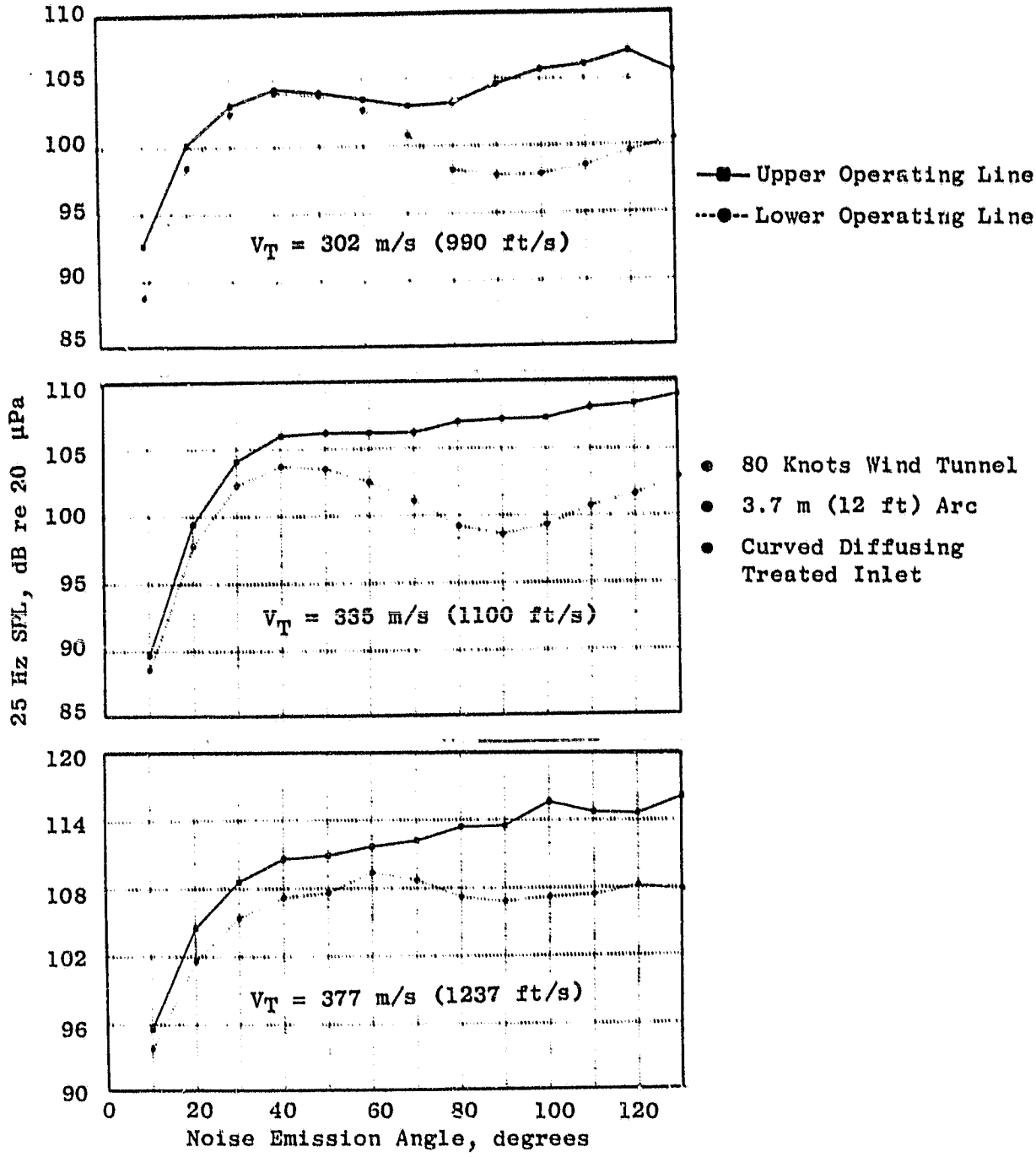

Figure 57. Scaled Perceived Noise Level Directivities for Two Fan Operating Lines.

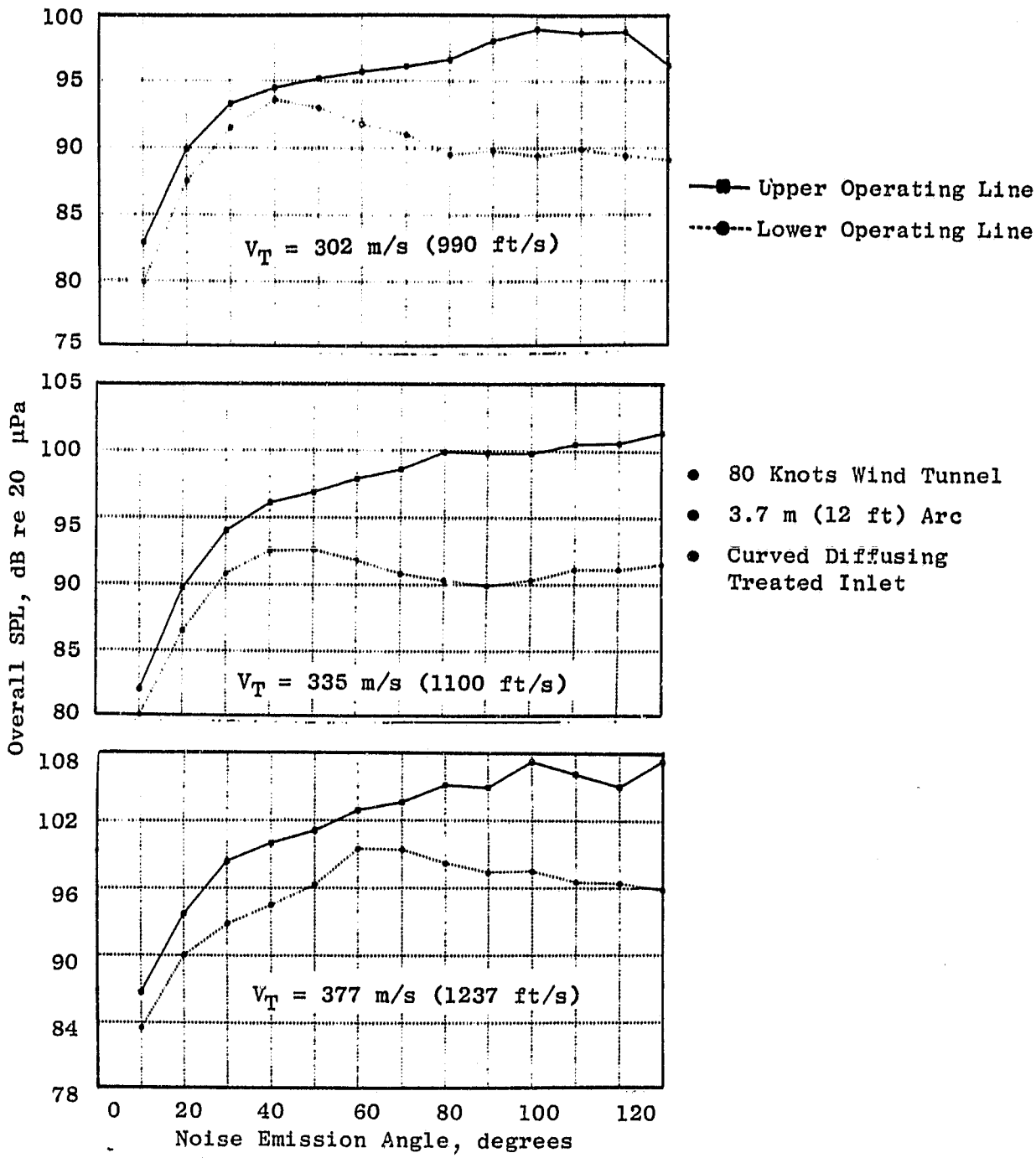

Figure 58. Scaled Overall Noise Level Directivities for Two Fan Operating Lines.

- 30° Noise Emission Angle
- 14.5 Foot Microphone
- Curved Diffusing Treated Inlet
- V_T = 302 m/s (990 ft/s)
- 80 Knots Wind Tunnel

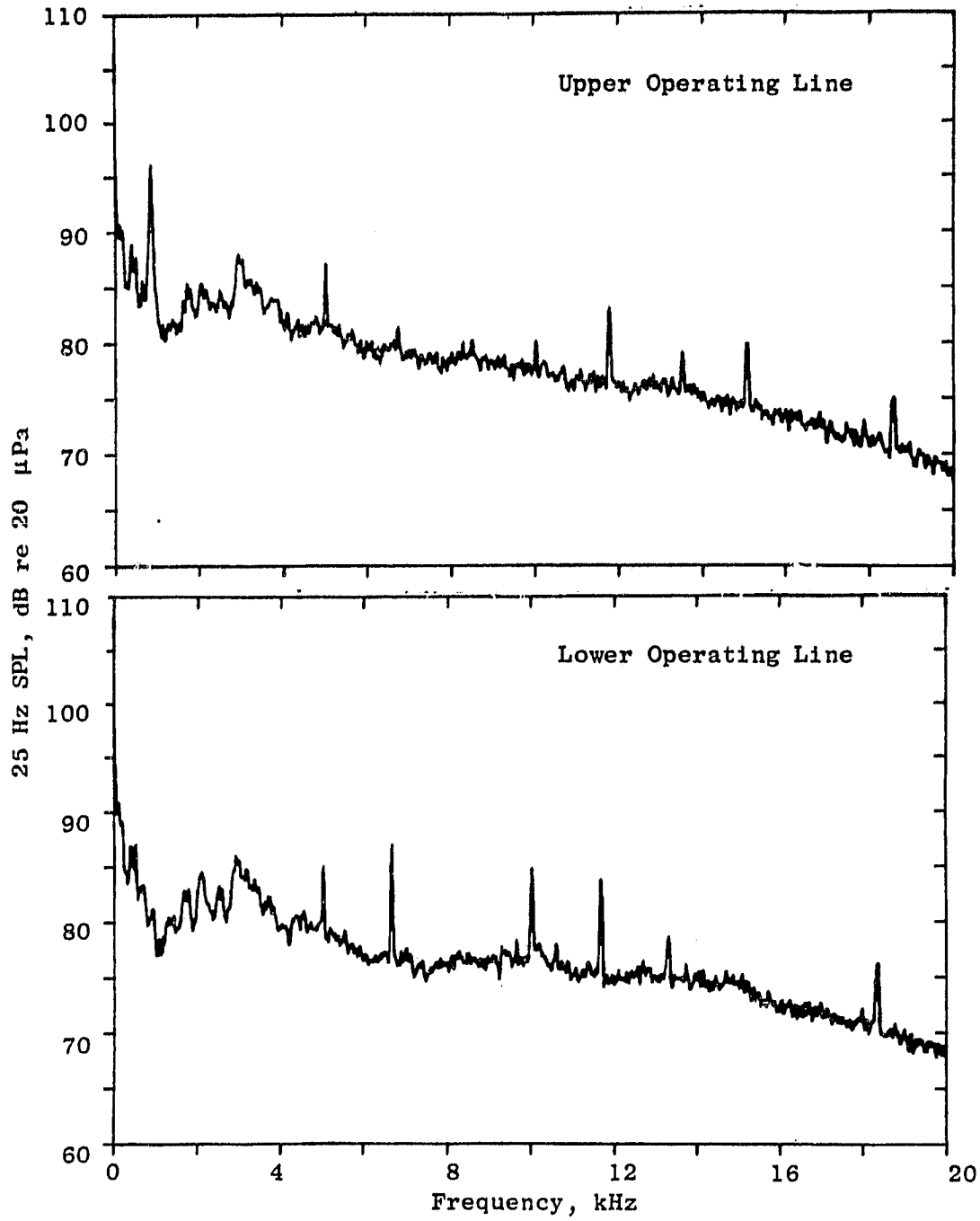

Figure 59. Comparison of Narrowband Spectra for Two Fan Operating Lines at Subsonic Tip Speed.

- 50° Noise Emission Angle
- 14.5 Foot Microphone
- Curved Diffusing Treated Inlet
- V_T = 302 m/s (990 ft/s)
- 80 Knots Wind Tunnel

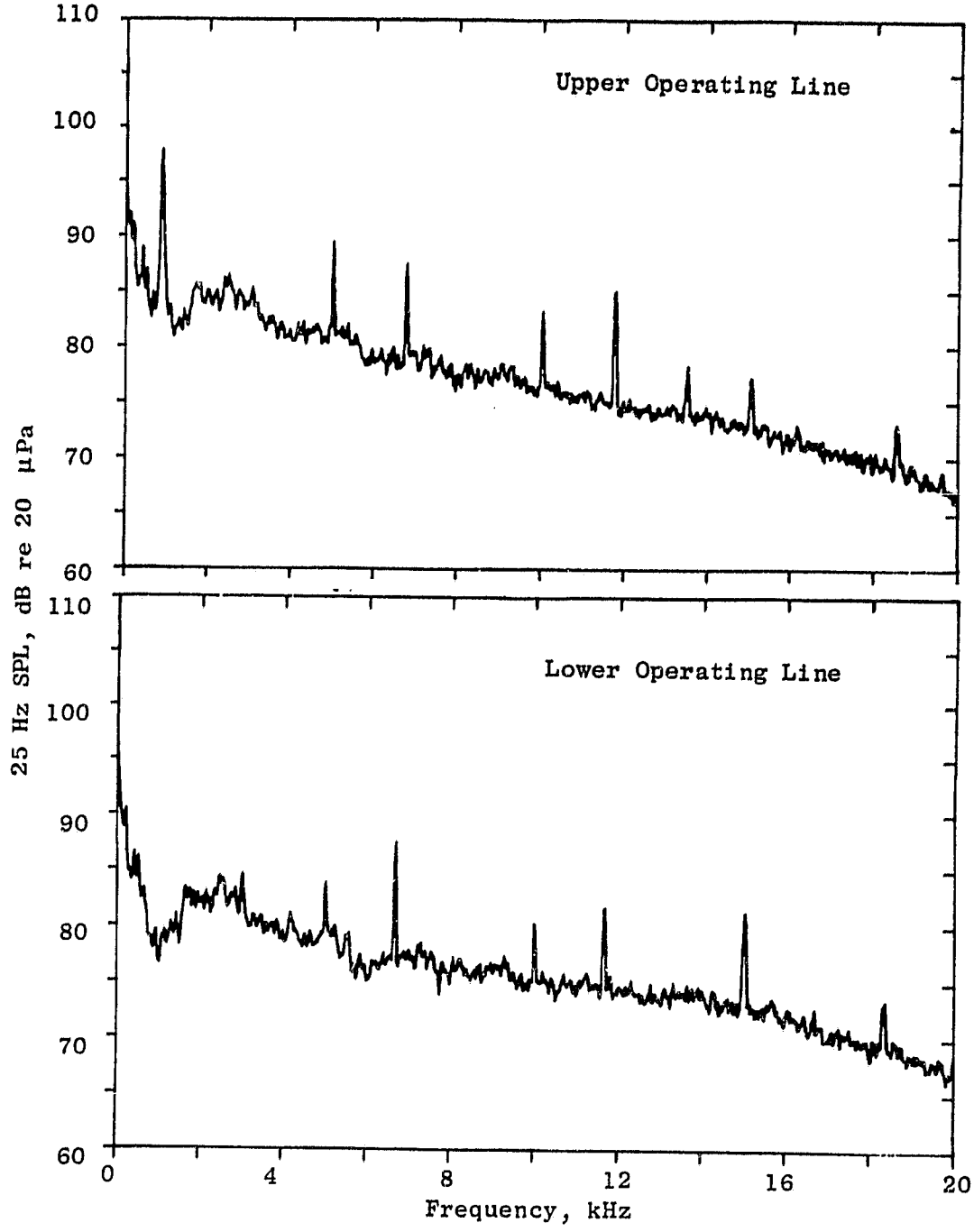

Figure 59. Comparison of Narrowband Spectra for Two Fan Operating Lines at Subsonic Tip Speed (Continued).

- 60° Noise Emission Angle
- 14.5 Foot Microphone
- Curved Diffusing Treated Inlet
- V_T = 302 m/s (990 ft/s)
- 80 Knots Wind Tunnel

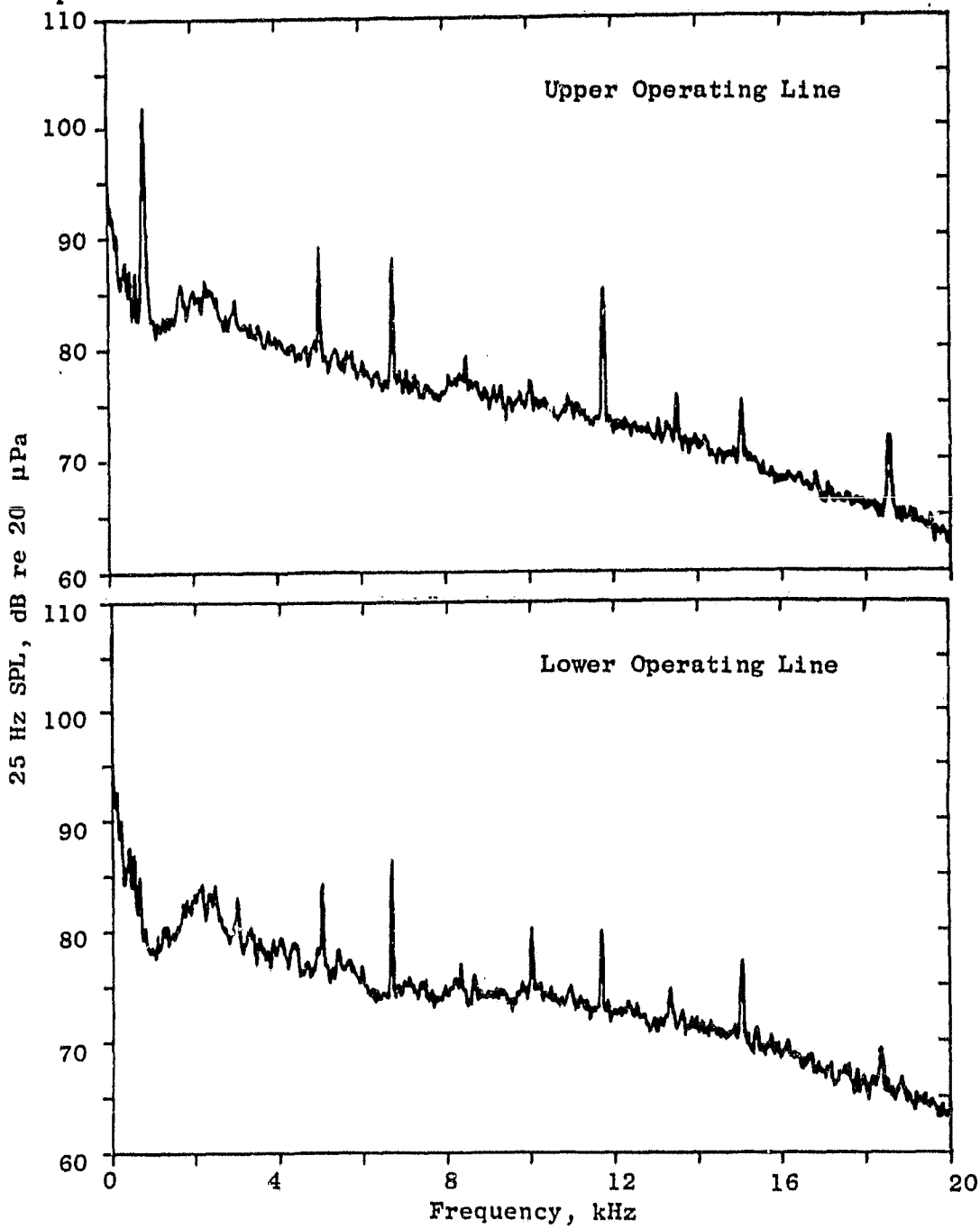

Figure 59. Comparison of Narrowband Spectra for Two Fan Operating Lines at Subsonic Tip Speed (Concluded).

- 30° Noise Emission Angle
- 14.5 Foot Microphone
- 80 Knots Wind Tunnel
- Curved Diffusing Treated Inlet
- V_T = 335 m/s (1100 ft/s)

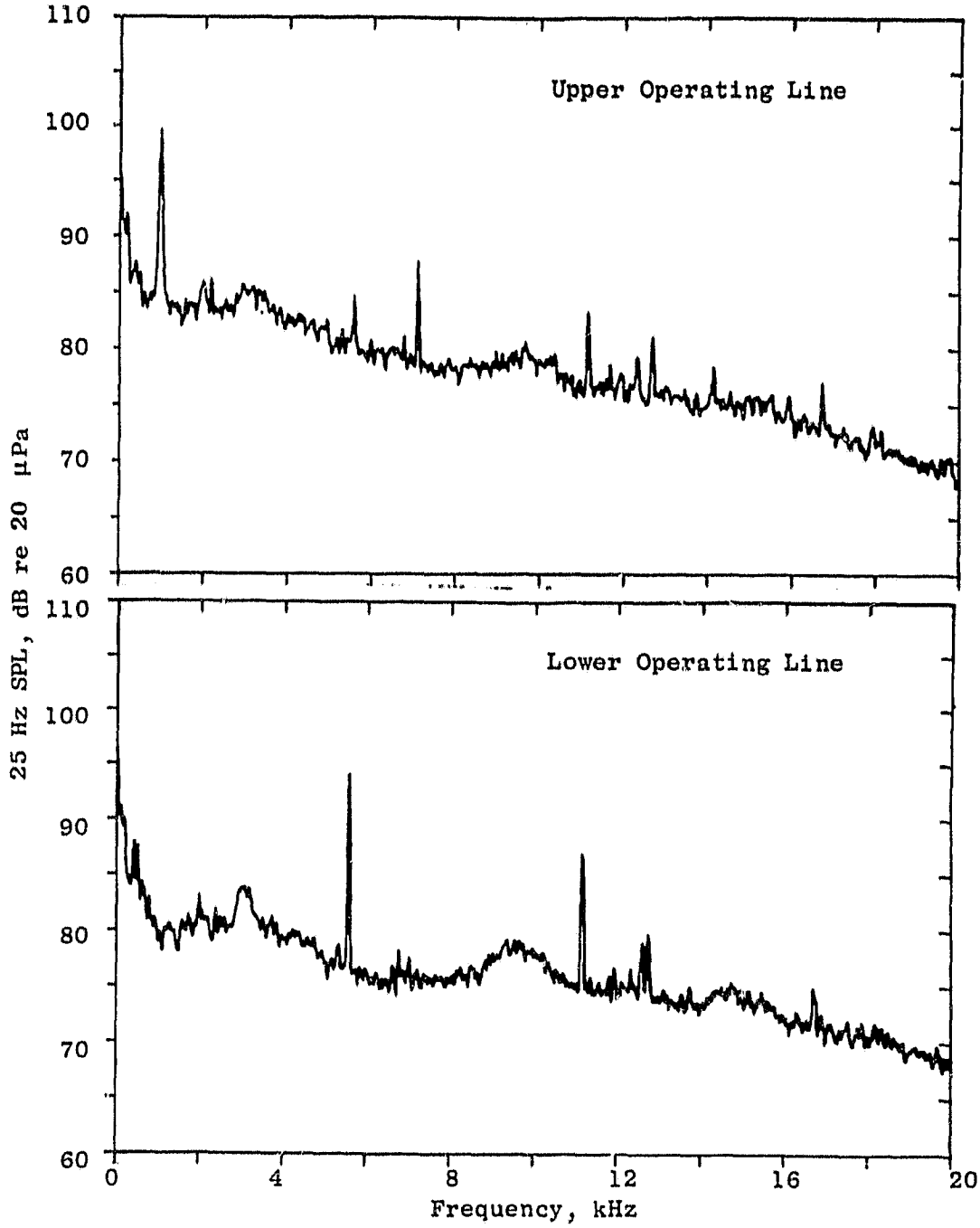

Figure 60. Comparison of Narrowband Spectra for Two Fan Operating Lines at Transonic Tip Speed.

- 50° Noise Emission Angle
- 14.5 Foot Microphone
- Curved Diffusing Treated Inlet
- V_T = 335 m/s (1100 ft/s)
- 80 Knots Wind Tunnel

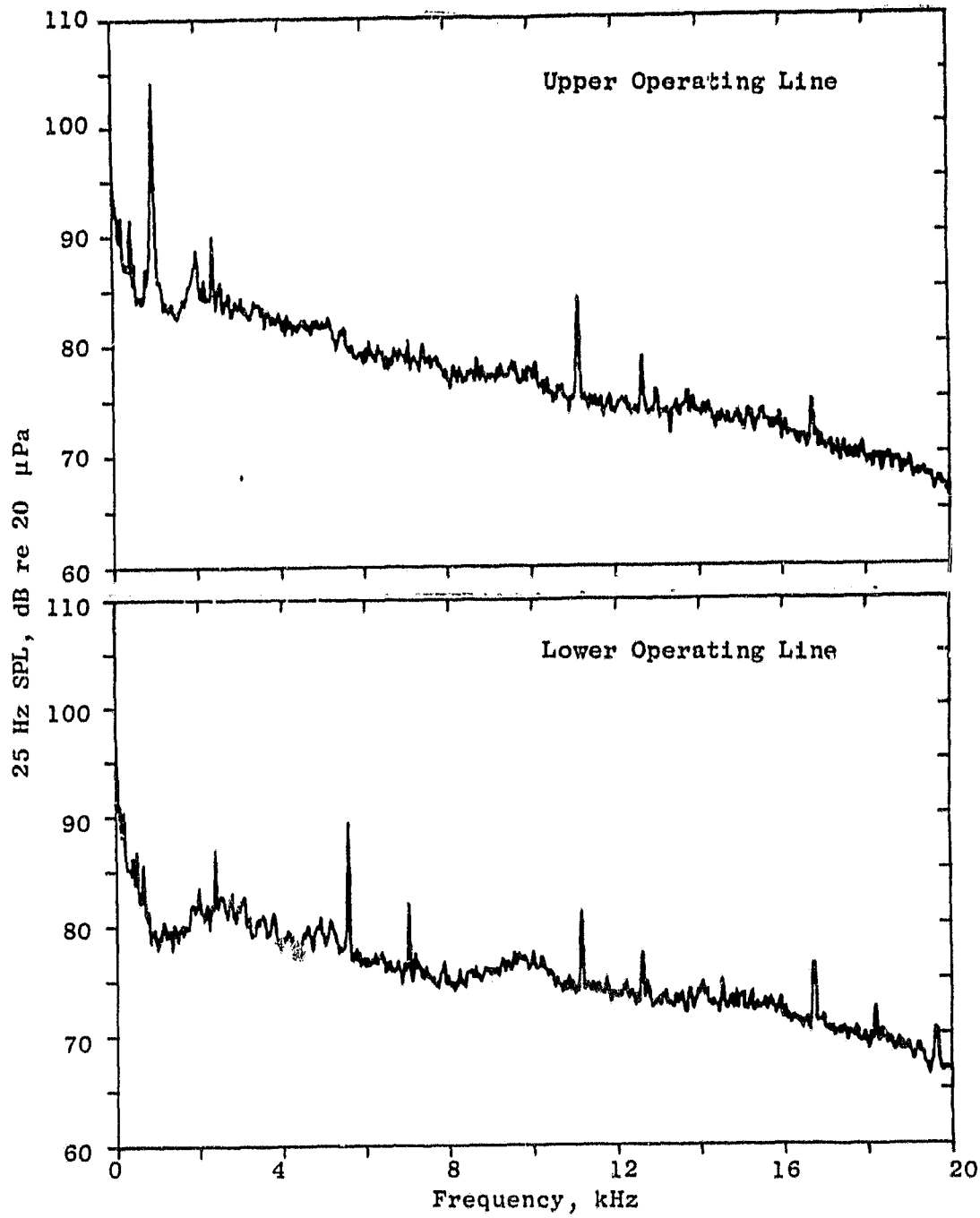

Figure 60. Comparison of Narrowband Spectra for Two Fan Operating Lines at Transonic Tip Speed (Continued).

- 60° Noise Emission Angle
- 14.5 Foot Microphone
- 80 Knots Wind Tunnel
- Curved Diffusing Treated Inlet
- V_T = 335 m/s (1100 ft/s)

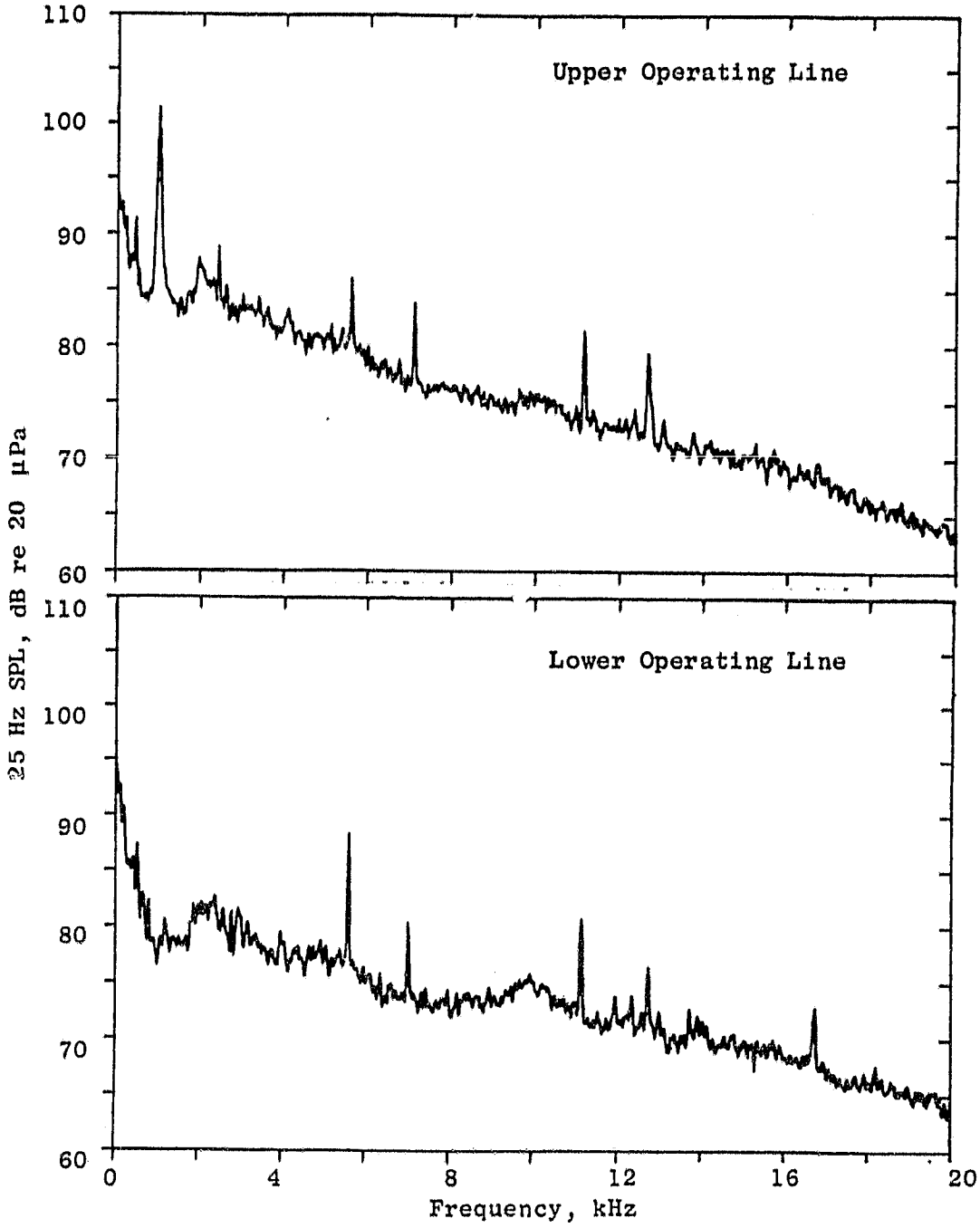

Figure 60. Comparison of Narrowband Spectra for Two Fan Operating Lines at Transonic Tip Speed (Concluded).

- 30° Noise Emission Angle
- 14.5 Foot Microphone
- Curved Diffusing Treated Inlet
- V_T = 377 m/s (1237 ft/s)
- 80 Knots Wind Tunnel

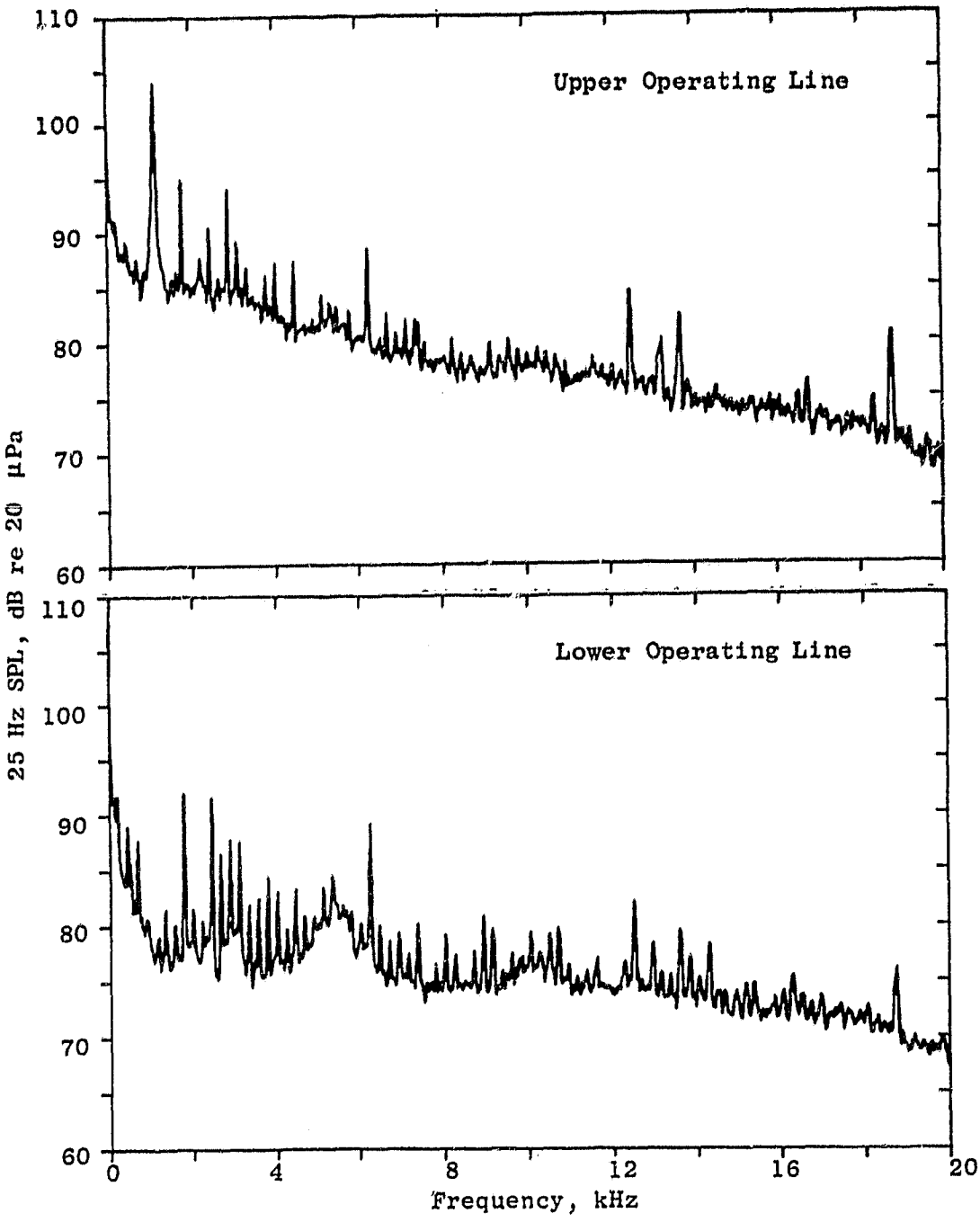

Figure 61. Comparison of Narrowband Spectra for Two Fan Operating Lines at Supersonic Tip Speed.

- 50° Noise Emission Angle
- 14.5 Foot Microphone
- Curved Diffusing Treated Inlet
- V_T = 377 m/s (1237 ft/s)
- 80 Knots Wind Tunnel

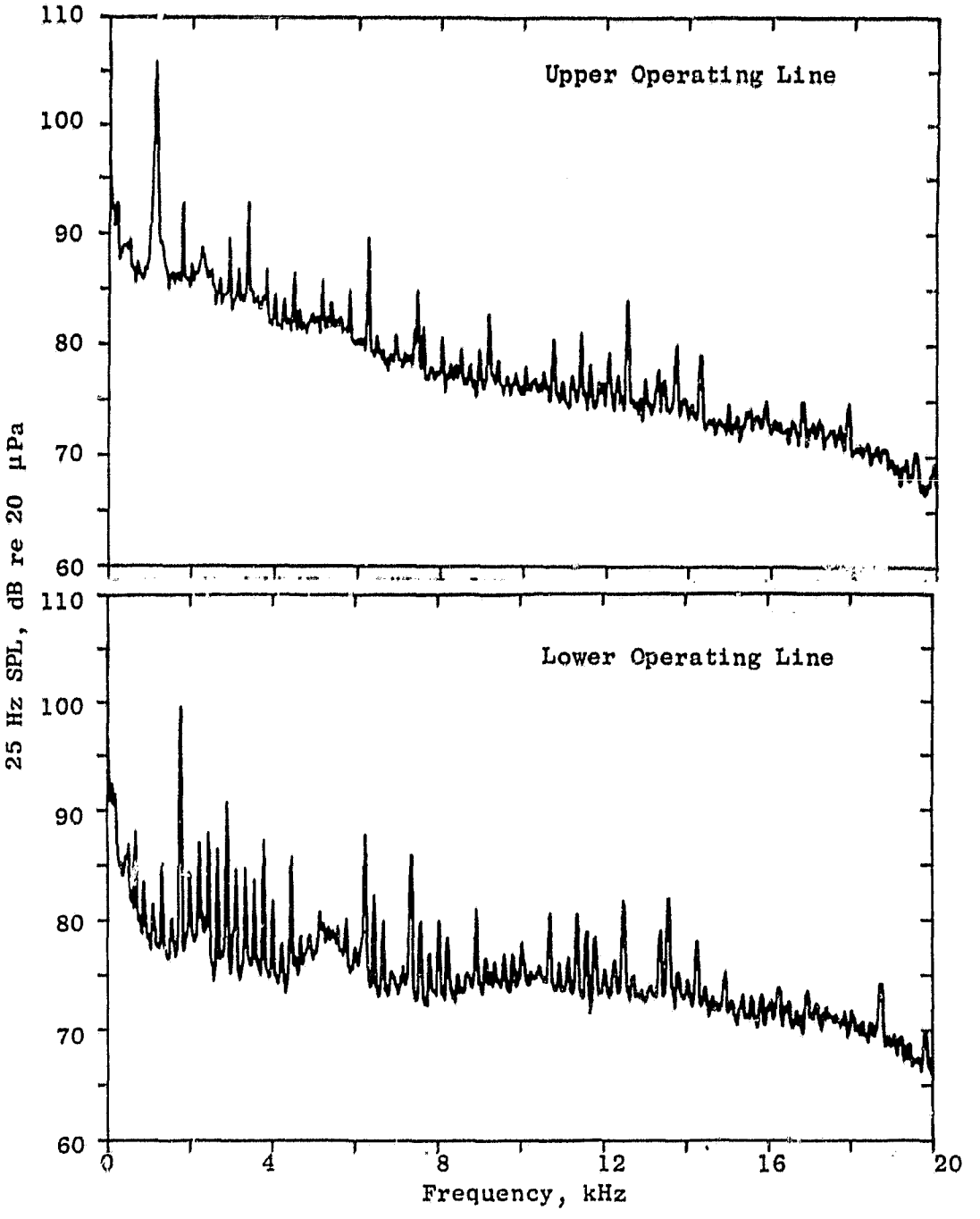

Figure 61. Comparison of Narrowband Spectra for Two Fan Operating Lines at Supersonic Tip Speed (Continued).

- 60° Noise Emission Angle
- 14.5 Foot Microphone
- 80 Knots Wind Tunnel
- Curved Diffusing Treated Inlet
- V_T = 377 m/s (1237 ft/s)

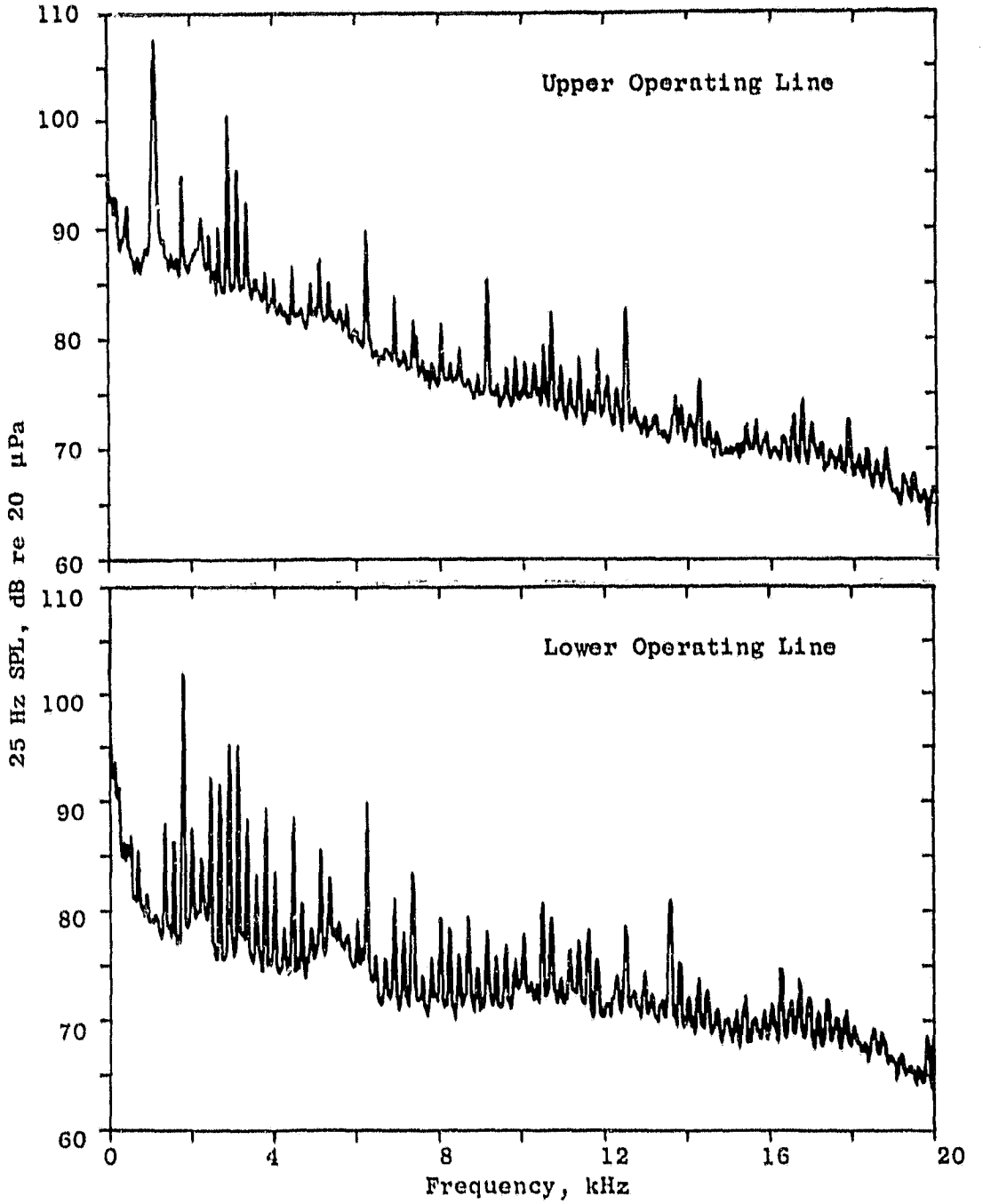

Figure 61. Comparison of Narrowband Spectra for Two Fan Operating Lines at Supersonic Tip Speed (Concluded).

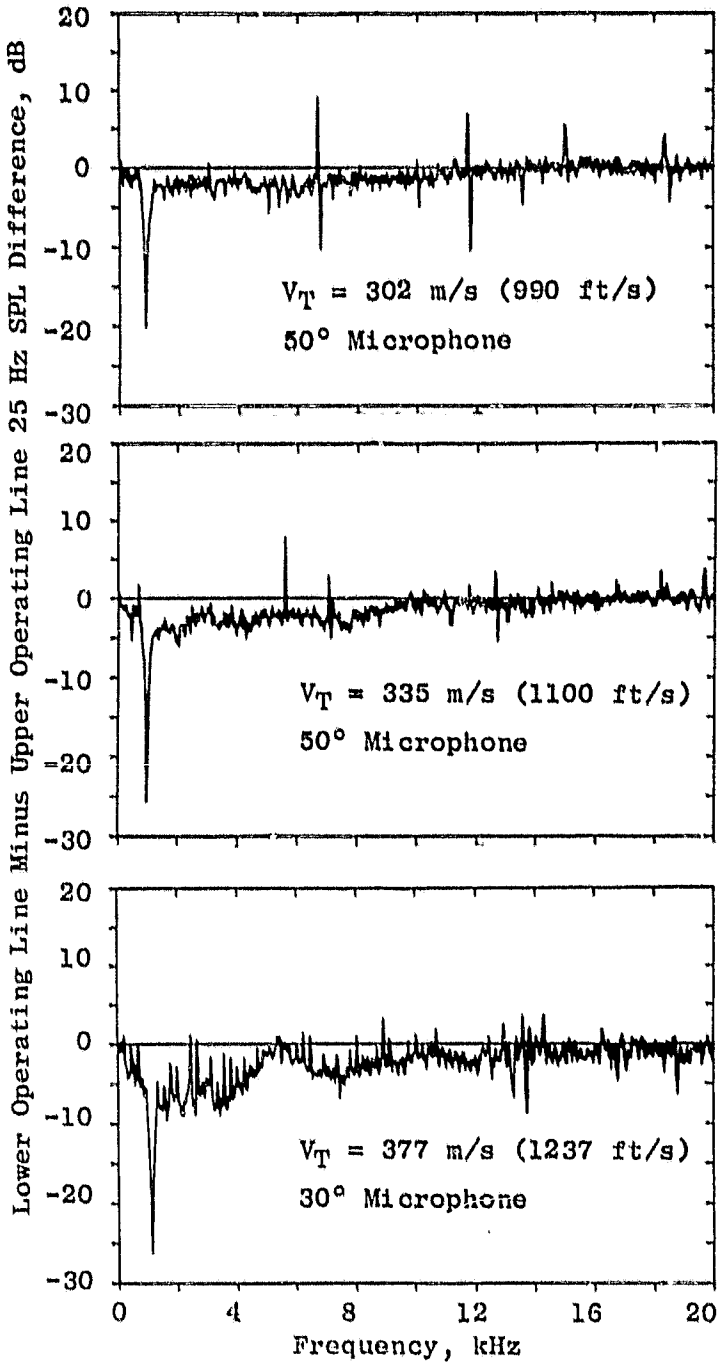

- 80 Knots Wind Tunnel
- 14.5 Foot Microphone
- Curved Diffusing Treated Inlet

Figure 62. Normalized Narrowband Spectral Differences Between Fan Operating Lines.

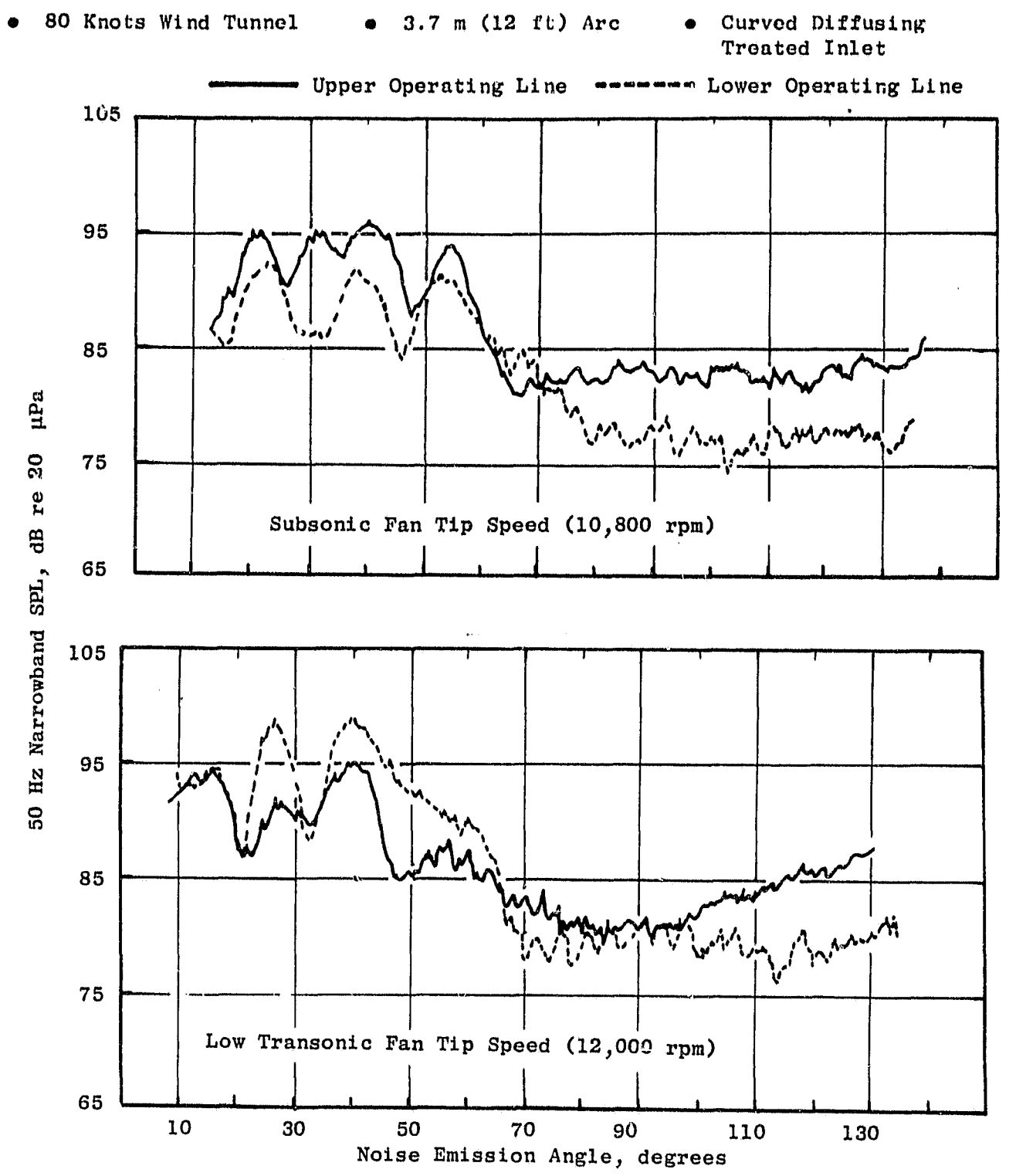

Figure 63. Narrowband BPF Directivities.

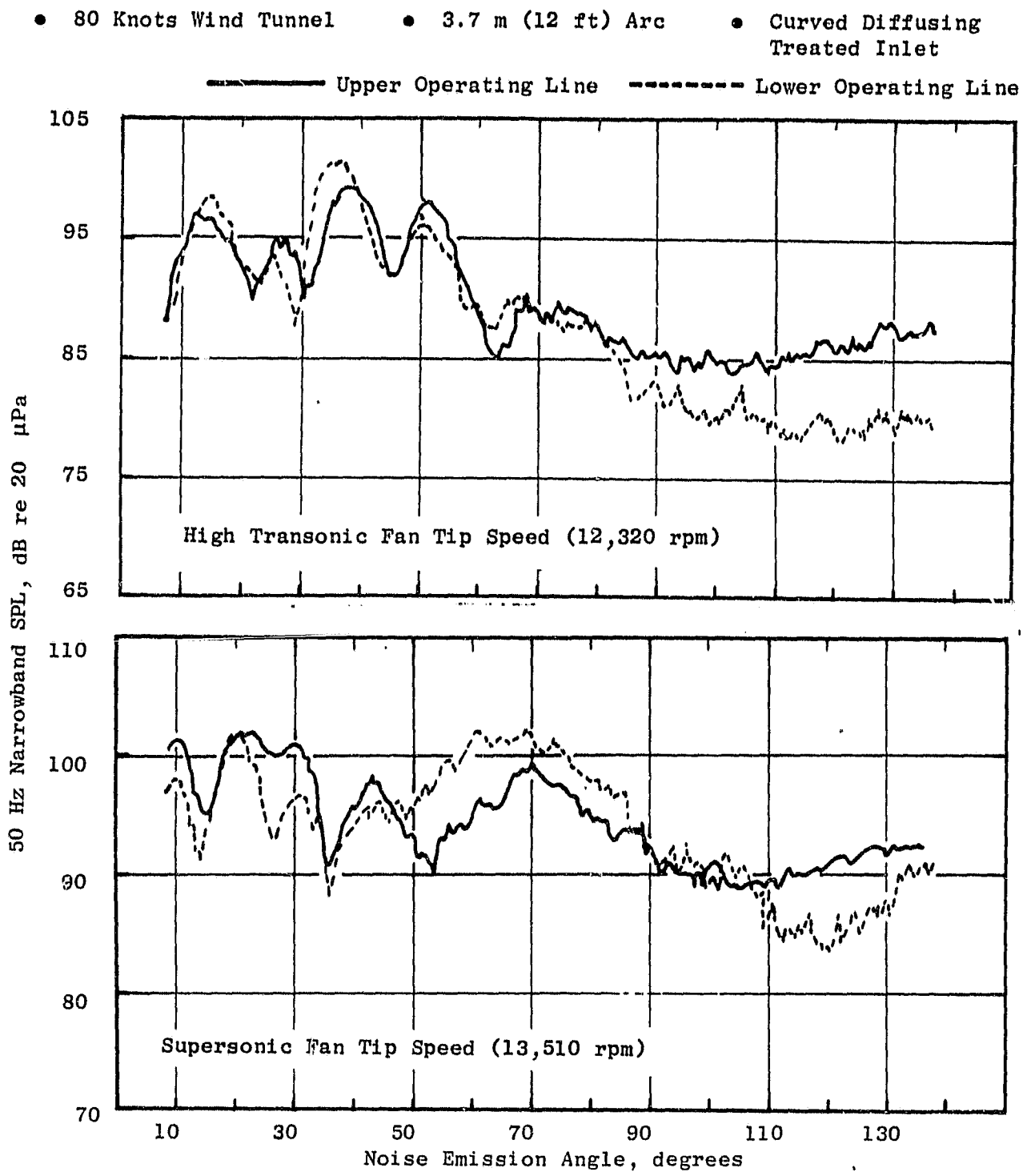

Figure 63. Narrowband BPF Directivities (Concluded).

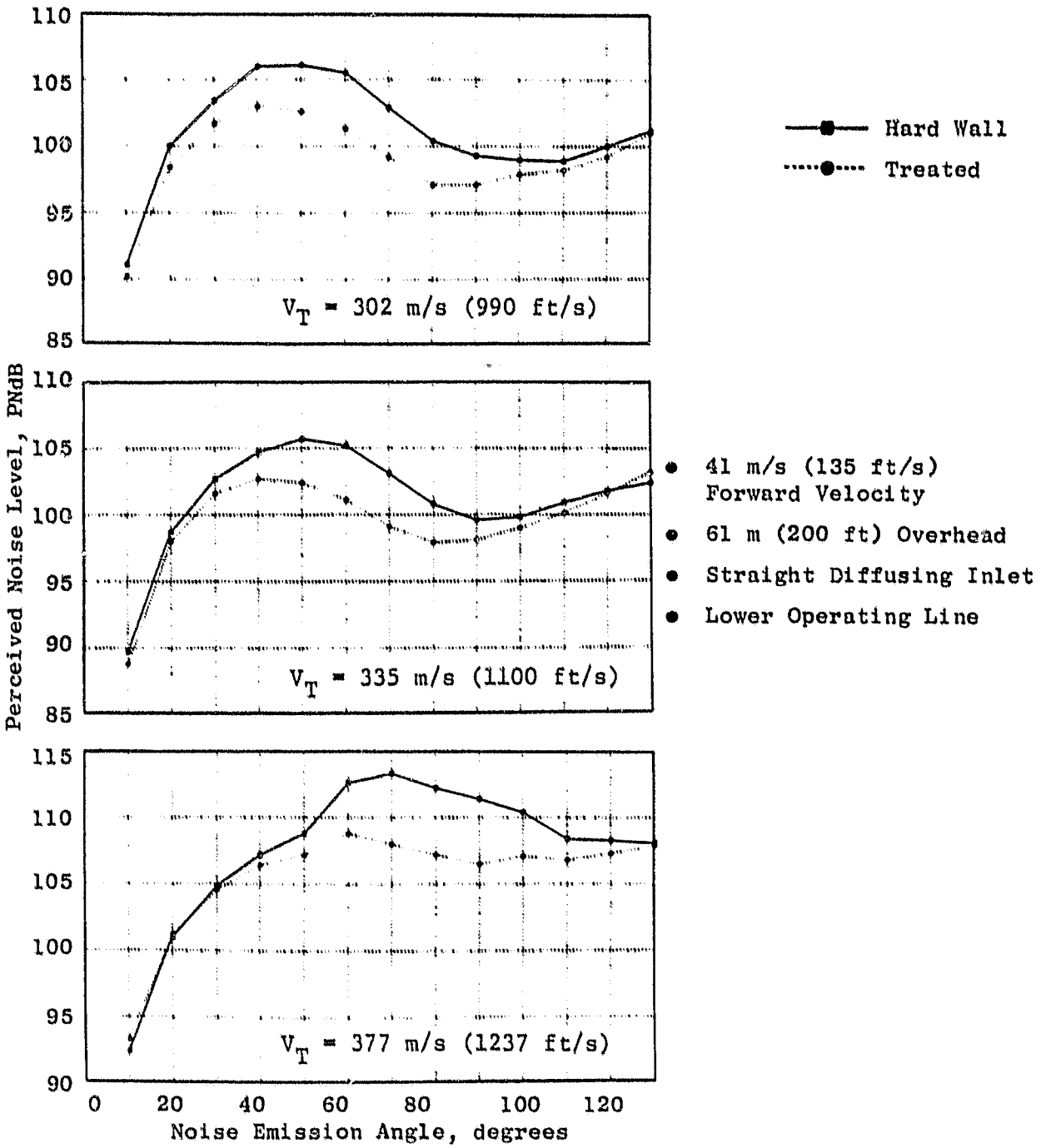

Figure 64. Scaled Perceived Noise Level Directivities for Subsonic, Transonic, and Supersonic Tip Speeds.

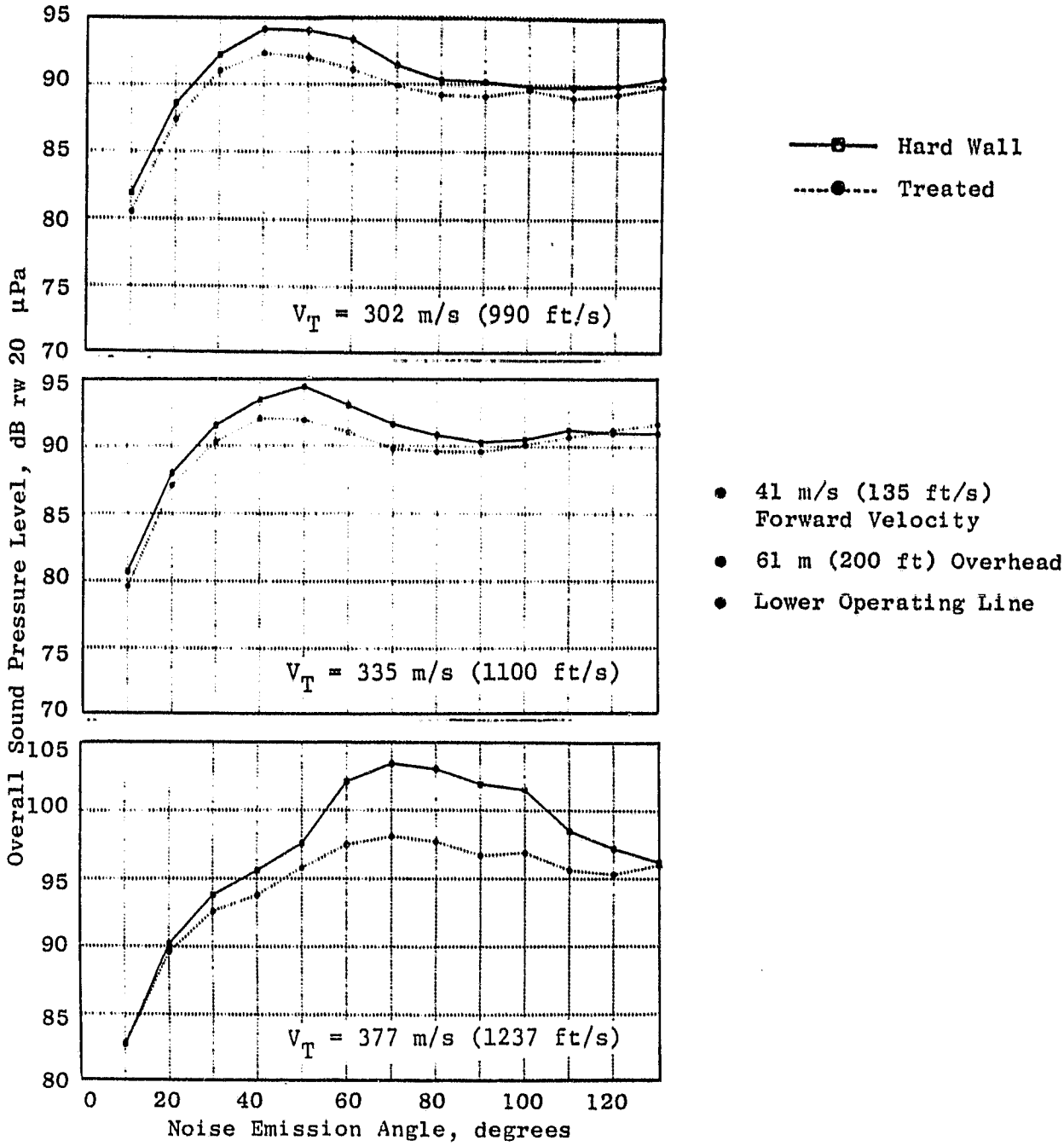

Figure 65. Scaled OASPL Directivities for Hard-Wall and Treated Straight Diffusing Inlet.

- 30° Noise Emission Angle
- 14.5 Foot Microphone
- Straight Diffusing Inlet
- V_T = 302 m/s (990 ft/s)
- 80 Knots Wind Tunnel
- Lower Operating Line

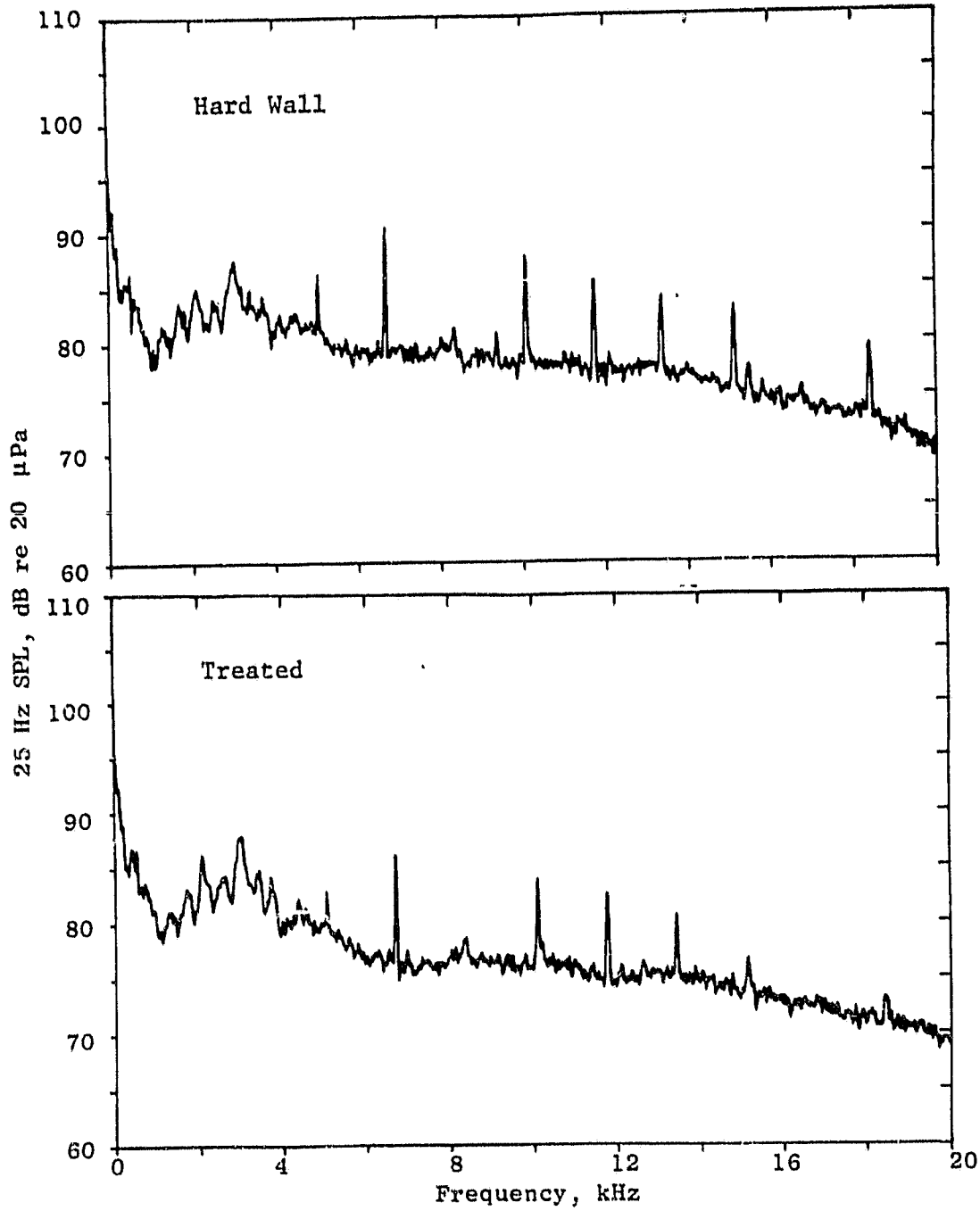

Figure 66. Comparison of Narrowband Spectra for Treated and Hard-Wall Configurations at Subsonic Tip Speed.

- 50° Noise Emission Angle
- 14.5 Foot Microphone
- Straight Diffusing Inlet
- V_T = 302 m/s (990 ft/s)
- 80 Knots Wind Tunnel
- Lower Operating Line

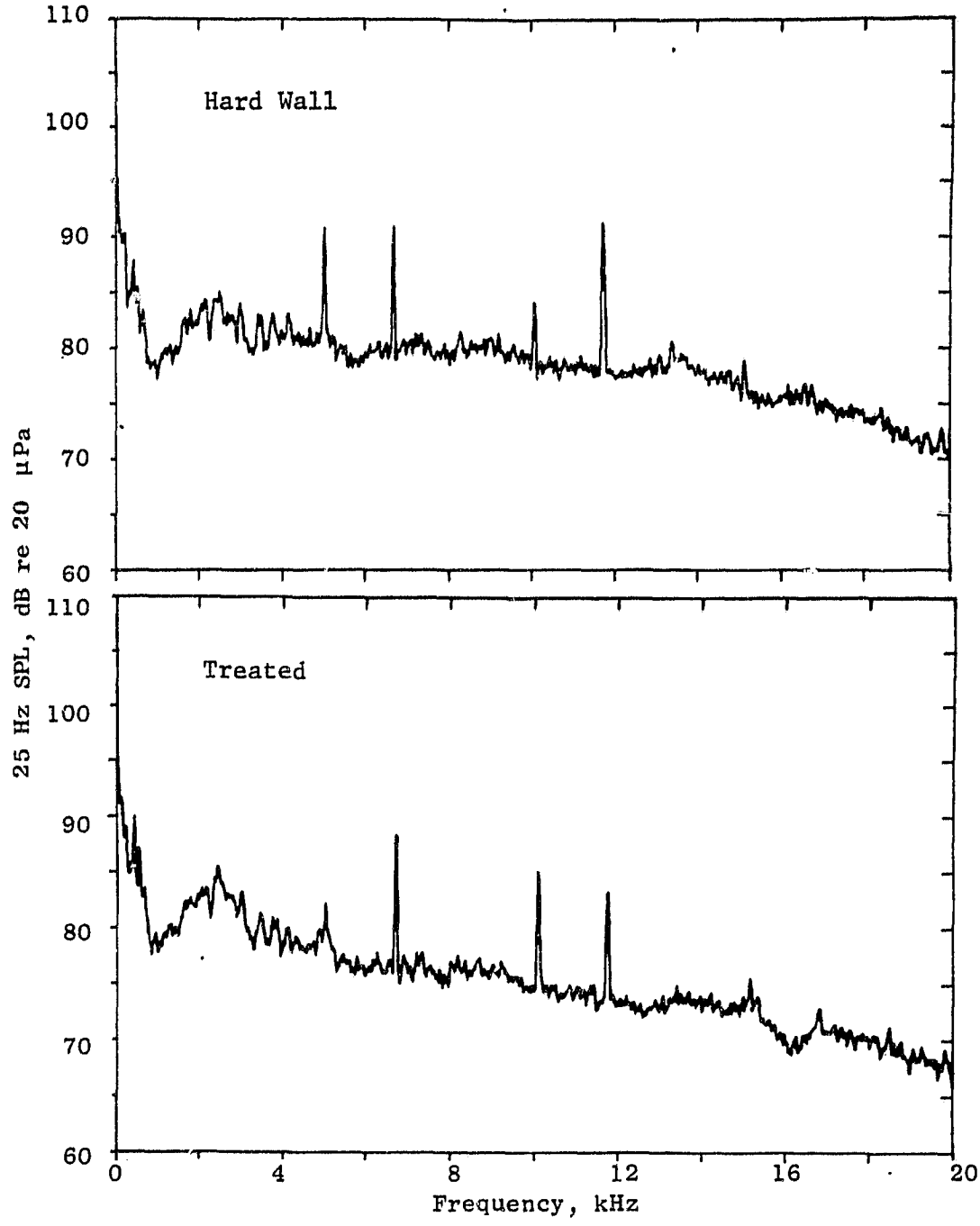

Figure 66. Comparison of Narrowband Spectra for Treated and Hard-Wall Configurations at Subsonic Tip Speed (Continued).

- 70° Noise Emission Angle
- 14.5 Foot Microphone
- Straight Diffusing Inlet
- V_T = 302 m/s (990 ft/s)
- 80 Knots Wind Tunnel
- Lower Operating Line

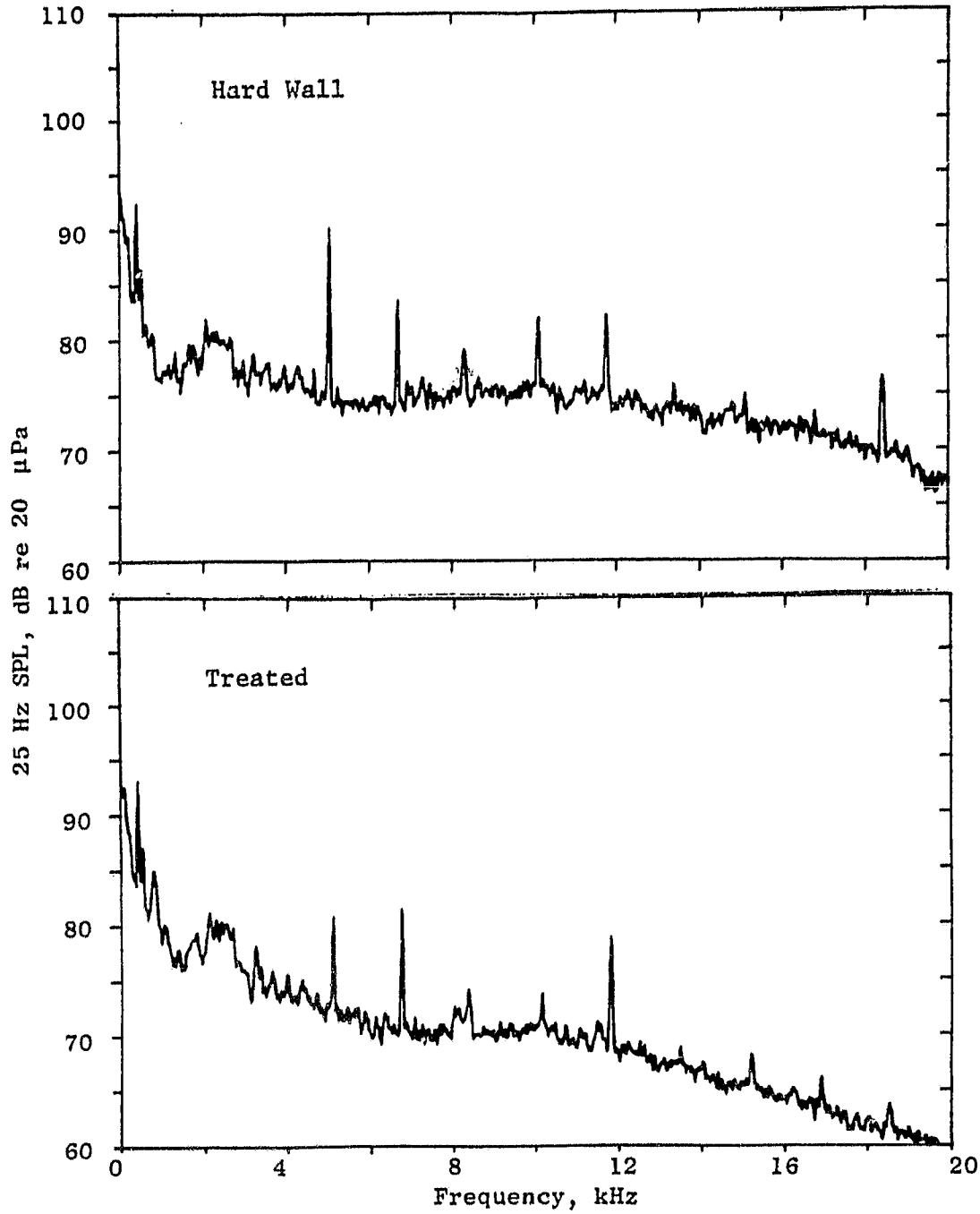

Figure 66. Comparison of Narrowband Spectra for Treated and Hard-Wall Configurations at Subsonic Tip Speed (Concluded).

- 30° Noise Emission Angle
- 14.5 Foot Microphone
- Straight Diffusing Inlet
- V_T = 335 m/s (1100 ft/s)
- 80 Knots Wind Tunnel
- Lower Operating Line

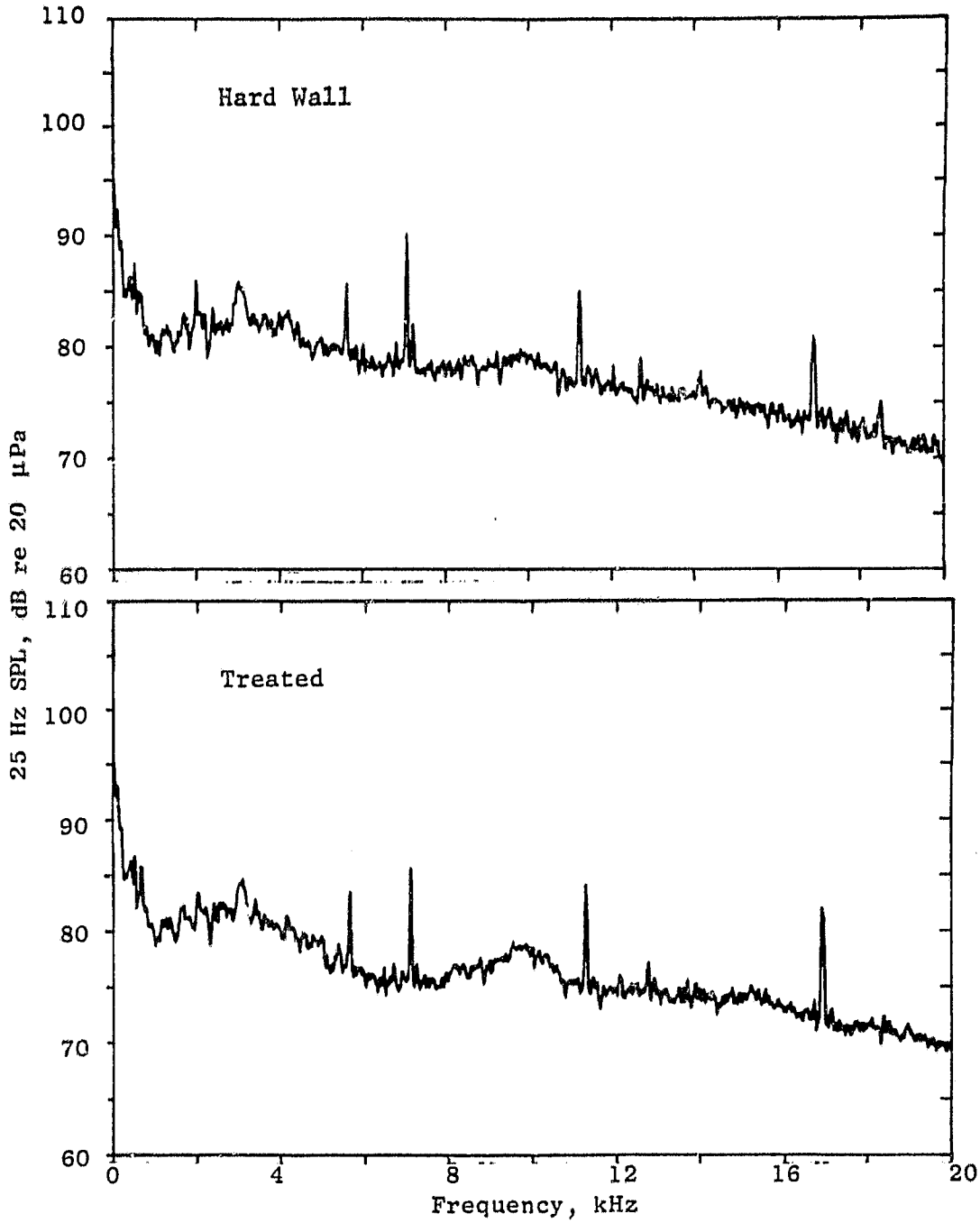

Figure 67. Comparison of Narrowband Spectra for Treated and Hard-Wall Configurations at Transonic Tip Speed.

- 50° Noise Emission Angle
- 14.5 Foot Microphone
- Straight Diffusing Inlet
- V_T = 335 m/s (1100 ft/s)
- 80 Knots Wind Tunnel
- Lower Operating Line

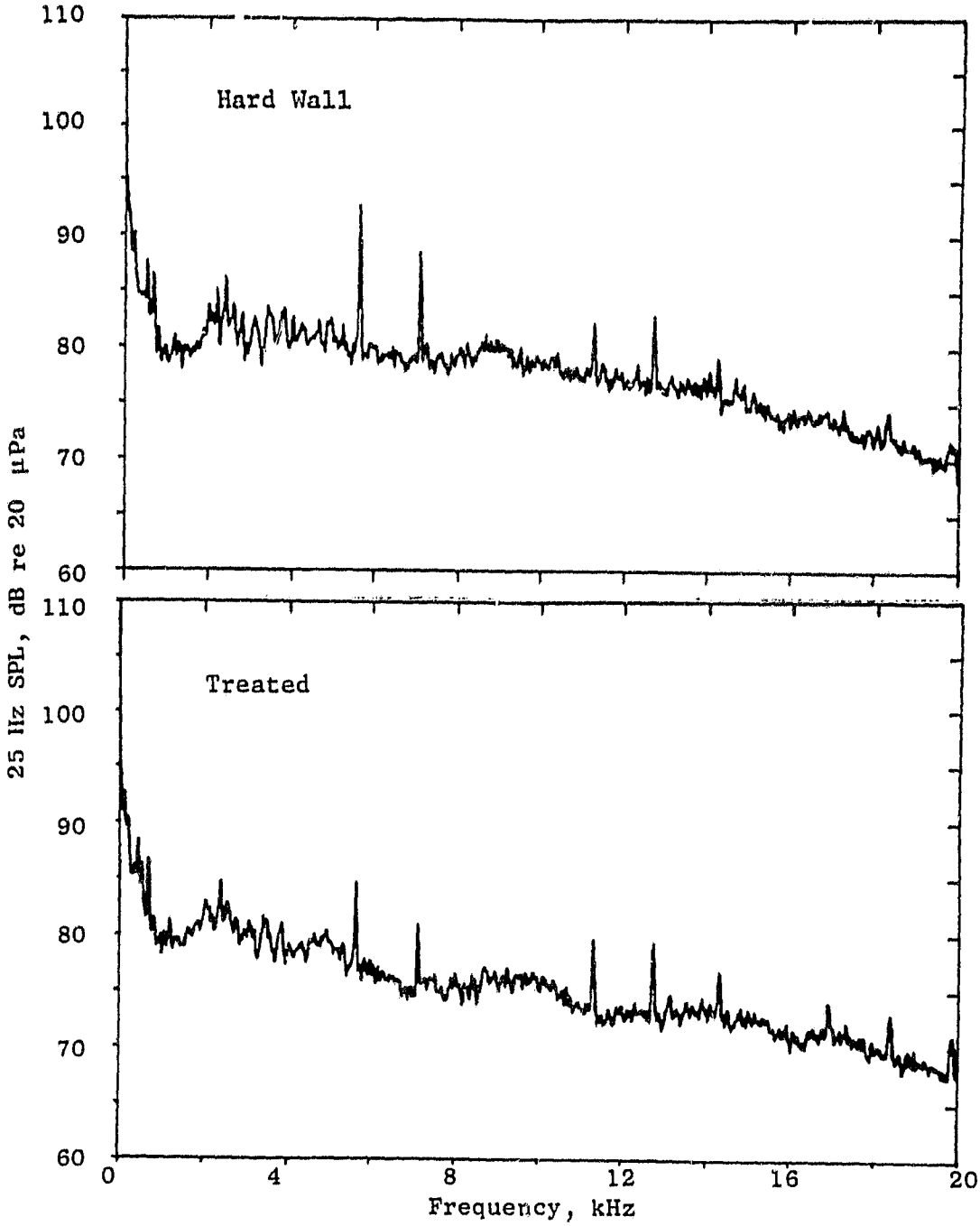

Figure 67. Comparison of Narrowband Spectra for Treated and Hard-Wall Configurations at Transonic Tip Speed (Continued).

- 70° Noise Emission Angle
- 14.5 Foot Microphone
- Straight Diffusing Inlet
- V_T = 335 m/s (1100 ft/s)
- 80 Knots Wind Tunnel
- Lower Operating Line

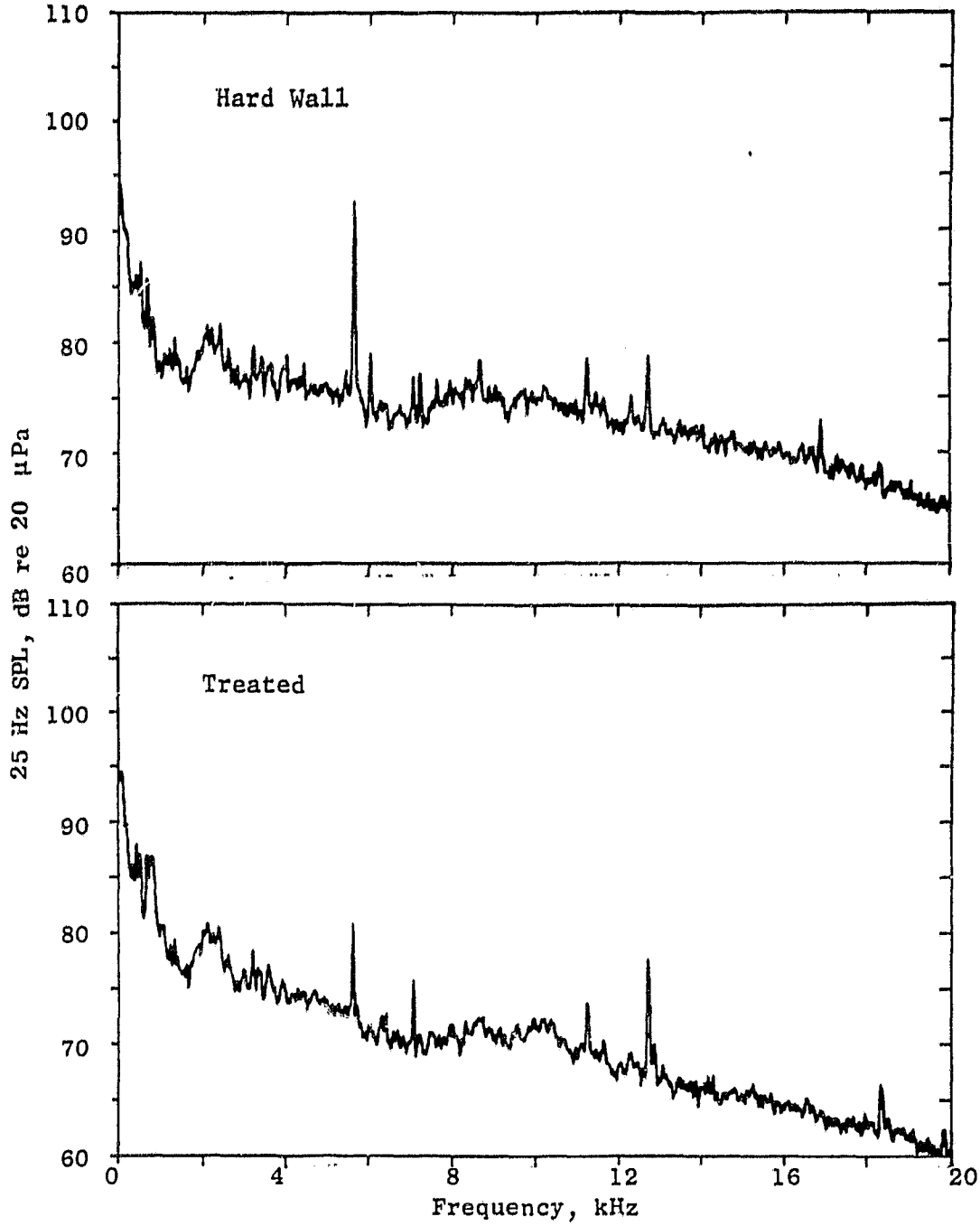

Figure 67. Comparison of Narrowband Spectra for Treated and Hard-Wall Configurations at Transonic Tip Speed (Concluded).

- 30° Noise Emission Angle
- 14.5 Foot Microphone
- Straight Diffusing Inlet
- V_T = 377 m/s (1237 ft/s)
- 80 Knots Wind Tunnel
- Lower Operating Line

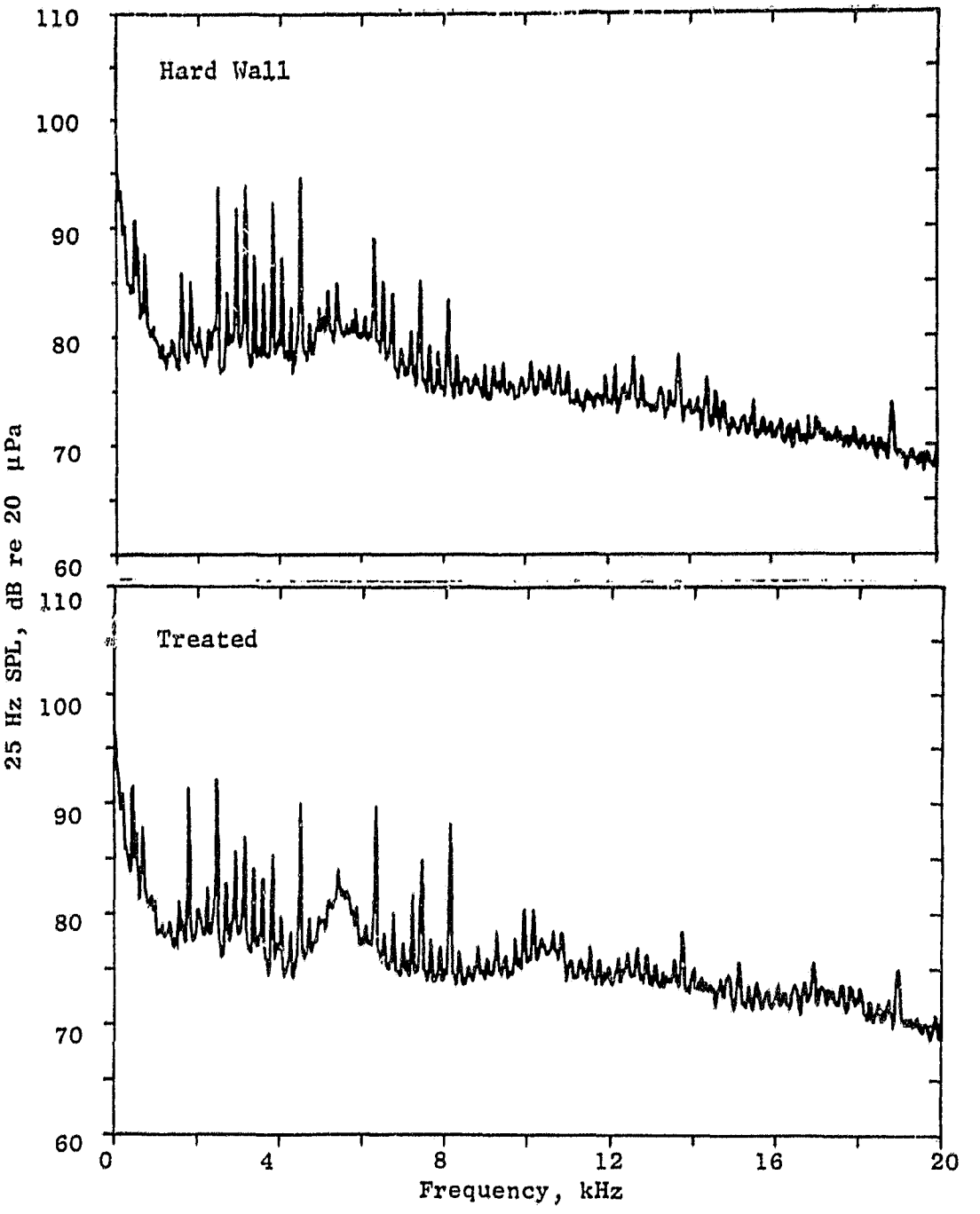

Figure 68. Comparison of Narrowband Spectra for Treated and Hard-Wall Configurations at Supersonic Tip Speed.

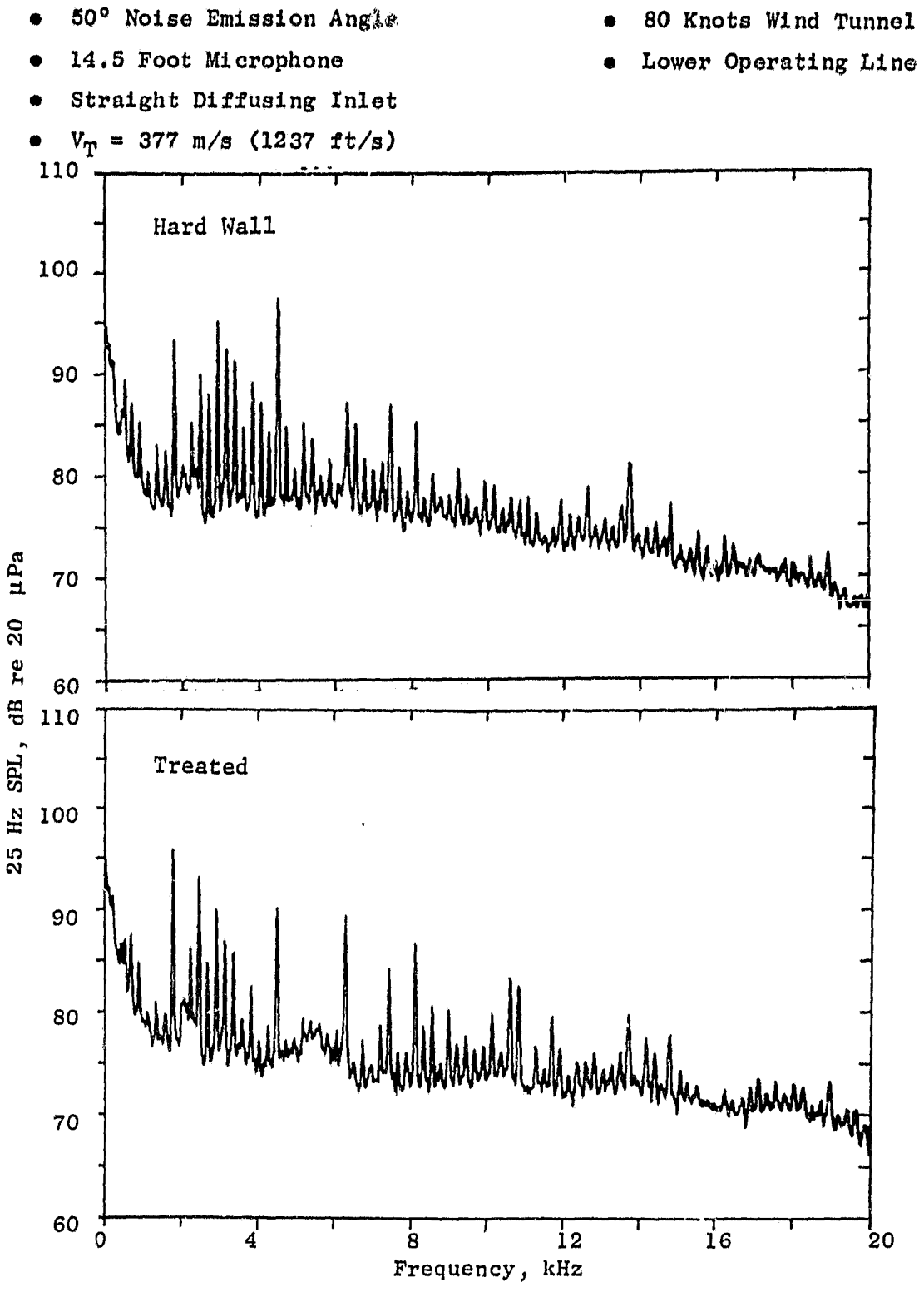

Figure 68. Comparison of Narrowband Spectra for Treated and Hard-Wall Configurations at Supersonic Tip Speed (Continued).

- 70° Noise Emission Angle
- 14.5 Foot Microphone
- Straight Diffusing Inlet
- V_T = 377 m/s (1237 ft/s)
- 80 Knots Wind Tunnel
- Lower Operating Line

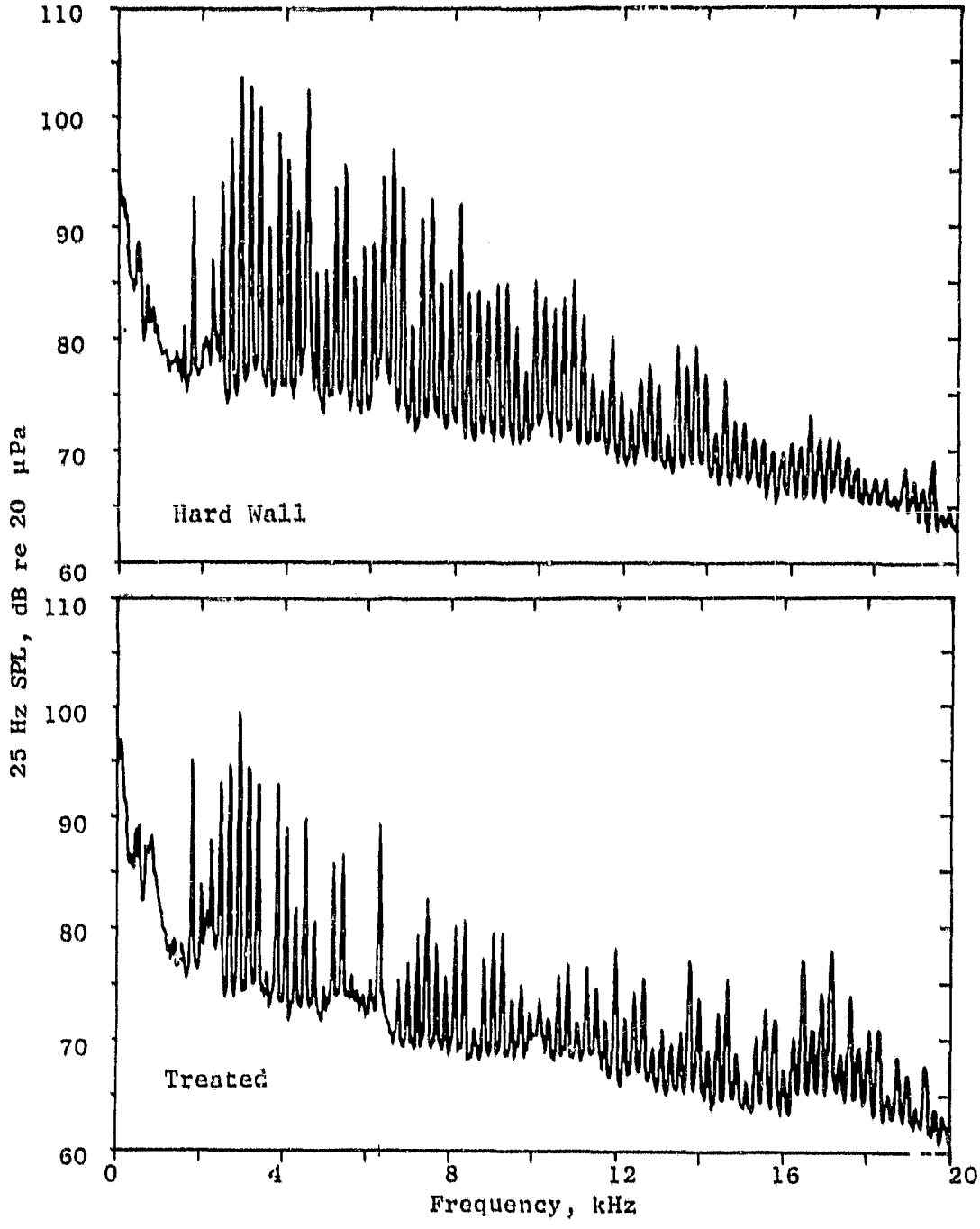

Figure 68. Comparison of Narrowband Spectra for Treated and Hard-Wall Configurations at Supersonic Tip Speed (Concluded).

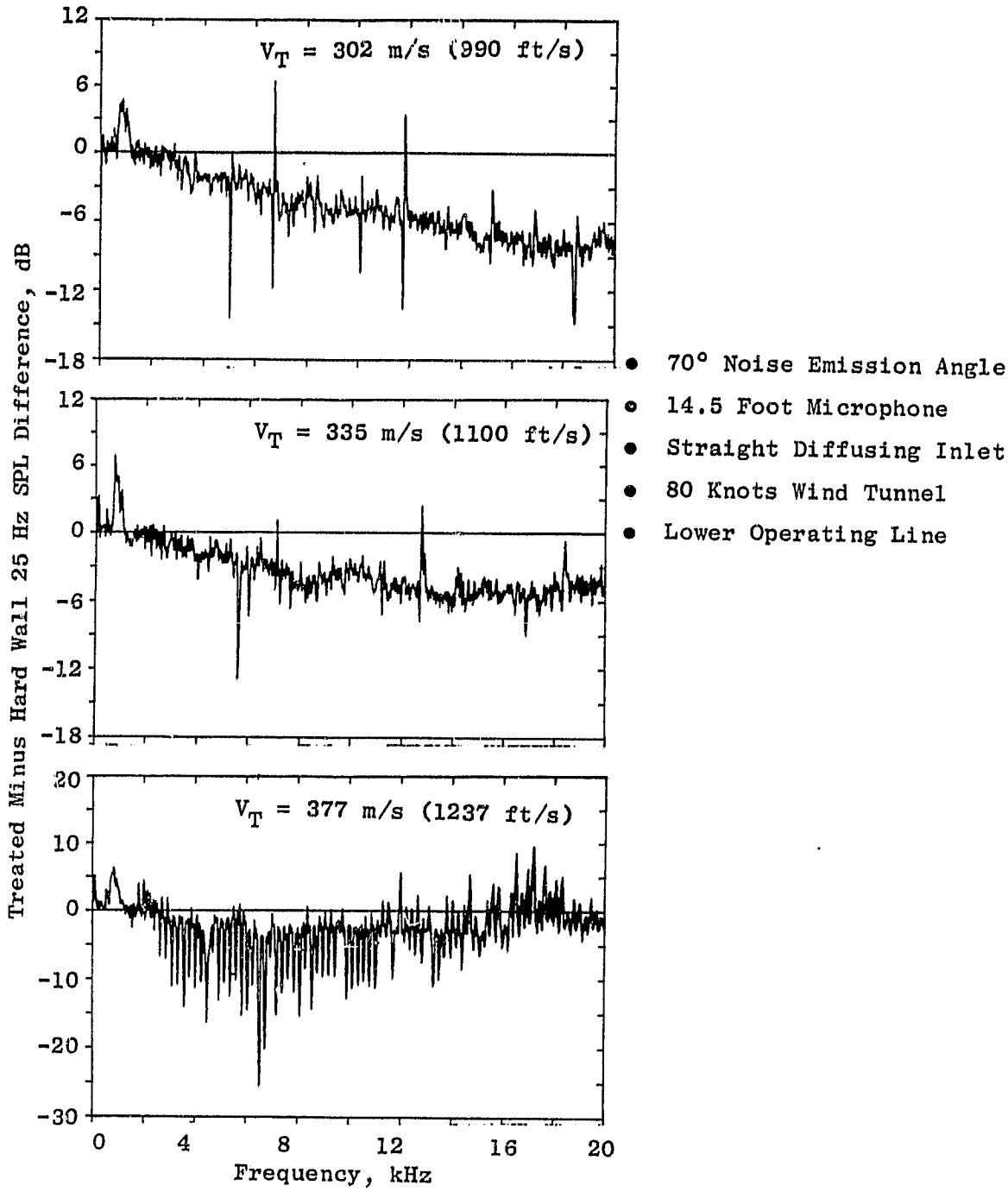

Figure 69. Normalized Narrowband Differences Between Treated and Untreated Inlet Configurations.

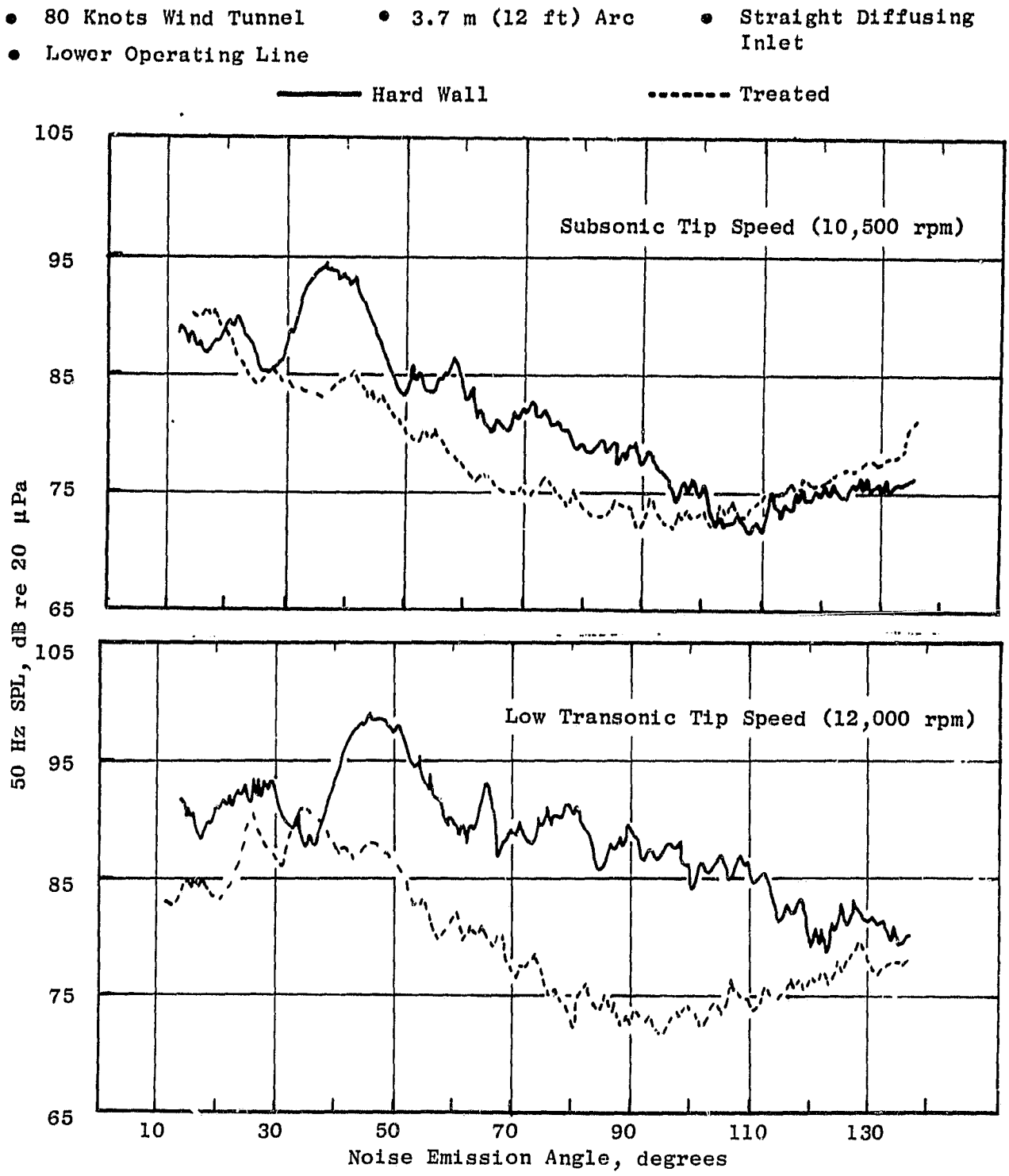

Figure 70. Comparison of Narrowband BPF Directivities for Hard-Wall and Treated Inlets.

- 80 Knots Wind Tunnel
- 3.7 m (12 ft) Arc
- Straight Diffusing Inlet
- Lower Operating Line

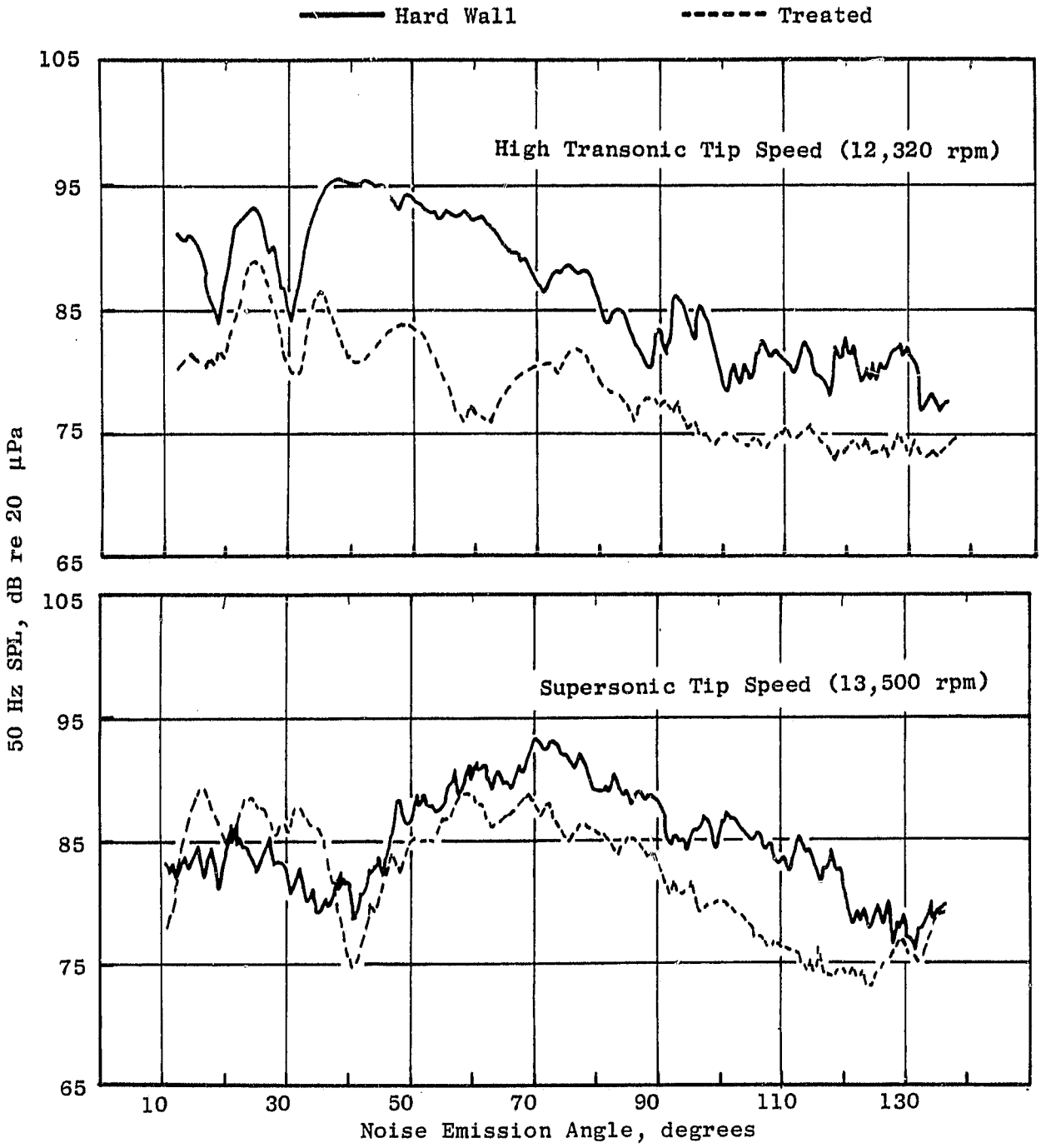

Figure 70. Comparison of Narrowband BPF Directivities for Hard-Wall and Treated Inlets (Concluded).

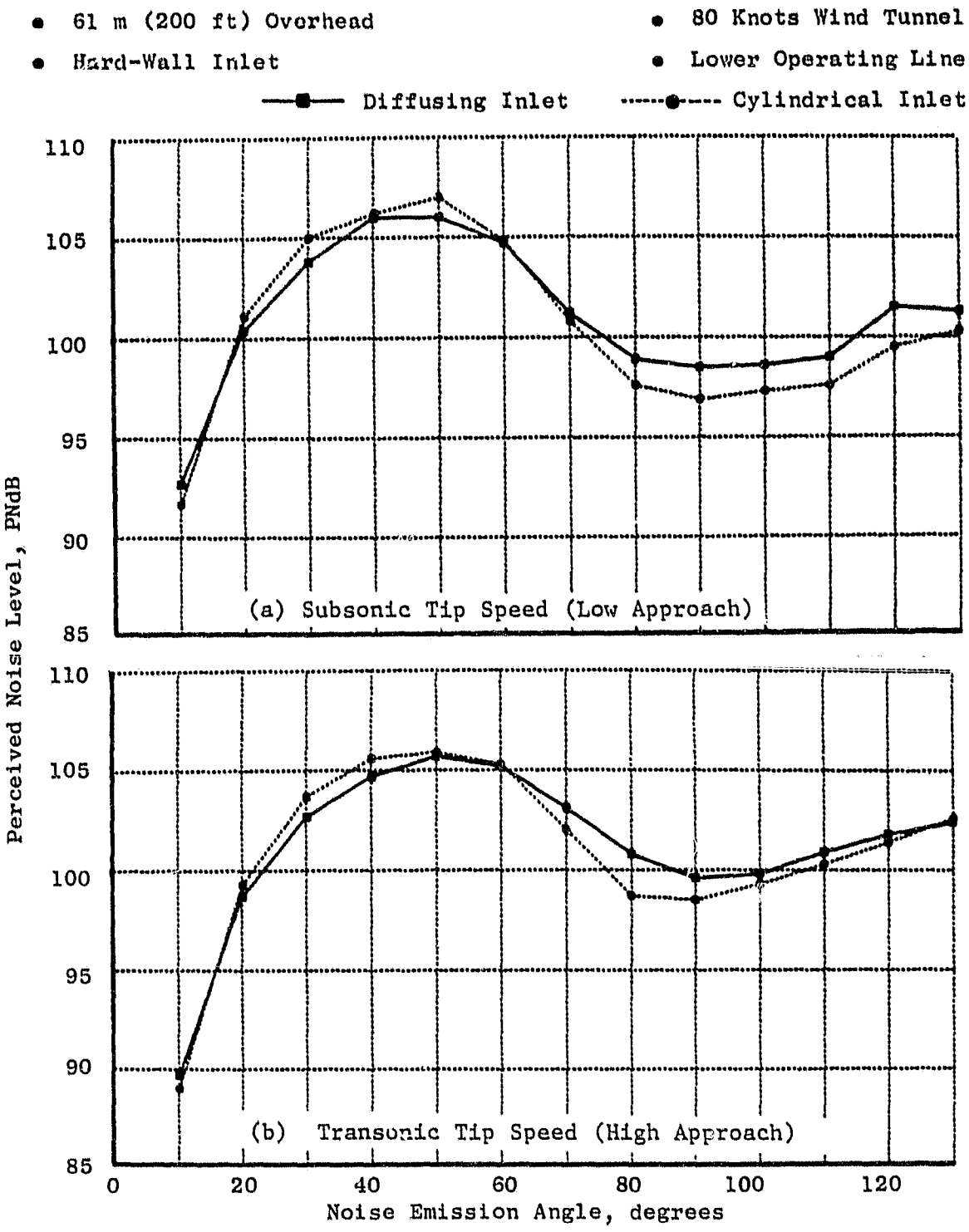

Figure 71. Scaled PNL Directivities for Diffusing and Cylindrical Inlets.

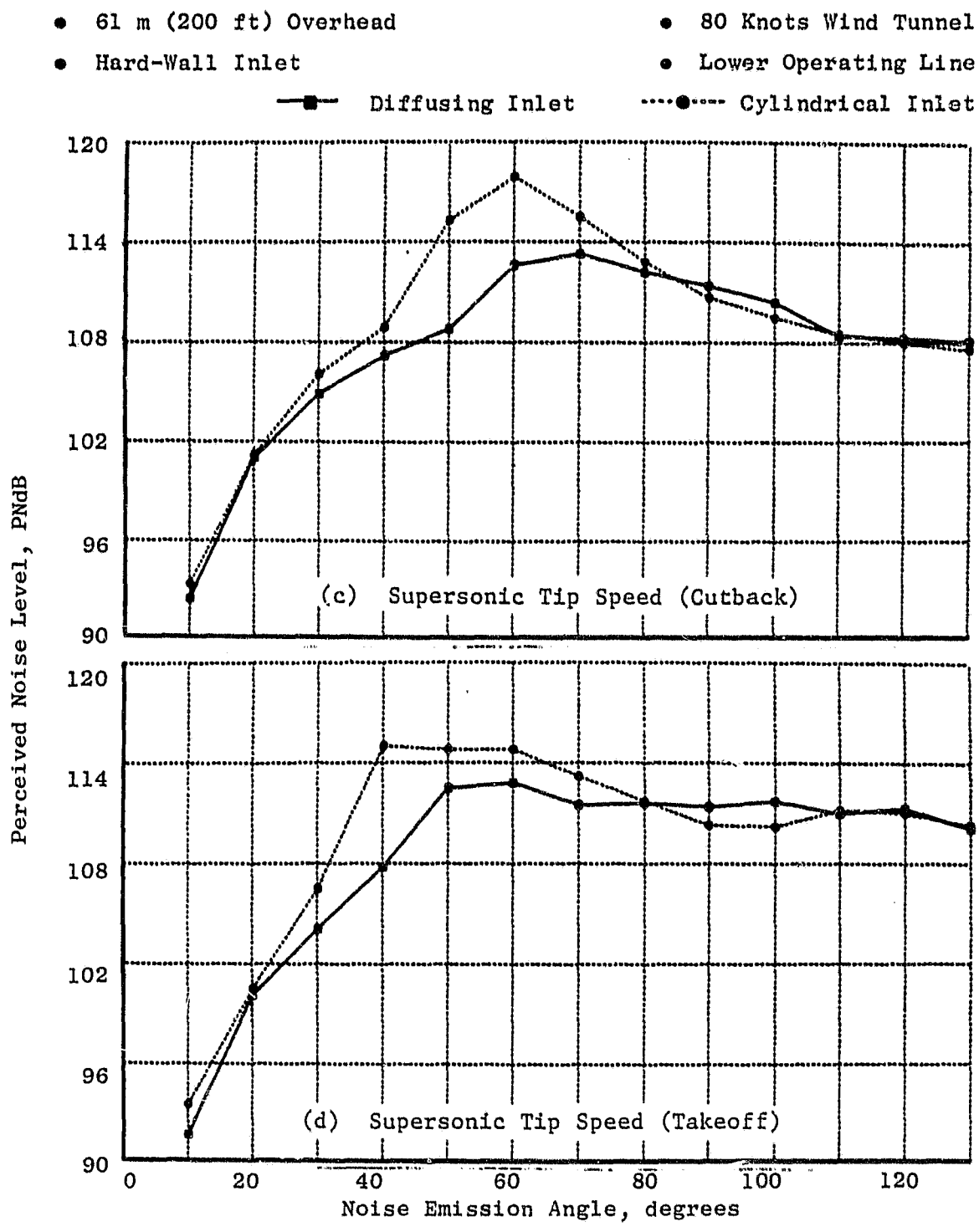

Figure 71. Scaled PNL Directivities for Diffusing and Cylindrical Inlets (Concluded).

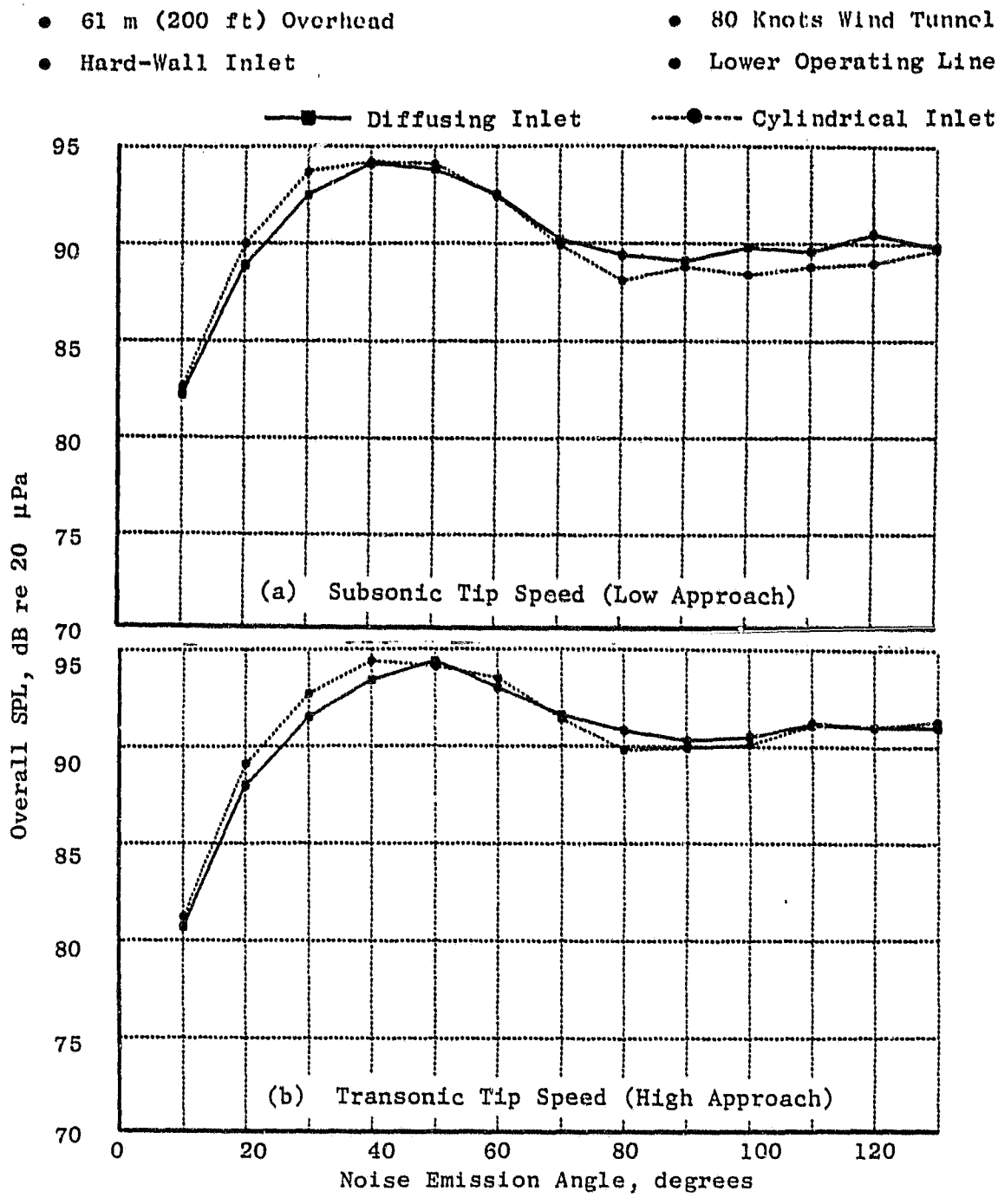

Figure 72. Scaled OASPL Directivities for Diffusing and Cylindrical Inlets.

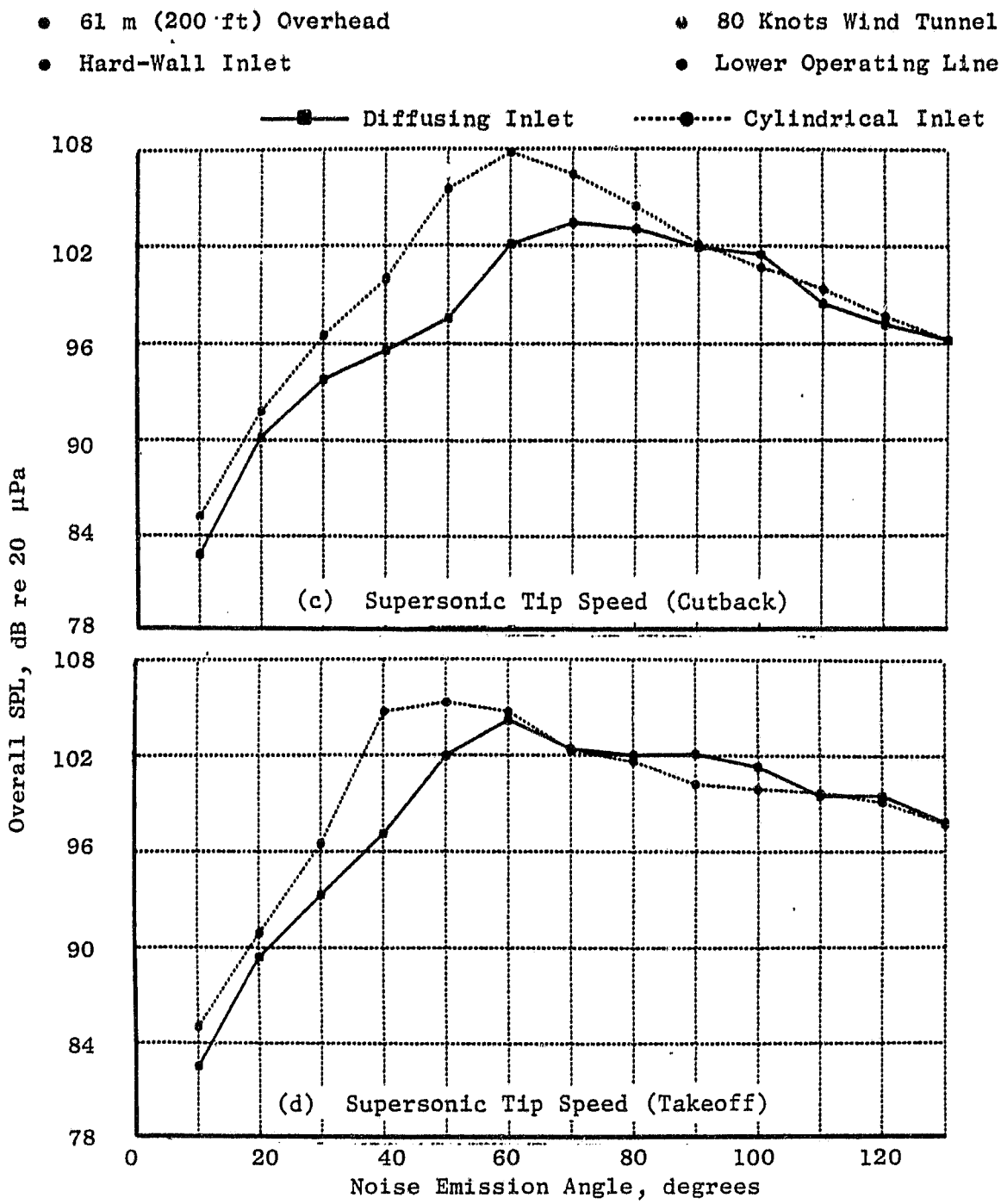

Figure 72. Scaled OASPL Directivities for Diffusing and Cylindrical Inlets (Concluded).

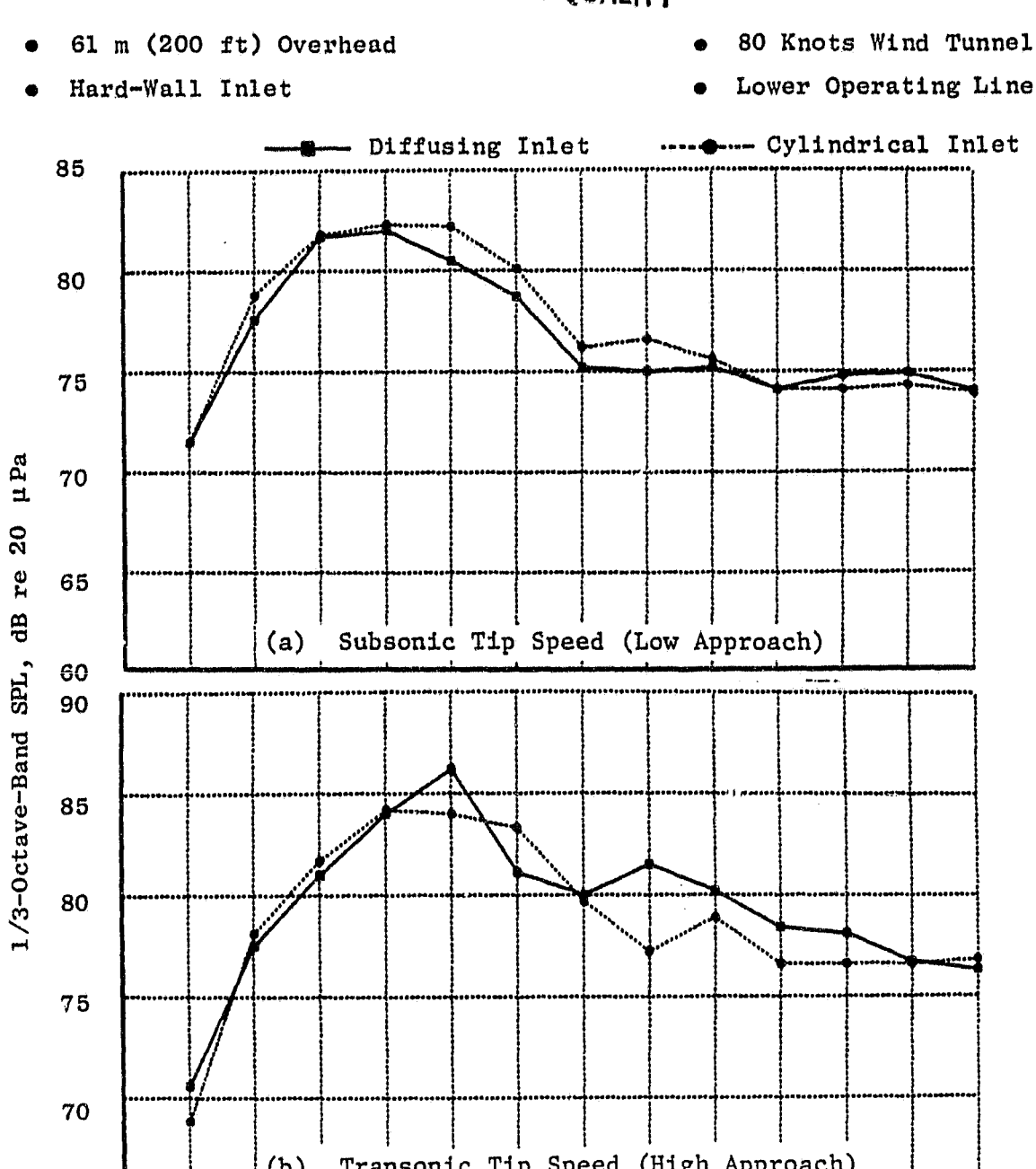

Figure 73. Scaled BPF 1/3-Octave-Band Directivities for Diffusing and Cylindrical Inlets.

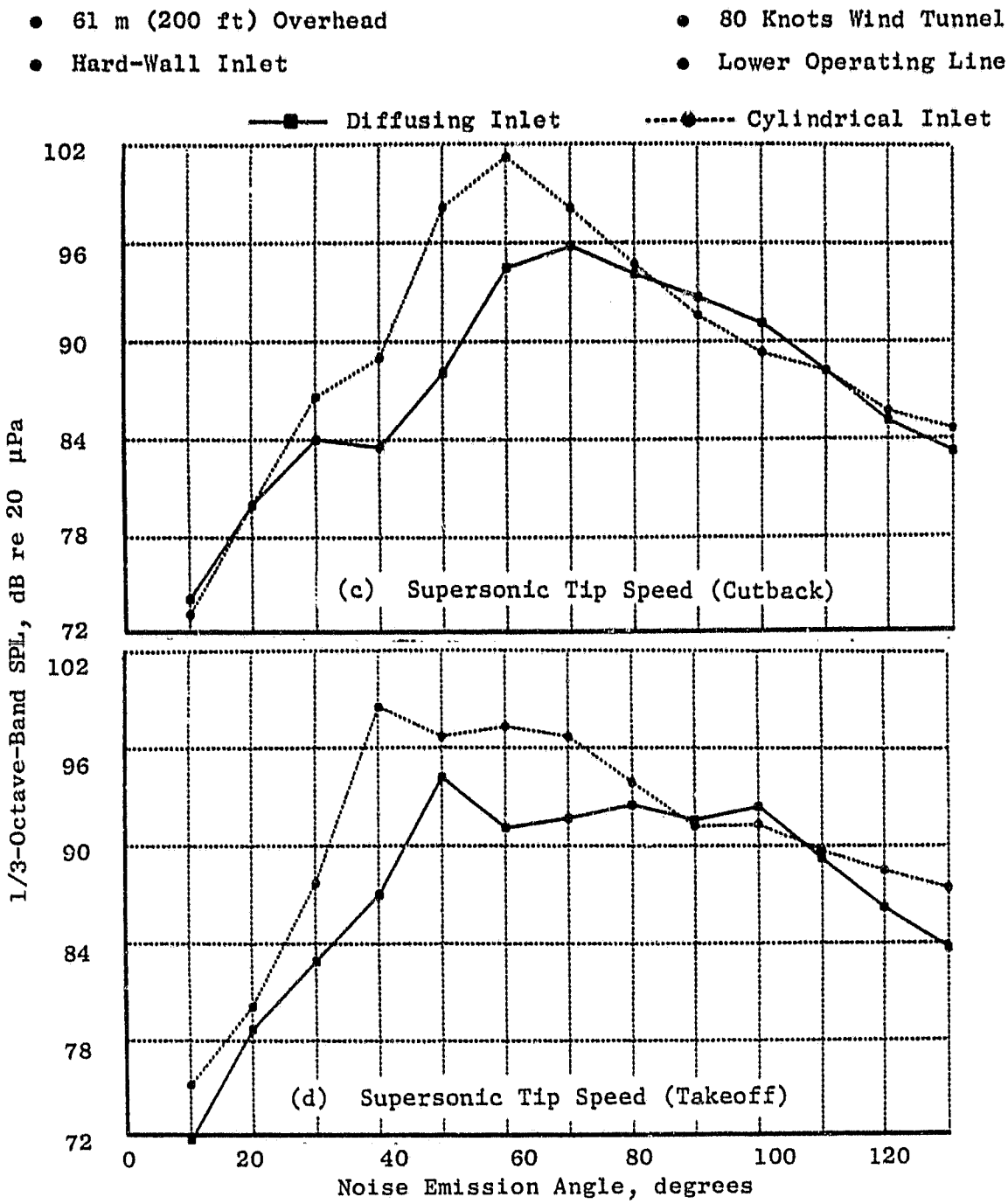

Figure 73. Scaled BPF 1/3-Octave-Band Directivities for Diffusing and Cylindrical Inlets (Concluded).

OASPL, and BPF 1/3-octave results at comparable speed points for cylindrical and diffusing hard-wall inlets. No differences are observed at lower subsonic fan tip speeds. However, at supersonic fan tip speeds consistent with throat Mach numbers greater than 0.55, a difference on the order of 2 dB is observed. This result is consistent with the earlier findings in Reference 1, which demonstrated significant flow acceleration suppression effects at throat Mach numbers in the 0.62 range.

4.6 INLET DESIGN INFLUENCE ON ACOUSTIC CHARACTERISTICS

Typical wing-mounted aircraft engines possess inlets that are canted downward relative to the rotational axis of the engine. This canting improves the installed aerodynamic performance of the engine, although it creates a circumferentially nonuniform static pressure distribution at the rotor face. The acoustic impact of this static pressure distortion, and its dependence on the flow turning in the inlet diffusing section, was investigated as part of this test program. Three inlets were tested to perform this assessment: a straight diffusing inlet, a conventionally canted inlet, and an inlet aerodynamically designed to reduce fan face static pressure distortion yet achieve the performance benefits of a canted inlet (i.e., a curved centerline inlet).

4.6.1 Comparison of Canted and Straight Inlet Acoustic Results

The results of earlier testing using a canted cylindrical inlet were reported in References 1 and 2. Two distinct differences between this test program and the former testing should be noted. One difference is that the latter testing utilized a diffusing inlet design [refer to Figure 7(a)] typical of conventional commercial engines rather than the nondiffusing cylindrical inlet geometry used in the previous test series shown in Figure 74. The other major difference is that testing was performed using an acoustically treated inlet as opposed to the untreated inlet. The prior results (see Figure 75) indicated a large increase in the sideline-radiated BPF 1/3-octave band noise for the canted cylindrical inlet relative to the straight cylindrical inlet. This increase occurred in the high subsonic and transonic speed ranges and was attributed to the static pressure distortion at the fan face. Refer to Figure 74(b). The reason this increase occurs at only these speeds is associated with the circumferential distortion, measured using wall static pressure taps, which induced a 1/rev fan blade loading functional generating a 27th order duct mode. The 27th duct mode becomes propagational at this high subsonic/transonic speed range as shown in Figure 51. It is postulated that as the fan tip speed becomes more supersonic, the rotor alone potential field becomes a substantially stronger noise source and masks the distortion noise making the BPF 1/3-octave band directivities comparable again.

Results of the straight and canted diffusing inlets are also presented in Figure 75 at similar fan speed ranges to those of the earlier tests. These results indicate substantially less difference in this high subsonic/transonic speed range. The diffusing treated results also are significantly lower than

a. Geometry Schematics

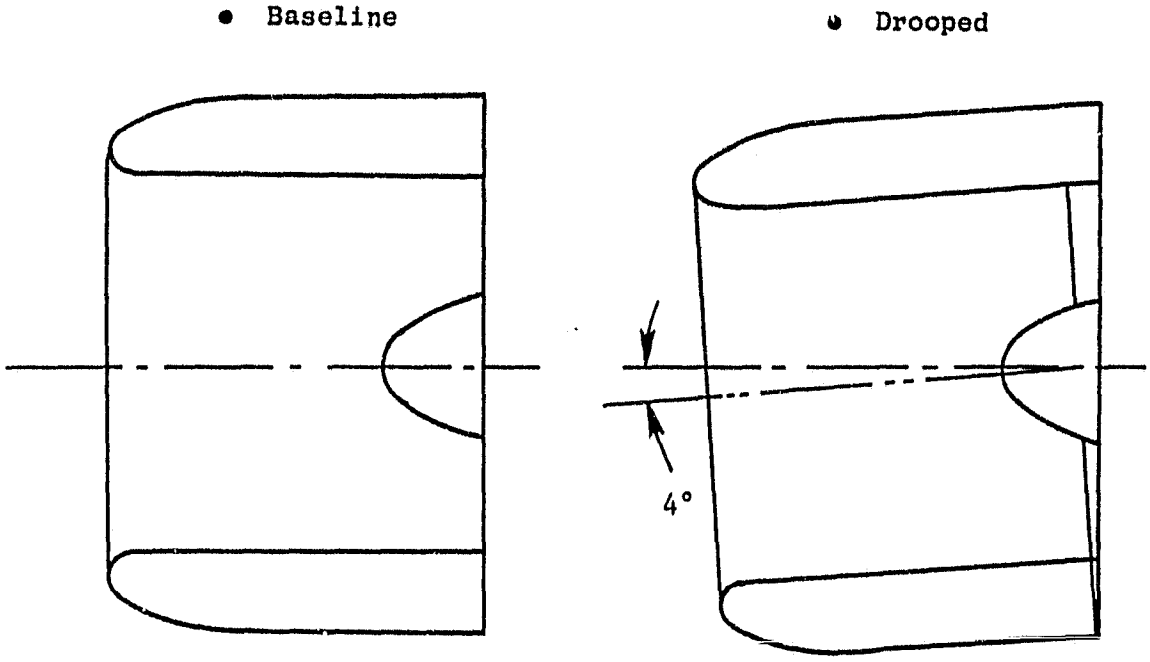

b. Inlet Circumferential Distortion at 80 Knots, V_T = 344 m/s (1129 ft/s)

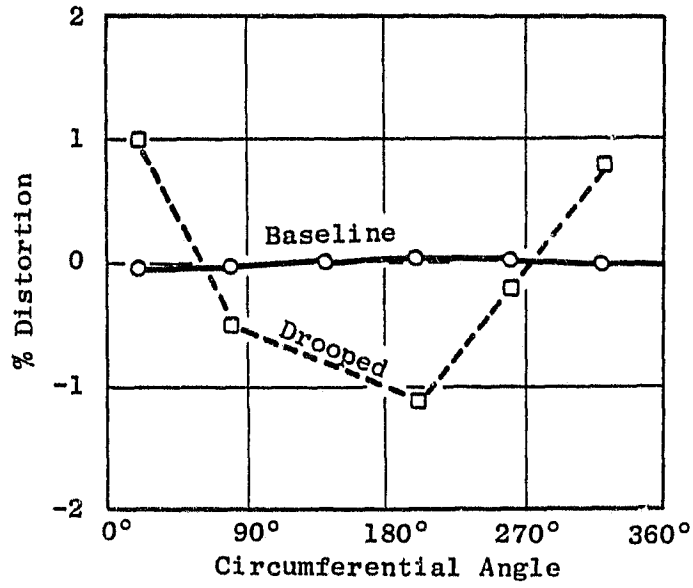

Figure 74. Baseline and Drooped Inlet Configurations.

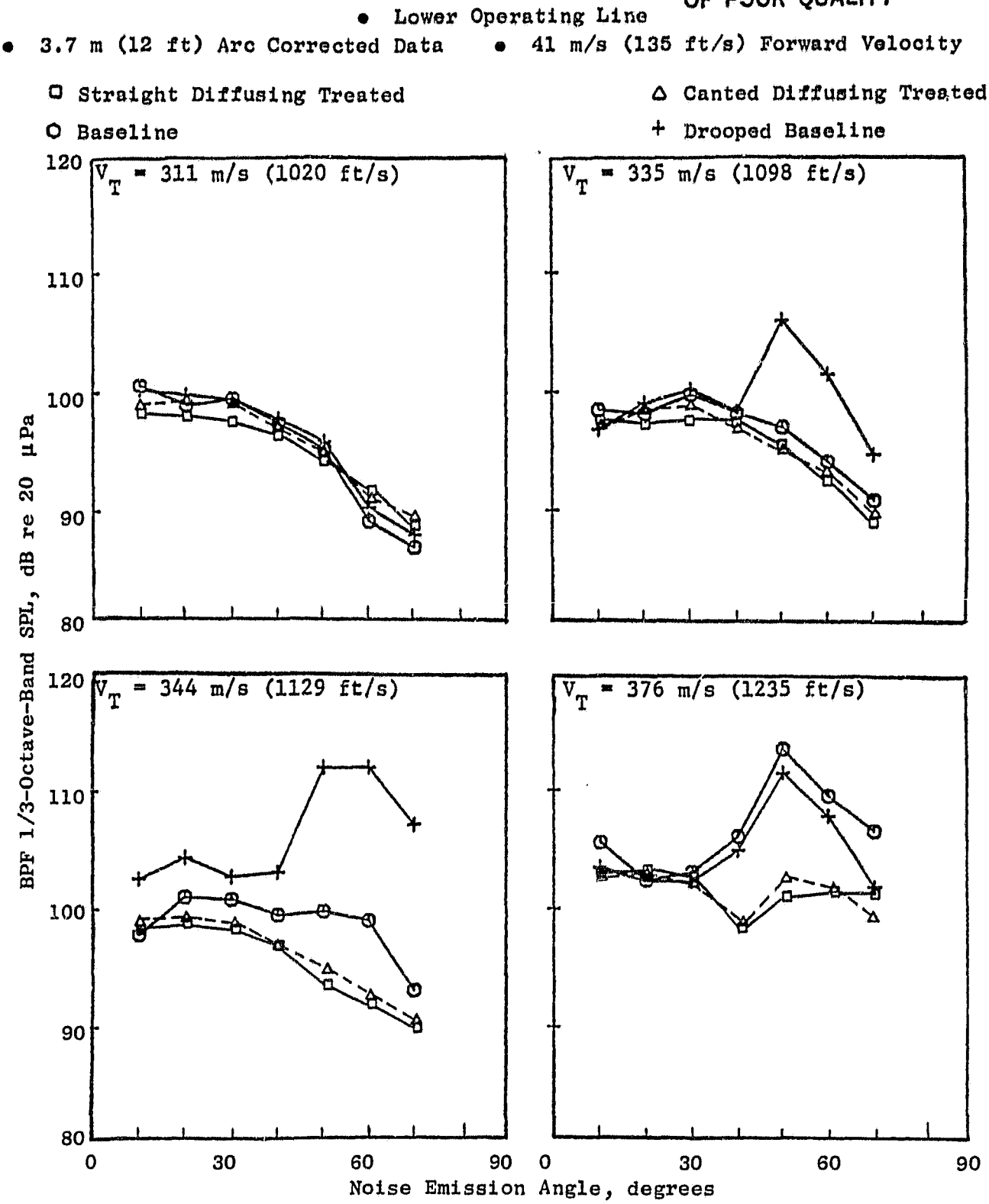

Figure 75. Blade-Passing Frequency, 1/3-Octave-Band Noise Directivity for Baseline and Drooped Baseline Inlets, Straight Diffusing and Canted Diffusing Inlets.

the nondiffusing hard-wall case as was reviewed in Section 4.5 dealing with inlet suppression. Hence, the treatment is believed responsible for the alleviation of the substantial noise increase attributable to canting the inlet. Note that the static pressure distortion of the canted diffusing geometry was of the same order of magnitude as the canted cylindrical geometry shown in Figures 74(b) and 30.

Narrowband results for the earlier canted inlet tests in the high subsonic/transonic fan tip speed are displayed in Figure 76. Similar comparative narrowband results for the straight and canted diffusing inlet geometries are presented in Figures 77 to 79. The narrowband tonal results represent single-point angular measuremets; thus, better definition of the angular distribution of tonal energy is obtained using the traverse microphone data in conjunction with a tracking filter tuned to the BPF tone.

Figure 80 presents the BPF directivities' various engine speed points for the diffusing inlets. These results were obtained using a 50-Hz bandwidth tracking filter. This technique was chosen to present the data, since the treatment effectiveness reported previously reduced tone levels so that tonal contributions to the BPF 1/3-octave band (as in Figure 75) were typically negligible. The results in Figure 80 demonstrate a somewhat similar trend to that formerly observed by the canted cylindrical testing. The noise level increases in the 60° to 90° sideline sensitive region for tip speeds in the transonic range. However, this region is also the region of peak acoustic treatment effectiveness, hence, the impact of this distortion noise source is greatly diminished. The peak sideline noise levels occur at much shallower angles where lower-order duct modes unrelated to the static pressure distortion would be increased. A study of the propagation of these lower-order duct modes is discussed in Reference 15.

4.6.2 Effect of Curved Inlet Design

The design premise of the curved inlet was to improve the fan face static pressure distortion as previously discussed. The aerodynamic improvement achieved was reported in Section 4.2. Another indirect measure of the potential abatement of this purported noise source mechanism are the enhanced waveform results of the BMT's and their harmonic spectra. These results are shown in Figure 81. The harmonic results for the first 50 contributions to the shaft-related revolutions are presented in this figure. It is noted that in the canted case, the 1/rev harmonic contribution is significantly higher than the straight and curved cases. This result is also observed directly by inspection of the waveforms displayed.

Another feature that is obvious from the waveforms is the importance of the 6/rev harmonic component. This component is apparently attributable to a six-strut assembly which forms the structural main frame, and provides a strong potential field seen by the rotor blades. The noise from this distortion component was discussed in References 3 and 4. An interesting result is observed with regard to the 6/rev component. The inlet geometry appears to

- Lower Operating Line
- 3.7 m (12 ft) Arc Uncorrected Data
- 41 m/s (135 ft/s) Forward Velocity

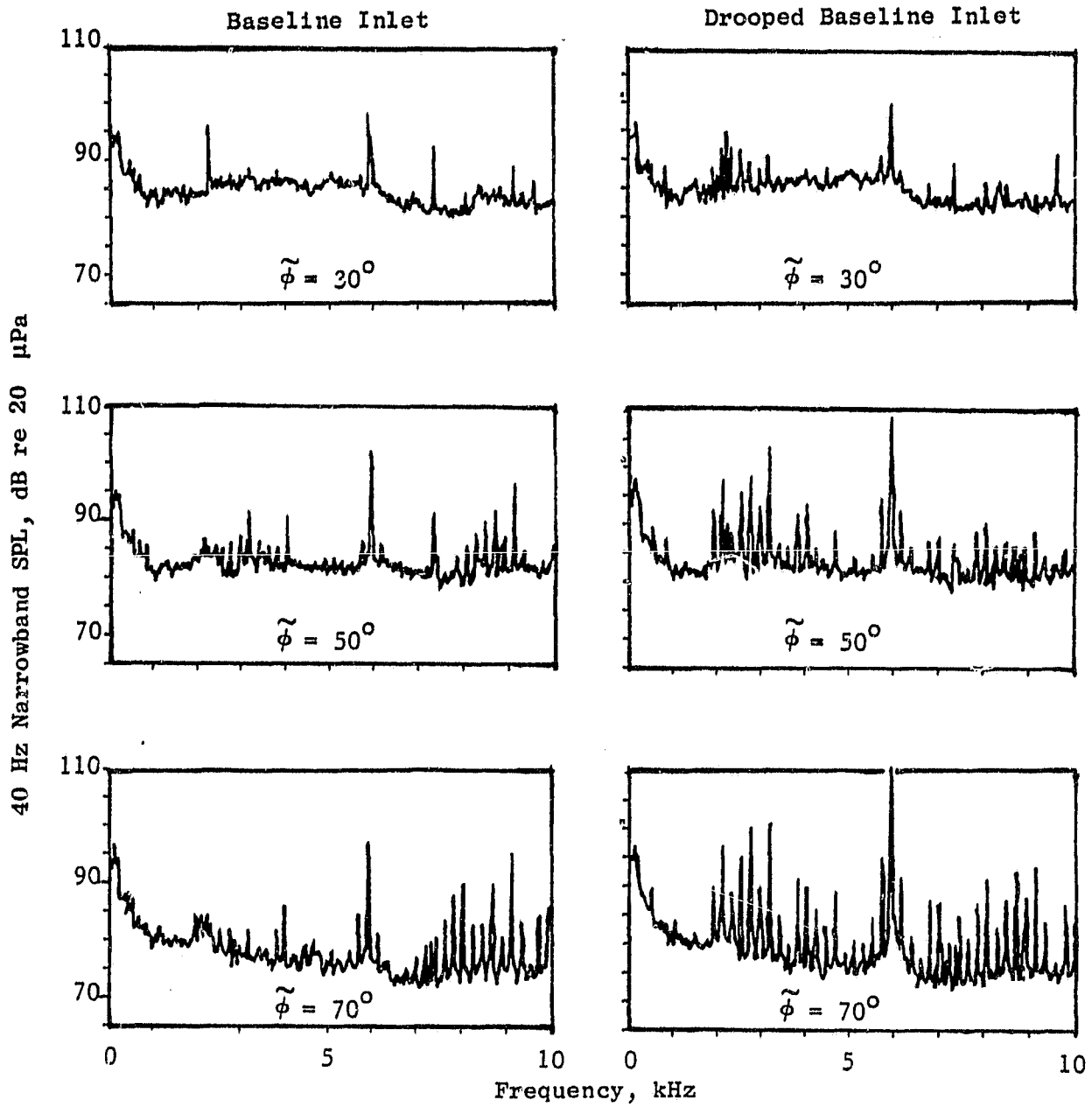

Figure 76. Narrowband Spectra for Baseline Inlet and Drooped Baseline Inlet at V_T = 344 m/s (1129 ft/s).

- 30° Noise Emission Angle
- 14.5 Foot Microphone
- V_T = 302 m/s (990 ft/s)
- 80 Knots Wir ; Tunnel
- Lower Operating Line

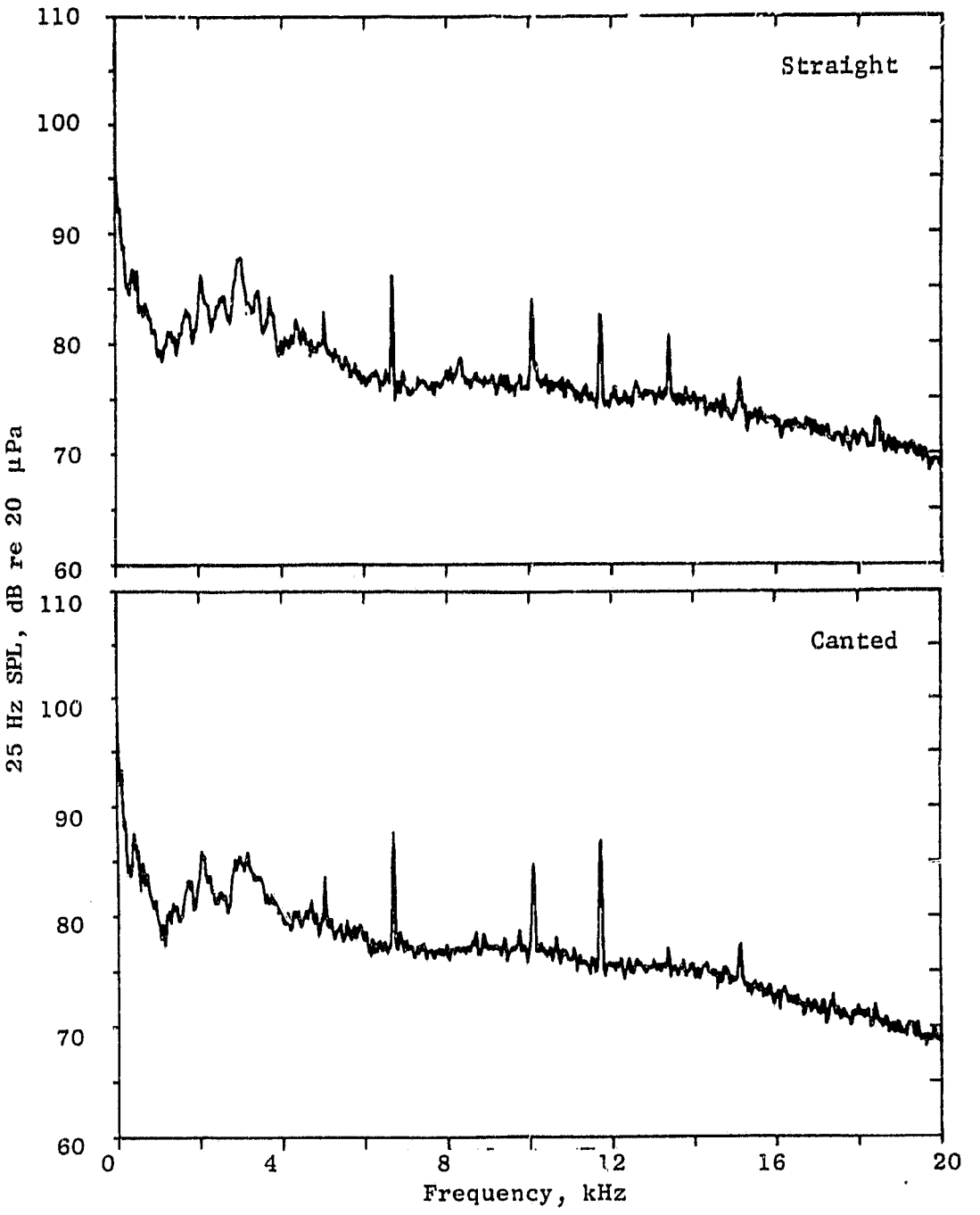

Figure 77. Comparison of Canted and Straight Diffusing Treated Inlet Narrowband Spectra at Subsonic Tip Speed.

- 50° Noise Emission Angle
- 14.5 Foot Microphone
- V_T = 302 m/s (990 ft/s)
- 80 Knots Wind Tunnel
- Lower Operating Line

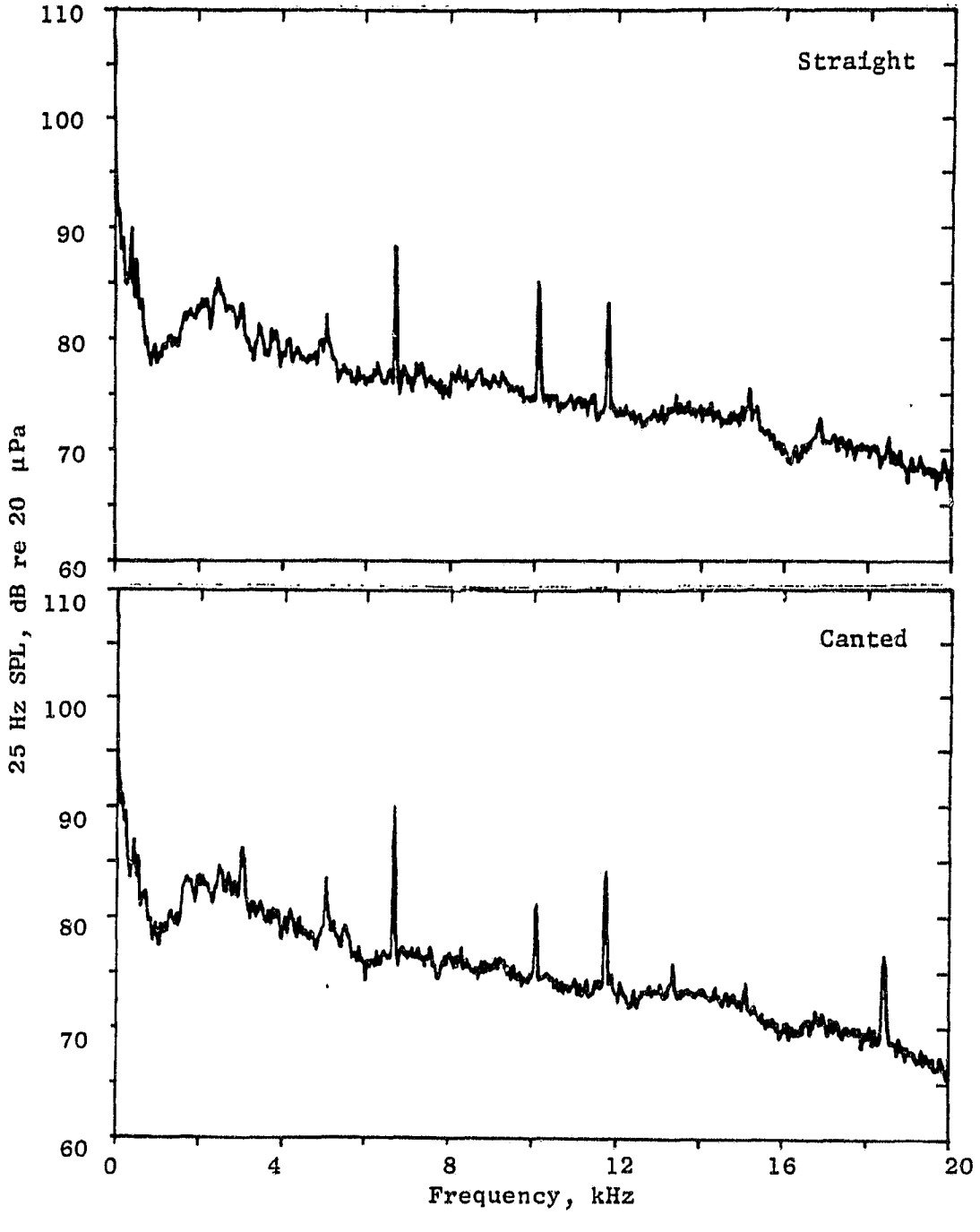

Figure 77. Comparison of Canted and Straight Diffusing Treated Inlet Narrowband Spectra at Subsonic Tip Speed (Continued).

- 70° Noise Emission Angle
- 14.5 Foot Microphone
- V_T = 302 m/s (990 ft/s)
- 80 Knots Wind Tunnel
- Lower Operating Line

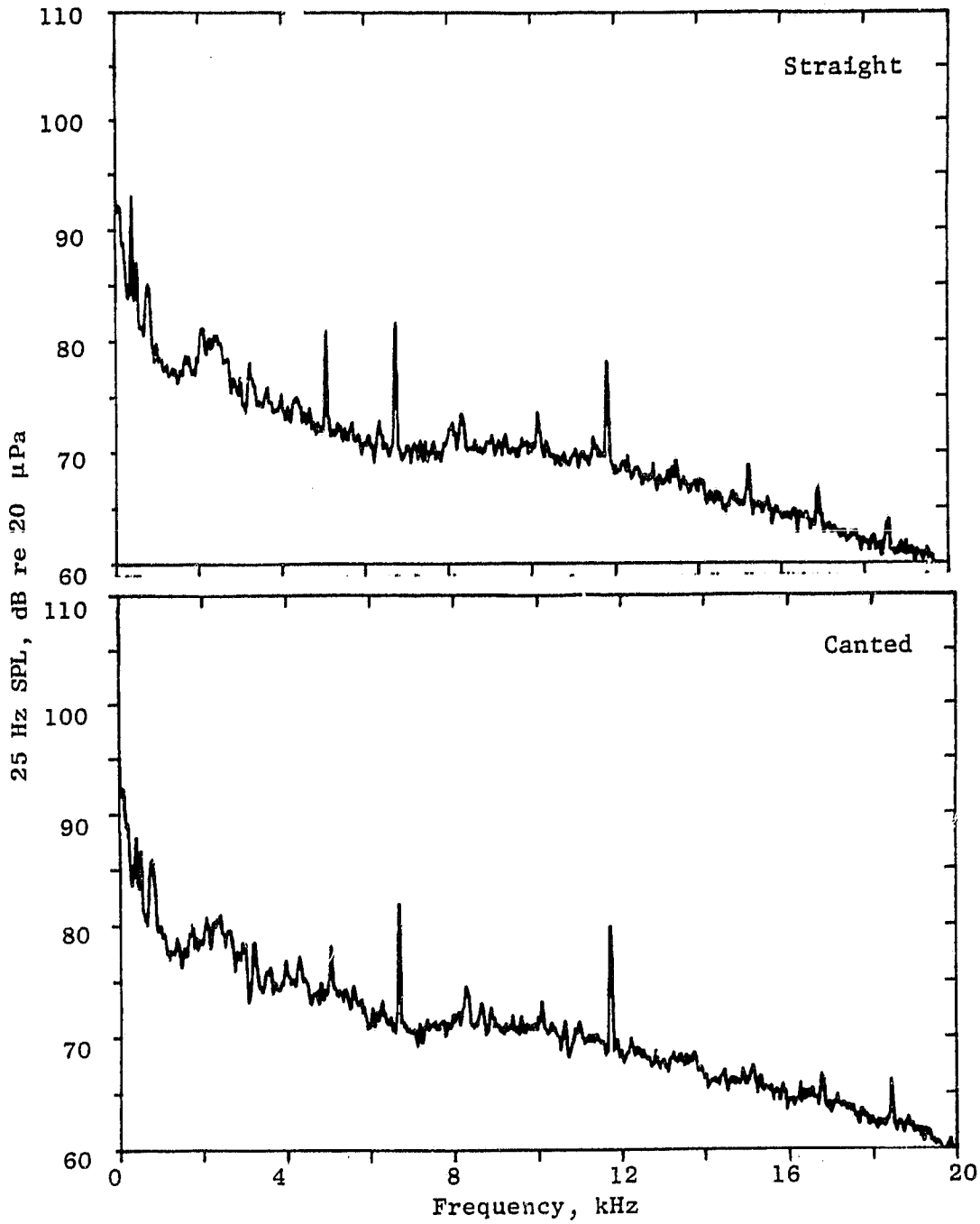

Figure 77. Comparison of Canted and Straight Diffusing Treated Inlet Narrowband Spectra at Subsonic Tip Speed (Concluded).

- 30° Noise Emission Angle
- 14.5 Foot Microphone
- V_T = 335 m/s (1100 ft/s)
- 80 Knots Wind Tunnel
- Lower Operating Line

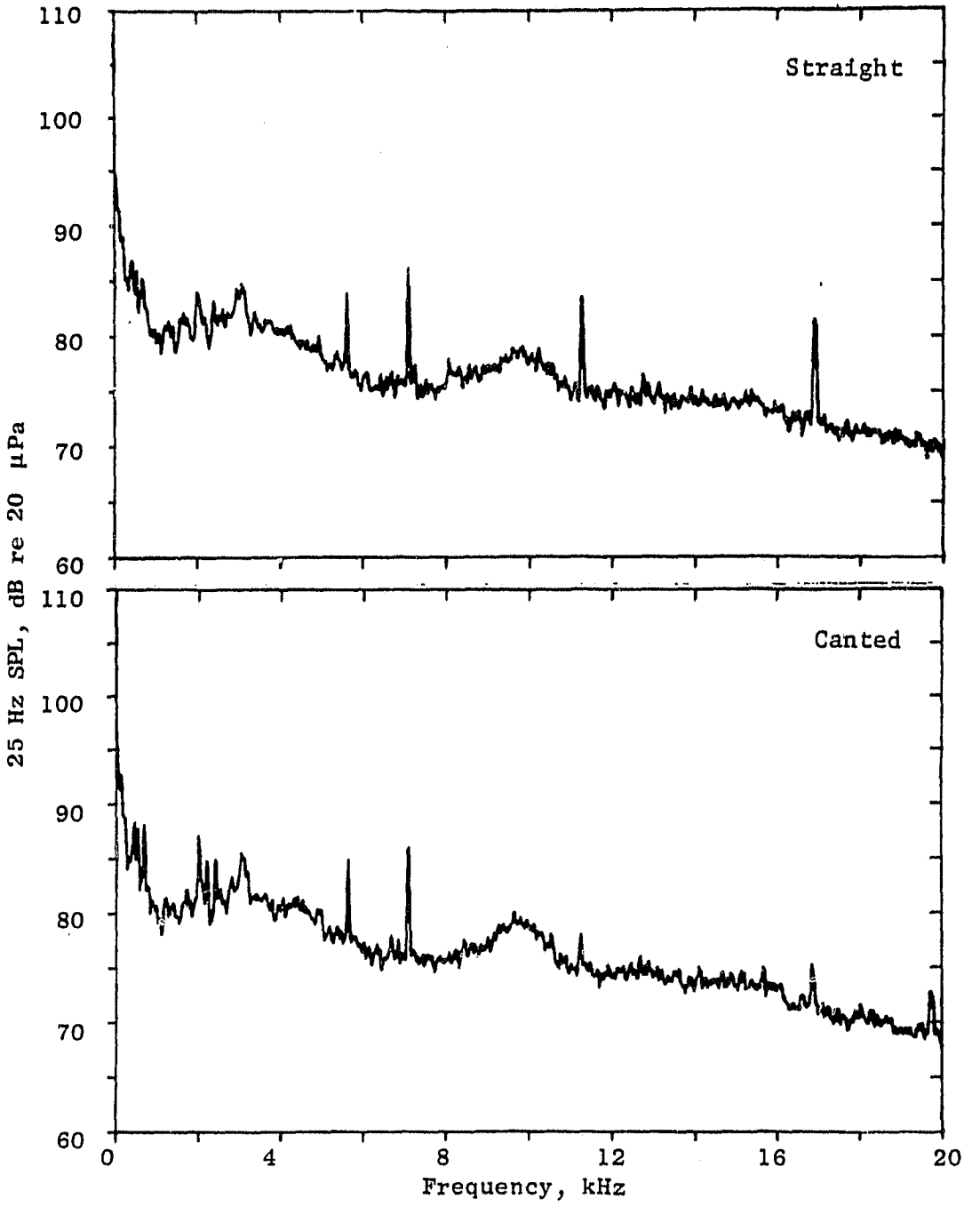

Figure 78. Comparison of Canted and Straight Diffusing Treated Inlet Narrowband Spectra at Transonic Tip Speed.

- 50° Noise Emission Angle
- 14.5 Foot Microphone
- V_T = 335 m/s (1100 ft/s)
- 80 Knots Wind Tunnel
- Lower Operating Line

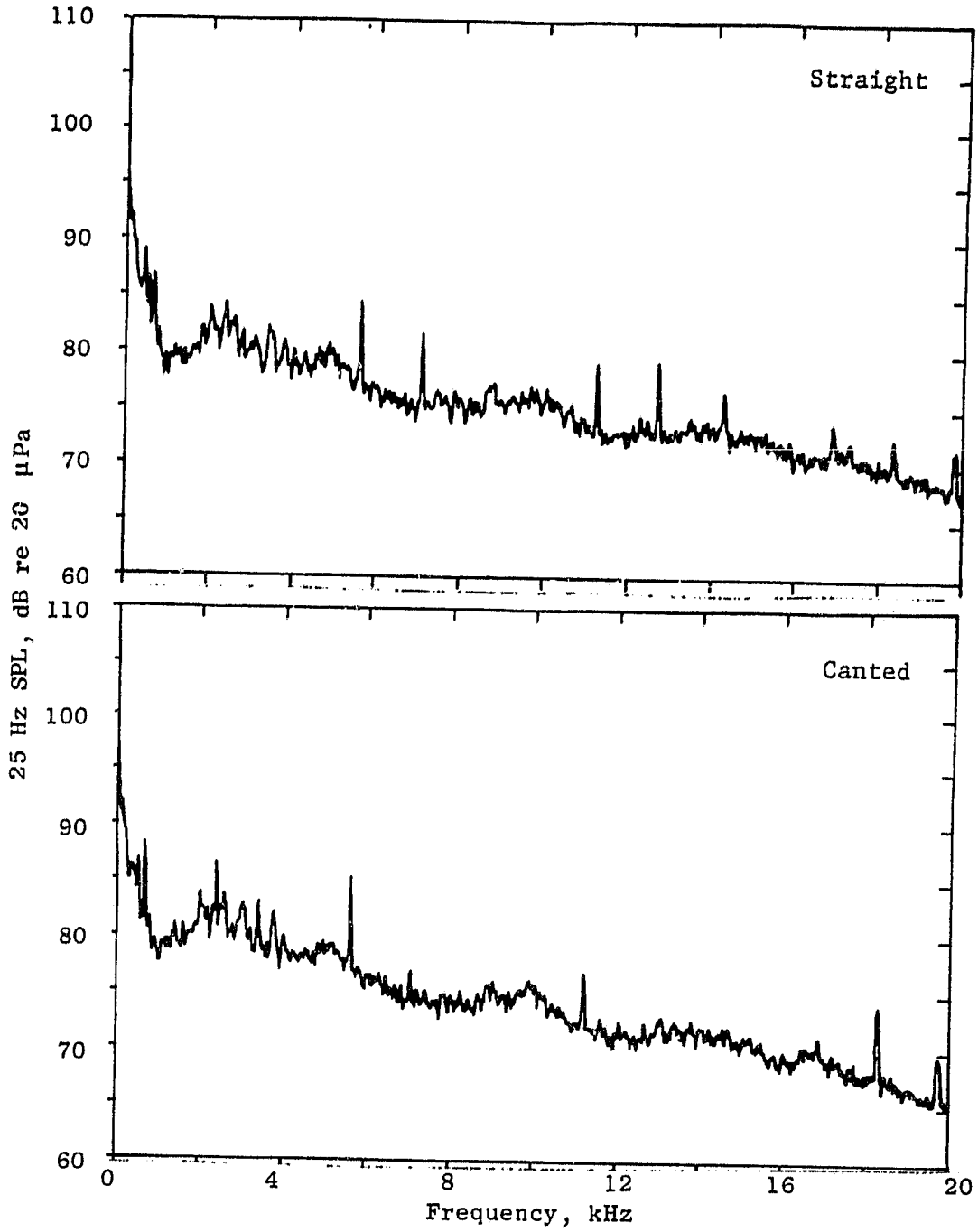

Figure 78. Comparison of Canted and Straight Diffusing Treated Inlet Narrowband Spectra at Transonic Tip Speed (Continued).

- 70° Noise Emission Angle
- 14.5 Foot Microphone
- V_T = 335 m/s (1100 ft/s)
- 80 Knots Wind Tunnel
- Lower Operating Line

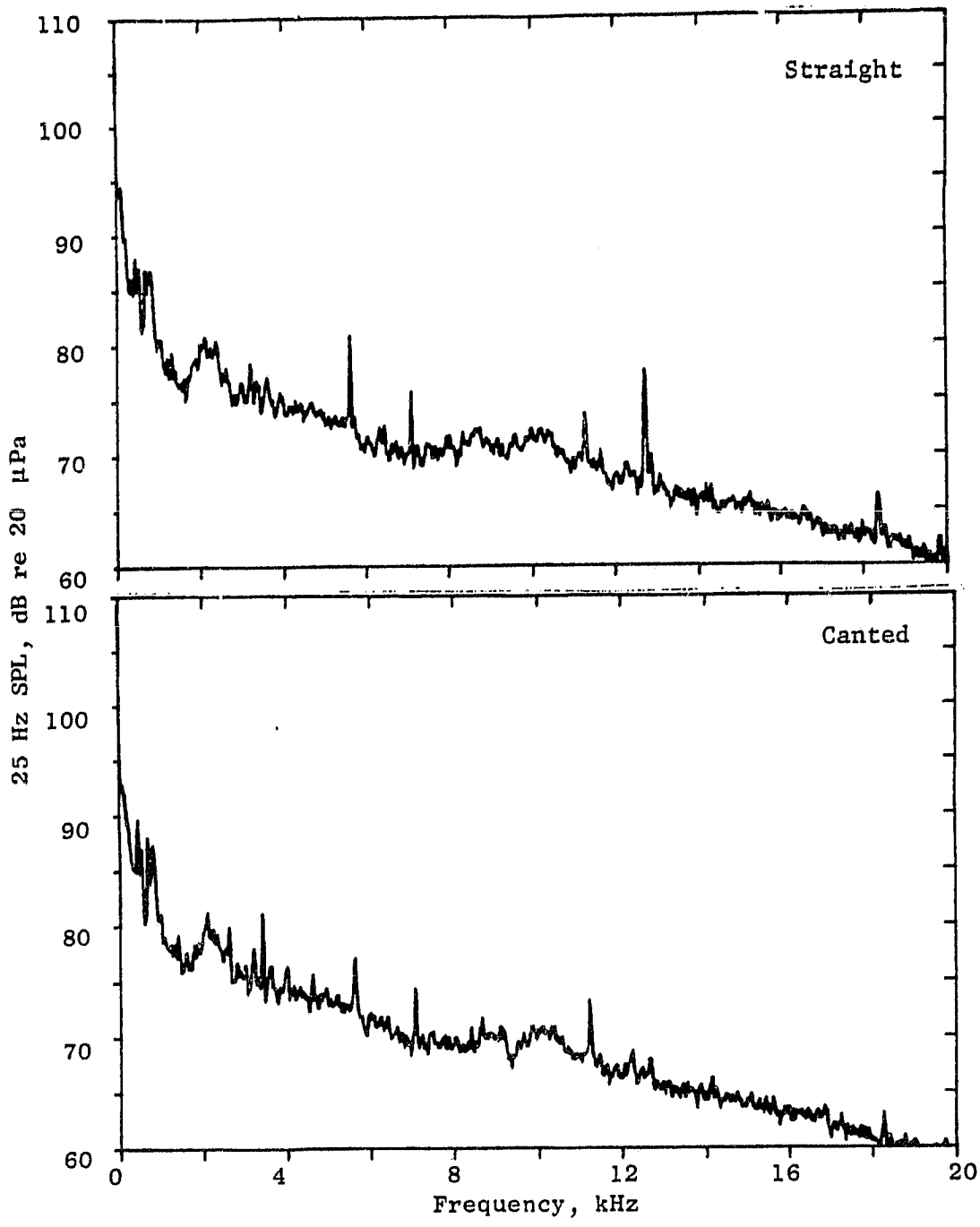

Figure 78. Comparison of Canted and Straight Diffusing Treated Inlet Narrowband Spectra at Transonic Tip Speed (Concluded).

- 30° Noise Emission Angle
- 14.5 Foot Microphone
- V_T = 377 m/s (1237 ft/s)
- 80 Knots Wind Tunnel
- Lower Operating Line

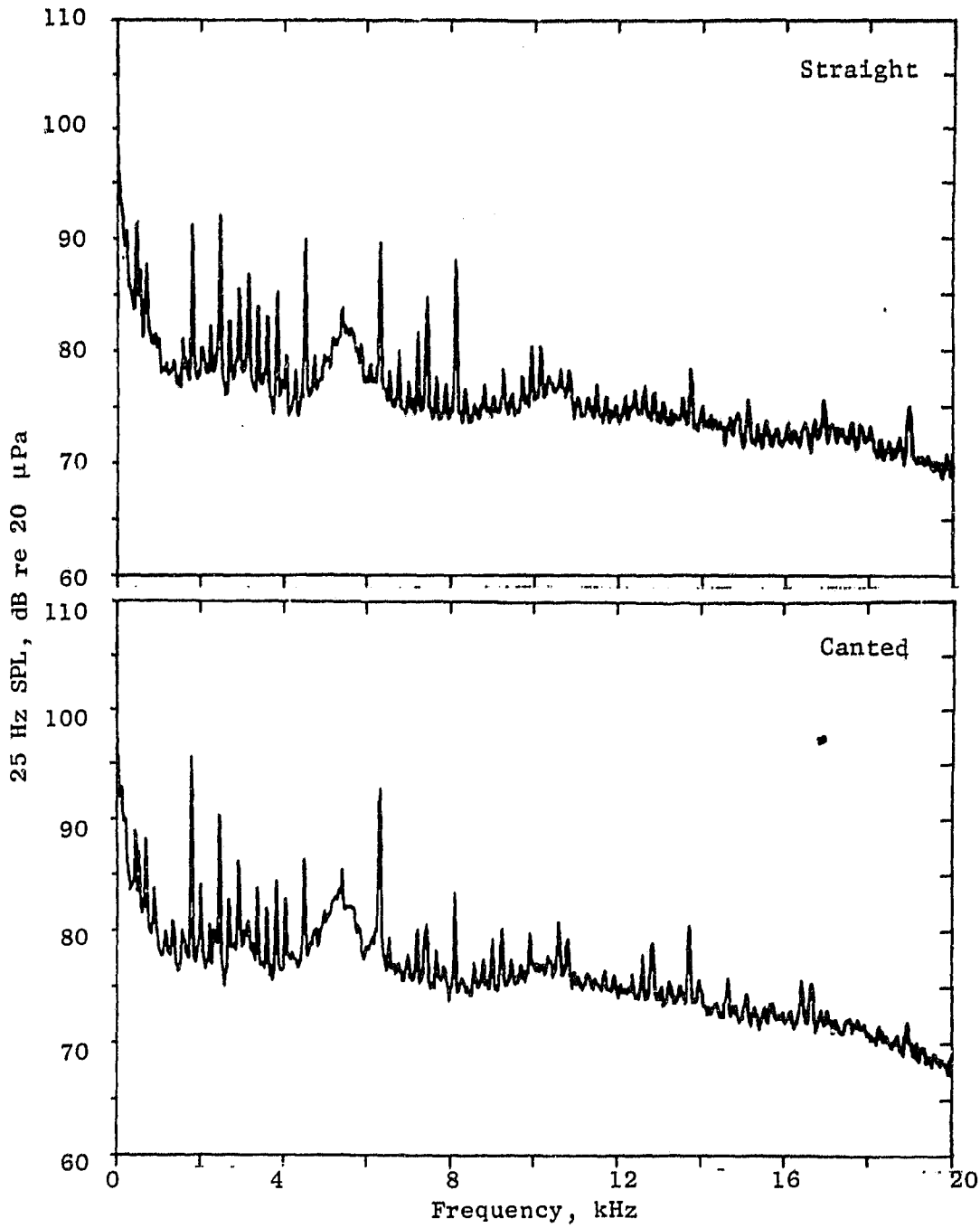

Figure 79. Comparison of Canted and Straight Diffusing Treated Inlet Narrowband Spectra at Supersonic Tip Speed.

- 50° Noise Emission Angle
- 14.5 Foot Microphone
- V_T = 377 m/s (1237 ft/s)
- 80 Knots Wind Tunnel
- Lower Operating Line

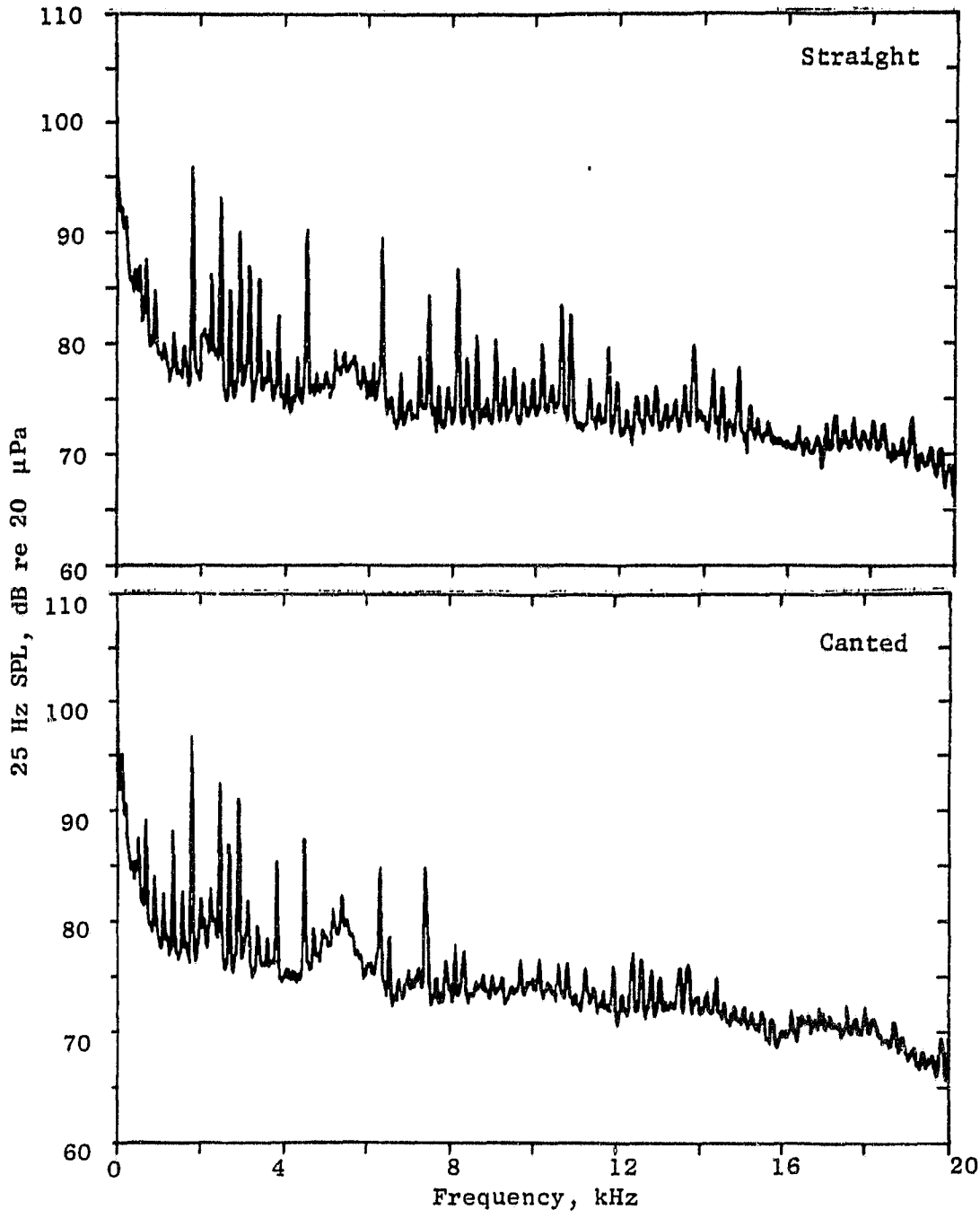

Figure 79. Comparison of Canted and Straight Diffusing Treated Inlet Narrowband Spectra at Supersonic Tip Speed (Continued).

- 70° Noise Emission Angle
- 14.5 Foot Microphone
- V_T = 377 m/s (1237 ft/s)
- 80 Knots Wind Tunnel
- Lower Operating Line

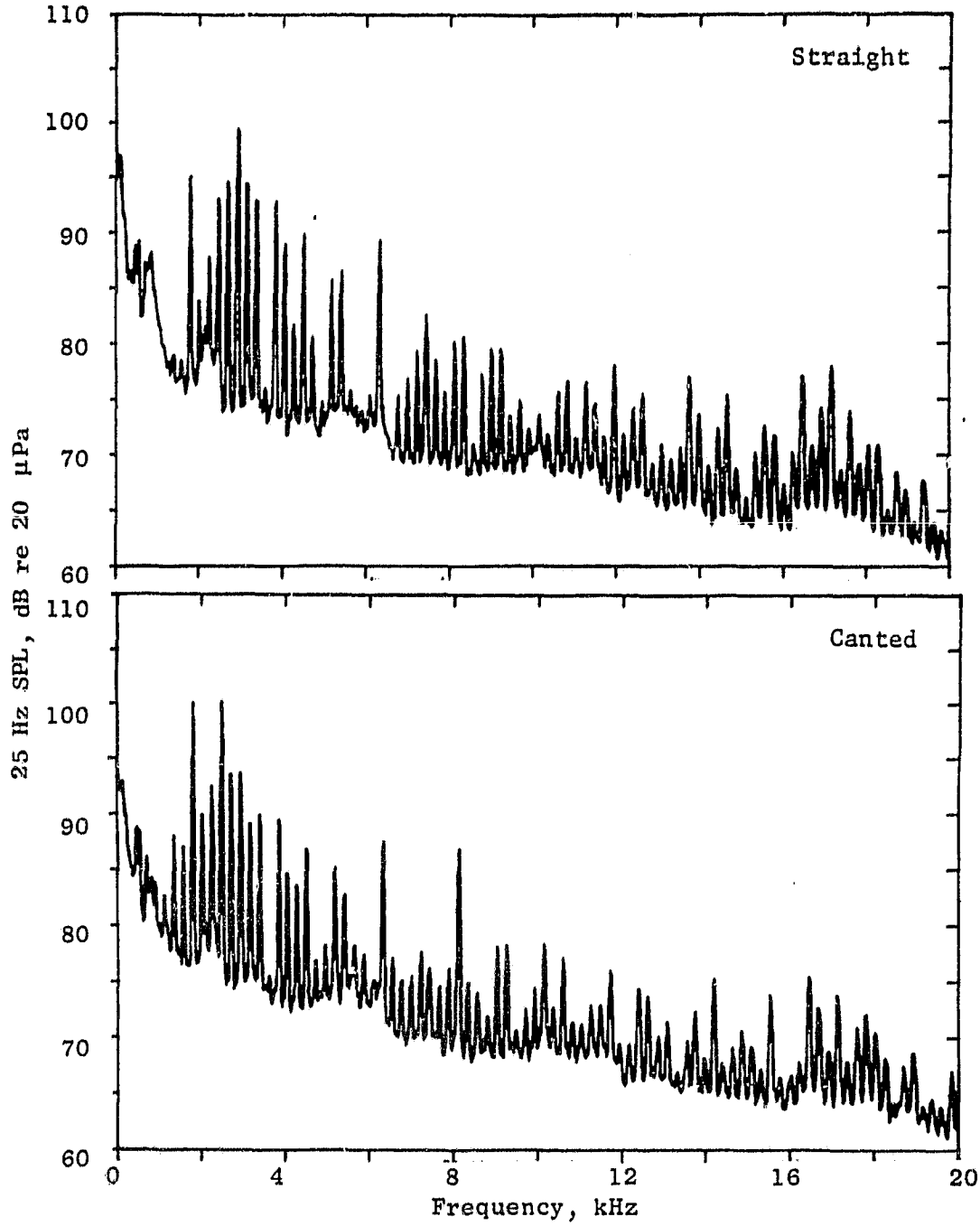

Figure 79. Comparison of Canted and Straight Diffusing Treated Inlet Narrowband Spectra at Supersonic Tip Speed (Concluded).

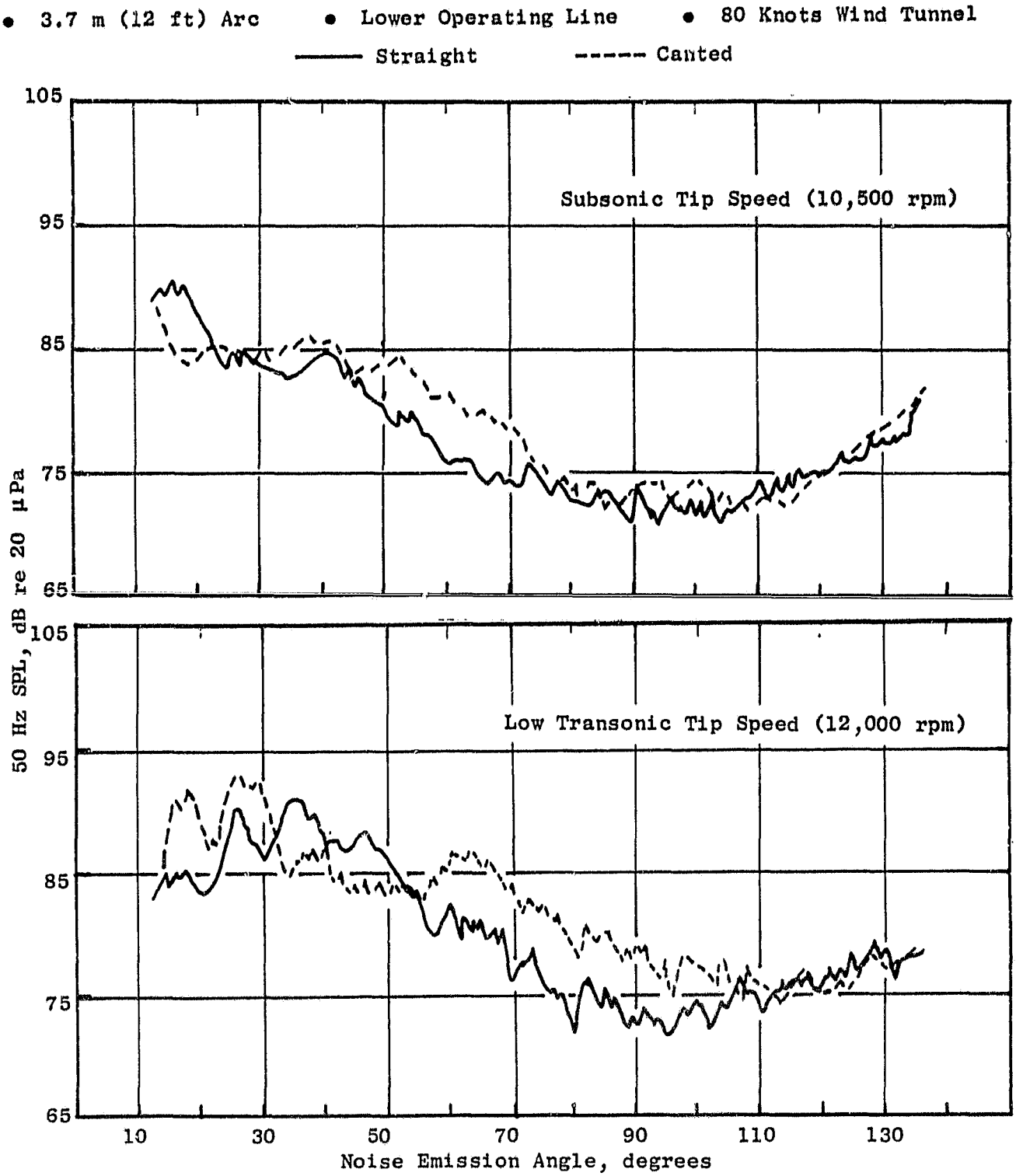

Figure 80. Comparison of BPF Directivities for Straight and Canted Diffusing Treated Inlets.

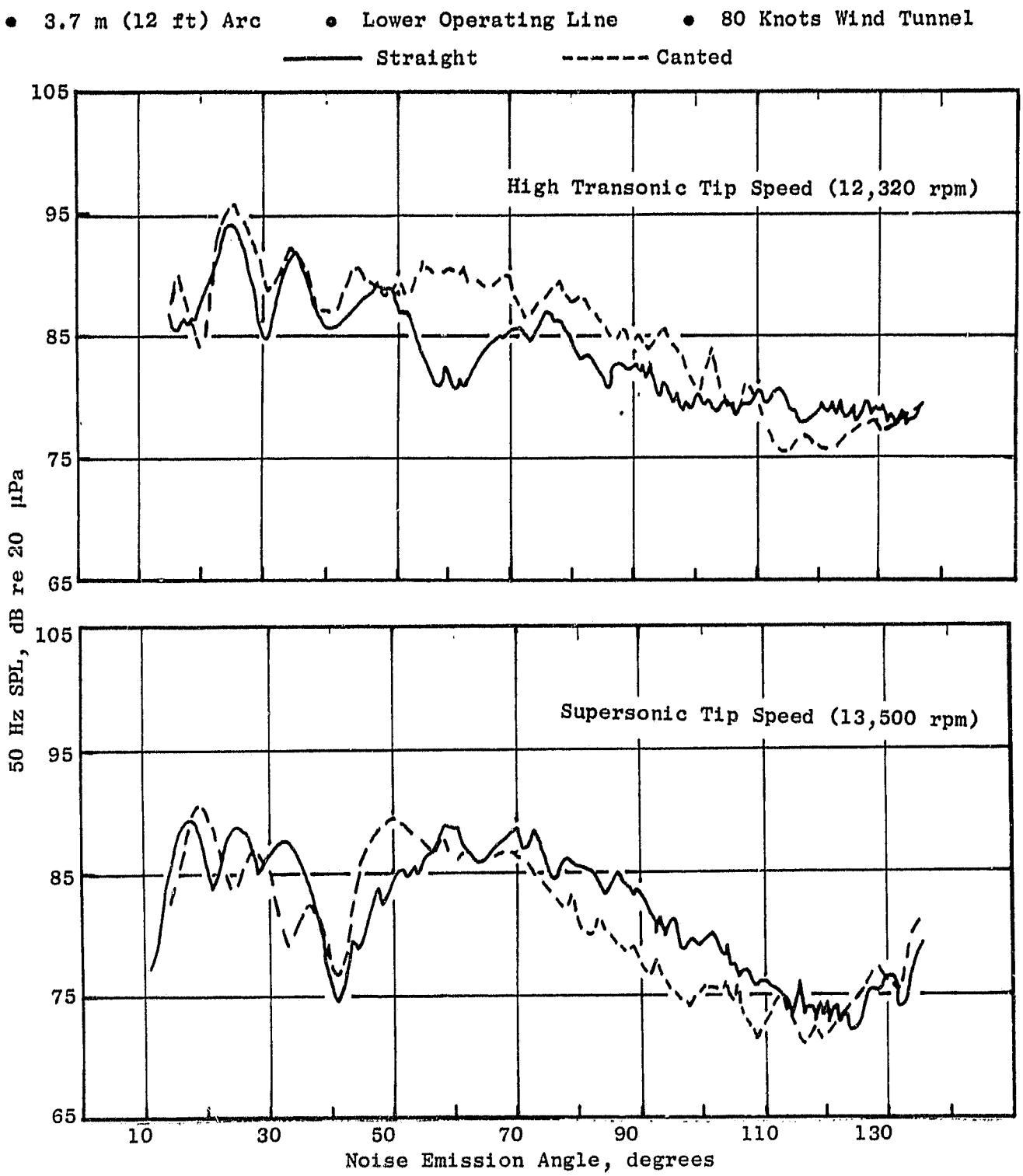

Figure 80. Comparison of BPF Directivities for Straight and Canted Diffusing Treated Inlets (Concluded).

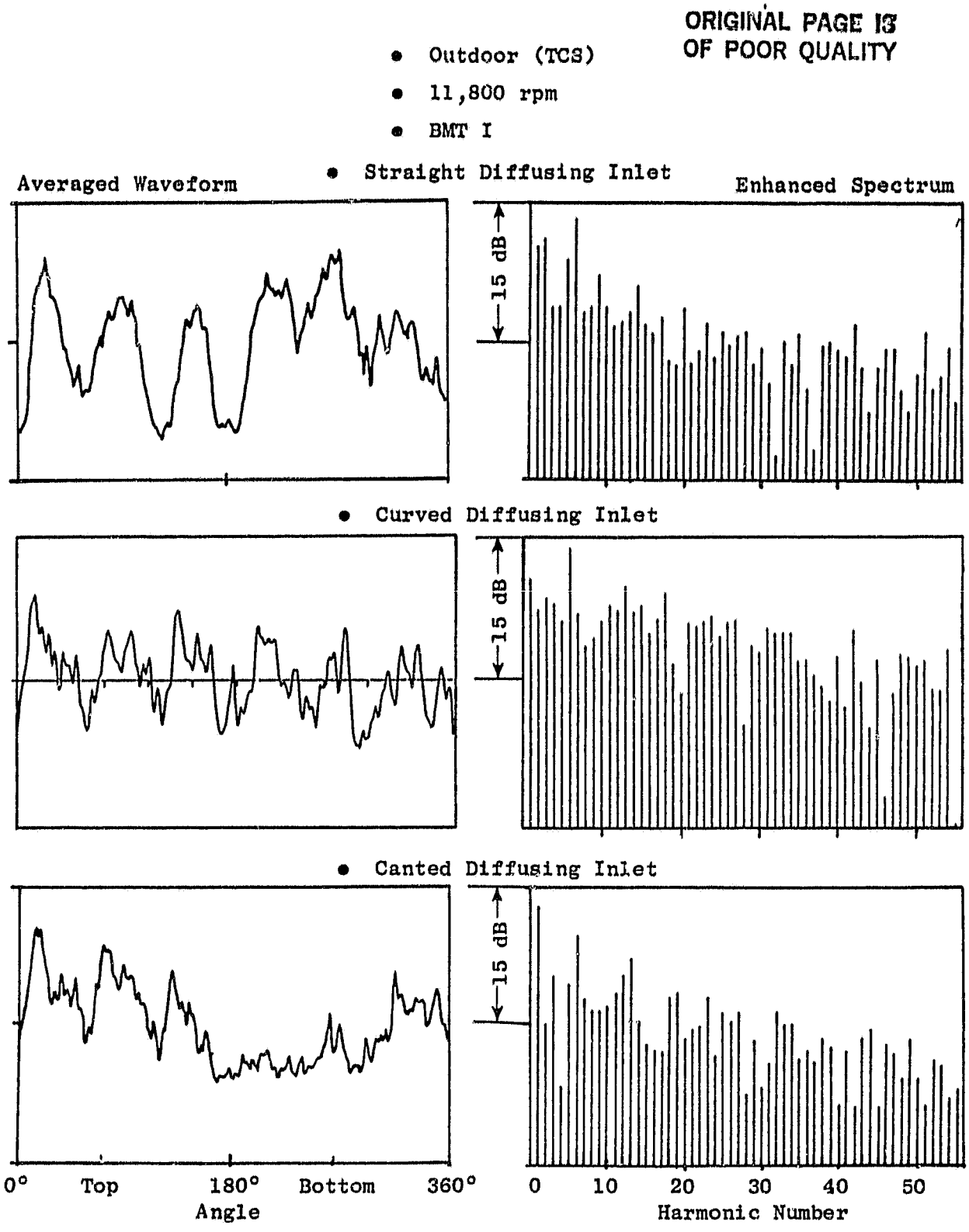

Figure 81. Enhancement Example.

disrupt the uniformity of its waveform as further noted by the reduced harmonic amplitudes in the curved and canted cases compared to the straight inlet case.

The variation of various BMT harmonic components with engine speed is displayed in Figure 82 for the canted and curved inlet cases. The results were obtained tracking the output of the BMT G signal during an engine speed acceleration. This inboard location was chosen for presentation since its enhanced and averaged spectral components for these harmonics were the same. At other BMT's closer to the tip, differences of greater than 12 dB were observed between canted and curved 1/rev components compared to the 7 dB in the BMT G case. The second harmonic is also noted to be higher for the canted case with the 6/rev contribution fairly similar.

More detailed studies are needed to quantify the 6/rev contribution since the outboard transducers and waveforms did indicate differences as shown in Figure 81.

Comparative scaled PNL and OASPL results for typical subsonic and transonic fan tip speed ranges are exhibited in Figures 83 and 84. The results indicate a systematic reduction in acoustic emission among the canted, curved, and straight treated diffusing inlets. The improvement is not always directly attributable to the scaled BPF 1/3-octave band as shown in Figure 85. Details of the narrowband spectra for the curved and canted inlets are shown in Figures 86 through 89 for outdoor testing on the design operating line. The lowered operating line results can be compared using Figures 59-61 and 77-79.

The comparison of the canted and curved inlet BPF directivities measured in the wind tunnel is accomplished using Figures 63 and 80. The results show relatively small differences in the 60°-90° sideline region with the curved inlet producing lower levels at the transonic speed point. The curved inlet did produce higher tone levels in the 10°-40° region at the transonic speed point.

The outdoor BPF tonal components are again compared using a 50-Hz tracking filter technique with the results presented in Figure 89. No systematic trends are observed to suggest the dominance of a particular BMT harmonic component or duct mode. Generally, the 60°-90° sideline region is composed of a broader lobe in the canted case and more well defined multiple lobes in the curved case. This finding suggests the propagation of lower order modes in the curved case and higher order modes in the canted case.

The effect of small angle of attack changes on the curved inlet BPF were relatively insignificant. Figure 90 exhibits the differences in BPF directivities for 0° and 5° angles of attack at an engine speed of 12,000 rpm. The results are also indicative of the reproducibility the wind tunnel directivity patterns exhibit during repeats of the same test condition.

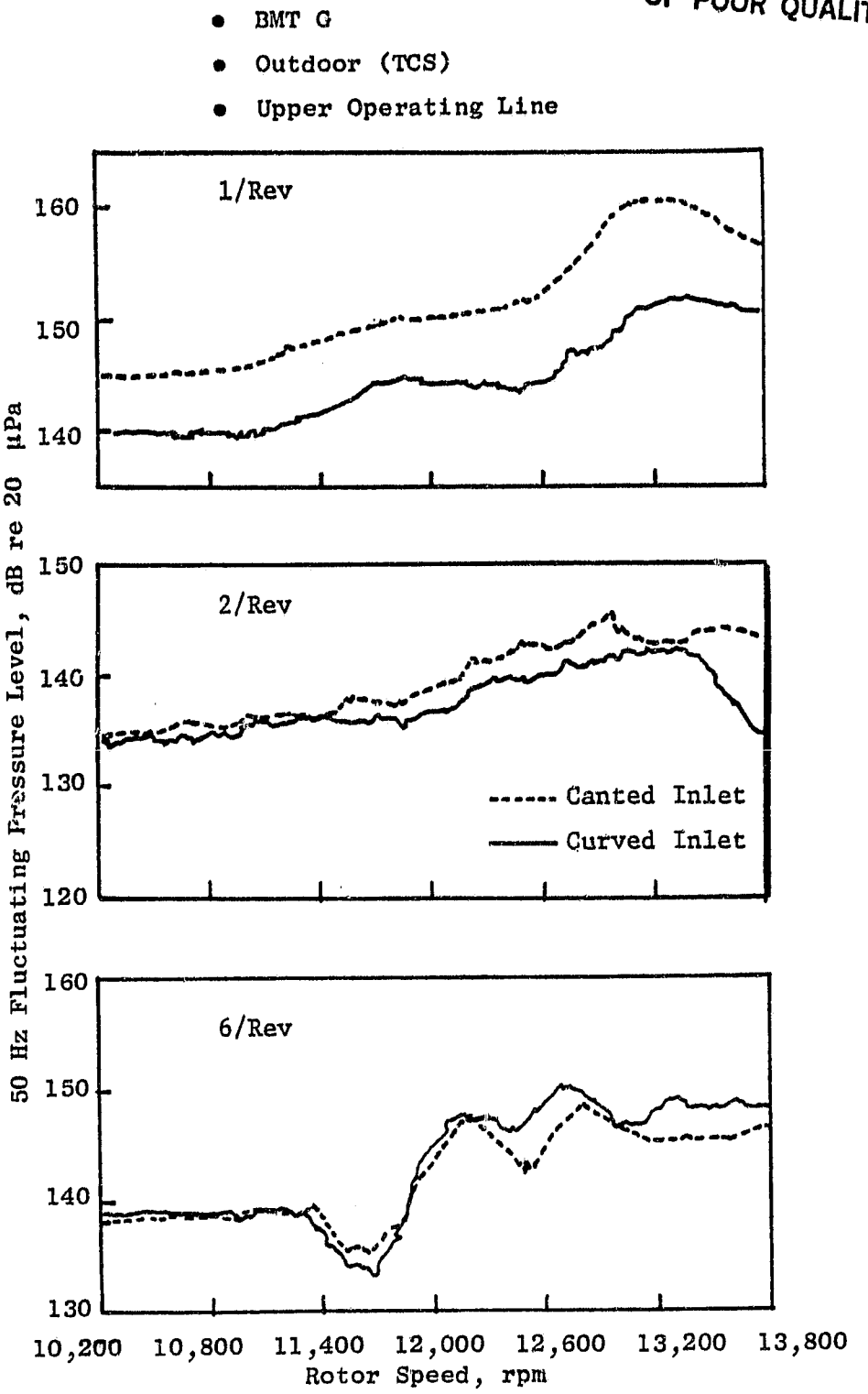

Figure 82. Blade Loading Harmonics.

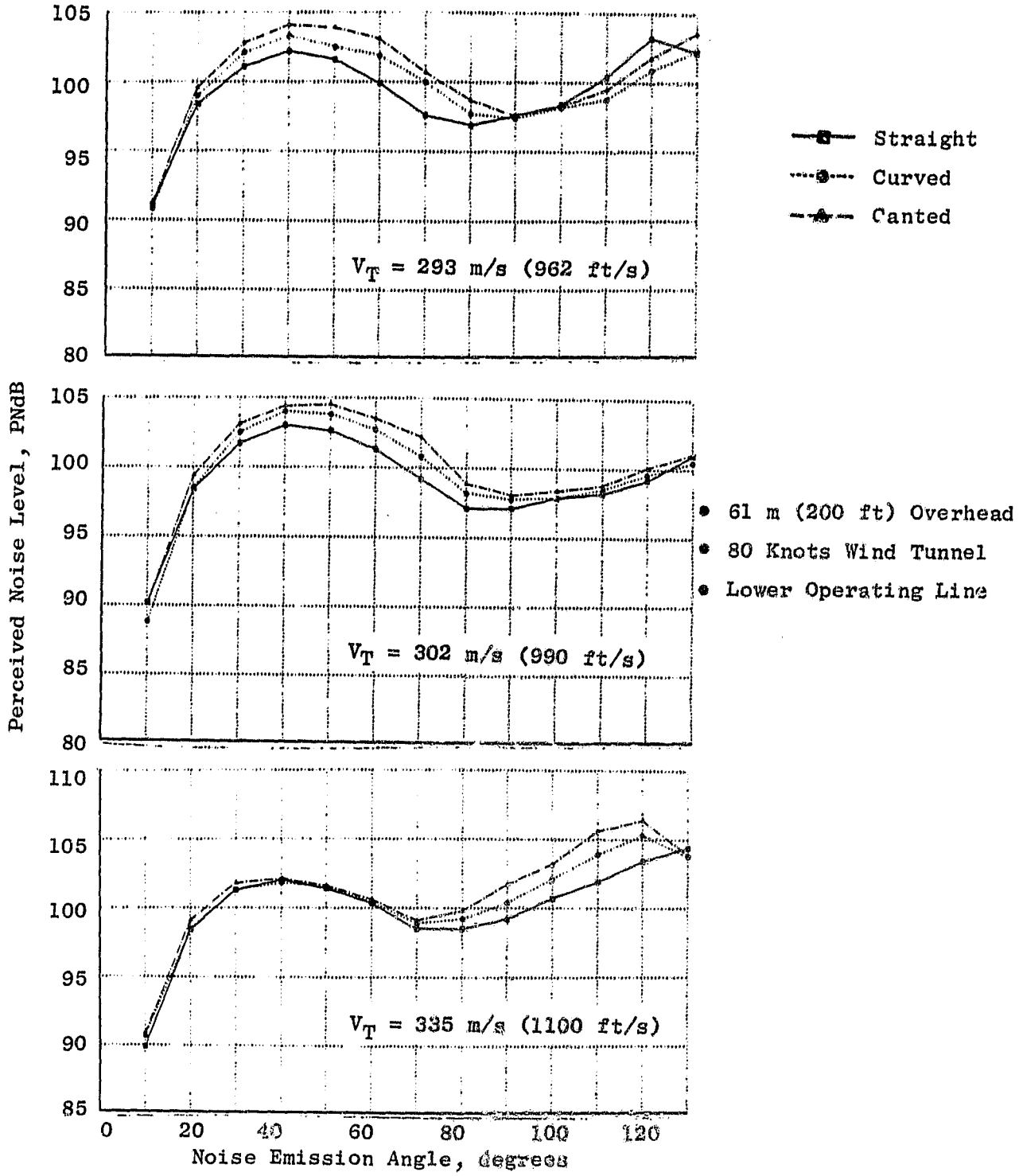

Figure 83. Comparison of Curved, Canted, and Straight Diffusing Treated Inlet Perceived Noise Level Directivities.

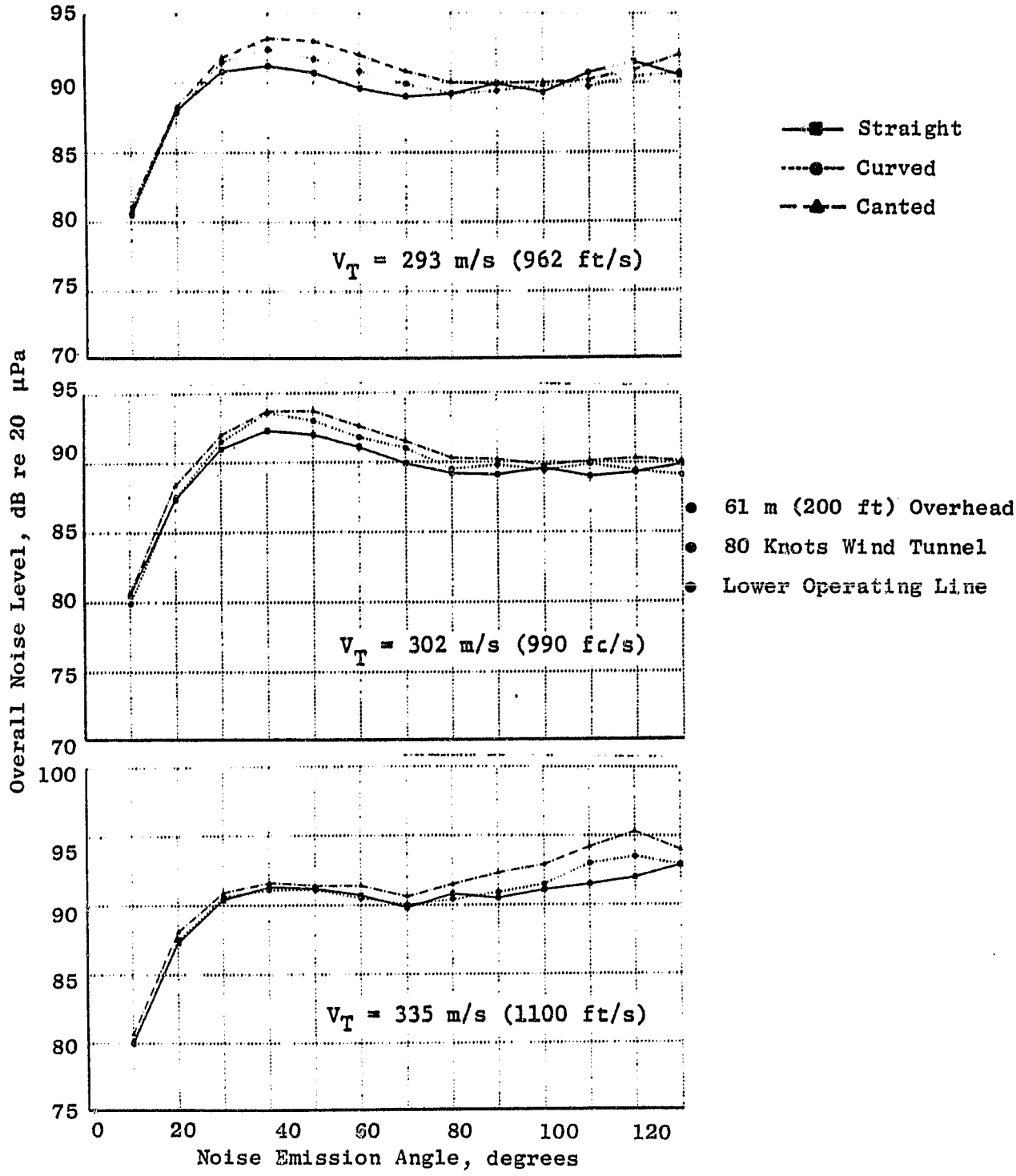

Figure 84. Comparison of Curved, Canted, and Straight Diffusing Treated Inlet Overall Noise Level Directivities.

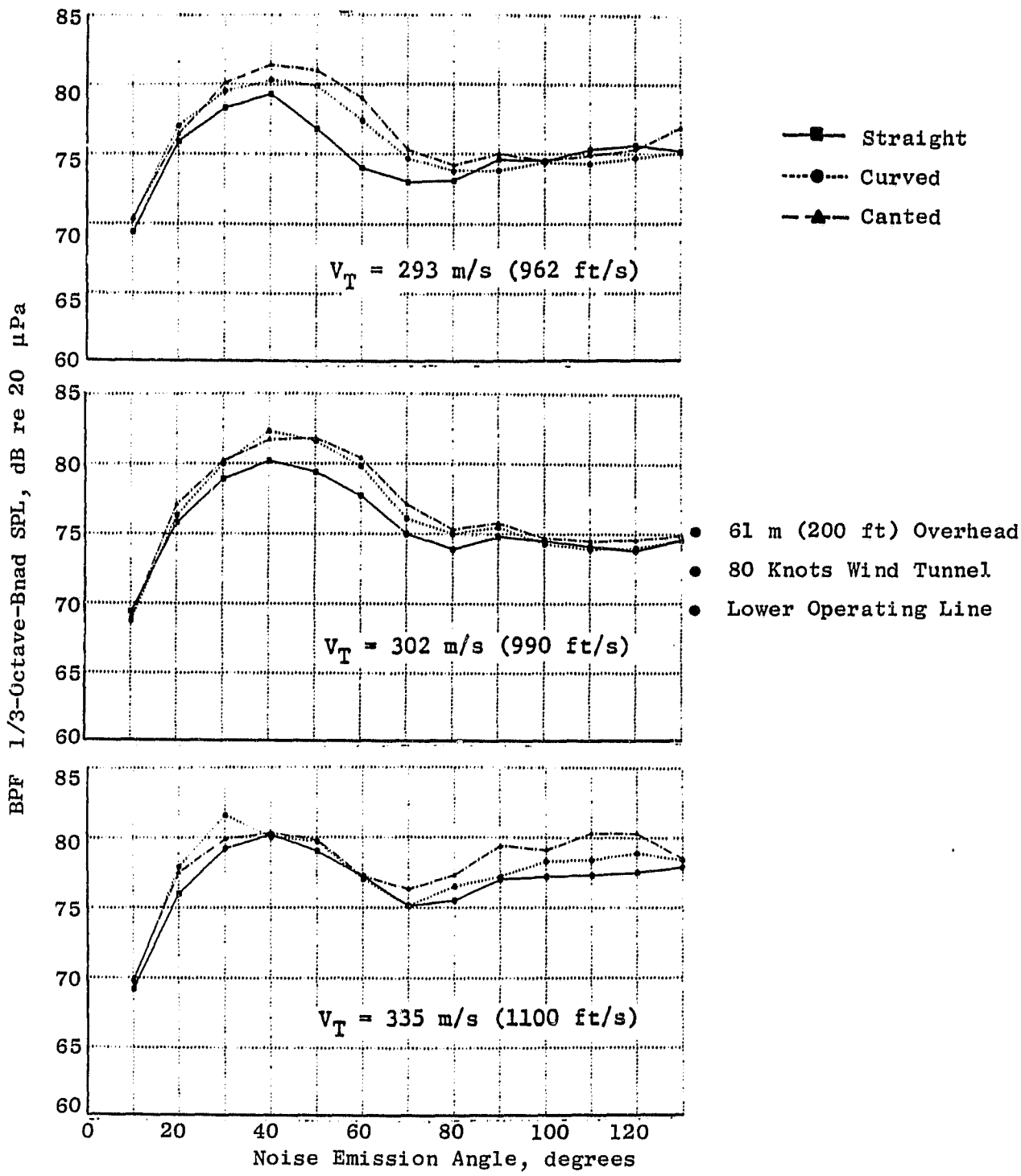

Figure 85. Comparison of Curved, Canted, and Straight Diffusing Treated Inlet 1/3-Octave-Band BPF Level Directivities.

- 30° Noise Emission Angle
- 14.5 Foot Microphone
- V_T = 302 m/s (990 ft/s)
- Outdoor (TCS)
- Upper Operating Line

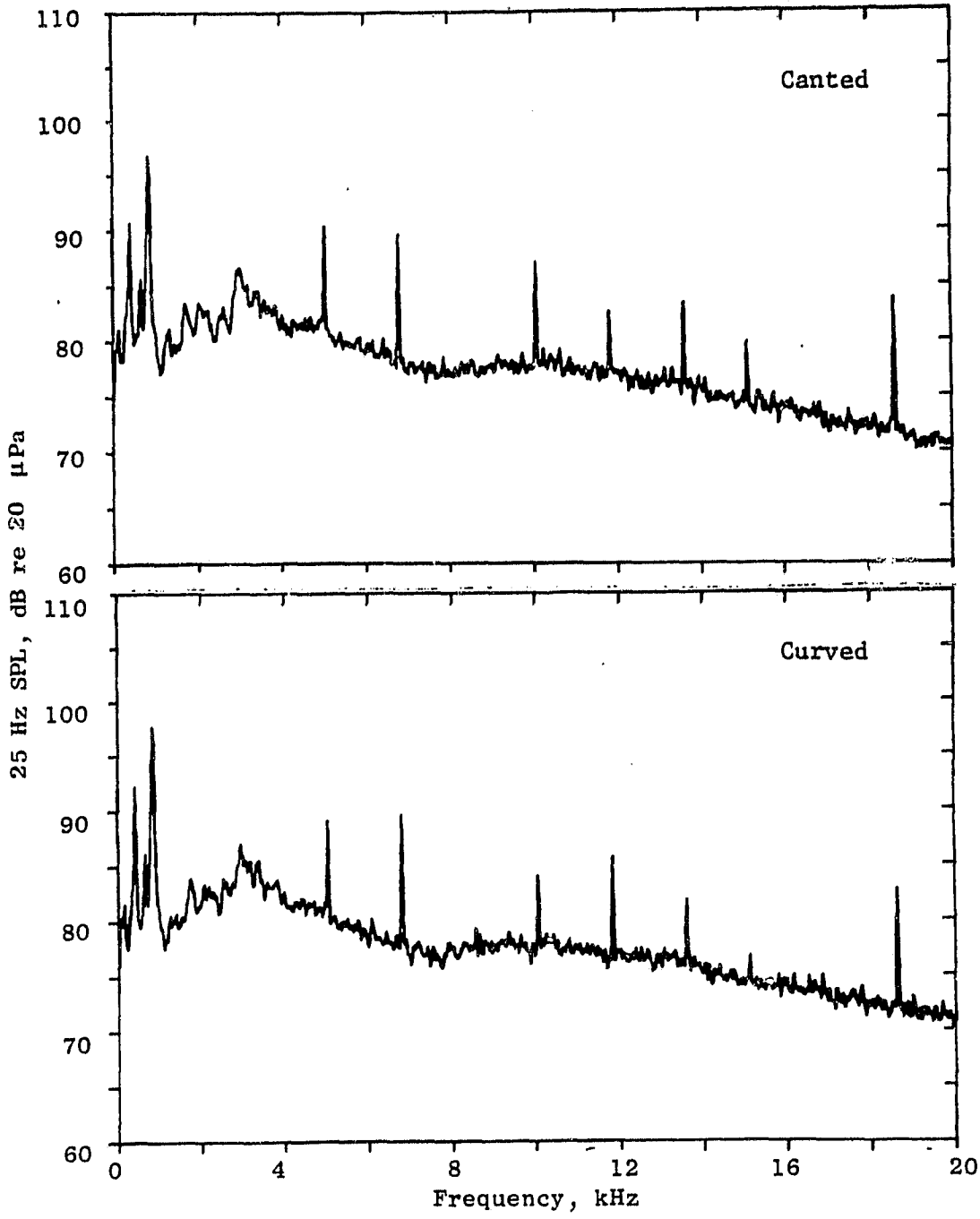

Figure 86. Comparison of Canted and Curved Diffusing Inlet Narrow-Band Spectra at Subsonic Tip Speed.

- 50° Noise Emission Angle
- 14.5 Foot Microphone
- V_T = 302 m/s (990 ft/s)
- Outdoor (TCS)
- Upper Operating Line

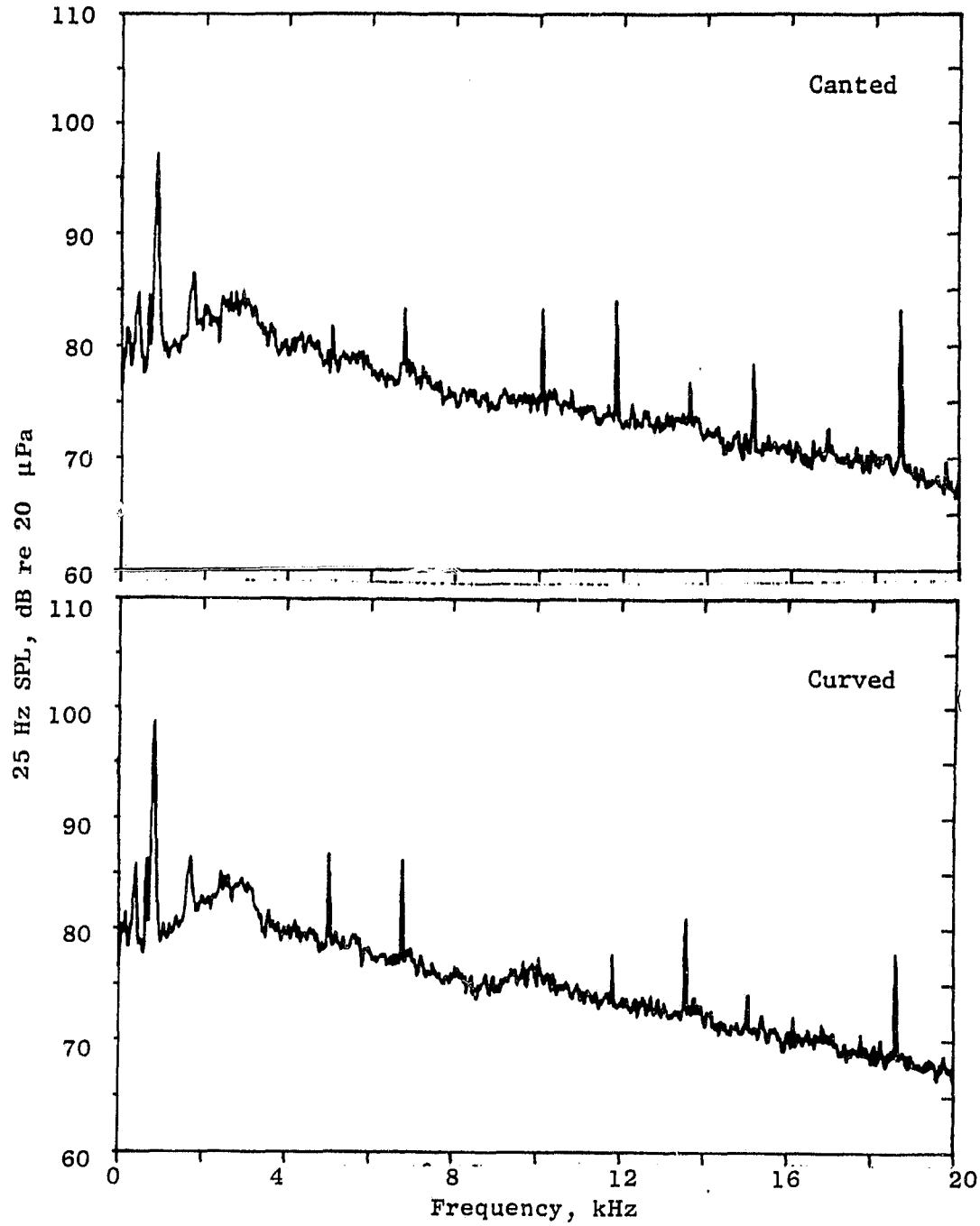

Figure 86. Comparison of Canted and Curved Diffusing Inlet Narrow-Band Spectra at Subsonic Tip Speed (Continued).

- 70° Noise Emission Angle
- 14.5 Foot Microphone
- V_T = 302 m/s (990 ft/s)
- Outdoor (TCS)
- Upper Operating Line

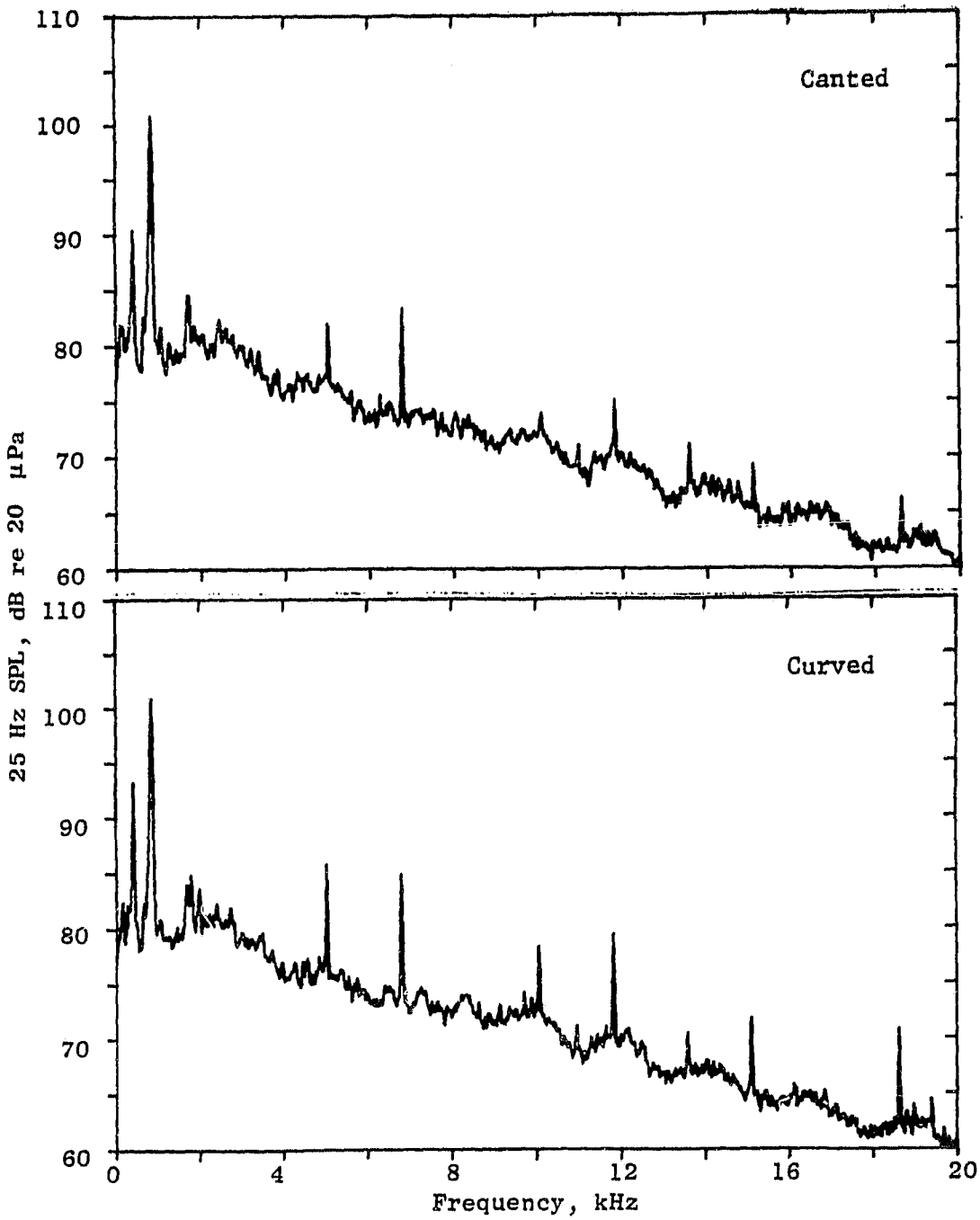

Figure 86. Comparison of Canted and Curved Diffusing Inlet Narrow-Band Spectra at Subsonic Tip Speed (Concluded).

- 30° Noise Emission Angle
- 14.5 Foot Microphone
- V_T = 335 m/s (1100 ft/s)
- Outdoor (TCS)
- Upper Operating Line

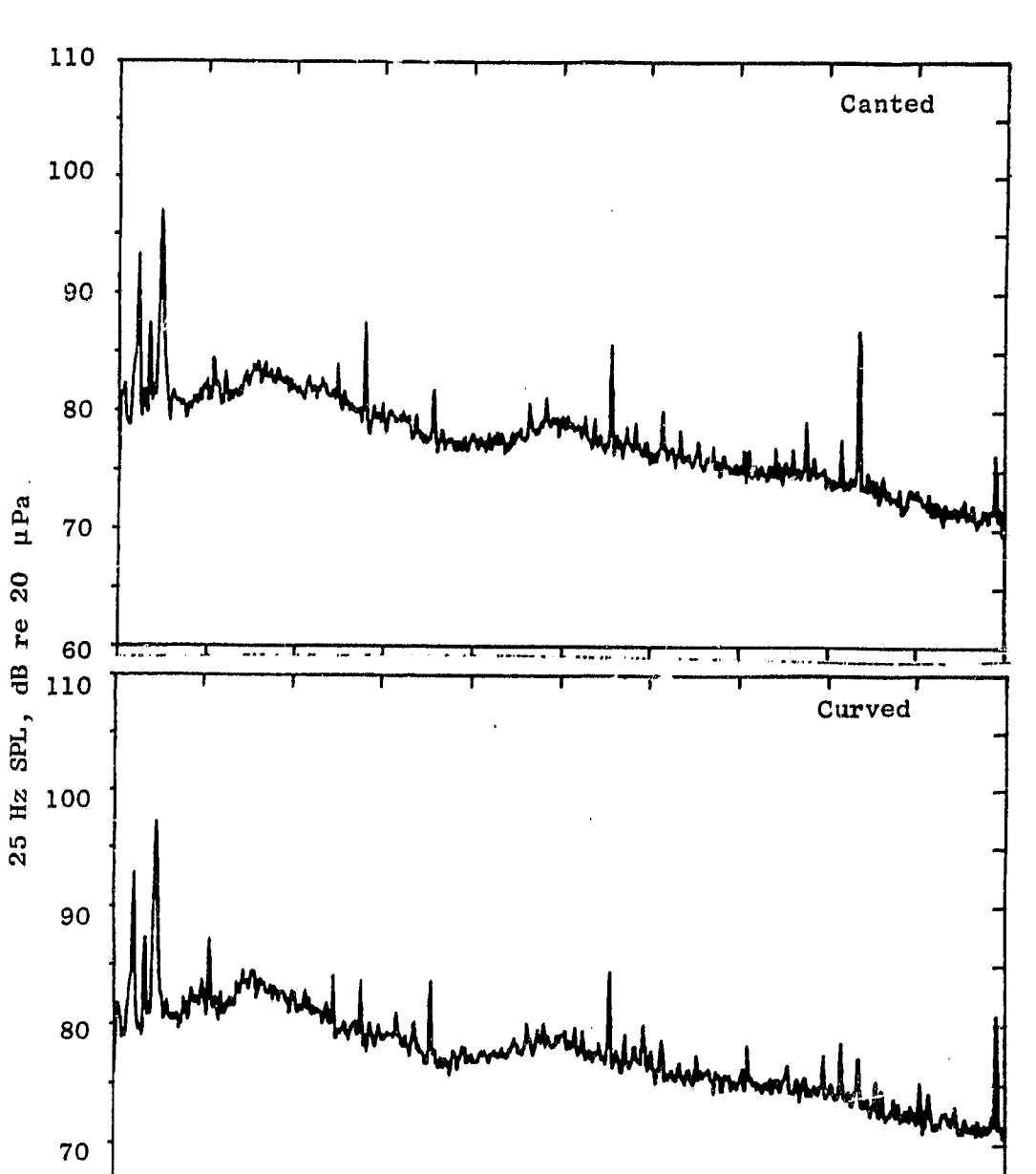

Figure 87. Comparison of Canted and Curved Diffusing Inlet Narrow-Band Spectra at Transonic Tip Speed.

- 50° Noise Emission Angle
- 14.5 Foot Microphone
- V_T = 335 m/s (1100 ft/s)
- Outdoor (TCS)
- Upper Operating Line

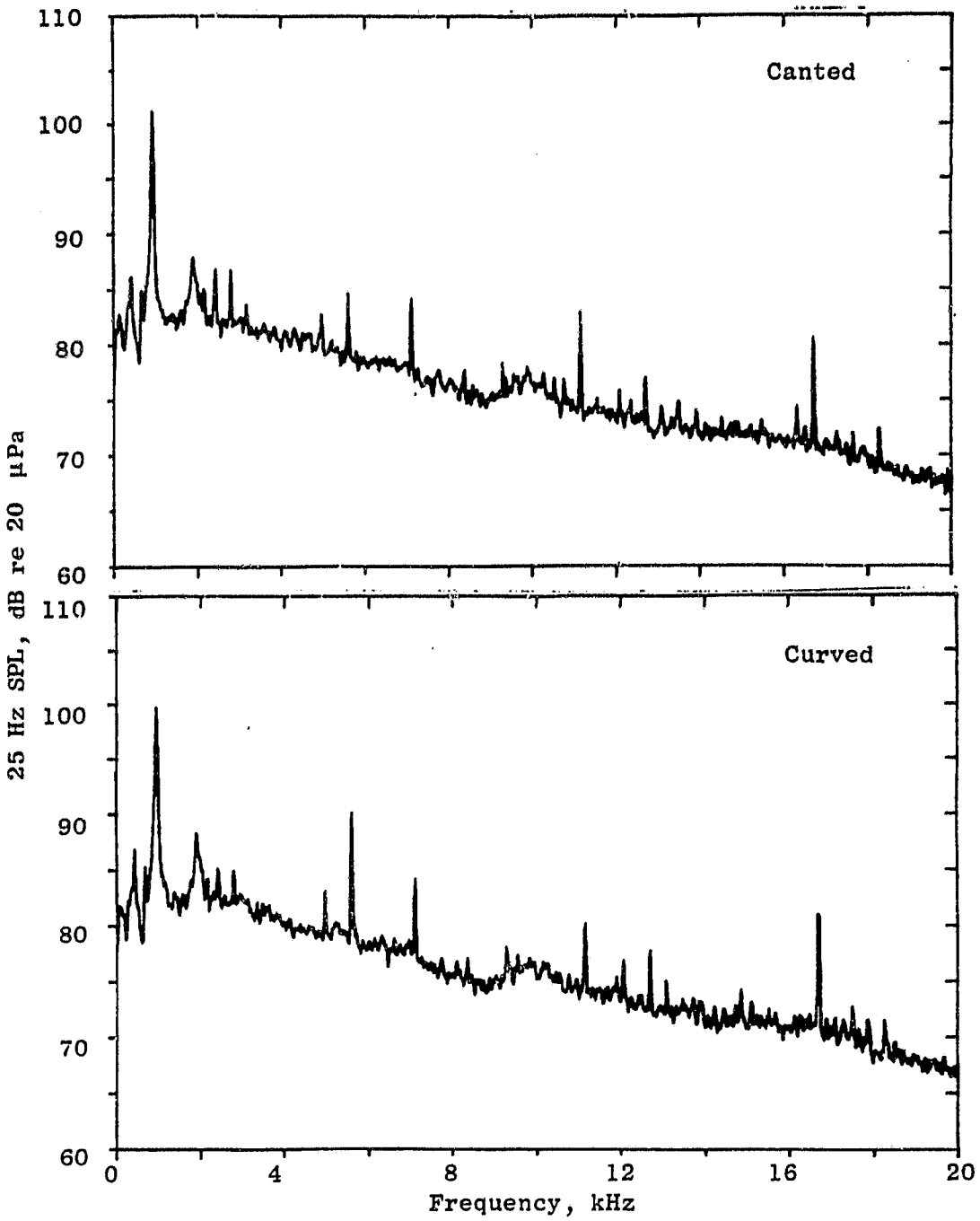

Figure 87. Comparison of Canted and Curved Diffusing Inlet Narrow-Band Spectra at Transonic Tip Speed (Continued).

- 70° Noise Emission Angle
- 14.5 Foot Microphone
- V_T = 335 m/s (1100 ft/s)
- Outdoor (TCS)
- Upper Operating Line

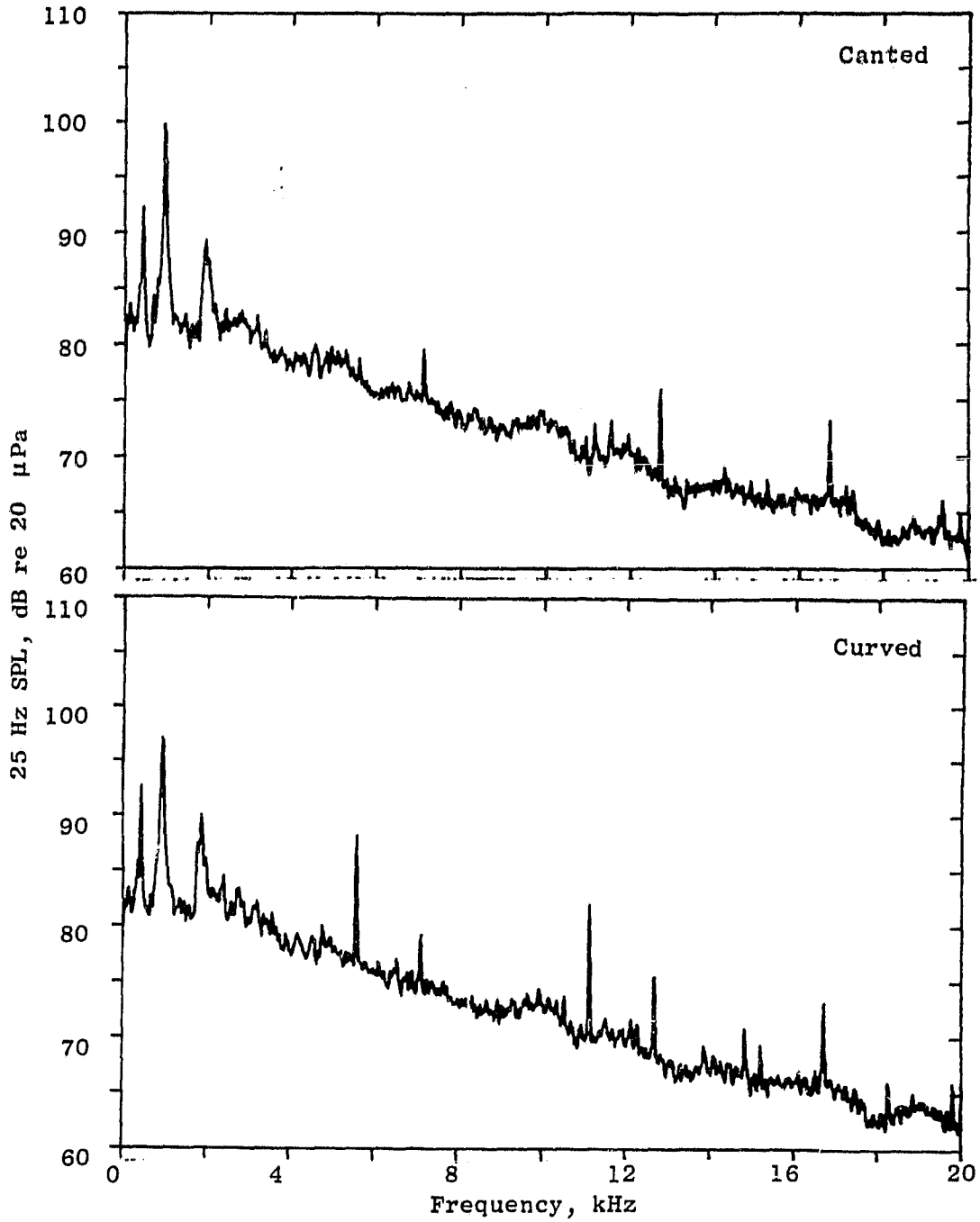

Figure 87. Comparison of Canted and Curved Diffusing Inlet Narrow-Band Spectra at Transonic Tip Speed (Concluded).

- 30° Noise Emission Angle
- 14.5 Foot Microphone
- V_T = 377 m/s (1237 ft/s)
- Outdoor (TCS)
- Upper Operating Line

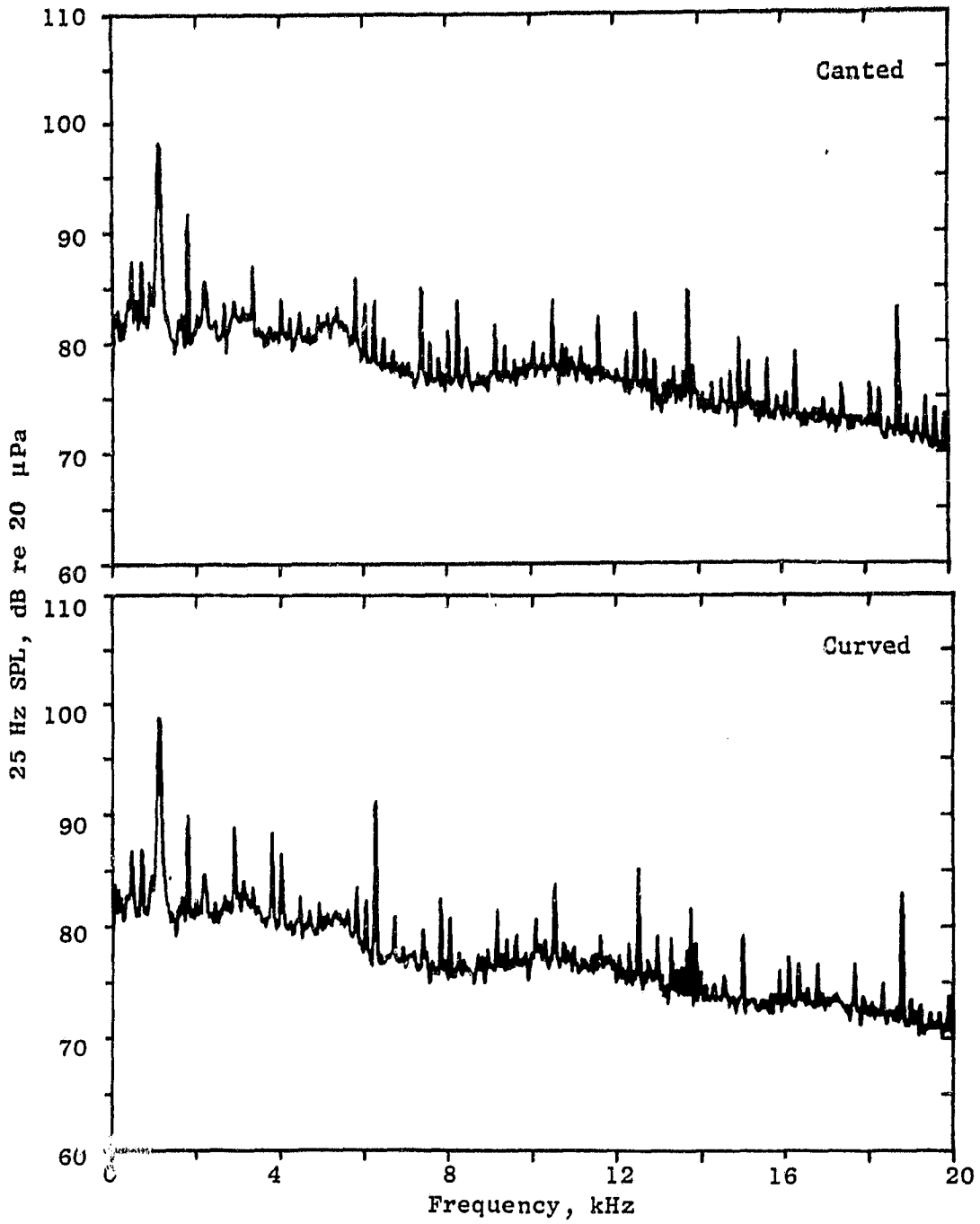

Figure 88. Comparison of Canted and Curved Diffusing Inlet Narrow-Band Spectra at Supersonic Tip Speed.

- 50° Noise Emission Angle
- 14.5 Foot Microphone
- V_T = 377 m/s (1237 ft/s)
- Outdoor (TCS)
- Upper Operating Line

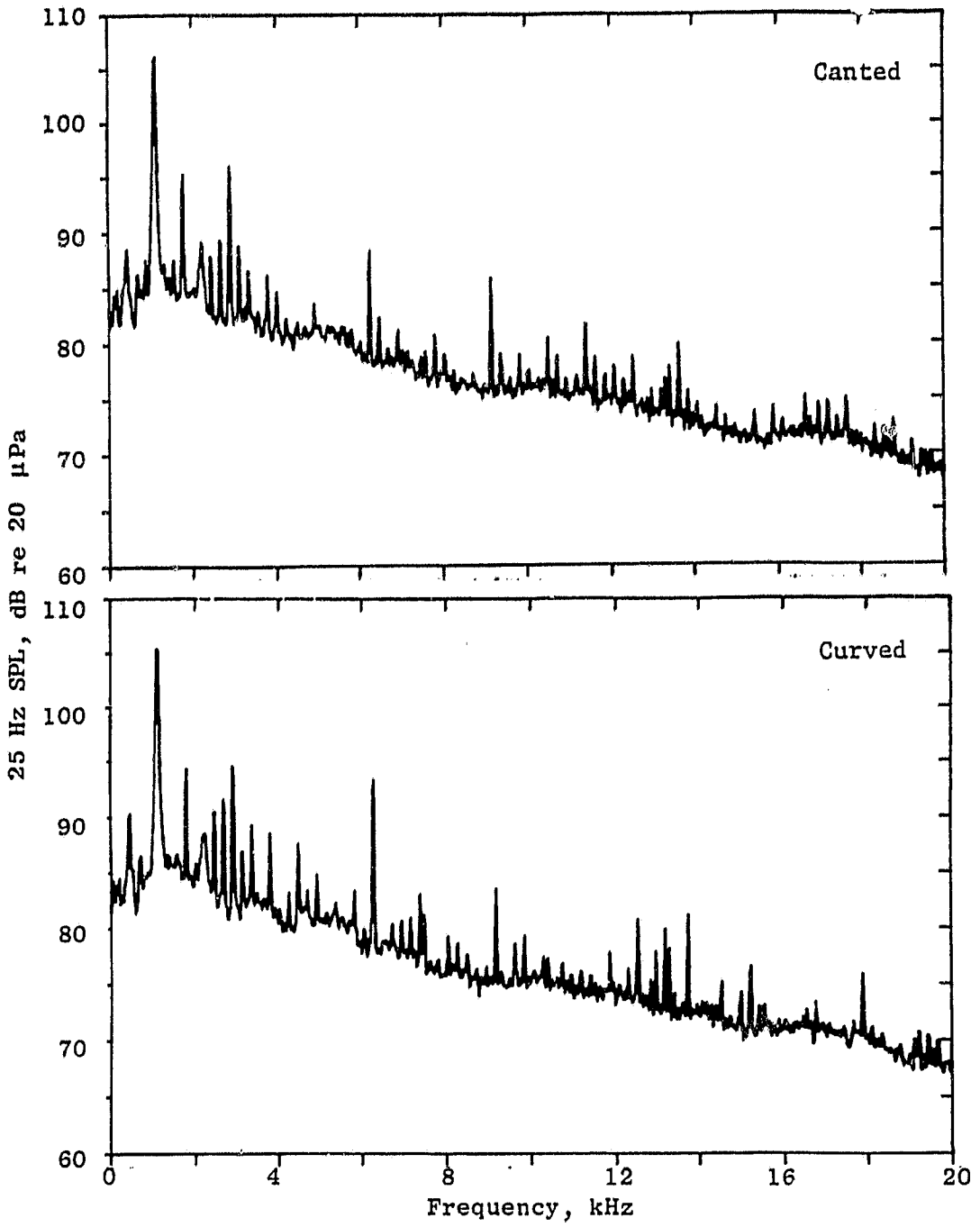

Figure 88. Comparison of Canted and Curved Diffusing Inlet Narrow-Band Spectra at Supersonic Tip Speed (Continued).

- 70° Noise Emission Angle
- 14.5 Foot Microphone
- V_T = 377 m/s (1237 ft/s)
- Outdoor (TCS)
- Upper Operating Line

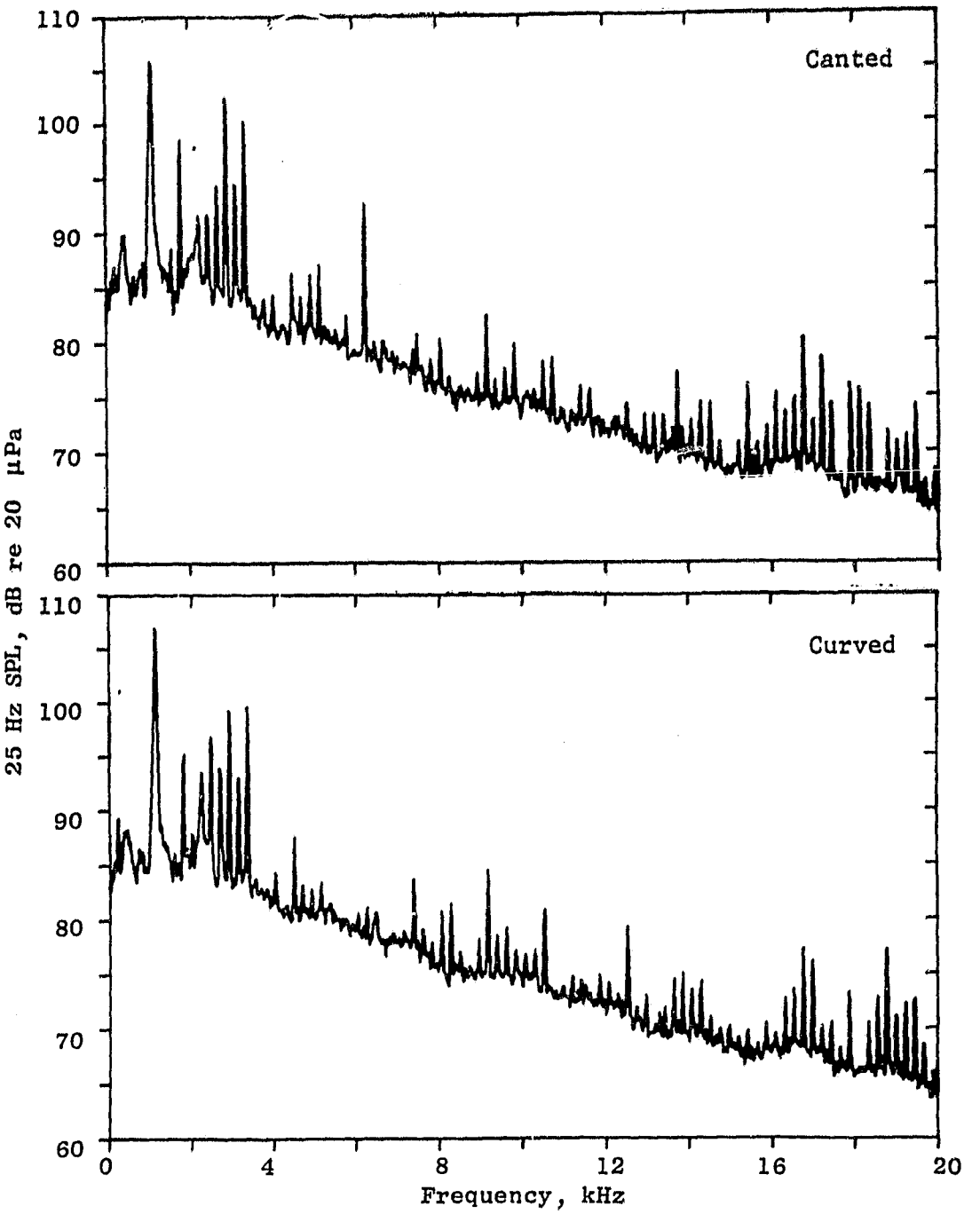

Figure 88. Comparison of Canted and Curved Diffusing Inlet Narrow-Band Spectra at Supersonic Tip Speed (Concluded).

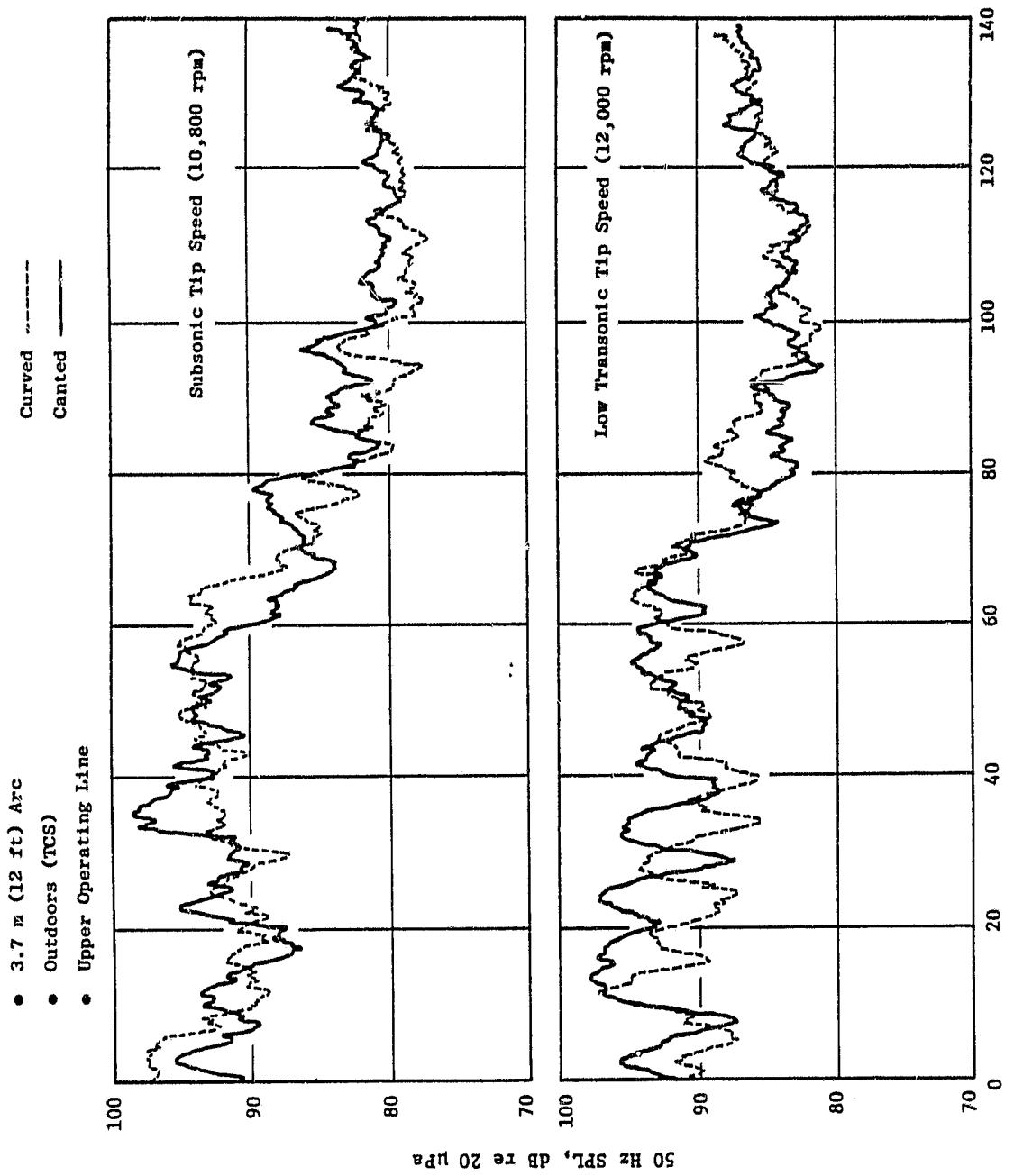

Figure 89. Comparison of BPF Directivities for Canted and Curved Diffusing Treated Inlets.

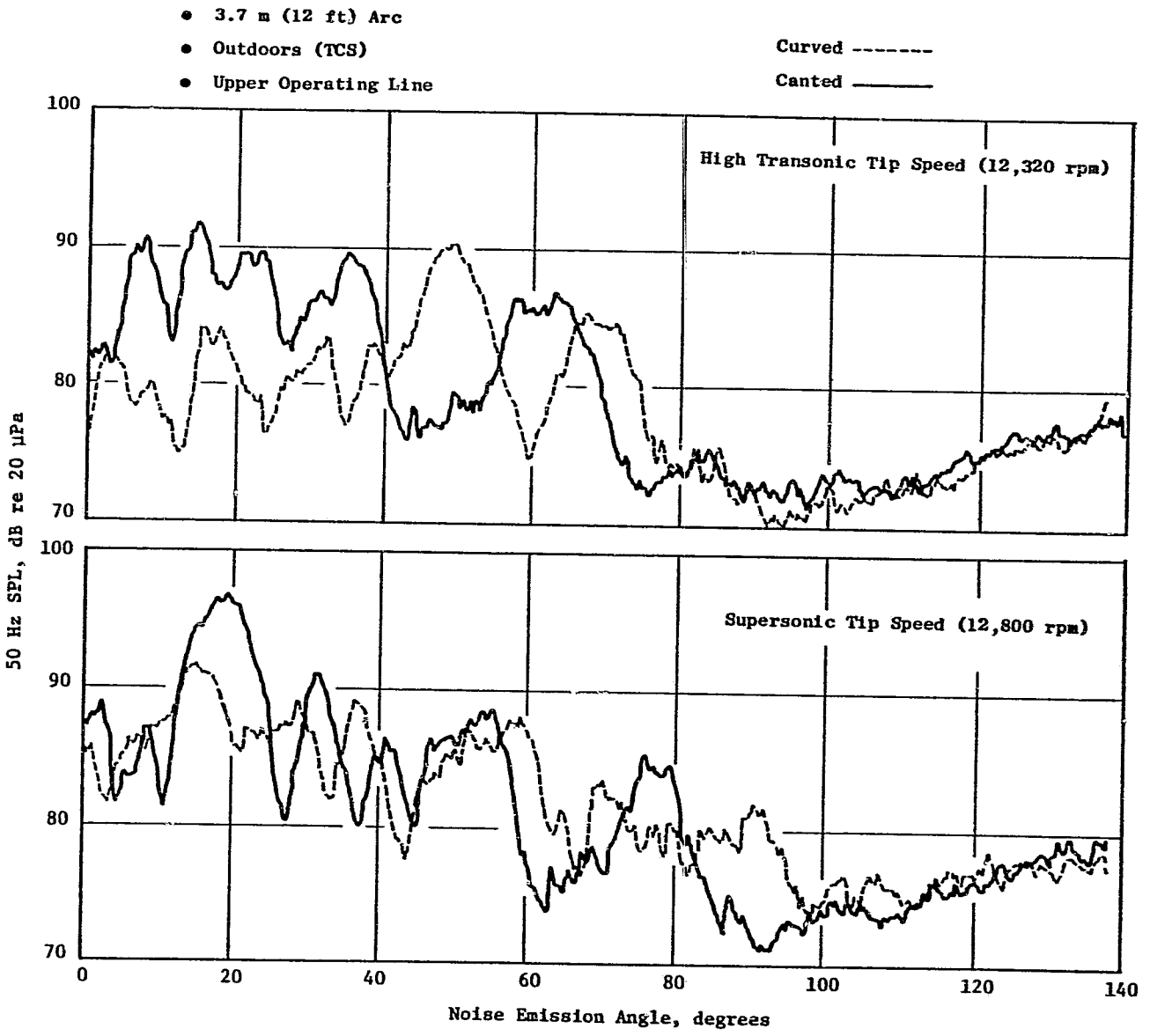

Figure 89. Comparison of BPF Directivities for Canted and Curved Diffusing Treated Inlets (Concluded).

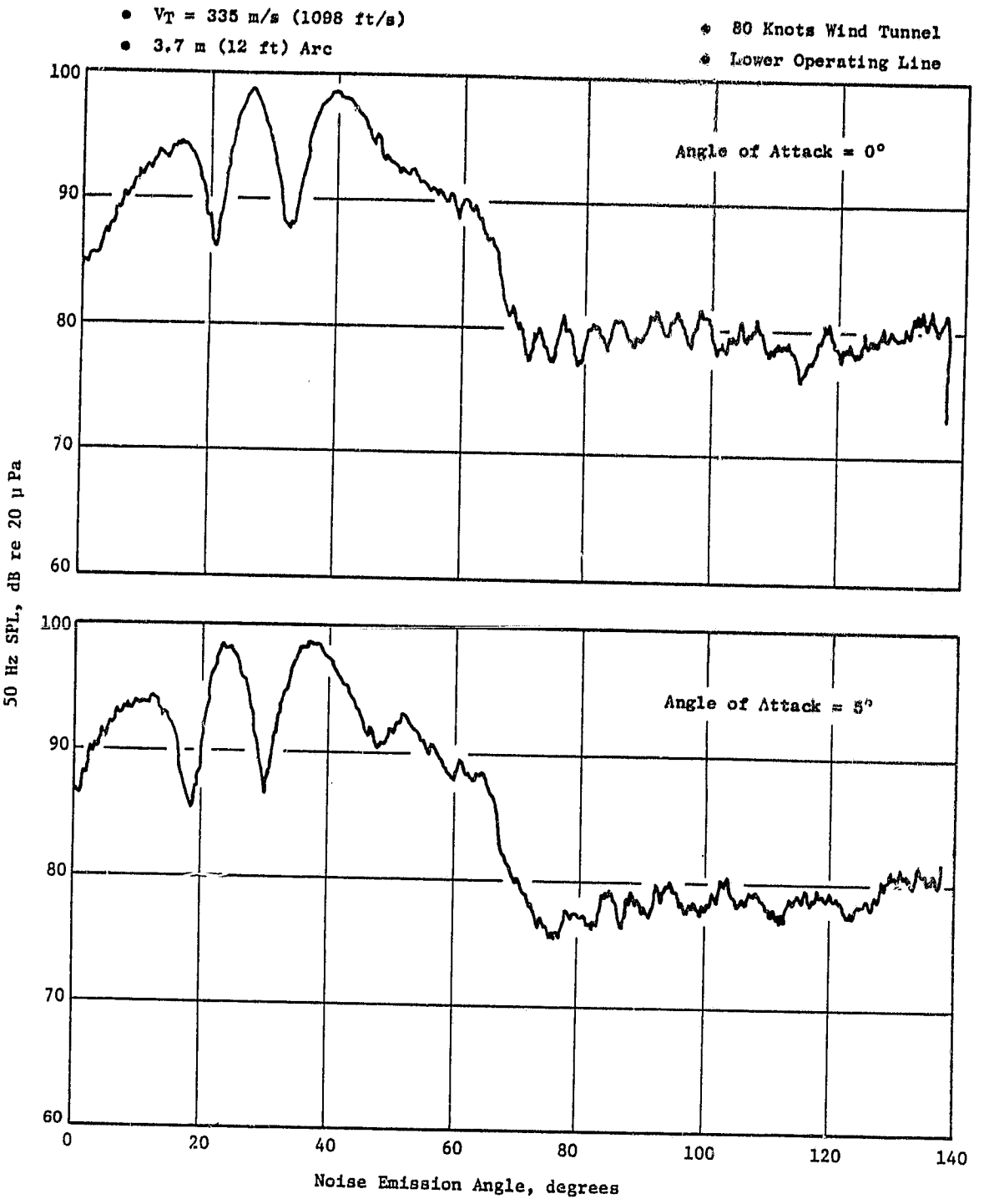

Figure 90. Curved Diffusing Treated Inlet BPF Directivity Pattern.

5.0 RECOMMENDATIONS AND CONCLUSIONS

This report is comparative in nature because the data analyses were performed to detect differences between configurations as opposed to the objective of determining absolute values such as in the certification of an aircraft engine configuration for use in commercial service. This perspective aligns with the research orientation of the test program and allows specific comparative conclusions to be reached. The general areas on which specific comments are made coincide with the topics discussed in the last four subsections of Section 4.0.

5.1 FAN NOISE TESTING TECHNIQUES

Ground-based static testing without a turbulence control device has been shown by many investigators, and reaffirmed in this study, to produce fan tone levels much higher than those measured using a turbulence control device. The use of a Turbulence Control Structure (TCS) in the static test program definitely reduced the fan noise level; however, the question of how well the TCS performs in the area of reproducing an accurate flight turbulence environment remains. Also, the issue of transmission loss through the TCS is raised as a result of some differences observed in comparative broadband spectra. At frequencies above 5 kHz, broadband levels differ by the order of 1 to 4 dB between TCS and non-TCS runs, with the greater differences occurring at higher frequencies.

A comparison of the wind tunnel test results to those derived out-of-doors with the TCS forms a basis for assessing how well the outdoor testing with the TCS matches the acoustics measurements obtained in the 40 x 80 at a tunnel velocity of 80 knots. This comparison at various engine speeds indicates that the broadband noise levels measured in the wind tunnel are higher than those obtained outdoors using the TCS. The increase is of the order of 1 to 3 dB and is not well accounted for by the theories dealing with the wind tunnel to static transformations. The increase in noise levels can in part be ascribed to a term called "dynamic effect." This finding provides a direct impact on how well dynamic effect corrections are utilized in making static-to-flight projections which can only be answered by flight testing. Should the flight data reproduce the wind tunnel data, then new dynamic-effect corrections to static data need to be applied to adequately and accurately estimate flight noise levels from statically measured noise quantities.

Although the integrated level of the BPF tone with the TCS installed is in relative agreement with the wind tunnel results, fundamental differences occur in the angular distribution of the tonal energy.

A comparison of BPF tonal directivities suggests that redirection of the tonal sound energy is not directly associated with the use of the TCS. However, the flow-field and lip shape differences between the outdoor static and

the wind tunnel configurations may cause more redistribution of sound energy than previously thought. The test results indicate that additional field testing of TCS devices with calibrated sources in flow environments should be accomplished along with theoretical studies which incorporate lip shape and flow-field effects into the problem of tonal radiation from ducts to assist in the resolution of these differences.

5.2 FAN OPERATING LINE ACOUSTIC CONSIDERATIONS

The testing of the JT15D on two operating lines demonstrated the importance of this aerodynamic parameter in performing acoustic measurements. At comparable corrected speed points, broadband noise differences of approximately 3 dB were measured as the fan's design operating line was reduced as shown in Figure 24. In addition, significant tonal differences were noted which could be attributed to the duct modal propagation effects.

5.3 INLET SUPPRESSION EFFECTS

The utilization of an advanced bulk absorber treatment design in a conventional aircraft inlet application was successfully demonstrated. Suppressions of up to 20 dB in the sideline fan BPF directivity pattern were measured at certain engine speeds. The design was based on the duct modal propagation concept; thus, the treatment's effectiveness gives enhanced credibility to this theory of treatment design. The testing of the fan in environments where turbulence was controlled to the extent that lobular BPF directivity patterns were obtained also establishes renewed faith in some of the earlier theories dealing with modal radiation.

5.4 INLET AEROACOUSTIC DESIGN CONSIDERATIONS

The aerodynamic superiority of the curved inlet concept over the canted inlet concept for reducing static pressure distortion was clearly demonstrated. This improvement of up to 12 dB in the blade-measured, 1/rev dynamic pressure component did not produce a substantial acoustic benefit in the BPF far-field tonal directivity pattern. The apparent reason for this minimal benefit is the treatment effectiveness which suppressed the sideline acoustic radiation of high-order modal patterns such as those generated by the 1/rev static pressure distortion. Another interesting aeroacoustic phenomenon appeared as a result of the testing: The forward acoustic radiation at shallow angles actually increased as a result of using the curved inlet. Observation of the BMT resultant enhanced waveforms, and spectra showed that the 6/rev component was somewhat disrupted by the static pressure distortion imposed from the canted inlet, thereby diminishing its harmonic amplitude. So if the 6/rev component is a strong contributor to the BPF far-field radiation pattern, as has been suggested by other investigators, then the higher acoustic levels measured with the curved inlet at some speeds are potentially attributable to this source

mechanism. Attempts to isolate such an effect during the course of this program were limited, and more in-depth studies should be performed using computer software specifically designed to evaluate this effect. The information contained on the BMT's may be a useful tool in this evalution.

The overall conclusion in the area of aeroacoustic design is that the curved diffusing treated inlet demonstrated improvements on the order of only 1 PNdB over the canted diffusing treated inlet in high subsonic speed ranges typical of a high-flap landing approach condition. The use of the curved inlet concept, coupled with the advanced bulk absorber concept, effectively eliminated the high sideline acoustic levels reported previously in the untreated nondiffusing canted case. A tradeoff between the use of the curved inlet concept and the shorter treated inlet design may be available as a result of this finding. The inlet design apparently impacted other aeroacoustically related quantities as indicated by the alteration in the fan-blade-measured 6/rev component attributed to the potential field from the six engine support struts.

REFERENCES

1. Moore, M.T., "Forward Velocity Effects on Fan Noise and the Suppression Characteristics of Advanced Inlets as Measured in the NASA-Ames 40 x 80 Foot Wind Tunnel," NASA CR-152328, September 1979.

2. Smith, E.B., Moore, M.T., and Gliebe, P.R., "Distortion - Rotor Interaction Noise Produced by a Drooped Inlet," AIAA Paper 80-1050, AIAA 6th Aeroacoustic Conference, June 4-6, 1980.

3. Hodder, B.K., "Further Studies of Static-to-Flight Effects on Fan Tone Noise Using Inlet Distortion Control for Source Identification," NASA TMX-73183, NASA-Ames Research Center, Moffett Field, California, December 1976.

4. McArdle, J.G., Jones, W.L., Heidelberg, L.J., and Homyak, L., "Comparison of Several Inflow Control Devices for Flight Simulation of Fan Tone Noise Using a JT15D-1 Engine," NASA TM-81505, AIAA 6th Aeroacoustics Conference, June 4-6, 1980.

5. Preisser, J.S., Schoenster, J.A., Golub, R.A., and Horne, C., "Unsteady Fan Blade Pressure and Acoustic Radiation from a JT15-D-1 Turbofan Engine at Simulated Forward Speed," AIAA Paper 81-0096, AIAA 19th Aerospace Sciences Meeting, January 12-15, 1981.

6. Evans, L.B., and Sutherland, L.C., "Absorption of Sound in Air," Wyle Lab Report WR 70-14, July 1970.

7. Rice, E.J., Heidmann, M.F., and Sofrin, T.G., "Modal Propagation Angles in a Cylindrical Duct with Flow and Their Relation to Sound Radiation," NASA TM-79030, AIAA Paper 79-0183, Aerospace Sciences Meeting, January 15-17, 1979.

8. Bendat, J.S., and Piersol, A.G., Random Data: Analysis and Measurement Procedures, John Wiley and Sons, Inc., 1971.

9. Ho, P.R., Smith, E.B., Kantola, R.A., "An Inflow Turbulence Reduction Structure for Scale Model Fan Testing," AIAA Paper 79-0655, 1979.

10. Kantola, R.A., Warren, R.E., "Basic Research in Fan Source Noise Inlet Distortion and Turbulence Noise, Final Report," NASA CR-17853, December 1978.

REFERENCES (Concluded)

11. Gedge, M.R., "A Design Procedure for Fan Inflow Control Structures," Pratt and Whitney - NASA CR-165625, September 1980.

12. Kerschen, E.J., Gliebe, P.R., "Fan Noise Caused by the Ingestion of Anisotropic Turbulence - a Model Based on Axisymmetric Turbulence Theory," AIAA Paper 80-1021, AIAA 6th Aeroacoustic Conference, June 4-6, 1980.

13. Ginder, R.B., and Newby, D.R., "An Improved Correlation for the Broad-band Noise of High-Speed Fans," AIAA J. of Aircraft, Vol. 14, No. 9, September 1977, pp. 844-849.

14. Gliebe, P.R., "Effect of Throttling on Forward Radiated Fan Noise," AIAA Paper 79-0640, March 1979.

15. Tyler, J.M., and Sofrin, T.G., "Axial Flow Compressor Noise Studies," SAE Transactions, Vol. 70, 1962, pp. 309-332.